# Synthesis of imprinted polymers for the detection of tamoxifen or its metabolites and evaluation of their potential as drug carriers.

A thesis submitted in partial fulfilment of the Degree of Doctor of Philosophy at the University of London

Fosca Mirata

August 2017

School of Biological and Chemical Sciences

Queen Mary University of London

## Statement of originality

I, Fosca Mirata, confirm that the research included within this thesis is my own work or that where it has been carried out in collaboration with, or supported by others, that this is duly acknowledged below and my contribution indicated. Previously published material is also acknowledged below.

I attest that I have exercised reasonable care to ensure that the work is original, and does not to the best of my knowledge break any UK law, infringe any third party's copyright or other Intellectual Property Right, or contain any confidential material.

I accept that the College has the right to use plagiarism detection software to check the electronic version of the thesis.

I confirm that this thesis has not been previously submitted for the award of a degree by this or any other university.



Signature: 

Date: 09-08-17

Details of collaboration and publications:

Chapter 3 of this thesis describes the work carried out on polymers obtained by Dr. J. V. Ray at Polyintell as part of a collaborative project. The results were published as an article in Analytical Bioanalytical Chemistry, doi.org/10.1007/s00216-015-9296-8

*This Thesis is dedicated to my wonderful family:*
*Mamma, Papà, Graziano and Anne.*

*Love you from the bottom of my heart.*

# Abstract

Recent advances in the area of nanotechnology have led to interesting applications of nanomaterials in medicine, especially in the areas of imaging and treatment. This thesis presents the development of two molecularly imprinted polymers (MIPs) based on the same fluorescent functional monomer. One MIP, prepared in the bulk format, is investigated for its ability to detect tamoxifen and its metabolites. The other MIP synthesised in the nanogel format, holds the potential to be used as pH-responsive drug delivery system.

Four objectives were identified within this project. The first was the design and synthesis of fluorescent functional monomer. Two coumarin derivatives carrying a polymerisable unit, for covalent bonding within the polymer, and a carboxylic moiety, for interaction site with the template, were synthesised and characterised. However, only one of them (the VCC: 6-vynilcoumarin-4-carboxylic acid) showed high fluorescent yield and was selected as functional monomer. The second objective involved the development of a detection system based on bulk MIP containing the VCC fluorescent monomer. This system proved effective in generating a detectable signal upon binding the analytes. The signal was observed as a quenching of the polymer fluorescence and it was proportional to the amount of target molecules detected. The third objective was the preparation of tamoxifen-imprinted nanogels for potential application in the drug delivery field. The optimisation of the procedure gave a set of NIP/MIP with the desired solubility, particle size and fluorescence emission. These nanogels were then employed in the last objective, which involved the toxicity study and evaluation of the drug loading on of transgenic line of zebrafish. The nanogels were non-toxic at the tested concentrations and the presence of tamoxifen was confirmed.

# Acknowledgements

The very first person I would like to thank is my supervisor Prof. Marina Resmini. Her continuous support, teaching, advice and her incredible patience have been precious to me during the last 4 years. She also gave me the opportunity to participate in some of the international meetings within the European network NANODRUG. That was a great experience during which I could meet amazing people and brilliant scientists.

My thanks and appreciation also goes to Dr. Caroline Brennan for her valuable help and support in the experiments involving the zebrafish. I would like to thank Ari and Luca for helping me over the years. Special thanks go to Judit for her time and for sharing her skills in imaging with me. Especially I am very grateful to Alistair for too many different reasons, but in particular for his constant encouragement and unconditional support.

I would also like to thank all the amazing people I was lucky enough to meet during my time at QMUL. From the people in the early days who offered a warm welcome to me and made me feel part of a new community, to the present members. Thanks especially to Martina, Jacopo, Giuseppe, Nolwenn, Sandra, Mark and John for unwinding together and for the usual Friday nights. Many thanks go to David and Indigo for being so supportive and friendly during my short working experience as teaching laboratory assistant. I could not thank enough Jay, Agha, Simona and all the technical and academic staff in the JP building for their help, kindness, stimulating chats and friendship.

The Resmini's group members deserve more than a simple thank you. They were not only colleagues but also good friends, with whom I shared joys and sorrows. Giorgio and Gabriele were the pillars of my PhD experience, both in the lab and outside; it would not have been the same without them. Yolanda, Katarzyna, and the present members Luca, Angelo, Rosemary, Charlie and Fei are all thanked for their advice and making the days in the lab even more enjoyable.

Thanks to Jess and Marzia for the incredible fun time spent together in the first years and keep on being present for each other.

Many thanks go to Sergio for his 10-years long encouragement and motivation.

Lastly, I am really grateful to Paolo and Lollo, who showed me that friendship could become even stronger when far apart. Thanks for the long-distance support, for travelling with and taking the time to come and visit.

# Abbreviations

°C = Celsius degree

$^{13}C$ = carbon, isotope 13 in NMR

$^{1}H$ = proton in NMR

4-OHT = 4-Hydroxytamoxifen

ACN = acetonitrile

AIBN = azobisisobutyronitrile

CLO = clomiphene

$C_M$ = monomer concentration

COSY = correlation Spectroscopy

DCM = dichloromethane

DDS = drug delivery system

DLS = dynamic light scattering

DMF = dimethylformamide

DMSO = dimethylsulfoxide

dpf = days post fertilisation

EBA = N,N' - ethylenebis(acrylamide)

eq = equivalents

EtOAc = ethyl Acetate

FM = functional monomer

FM-PX = nanogels formulations, where X is the number of the preparation

GC-MS = gas chromatography-mass spectrometry

HCl = hydrochloric acid

hpf = hours post fertilisation

HPLC = high Performance Liquid Chromatography

$J_{H-H}$ = vicinal proton coupling constant

KDa = kilo Dalton

LC-MS = liquid chromatography-mass spectrometry

MBA = N,N'-methylenebis(acrylamide)

MeOH = methanol

MIP = molecularly imprinted polymer

mmol = millimoles

mol = moles

$N_2$ = nitrogen gas

$NaHCO_3$ = sodium bicarbonate

NIP = non-imprinted polymer

NIPAM = N-isopropylacrylamide

nm = nanomoles

NMR = nuclear magnetic resonance

NP = nanoparticle

PBS = phosphate buffer solution

PFA = paraformaldehyde

ppm = parts per million

QDs = quantum dots

$R_f$ = retention factor

SPE = solid-phase extraction

T = template

TAM = tamoxifen

TCA = 7- acrylamidecoumarin-4-trifluoromethyl

TLC = thin layer chromatography

THF = tetrahydrofuran

UV-Vis = ultraviolet-visible radiation

v/v = volume/volume

VCC = 6-vynilcoumarin-4-carboxylic acid

w/v = weight/volume

XL = cross-linker

$\lambda$ = wavelength

$\lambda_{exc}$ or $\lambda_{em}$ = excitation/emission wavelength

$\mu$M = micromolar

Table of Content

# Chapter 1

## Introduction

# 1. Introduction

## 1.1. Nanomaterials in medicine

Nanotechnology is the branch of technology that studies materials with length size between 1-100nm, defined as "nanomaterials".[1] Nanotechnology is currently in its most flourishing period and it is considered one of the most innovative and cutting-edge fields of science. The spotlight is on nanomaterials and their unique features, which are very different from the bulk systems due to their small size.[2] Nanomaterials and their applications have revolutionised a wide range of fields including physics, chemistry, engineering and medicine.[3] In particular, nanomaterials applied in medicine have seen a rapid growth in the last few decades, covering a multitude of different areas. For example, nanomaterials can be engineered in order to enhance tissue repair and enable the body to heal itself, thus being largely useful in regenerative medicine.[4-6]

Nanomaterials are also used to a great extent in diagnostic imaging, contributing to an increase in the resolution and sensitivity compared to traditional techniques (i.e. magnetic resonance imaging, ultra-sounds, positron-emission tomography).[7] Furthermore, nanosystems play an important part in the study of human biochemical processes *in vivo*, allowing an early detection of disease and the monitoring of their different stages.[8-10]

Nanosized materials find application also in immunotherapy, which is a cancer treatment aiming to improve the natural defence of the body and activating its immune response. Nanoparticles were successfully used to develop an antigen-capturing system, which demonstrated an enhanced response rate of the therapy and improved the efficacy of the treatment.[11]

Although nanomaterials have many medical applications, there two areas that have particularly benefitted from the development of such materials: sensing [12] and smart delivery systems. [13] Therapeutic drugs monitoring (TDM) is one of the many interesting use of nanomaterials in sensing. [14] TDM involves the active evaluation of the drug concentration in patients' organic fluids to assess the pharmacokinetics of the administrated drug. Amongst a number of advantages, TDM implements a personalised medicine approach, which is tailored to meet the different needs of each patients, adjusting the dosage of the therapy or intervening medically if required.

Molecular recognition, in terms of specificity and high binding ability is the key requirement for the successful application of nanomaterials in medicine. Amongst the different approaches utilised for the generation of high molecular recognition, molecular imprinting has attracted a large volume of research, as evidenced by the number of publications in the literature on this topic, with more than 1500 papers published over the last two years. [15]

## 1.2. Molecular imprinting approach

Molecular imprinting is a particularly useful process for developing materials with high recognition properties and selectivity. Using a template-casting technique the functional monomers interact with the template molecule, forming a pre-polymerisation complex. The polymerisation then occurs in the presence of the initiator and the cross-linker. The polymers obtained with this procedure are called molecularly imprinted polymers (MIPs). When the template is removed, 3D cavities, complementary in shape and functionalities to the template, are left in the matrix (figure 1.1) and are able to selectively recognise and rebind the target analyte. [16]

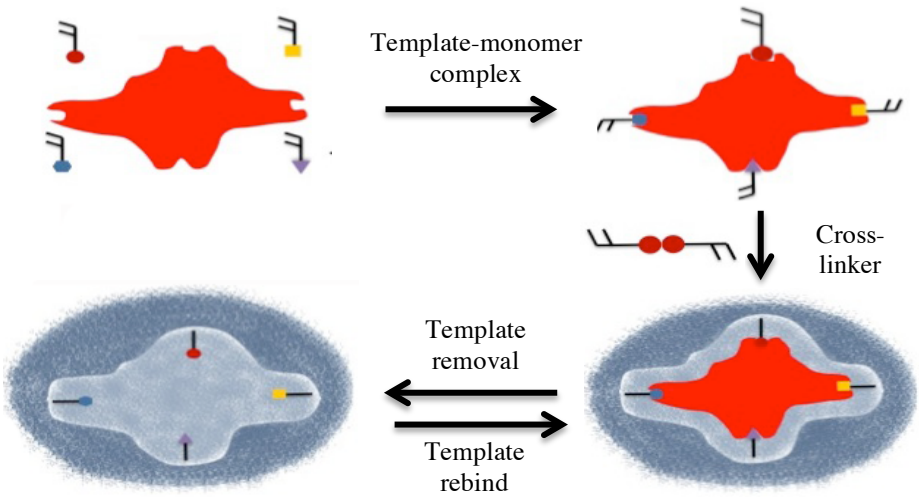


**Figure 1.1.** Representation of the molecular imprinting process. It starts with the formation of a pre-polymerisation template-monomer complex, which polymerises in the presence of cross-linker and initiator. The cavities can then rebind the template.

Three main approaches to successful imprinting have been investigated over the years, namely covalent, non-covalent and semi-covalent. [17] These relate to the different type of interactions taking place between the template (T) and functional monomer (FM) and are often chosen according to the application of the MIPs. In the first approach, covalent bonds occur between the functional monomer and the template before the polymerisation process. Although the polymer, produced with this process, is more stable and has exact stoichiometry between FM and T, it has slow kinetics, both in the formation and in the cleavage of the bond. Therefore, the reversibility of the system is limited as well as its applications, especially when fast equilibrium is required. In the non-covalent approach the interactions between the FM and the T occur through non-covalent bonds, namely hydrogen bonding or electrostatic interactions. This way the template extraction and the equilibration are favourite and more rapid. However, the ability of template re-uptake is limited, as 85% of the cavities shrink and loose their selectivity. [18] Whereas, the semi-covalent approach involves the formation of covalent bonds before the polymerisation process and the formation of non-covalent bonds when

the polymer re-binds the analyte. This procedure combines the high stability of the covalent interaction between the FM and T with the reversibility and rapid equilibration of the non-covalent interactions. Due to the different interactions involved, every approach requires a specific ratio of T to FM in order to ensure the best results of imprinting in the final polymer. Typically, the ratio used in covalent and semi-covalent approaches is 1:1 or 1:2 T to FM. The non-covalent procedure requires higher ratios, typically 1:4 - 1:8, to push the equilibrium towards the formation of the complex, though there is a substantial risk to form non-specific binding sites. Nevertheless, the appropriate ratio depends on the complexity of the template and the affinity between the functional monomer and the template. Another option is the stoichiometric/non-covalent interactions, which is achieved when the pre-polymerisation complex is strong enough and involves high association constants. [18] This way it is possible to combine the fast rebinding kinetics, characteristic of the non-covalent/non-stoichiometric procedure, with the high stability and accessibility of the cavities, typical of the covalent approach, without the aforementioned disadvantages involved in the two procedures. Therefore, the key step to having polymers with high selectivity is to use strong and defined interactions in the pre-polymerisable complex.

Literature offers many examples of the range of applications of MIPs. [19,20] In particular, the use of MIPs as sensor [21,22] and drug delivery system [23] has seen a significant growth in the last few years. For instance, MIPs were used to replace the antibodies in ELISA tests (enzyme-linked immunosorbent assay) to overcome the disadvantages of using antibodies, such as the related high costs and poor stability. [24] The assay employing MIP nanoparticles showed lower detection limit than the ELISA equivalent, detecting the analyte in real samples with mean accuracy of 98%. Moreover, such device was stable

to high temperature overtime and also versatile, as it was employed for detection of a variety of analytes, including drugs and toxins.

Ton *et al*. reported another noteworthy example of MIP used as sensor for herbicides and mycotoxins. [25] The group developed a disposable evanescent wave fibre optic sensor in which the polystyrene waveguide was coated with MIP, specific for the selected analytes. The MIPs were also equipped with a fluorophore that provided fluorescence enhancement upon binding of the analytes. Such sensors showed detection of analytes in the order of nM or μM, and were proposed as screening tools for fast and on-site monitoring of herbicides and mycotoxins in environmental or food samples.

In the literature there are also very good reports on the applications of MIP in drug delivery. [26] For example the use of MIPs for ocular delivery is a very fascinating one. MIPs contributed to overcome issues linked to the ocular protective mechanisms and high lachrymal turnover, which reduces the bioavailability of the already available ophthalmic medications. Imprinted hydrogels have been developed for uses as soft contact lenses that offer a sustained drug release. [27] Such MIPs, characterised by a low content of cross-linker in order to ensure transparency and flexibility to the system, have the potential to improve the treatments of ocular diseases enhancing the efficacy and efficiency of the lenses.

### 1.2.1. Format of molecularly imprinted polymers

Molecularly imprinted polymers can be prepared in a variety of formats that provide different characteristics and properties of the matrices. The choice of format and method of preparation, therefore, is strongly dependent on the final applications of the MIPs. Common formats are nano- or micro-beads, thin films, membranes, gels or bulk polymers, all of which can be obtained by controlling different parameters. [28]

Chronologically, the first format of MIP ever proposed was in the format of bulk polymer. In his first work on molecular imprinting published in 1973, Wulff describes the formation of an imprinted organic bulk polymer able to separate a racemic mixture.[29] Within the following 10 years after Wulff's first paper, the number of groups who contributed to the innovation of this field grew considerably. In 1978 Shea and Thompson published their first work in which the two presented a bulk polymer able to achieve stereo-specific reactions. [30] In 1997 Damen and Neckers developed a highly cross-linked styrene-divinylbenzene copolymer prepared in the bulk format, which was able to recognize stereoisomers. [31] Mosbach's group gave great impact to MIP synthesis and application when, in 1981, they introduced molecular imprinting in synthetic bulk MIP with non-covalent interactions. [32]

The bulk preparation consists on the synthesis of a polymer monolith, which is then crushed and grounded, following by sieving of the particles into the desired size ranges. The preparation of bulk polymers is time-consuming and more than 50% of the polymer is wasted in the process of grinding and sieving, however this method is the most straightforward and widely used. [33, 34] Bulk polymerization requires fewer optimization steps compared to other methods, it is fast and simple to set up and the resulting monoliths are easy to handle. [20, 35] Bulk polymers are still the most preferred matrices for sensing applications. In 2016, Hu *et al*. presented a sensor based on bulk MIP integrated with silver nanoparticles. The sensor was able to specifically separate and detects trace level of melamine in tap water and milk samples in 18 min and 25 min, respectively. [36] A few months later Ji *et al*. published a study, which described the synthesis of molecularly imprinted polymers for the recognition of glycosides in aqueous media characterized by excellent hydrophilicity. [37]

Another common format for imprinted polymers is nanogels. Nanogels are defined as intra-molecularly cross-linked polymeric particles, which are able to swell or aggregate according to the solvent used. Nanogels form three-dimensional network in which at least one dimension is in the nanometre size (between 1 and 100nm).[38] These materials combine the advantages of the polymeric nanoparticles, such as physical stability, and ease of surface modification,[39] together with the typical features of the hydrogels of swelling, biocompatibility and low surface tension.[40] Such characteristics have attracted considerable interest towards the use of nanogels and their applications have covered a large variety of topics, from imaging,[41 41b] to sensing[42 43] and also coating.[44] Nanogels pose also as very promising drug delivery systems (DDS). In fact, some of their features are compatible with those of the ideal DDS such as: high loading capacities of the swollen network without involving chemical reactions, thus reducing the amount of carrier required and protecting the drug activity; ease control of the particle size in order to obtain nanogels small enough to be able to reach the small capillary vessels and penetrate the tissues; and the possibility to acquire a controlled and sustained release of the therapeutic at the target site.[45] Nanogels have been employed as DDS *in vivo* and in human clinical trial since the early 2000s, showing encouraging results. Shimizu *et al*. applied cholesterol-bearing pullulan (CHP)-based nanogels to administration *in vivo* of anti-cancer interleukin-12 (IL-12), using murine model. Preliminary studies *in vivo* demonstrated that, although the IL-12 resulted in a complete remission of the cancer, it showed systemic toxicity and short half-life. Nevertheless, the incorporation of recombinant IL-12 within CHP nanogels allowed the administration of the drug in a reduced dose so to minimise its toxic effect, while obtaining a suppression of the tumour growth in the animal.[46] CHP nanogels were also used to load antigens and prepare a CHP-HER2 vaccine, which was used in a phase I clinical trial to assess the

safety of the vaccine and HER2-specific T-cell immune responses. Following the treatments, the only adverse event showed by the patients was a mild skin irritation at the site of vaccine injection. The vaccine was deemed to be safe and HER2-specific immune responses of T-cells, as well as antibody production, were detected. [47, 48] Nukolova *et al*. presented another interesting work that highlighted the use of nanogels as promising DDS towards ovarian carcinoma. [49] The nanogels were conjugated to folic acid (FA), a targeting moiety capable of specific interaction with folate receptor, which is overexpressed in ovary cancer cells. This system showed very good anti-cancer drug uploading and cellular uptake. The DDS proved to inhibit the tumour growth and exhibited lower toxicity (i.e. body weight loss) compared to the free drug. Moreover, the bio-conjugation with the FA allowed the release of the drug only in the cancer cells, reducing eventual side effects connected to the drug accumulation in healthy tissues.

In the context of this project there was the desire to contribute to study the potential of the molecular imprinting approach for the development of polymers to be used as sensing unit for a specific drug as well as drug delivery system. In particular it was decided to use the same target drug, Tamoxifen, for both applications given its importance and wide use in the clinics. The choice of drug was a very important one, as it determined the type of monomers that could be used.

## 1.3. Tamoxifen as model drug

Tamoxifen (figure 1.2) is a British discovery. It was first synthesised in 1966 by researchers at Imperial Chemical Industries, but was only licensed for the treatment of breast cancer in the early 1980s, becoming one of the very successful drugs in the history of medical oncology.

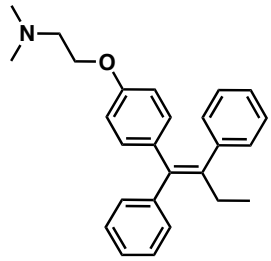

**Figure 1.2.** Molecular structure of tamoxifen.

Drugs such as tamoxifen belong to a class of compounds known as SERMs (selective oestrogen receptor modulators), acting as oestrogen agonist or antagonist depending on the target tissues. Tamoxifen has an oestrogen antagonist effect on breast tissues, but it also exhibits an oestrogen-like action on bones and uterus tissue. [50] Tamoxifen is a widely used anticancer drug, both in prevention and in the treatment of all stages of breast cancer. 80% of the breast cancer is oestrogen receptors positive, in other words the growth of the tumour is promoted by signals received from oestrogens. The antagonistic effect of TAM on oestrogen receptors in breast tissues involves preventing oestrogen from exerting its normal effect, thus inhibiting the proliferation of breast cells and hence the propagation of the tumour. [51] Tamoxifen has also an effect on bones and endometrium, as agonist for oestrogen receptors located in these tissues. On one side TAM helps to preserve the density in the bones, [52] on the other tamoxifen-treated patients have a small risk (2 per 1000 women per year) of low-grade endometrial cancer insurgence. However, the benefits of tamoxifen in breast cancer treatment outweigh the risk associated with endometrial tumour. [53]

Interestingly, as a result of its anti-oestrogenic activity in breast tissues, tamoxifen is also largely abused by bodybuilders and athletes to mask the side effects of doping with anabolic androgenic steroids (AAS). AAS aromatise during the metabolism, forming oestrogens, which cause the development of breast tissues in man (*gynecomastia*).

Tamoxifen is, therefore, used in conjunction with AAS as it binds the oestrogen receptors, stopping *gynecomastia*. For this inappropriate use, the World Anti-doping Authority (WADA) and the International Olympic Committee (IOC) banned tamoxifen in sports and competitions. [54, 55]

Tamoxifen is extensively metabolised after oral administration. The metabolism of this drug is mediated by the hepatic cytochrome P450 (P450), which is a family of enzymes responsible for the biotransformation of many potentially toxic compound. [56] Two main routes of metabolism have been identified: 4-hydroxylation and N-demethylation, which give hydroxylated and demethylated metabolites, respectively. 4-hydroxytamoxifen (4-OHT) and N-desmethyltamoxifen are the main metabolites of these two pathways. The latter metabolite is further transformed into into 4-hydroxy-N-desmethyltamoxifen, also known as endoxifen (figure 1.3).

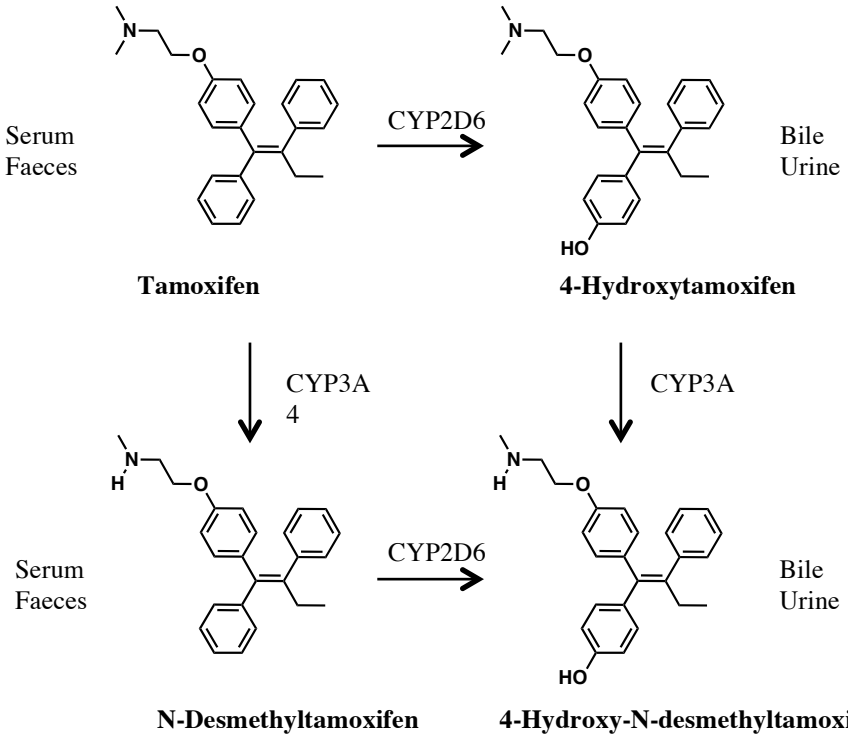


**Figure1.3.** Structure of tamoxifen and its primary metabolites. The relevant cytochromes responsible for each bio-transformation are also indicated, together with the organic fluid in which each metabolite is mainly excreted.

Each metabolite shows a specific binding affinity for the oestrogen receptors. In particular it was found that 4-OHT and endoxifen are the major active metabolites in tamoxifen treatment. Both metabolites exhibit a higher anti-oestrogenic activity than TAM or other studied metabolites, however the concentration in plasma of endoxifen is higher than 4-OHT. [57] The concentration of metabolites in the serum is different in each individual and it influences the efficacy of the drug. The polymorphic of the enzymes responsible for tamoxifen metabolism, together with potential additional contributors, not yet fully understood, are responsible for such difference in concentration. [58]

There are two major issues related to the use of tamoxifen. On one hand, although tamoxifen is pharmacologically important, it suffers from low solubility and bioavailability, together with poor selectivity towards the affected area. This involves significant side effects for the patients' health, such as a higher risk to have uterine cancer and venous thromboembolism. [59] The development of a delivery vehicle could contribute to increase the bioavailability of the drug and target only the malignant tissues, thus reducing the side effects. More details will be given in section 1.3.2.

On the other hand, the detection and quantification of tamoxifen and its metabolites remains a challenging problem that has attracted a variety of approaches. The development of a fast, easy and reliable sensor, which does not involve complex instruments, for the evaluation of tamoxifen and/or its metabolites in urine or serum would have a large impact on many aspects. It would help fighting the illicit use of tamoxifen, and, in case of breast cancer, it would provide an instrument for monitoring the response of the tumour to tamoxifen and the treatment status. In the next section the key findings and the state of the art for the detection of tamoxifen will be given.

### 1.3.1. Detection and quantification of tamoxifen and metabolites

Since the late 1970s, when tamoxifen became one of the most successful drugs in the treatment of breast cancer, multiple resources and funds have been committed to the identification, detection and quantification of the drug or its metabolites in plasma, serum and bile. One of the first examples in literature is from 1979. Daniel *et al*. reported the detection of tamoxifen and one of its hydroxylated metabolites in plasma samples obtained from patients treated with tamoxifen. [60] The samples were extracted with organic solvent and purified by ion-exchange chromatography. The samples were then analysed by gas chromatography coupled with mass spectrometry (GC-MS) and quantified by means of a standard curve.

In the early 1980s Kemp *et al*. reported another interesting work on the identification and quantification of tamoxifen and metabolites using GC-MS. [61] The group reported a method based on thin-layer densitometry as a technique to separate N-desmethyltamoxifen, N-desdimethyltamoxifen and tamoxifen's primary alcohol, which structures are shown in figure 1.4.

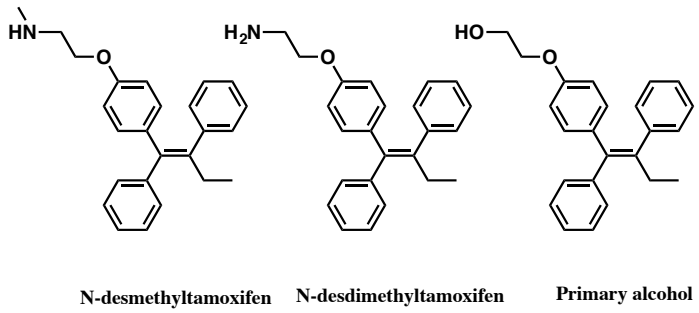


**Figure 1.4.** Chemical structures of tamoxifen metabolites investigated in Kemp's work [61]

Serum samples were obtained from patients who had received 100 mg b.d (twice a day) of Nolvadex® (tamoxifen citrate). The three metabolites were extracted from serum at different pH using an organic solvent and separated on thin-layer chromatography. The plate was then irradiated with a source of ultra-violet light in order to convert the non-

fluorescent metabolites containing the triphenylethylene group into highly fluorescent phenanthrene derivatives (figure 1.5). The quantification was then carried out employing densitometry.

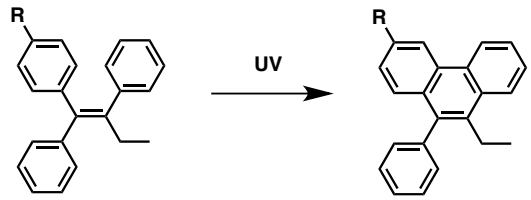


**Figure 1.5.** Photoreaction of tamoxifen and metabolites. By UV irradiation the molecules containing triphenylethylene moiety are converted into phenantrene derivatives, which are high fluorescent

The authors identified the metabolites using three independent methods: 1) by assessment of their extractability under different pH conditions; 2) by comparison of the retention factor (Rf) of the extracted compounds with the Rf of the synthesised ones; 3) by using gas chromatography coupled with mass spectrometer (GC-MS) and analysis of the fragmentation pattern.

Although GC-MS is characterised by high-resolution power and sensitivity, it requires complicated samples preparation prior the analysis. The biologic samples need to be treated to separate the analytes from the matrix or background material, as described in the previous example. [61] A far more convenient method is based on high performance liquid chromatography (HPLC).

Golander *et al*. [62] and Stevenson *et al*. [63] presented interesting methods of identification and quantification of tamoxifen and its metabolites that involved HPLC coupled with fluorimeter. After photochemical reaction induced by UV-light source, as showed in figure 1.5, the reaction mixture was separated onto HPLC columns. The analytes were quantified as photoreaction products, by measuring the peak area and comparing it with a standard curve. In these examples the technique employed was “off-line”, as the photoreaction was carried out before the chromatographic separation. However, the

phenantrene derivatives produced during the irradiation of the sample was subject to photodegradation over time, which led to complex chromatograms and poorer resolution. In order to overcome the disadvantages caused by the off-line approach, the photoreaction was introduced after chromatographic separation. This new procedure took the name of "on-line" approach, in which the UV-absorbing materials were separated from the compounds of interest before irradiation. This way the risk of fluorescence quenching or photochemical side products was minimised. The on-line procedure was, therefore, more reproducible and sensitive than the off-line photoconversion. In the "on-line" approach the photoreaction was coupled into a HPLC system. After the separation, the elute was illuminated by a UV-light source before passing through the fluorescent detector. An example of this approach was given by Nieder *et al*. who focused on the optimisation of a method for detection of tamoxifen and N-desmethyltamoxifen in plasma. [64] A few years later Kikuta *et al*. used the same approach for the detection of tamoxifen, N-desmethyltamoxifen and 4-hydroxytamoxifen. [65] However, the authors introduced innovation to the preparation of the sample and in the photoconversion. Plasma samples were treated with HCl and centrifuged to remove solid material. The pre-column was conditioned with methanol-water-HCl, the supernatant was then loaded onto the pre-column, which was washed with water before switching into HPLC stream (figure 1.6). The authors introduced a newly designed photoreactor with a 3D configuration, which allowed a faster and more efficient conversion of the analytes in the fluorescent products. The resulted system was characterised by high selectivity and specificity of separation and detection. Moreover, results showed sensitivity for tamoxifen and metabolites in plasma samples down to subnanogram levels.


**Figure 1.6.** Schematic representation of Kikuta detection system.

Lien *et al*. picked up on the same path of Kikuta and developed a fully automated assay able to detect the tamoxifen and four metabolites in human serum. [66] The sample preparation consisted in only one step, deproteinisation of the serum and its centrifugation to remove the precipitated protein. The supernatant was then injected into a small pre-column and equilibrated in order to concentrate the analytes. An automated column-switching valve allows the direction of the flow from the pre-column to the reversed-phase analytical column after which the cyclisation occurred *via* UV irradiation, converting the analytes in phenantrene derivatives to be detected. The in-column concentration of the sample increased the sensitivity and reproducibility of the whole system. This fully automated assay was characterized by simple sample processing, high recovery of analytes, precision, and simultaneous quantification of the parent drug and four serum metabolites. One year later the group applied the same method to human bile samples. [67] Results showed the presence of a new peak, not present in serum samples, which was identified as 4-hydroxy-N-desmethyltamoxifen, also known as endoxifen (figure 1.7).

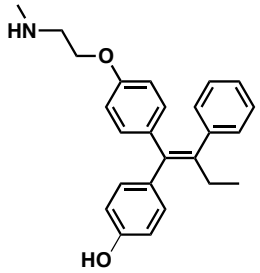


**Figure 1.7.** 4-hydroxy-N-desmethyltamoxifen, metabolite found in bile samples.

An alternative to on-line in-column pre-concentration of the analytes with no sample treatment was possible in the 90's with the development of solid-phase extraction systems (SPE). The extraction of the analytes from complex biological matrices such as plasma[68] and urine[69] became fast, noise-free and easy with the SPE. Although the extraction efficiency obtained with the on-line extraction were higher that that observed with SPE, this technique overcome the time-consuming organic extraction of samples and the use of complicated pre-column and column-switching valves. McCullum *et al*. demonstrated that the levels of tamoxifen and N-desmethyltamoxifen detected in plasma using SPE for extraction and HPLC assay for separation and detection of the analytes were similar to those obtained with previous methods with same detection limits.[68] With the development of the SPE, which make the extraction fast and easy, also GC-MS became a viable alternative to the HPLC. [69, 70]

As described in section 1.2, molecularly imprinted polymers provide high selectivity and affinity for the target analyte. MIPs, therefore, represent the perfect sorbent materials for SPE, which allows to selectively isolating biological analytes from complex matrices. MIP-SPE have successfully been used for the specific extraction of tamoxifen followed by quantification *via* HPLC. [71-73]

In the last few years MIPs have also found application in the development of sensor for the detection and quantification of tamoxifen and its metabolites. In 2005 Nie *et al*. developed a new material in which MIPs, packed into a column, provided the recognition material to a system based on chemiluminescence. [74] The group found that the reaction of tamoxifen with Mn (IV) produced a detectable chemiluminescence signal. However, other substances in the samples could react in the same way with Mn (IV), producing the same signal. In order to introduce selectivity towards tamoxifen, the sample solution was pumped through the MIP column specific for the drug. A solution

of Mn (IV) was then pumped in the column in which it reacted with tamoxifen, incorporated within the MIP matrix, producing the signal. Such system was successfully used to determine the drug in urine collected from breast cancer patients treated with tamoxifen, obtaining good analytical parameters and low detection limit. Another recent example of MIP employed in the detection of tamoxifen was reported by Yarman *et* al.[75] The group developed an electrochemical MIP sensor in the format of film in which the detection of the drug was achieved by an indirect method. The binding event of tamoxifen on the MIP film caused the suppression of the signal produced by the reduction of the ferricyanide redox probe. The sensor proved a fast rebinding of the analyte and a linear range from 1 to 100 nM, reaching saturation above it.

Although different methods for the detection and quantification of tamoxifen and its metabolites have been suggested, the reviewed methodologies depend on complex instrumentation, which involve trained staff and high cost. Nevertheless, the use of MIP opens new opportunities for the development of a new range of sensors, which could provide fast and reliable analysis. In relation to tamoxifen, in addition to the detection of the drug, its delivery by means of nanomaterials has also attracted interesting studies, which are summarised and discussed in the next section.

### 1.3.2. Drug delivery systems for tamoxifen

Drug delivery systems (DDS) are specialised devices used for the delivery of therapeutics, allowing improvement of the selectivity, effectiveness and safety of drug administration. The ideal drug delivery system should be able to transport the active substance in the affected area and release the drug in a controlled and sustained manner. By using DDS it is possible to increase the stability and bioavailability of drugs otherwise having poor solubility in water and thus limited administration. The increased

bioavailability also allows a reduction of the overall dosage and frequency of administration of the therapeutics in question. This way the adverse effects caused by higher dosage and accumulation of the drug in areas of the body other than the affected one are reduced. [76] The routes of drug administration are mainly divided in enteral, parenteral and topical, among others. Each one of the administration routes, with its advantages and disadvantages, affects the drug metabolism and clearance therefore influencing its dosage. In other words, the total amount of drug that arrives at the target area of action is largely dependent on how the medication is administrated in the body.[77] All the routes of administration need to face the problem of the lack of bioavailability of the drugs. The bioavailability is influenced by several factors such as the first-pass metabolism, the solubility of the drug and its chemical instability to acidic pH of the stomach. One possible way to overcome these issues it to apply nanotechnology to drug delivery. Nanomaterials, characterised by their size in the order of nanometres and their large surface-to-volume ratio, can be modulated in order to protect the drugs from metabolising enzymes. Nanoformulation can also improve the hydrophilicity of the drugs *via* conjugation or encapsulation within nano-vehicles, providing an increased deliverability of such drugs. Moreover, nanomaterials can influence the chemical stability of the medication, protecting it from harsh conditions. Nanomaterials can also be designed in such a way to be attracted to diseased cells and activated to release therapeutic in response to a trigger, thus allowing direct treatment of those cells sparing the healthy ones and reducing the potential accumulation off-target. [78] Nanomaterials, therefore, contribute to increase the bioavailability of the drugs, resulting in an extended blood circulation time, and deliver the therapeutics specifically in the affected area.

When a medication is administered in the body, regardless of the route of administration, several barriers need to be crossed before the therapeutic substances reach the site of

action, and only a small portion of the drug reaches the targeted organs. [79] The use of nanomaterials as drug carriers was shown to assist the drugs in traveling across these barriers. However, only particles with size < 200nm are considered suitable for drug delivery applications. The recent progress in the field of nanotechnology positively influenced the development of drug delivery systems, moving from macro- to nano-sized drug vehicles. [80, 81] Nanomaterials can penetrate even small capillaries, with 5–6 μm in diameter, and are characterised by higher intracellular uptake, compared to microparticles, which allows efficient drug accumulation at the target sites in the body.[82,83] As shown by Desai *et al*. in their study carried out on adult rats, 100 nm particles were able to penetrate the submucosal layer while larger microparticle were concentrated in the epithelium. [84] As aforementioned, nanomaterials have a high surface-to-volume ratio, which implies that a significant amount of material can be loaded in the network maintaining the stability of the material. Moreover, the large surface can be functionalised and modified in order to generate conjugation with biomolecules, making the nanomaterials more reactive compared to larger molecules or bulk counterparts. The high surface area can also improve the water solubility and the bioavailability of such nanomaterials. [85] However, being able to cross the barriers and deliver the therapeutics in the targeted region in a controlled release rate, are not the only challenges that are faced during the development of a DDS. The ideal DDS should have the capability to transport the therapeutics without any loss before reaching the targeted location. The release of the drug is required at the most appropriate time and dose only upon reaching the affected area. Any release of the medication in areas other than the targets could have toxic effects and serious side effects for the patients. Four different mechanisms of drug release have been identified: diffusion-controlled, swelling-controlled, erosion-controlled and stimuli-controlled release (figure 1.8).[86]

| **Diffusion Controlled** | **Swelling Controlled** | **Erosion Controlled** | **Stimuli Controlled** |
|---|---|---|---|
| – Drug release controlled by diffusion down a concentration gradient | – Drug release controlled by degree of swelling, the drug diffuse out when the $H_2O$ penetrate in the matrix | – Drug release controlled by the physical or chemical degradation of the polymer | – Drug release controlled by external stimuli, which trigger a change in the system |

**Figure 1. 8.** Representation of the different possible mechanisms of drug release

In the last two decades drug delivery nanosystems with stimuli-responsive features have been largely studied and reviewed. [87-89] Such systems respond to environmental stimuli, which trigger a physicochemical change of the nanocarriers, thus promoting the release of the medication. Such triggers could be external (e.g. electric field, ultrasound, magnetic field) or internal (e.g. difference in pH, temperature, and ionic environment). Literature data suggest that polymeric nanoparticles have lately attracted much interest as drug delivery vehicle[90] due to their high physical stability, biocompatibility, ease of surface modification, biodegradability, just to cite some of their characteristics. [39] Different formats have been studied and developed such as polymeric micelles, [91] dendrimers[92] and coated nanoparticles[93, 94] among others. In particular, the number of nanomaterials developed as vehicles for the delivery of tamoxifen, considerably increased during the last decade. As mentioned in section 1.3, tamoxifen suffers from poor hydrophilicity and low bioavailability together with scarce specificity and insurgence of side effects, such as increased risk of endometrium tumour and thromboembolic events. Such issues could be overcome with the aid of nano-DDS. Very recently, $C_{60}$-fullerenes have been used for delivery of N-desmethyltamoxifen, one of tamoxifen metabolites, to cancer sites in a controlled and sustained manner. [95] Promising results showed that this system was internalised by cancer cells in which it

exhibited enhanced cytotoxicity. The nanostructure also improved the bioavailability of the drug and modified its pharmacokinetic profile decreasing its clearance time, therefore requiring smaller doses.

Other recent examples of nanocarriers of tamoxifen include the development of biocompatible micelles based on natural compounds as polyunsaturated fatty acid (i.e. peanut oil, corn oil, sesame oil, soya bean oil, sunflower oil) with self-nanoemulsifying properties. [96] The nanosystem demonstrated to have good cellular uptake compared to the control system or to a tamoxifen suspension, in fact the steady concentration of tamoxifen in plasma increase of 5.6 fold when the nanoemulsion was used. Also, the permeability of the drug increased due to the effect of the nanosystem. Furthermore, the nanoemulsion improved the anti-cancer activity of the drug, reducing the size of the induced breast tumour in female rats after repetitive oral dose of the nanosystem for thirty days.

Thakur *et al*.[97] incorporated tamoxifen into polymeric micelles based on the biodegradable poly (lactic-co-glycolic) acid (PGA) and on the non-toxic polysaccharide chitosan. Such chitosan-PGA micelles exhibited good drug release at the cancer cell pH and also high drug loading and good uptake by cancer cells with resulting enhancement of cytotoxicity.

Magnetic nanoparticles, functionalised with PEG (polyethylene glycol) have also been applied for tamoxifen, obtaining good levels of drug loading within the system, increased cytotoxicity of cancer cells and bioavailability of tamoxifen. [98]

The monitoring of the drug delivery systems, both *in vivo* and *in vitro*, is a key requirement to obtain information regarding the safety and efficacy of the nanosystem, prior to start human clinical trials. Although a variety of approaches (i.e. magnetic resonance imaging, computed tomography, positron emission tomography, optical

imaging or ultrasound) are conventionally utilised for imaging, fluorescence spectroscopy has recently attracted much attention. [99] In fact, the above-mentioned nanocarriers, developed for the delivery of tamoxifen, were all conjugated with fluorescent tags in order to allow an easy tracking of the nanomaterials.

In the next section the basics of fluorescence spectroscopy, together with its advantages in imaging and the different available fluorophores will be described.

## 1.4. Fluorescence

Fluorescence occurs when a particular fluorescent molecule, also called a fluorophore, emits light after previous absorption. [100] The fluorescence process is therefore divided in two steps: the absorption (excitation) and the emission of light (figure 1.9). During the excitation step, an electron of a fluorescent molecule exposed to UV light absorbs a photon of energy, which results in the formation of an unstable excited electronic state ($\mathbf{S}_1$). The lifetime of the excited state is in the order of a few nanoseconds, during this time the molecule relaxes towards the lowest vibrational energy level ($\mathbf{S}_1^0$) within the electronic excited state via non-radiative transition, dissipating the energy as heat to the solvent. The fluorescence originates when a photon is emitted during the relaxation of the electron back towards the ground state ($\mathbf{S}_0$).

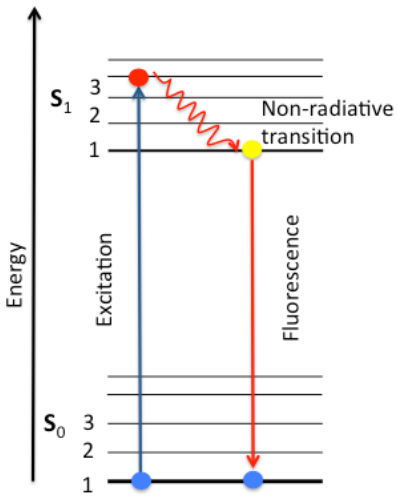


**Figure 1.9.** Representation of Jablonski diagram in which the electronic states and the transition of the electrons are illustrated. The electron is excited to $\mathbf{S}_1$ level after absorption of a photon; the electron then quickly relaxes to the lower level of the excited state by non-radiative transition. The further relaxation back to $\mathbf{S}_0$ occurs with emission of a photon generating the fluorescence

As the energy acquired during the excitation is partly dissipated by non-radiative transition, the emitted photon carries less energy and it is therefore characterised by longer wavelength compared to the absorption wavelength. The difference between the two wavelengths (excitation and emission) is called the Stokes shift. This is characteristic of each fluorophores and defines the sensitivity of the fluorescence technique. Large Stokes shifts are desirable to enhance the signal-to-noise ratio and for high quality optical imaging. The excitation/emission of a fluorophore is cyclical; the fluorescent molecule can be excited again after emission. However, the fluorescence emission of the fluorophores fades over time, giving rise to the phenomenon called photobleaching.[101] This is an irreversible loss of fluorescence signal due to photochemical changes of the fluorescent molecule, including reactions with neighbouring dye molecules. The choice of photo-stable fluorophores and the use of high sensitivity detector can prevent the photobleaching.

Fluorophores, are widely used in imaging, tracking and detection. Fluorescence spectroscopy, compared to other methods of detection and imaging (based on X-Rays, IR, microwaves, electromagnetism etc.) has many advantages. It is characterized by high efficiency, versatility, sensitivity and sensibility and in fact fluorescence is frequently used for the detection of small quantities. Moreover the fluorescence of the fluorophores can be modulated by interaction with other molecules therefore providing a detectable signal, useful in sensing application. The number of available fluorophores, with different characteristics and performance, provides flexibility for research application. The fluorophores are generally divided into three general groups, namely biological fluorophores, quantum dots and organic dyes; each of this subgroup is defined by their specific characteristics in terms of stability, availability and sensitivity.

The biological fluorophores are fluorescent proteins such as the green fluorescent protein (GFP), which was first cloned in the early 1990s by jellyfish *Aequorea victoria*.[102] Since its discovery, GFP has largely been used as gene expression reporter,[103, 104] or successfully incorporated into herpes virus in order to analyse the kinetics and the effect of the virus infections. [105] Moreover, GFP was found to have no effect on the cell growth, resulting to be not toxic. [106]

Quantum dots (QD) are nanosized fluorophores characterised by broad excitation and narrow emission, high quantum yields, photostability and resistance to photobleaching (the irreversible destruction of fluorophores). The emission bands of the quantum dots can be tuned by changing their size. Bigger dots with radius of 5-6 nm emit longer wavelengths compared to smaller QDs, 2-3 nm in radius. However the specific emissions also depend on the shape and composition of the QDs. [107, 108] The characteristics of QDs make them appropriate for biological applications such as labelling of living cells[109,110] tracking cancer cells, [111] or dynamic trackers for biological

events. For example it was possible to track the glycine receptors and to observe their entry into synapses by diffusion. [112]

The organic dyes are synthetic fluorophore molecules. Amongst this class, fluorescein and its derivatives are the most commonly used as tags and imaging agents for a variety of applications. [113] In particular, since its synthesis in the 80's, fluorescein has been largely used in health care as diagnostic tool in gastrointestinal endoscopy[114,115] and ophthalmic angiograms. [116] In order to be suitable fluorophores the synthetic dyes need to have the following characteristics: high visible extinction coefficient, which allow them to absorb the visible light even at low concentrations; high fluorescence quantum yield, which is an indication of the minimum concentration required for fluorescence detection; high ability of tissues penetration in order to observe sufficient fluorescence *in vivo*. [113] These features are easily addressable by chemical modifications. The addition of specific functional groups can change the emission wavelength, the hydrophilicity, the photostability, and can introduce specific binding sites to conjugate the fluorophore to biomolecules or nanosystem. [117] In fact, a range of synthetic fluorophores has been used over the past few years for nanocarrier labelling. Two recent examples are reported by Dong *et al*.[118] and by Saxena and Jayajannan. [119] The two groups proposed nanovehicles conjugated with fluorophores to simultaneously track the cellular uptake of the systems and monitor the tumour therapy efficacy.

As this class of fluorophores is quite versatile and the chemical structure can be modified to satisfy the requirements for the specific applications, it was decided to adopt organic synthetic fluorophores for the preparation of fluorescent MIP with potential application as detector and drug carrier. This will be explained in details in the following section.

## 1.5. Aim and objectives

The overall aim of this project is to develop novel polymers based on molecular imprinting and labelled with a fluorescent tag, which could be applied in sensing and delivery using tamoxifen as the drug target. Four main objectives were identified: i) synthesis and characterisation of polymerisable coumarin derivatives with dual functionality, fluorescence and pH-responsive; ii) development of coumarin-based MIPs in bulk format to be potentially used for tamoxifen sensing; iii) synthesis and characterisation of coumarin-based MIPs in nanogel format for application as drug delivery system; iv) toxicity study and evaluation of the drug loading of nanogels in transgenic zebrafish.

In order to simplify the discussion of the results, the data for each of the above objectives are presented in a dedicated chapter, as summarised here below.

**Chapter 2** presents the design and synthesis of the fluorescent functional monomers. To this purpose, three main features were identified as essential: 1) good fluorescence yield and production of a detectable signal upon binding the analytes; 2) polymerisable unit to covalently link the molecule to the polymer; 3) functional groups to anchor the template. A novel synthetic pathway was developed and two different coumarin derivatives monomers were synthesised and characterised by NMR and fluorescence emission. However, only one monomer (VCC, 6-vynilcoumarin-4-carboxylic acid) was taken to the next stage.

**Chapter 3** describes the use of the MIP bulk polymer (obtained at Polyintell by Dr. Ray) based on the VCC fluorescent monomer and its potential as detector for tamoxifen and its metabolite, 4-hydroxytamoxifen. Initially, the interactions between the functional monomer and the analytes clomiphene (the drug analogue employed as template), tamoxifen, and 4-hydroxytamoxifen were studied, demonstrating a

fluorescence quenching of the VCC upon binding of the analytes. Finally, the MIP was tested against the same analytes, ensuring the formation of interactions that quenched the fluorescence of the polymeric matrix. The generation of the signal in the presence of the analytes was also assessed by naked eye, thus confirming the potential of the system to be used as detector.

**Chapter 4** covers the work done on the synthesis and optimisation of NIPAM-based, water-soluble nanogels imprinted with tamoxifen with potential application in drug delivery. The fluorescent functional monomer VCC was employed to provide a specific binding site for the drug, stimuli-responsiveness to the final matrix as well as the opportunity to track the nanosystem *via* fluorescence. Different sets of MIP and NIP were obtained and optimisation was done based on solubility, fluorescence emission and particle size. The polymerisation of the fluorescent monomer was confirmed followed by sample treatment with MeOH and dialysis. Finally, the quantification of the drug in the MIP was carried out by indirect method. The tamoxifen, loaded in the matrix, was converted into a phenantrene derivative by UV irradiation of the MIP solution, which gives a new absorbance peak. Tamoxifen was, thus quantified as its photochemical product using a reference line.

**Chapter 5** presents the *in vivo* studies of the nanogels presented in chapter 4. The zebrafish tamoxifen reporter line ubi:loxP-EGFP-loxP-mCherry (ubi:switch) was utilised for toxicology studies and for evaluation of the drug loaded in the MIP nanogel. Ubi:switch larvae were first treated with two different concentrations of tamoxifen in order to confirm the activation of the genetic system, which generated a red fluorescence when the drug was present in the organism. Afterwards, the ubi:switch embryos were fed with fish water solution of NIP and MIP. The nanogels were non-

toxic to the zebrafish at the tested concentrations and the presence of tamoxifen loaded in the imprinted nanogel was confirmed by exhibition of red fluorescence.

**Chapter 6** describes the experimental conditions and methodologies together with the materials and instruments employed in this work.

## 1.6. References


1. Theis, T.; Parr, D.; Binks, P.; Ying, J.; Drexler, K. E.; Schepers, E.; Mullis, K.; Bai, C.; Boland, J. J.; Langer, R.; Dobson, P.; Rao, C. N.; Ferrari, M., nan'o.tech.nol'o.gy n. *Nature nanotechnology* **2006,** *1* (1), 8-10.

2. Andrews, D. L.; Scholes, G. D.; Wiederrecht, G. P., Comprehensive Nanoscience and Technology. *Academic Press* **2010**.

3. Tegart, G., Nanotechnology: The Technology for the 21st Century. *The APEC Center for Technology Foresight Bangkok, Thailand* **2002**.

4. Barnes, C. P.; Sell, S. A.; Boland, E. D.; Simpson, D. G.; Bowlin, G. L., Nanofiber technology: designing the next generation of tissue engineering scaffolds. *Advanced drug delivery reviews* **2007,** *59* (14), 1413-33.

5. Shekaran, A.; Garcia, A. J., Nanoscale engineering of extracellular matrix-mimetic bioadhesive surfaces and implants for tissue engineering. *Biochim Biophys Acta* **2011,** *1810* (3), 350-60.

6. Cassidy, J. W., Nanotechnology in the Regeneration of Complex Tissues. *Bone and tissue regeneration insights* **2014,** *5*, 25-35.

7. Smith, B. R.; Gambhir, S. S., Nanomaterials for In Vivo Imaging. *Chemical reviews* **2017,** *117* (3), 901-986.

8. Estelrich, J.; Sanchez-Martin, M. J.; Busquets, M. A., Nanoparticles in magnetic resonance imaging: from simple to dual contrast agents. *International journal of nanomedicine* **2015,** *10*, 1727-41.

9. Chapman, S.; Dobrovolskaia, M.; Farahani, K.; Goodwin, A.; Joshi, A.; Lee, H.; Meade, T.; Pomper, M.; Ptak, K.; Rao, J.; Singh, R.; Sridhar, S.; Stern, S.; Wang, A.; Weaver, J. B.; Woloschak, G.; Yang, L., Nanoparticles for cancer imaging: The good, the bad, and the promise. *Nano today* **2013,** *8* (5), 454-460.

10. Nune, S. K.; Gunda, P.; Thallapally, P. K.; Lin, Y. Y.; Forrest, M. L.; Berkland, C. J., Nanoparticles for biomedical imaging. *Expert opinion on drug delivery* **2009,** *6* (11), 1175-94.

11. Min, Y.; Roche, K. C.; Tian, S.; Eblan, M. J.; McKinnon, K. P.; Caster, J. M.; Chai, S.; Herring, L. E.; Zhang, L.; Zhang, T.; DeSimone, J. M.; Tepper, J. E.; Vincent, B. G.; Serody, J. S.; Wang, A. Z., Antigen-capturing nanoparticles improve the abscopal effect and cancer immunotherapy. *Nature nanotechnology* **2017**.

12. Holzinger, M.; Le Goff, A.; Cosnier, S., Nanomaterials for biosensing applications: a review. *Frontiers in chemistry* **2014,** *2*, 63.

13. Safari, J.; Zarnegar, Z., Advanced drug delivery systems: Nanotechnology of health design A review. *Journal of Saudi Chemical Society* **2014,** *18* (2), 85-99.

14. McKeating, K. S.; Aube, A.; Masson, J. F., Biosensors and nanobiosensors for therapeutic drug and response monitoring. *The Analyst* **2016,** *141* (2), 429-49.

15. source: web of knowledge database, research conducted on the 28-07-17, apps.webofknoweldge.com

16. Wulff, G., Fourty years of molecular imprinting in synthetic polymers: origin, features and perspectives. *Microchimica Acta* **2013,** *180* (15-16), 1359-1370.

17. Beltran, A.; Borrull, F.; Cormack, P. A. G.; Marce, R. M., Molecularly-imprinted polymers: useful sorbents for selective extractions. *Trends in Analytical Chemistry* **2010,** *29*, 1363-1375.

18. Wulff, G.; Knorr, K., Stoichiometric noncovalent interaction in molecular imprinting. *Bioseparation* **2002,** *10*, 257–276.

19. Alexander, C.; Andersson, H. S.; Andersson, L. I.; Ansell, R. J.; Kirsch, N.; Nicholls, I. A.; O'Mahony, J.; Whitcombe, M. J., Molecular imprinting science and technology: a survey of the literature for the years up to and including 2003. *Journal of molecular recognition : JMR* **2006,** *19* (2), 106-80.

20. Vasapollo, G.; Sole, R. D.; Mergola, L.; Lazzoi, M. R.; Scardino, A.; Scorrano, S.; Mele, G., Molecularly imprinted polymers: present and future prospective. *International journal of molecular sciences* **2011,** *12* (9), 5908-45.

21. Haupt, K.; Mosbach, K., Molecularly Imprinted Polymers and Their Use in Biomimetic Sensors. *Chem. Rev.* **2000,** *100*, 2495−2504.

22. Tokonami, S.; Shiigi, H.; Nagaoka, T., Review: micro- and nanosized molecularly imprinted polymers for high-throughput analytical applications. *Analytica chimica acta* **2009,** *641* (1-2), 7-13.

23. Sellergren, B.; Allender, C. J., Molecularly imprinted polymers: a bridge to advanced drug delivery. *Advanced drug delivery reviews* **2005,** *57* (12), 1733-41.

24. Chianella, I.; Guerreiro, A.; Moczko, E.; Caygill, J. S.; Piletska, E. V.; De Vargas Sansalvador, I. M.; Whitcombe, M. J.; Piletsky, S. A., Direct replacement of antibodies with molecularly imprinted polymer nanoparticles in ELISA--development of a novel assay for vancomycin. *Analytical chemistry* **2013,** *85* (17), 8462-8.

25. Ton, X. A.; Acha, V.; Bonomi, P.; Tse Sum Bui, B.; Haupt, K., A disposable evanescent wave fiber optic sensor coated with a molecularly imprinted polymer as a selective fluorescence probe. *Biosensors & bioelectronics* **2015,** *64*, 359-66.

26. Lulinski, P., Molecularly Imprinted Polymers As The Future Drug Delivery Devices. *Acta Poloniae Pharmaceutica-Drug Research* **2013,** *70*, 601-609.

27. Tashakori-Sabzevar, F.; Mohajeri, S. A., Development of ocular drug delivery systems using molecularly imprinted soft contact lenses. *Drug development and industrial pharmacy* **2015,** *41* (5), 703-13.

28. Pérez-Moral, N.; Mayes, A. G., Comparative study of imprinted polymer particles prepared by different polymerisation methods. *Analytica Chimica Acta* **2004,** *504* (1), 15-21.

29. G. Wulff, A. S., K. Zabrocki, Enzyme-analogue built polymers and their use for the resolution of racematbs. *Tetrahedron Letter8* **1973,** *44*, 4329 - 4332.

30. Kenneth J. Shea, E. A. T., Template synthesis of macromolecules. selective functionalization of an organic polymer *J. Org. Chem* **1978,** *43* (21), 4253-4255.

31. Julien Damen, D. C. N., Memory of Synthesized Vinyl Polymers for Their Origins. *J. Org. Chem* **1980,** *45* (8), 1382-1387.

32. Reza Arshady, K. M., Synthesis of substrate-selective polymers by host-guest polymerization. *Makromol. Chem* **1981,** *182*, 687- 692.

33. Lai, J. P.; Yang, M. L.; Niessner, R.; Knopp, D., Molecularly imprinted microspheres and nanospheres for di(2-ethylhexyl)phthalate prepared by precipitation polymerization. *Analytical and bioanalytical chemistry* **2007,** *389* (2), 405-12.

34. Mohajeri, S. A.; Karimi, G.; Aghamohammadian, J.; Khansari, M. R., Clozapine recognition via molecularly imprinted polymers; bulk polymerization versus precipitation method. *Journal of Applied Polymer Science* **2011,** *121* (6), 3590-3595.

35. Shuting Wei, B. M., Recent advances on noncovalent molecular imprints for affinity separations. *J. Sep. Sci.* **2007,** *30*, 1794-1805.

36. Hu, Y.; Lu, X., Rapid Detection of Melamine in Tap Water and Milk Using Conjugated "One-Step" Molecularly Imprinted Polymers-Surface Enhanced Raman Spectroscopic Sensor. *Journal of food science* **2016,** *81* (5), N1272-80.

37. Ji, W.; Zhang, M.; Gao, Q.; Cui, L.; Chen, L.; Wang, X., Preparation of hydrophilic molecularly imprinted polymers via bulk polymerization combined with hydrolysis of ester groups for selective recognition of iridoid glycosides. *Analytical and bioanalytical chemistry* **2016,** *408* (19), 5319-28.

38. Soussan, E.; Cassel, S.; Blanzat, M.; Rico-Lattes, I., Drug delivery by soft matter: matrix and vesicular carriers. *Angewandte Chemie* **2009,** *48* (2), 274-88.

39. Nahar, M.; Dutta, T.; Murugesan, S.; Asthana, A.; Mishra, D.; Rajkumar, V.; Tare, M.; Saraf, S.; Jain, N. K., Functional polymeric nanoparticles: an efficient and promising tool for active delivery of bioactives. *Crit. Rev. Ther. Drug Carrier Syst.* **2006,** *23*, 259-318.

40. Zhang, H.; Zhai, Y.; Wang, J.; Zhai, G., New progress and prospects: The application of nanogel in drug delivery. *Materials science & engineering. C, Materials for biological applications* **2016,** *60*, 560-8.

41. (a) Oishi, M.; Tamura, A.; Nakamura, T.; Nagasaki, Y., A Smart Nanoprobe Based On Fluorescence Quenching PEGylated Nanogels Containing Gold Nanoparticles for Monitoring the Response to Cancer Therapy. *Adv. Funct. Mater.* **2009,** *19*, 827–834; (b) Chan, M.; Almutairi, A., Nanogels as imaging agents for modalities spanning the electromagnetic spectrum. *Materials horizons* **2016,** *3* (1), 21-40.

42. Wu, W.; Zhou, S., Hybrid micro-/nanogels for optical sensing and intracellular imaging. *Nano reviews* **2010,** *1*.

43. Wu, W.; Shen, J.; Banerjee, P.; Zhou, S., Core-shell hybrid nanogels for integration of optical temperature-sensing, targeted tumor cell imaging, and combined chemo-photothermal treatment. *Biomaterials* **2010,** *31* (29), 7555-66.

44. Tessler, L. A.; Donahoe, C. D.; Garcia, D. J.; Jun, Y. S.; Elbert, D. L.; Mitra, R. D., Nanogel surface coatings for improved single-molecule imaging substrates. *Journal of the Royal Society, Interface* **2011,** *8* (63), 1400-8.

45. Sultana, F.; Manirujjaman.; Imran-Ul-Haque; Arafat, M.; Sharmin, S., An Overview of Nanogel Drug Delivery System. *Journal of Applied Pharmaceutical Science* **2013,** *3*, S95-S105.

46. Shimizu, T.; Kishida, T.; Hasegawa, U.; Ueda, Y.; Imanishi, J.; Yamagishi, H.; Akiyoshi, K.; Otsuji, E.; Mazda, O., Nanogel DDS enables sustained release of IL-12 for tumor immunotherapy. *Biochemical and biophysical research communications* **2008,** *367* (2), 330-5.

47. Kitano, S.; Kageyama, S.; Nagata, Y.; Miyahara, Y.; Hiasa, A.; Naota, H.; Okumura, S.; Imai, H.; Shiraishi, T.; Masuya, M.; Nishikawa, M.; Sunamoto, J.; Akiyoshi, K.; Kanematsu, T.; Scott, A. M.; Murphy, R.; Hoffman, E. W.; Old, L. J.; Shiku, H., HER2-specific T-cell immune responses in patients vaccinated with truncated HER2 protein complexed with nanogels of cholesteryl pullulan. *Clinical cancer research : an official journal of the American Association for Cancer Research* **2006,** *12* (24), 7397-405.

48. Kageyama, S.; Kitano, S.; Hirayama, M.; Nagata, Y.; Imai, H.; Shiraishi, T.; Akiyoshi, K.; Scott, A. M.; Murphy, R.; Hoffman, E. W.; Old, L. J.; Katayama, N.; Shiku, H., Humoral immune responses in patients vaccinated with 1-146 HER2 protein complexed with cholesteryl pullulan nanogel. *Cancer science* **2008,** *99* (3), 601-7.

49. Nukolova, N. V.; Oberoi, H. S.; Cohen, S. M.; Kabanov, A. V.; Bronich, T. K., Folate-decorated nanogels for targeted therapy of ovarian cancer. *Biomaterials* **2011,** *32* (23), 5417-26.

50. Macgregor, J. I.; Jordan, V. G., Basic Guide to the Mechanisms of Antiestrogen Action. *Pharmacological Reviews* **1998,** *50*, 151-196.

51. Jordan, V. C., Designer Estrogens. *Scientific American* **1998,** *279*, 60-67.

52. Love, R. R.; Barden, H. S.; Mazess, R. B.; Epstein, S.; Chappell, R. J., Effect of Tamoxifen on Lumbar Spine Bone Mineral Density in Postmenopausal Women After 5 Years. *Archives of Internal Medicine* **1994,** *154*, 2585-2588.

53. Assikis, V. J.; Jordan, V. C., Gynecologic effects of tamoxifen and the association with endometrial carcinoma. *International Journal of Gynecology & Obstetrics* **1995,** *49* (3), 241-257.

54. Báez, H.; Camargo, C.; Osorio, H.; Umpiérrez, F., Detection of Tamoxifen Metabolites by GC–MSD. *Journal of Chromatographic Science* **2004,** *42*.

55. Baker, J. S.; Graham, M. R.; Davies, B., Steroid and prescription medicine abuse in the health and fitness community: A regional study. *European journal of internal medicine* **2006,** *17* (7), 479-84.

56. Crewe, H. K.; Notley, L. M.; Wunsch, R. W.; Lennard, M. S.; Gillam, E. M. J., Metabolism Of Tamoxifen By Recombinant Human Cytochrome P450 Enzymes: Formation Of The 4-Hydroxy, 4!-Hydroxy And N-Desmethyl Metabolites And Isomerization Of Trans-4-Hydroxytamoxifen. *Drug Metabolism And Disposition* **2002,** *30*, 869–874.

57. Murdter, T. E.; Schroth, W.; Bacchus-Gerybadze, L.; Winter, S.; Heinkele, G.; Simon, W.; Fasching, P. A.; Fehm, T.; German, T.; Group, A. I. C.; Eichelbaum, M.; Schwab, M.; Brauch, H., Activity levels of tamoxifen metabolites at the estrogen receptor and the impact of genetic polymorphisms of phase I and II enzymes on their concentration levels in plasma. *Clinical pharmacology and therapeutics* **2011,** *89* (5), 708-17.

58. Cronin-Fenton, D. P.; Damkier, P.; Lash, T. L., Metabolism and transport of tamoxifen in relation to its effectiveness: new perspectives on an ongoing controversy. *Future oncology* **2014,** *10* (1), 107-22.

59. Meier, C. R.; Jick, H., Tamoxifen and risk of idiopathic venous thromboembolism. *Br J Clin Pharmacol* **1998,** *45*, 608–612.

60. Daniel, C. P.; Gaskell, S. J.; Bishop, H.; NIcholson, R. I., Determination of tamoxifen and an hydroxylated metabolite in plasma from patients with advanced breast cancer using gas chromatography-mass spectrometry. *J. Endocr.* **1979,** *83*, 401-408.

61. Kemp, J. V.; Adam, H. K.; Wakeling, A. E.; Slater, R., Identification and biological activity of tamoxifen metabolites in human serum. *Biochemical Pharmacology* **1983,** *32*, 2045-2052.

62. Golander, Y.; Sternson, L. A., Paired-Ion Chromatographic Analysis Of Tamoxifen And Two Major Metaboutes In Plasma. *Journal of Chromatography* **1960,** *181*, 41-49.

63. Stevenson, D.; Briggs, R. J.; Chapman, D. J.; De Vos, D., Determination of tamoxifen and five metabolites in plasma. *Journal of Pharmaceutical & Biomedical Analysis* **1988,** *6*, 1065-1068.

64. Nieder, M.; Jaeger, H., Quantification of tamoxifen and n-desmethyltamoxifen in human plasma by high-performance liquid chromatography, photochemical reaction and fluorescence detection, and its application to biopharmaceutic investigations. *Journal of Chromatography* **1987,** *413*, 207-217.

65. Kikuta, C.; Schmid, R., Specific high-performance liquid chromatographic analysis of tamoxifen and its major metabolites by "on-line" extraction and post-column photochemical reaction. *Journal of Pharmaceuacal & BiomedicalAnalysis* **1989,** *7*, 329-337.

66. Lien, E. A.; Ueland, P. M.; Solhelm, E.; Kvlnnslan, S., Determination of Tamoxifen and four Metabolites in Serum by Low-Dispersion Liquid Chromatography. *Clin. Chem.* **1987,** *33* (9), 1608-1614.

67. Lien, E. A.; Solheim, E.; Kvinnsland, S.; Ueland, P. M., Identification of 4-Hydroxy-N-desmethyltamoxifen as a Metabolite of Tamoxifen in Human Bile. *Cancer Research* **1988,** *48*, 2304-2308.

68. MacCallum, J.; Cummings, J.; Dixon, J. M.; Miller, W. R., Solid-phase extraction and high-performance liquid chromatographic determination of tamoxifen and its major metabolites in plasma. *Journal of Chromatography B* **1996,** *678*, 317-323.

69. Mihailescu, R.; Aboul-Enein, H. Y.; Efstatide, M. D., Identification of tamoxifen and metabolites in human male urine by GC/MS. *Biomedical chromatography* **2000,** *14*, 180-183.

70. Báez, H.; Camargo, C.; Osorio, H.; Umpiérrez, F., Detection of Tamoxifen Metabolites by GC–MSD. *Journal of Chromatographic Science* **2004,** *42*.

71. Claude, B.; Morin, P.; Bayoudh, S.; de Ceaurriz, J., Interest of molecularly imprinted polymers in the fight against doping. Extraction of tamoxifen and its main metabolite from urine followed by high-performance liquid chromatography with UV detection. *Journal of chromatography. A* **2008,** *1196-1197*, 81-8.

72. Rashid, B. A.; Briggs, R. J.; Hay, J. N.; Stevenson, D., Communications Preliminary Evaluation of a Molecular Imprinted Polymer for Solid-phase Extraction of Tamoxifen. *Analytical Communications* **1997,** *34*, 303–305.

73. Martin, P. D.; Wilson, T. D.; Wilson, I. D.; Jones, G. R., An unexpected selectivity of a propranolol-derived molecular imprint for tamoxifen. *The Analyst* **2001,** *126* (6), 757-759.

74. Nie, F.; Lu, J.; He, Y.; Du, J., Use of molecule imprinting-chemiluminescence method for the determination of tamoxifen in breast cancer sufferers' urine. *Luminescence* **2005,** *20* (4-5), 315-20.

75. Yarman, A.; Scheller, F. W., The first electrochemical MIP sensor for tamoxifen. *Sensors* **2014,** *14* (5), 7647-54.

76. Tiwari, G.; Tiwari, R.; Sriwastawa, B.; Bhati, L.; Pandey, S.; Pandey, P.; Bannerjee, S. K., Drug delivery systems: An updated review. *International journal of pharmaceutical investigation* **2012,** *2* (1), 2-11.

77. Whalen, K., Lippincott Illustrated Reviews. *Pharmacology Sixth Edition*.

78. Skandalis, S. S.; Gialeli, C.; Theocharis, A. D.; Karamanos, N. K., Advances and advantages of nanomedicine in the pharmacological targeting of hyaluronan-CD44 interactions and signaling in cancer. *Advances in cancer research* **2014,** *123*, 277-317.

79. Hubbell, J. A.; Chilkoti, A., Nanomaterials for Drug Delivery. *Science* **2012,** *337* (6092), 303-305.

80. Hoffman, A. S., The origins and evolution of "controlled" drug delivery systems. *Journal of controlled release : official journal of the Controlled Release Society* **2008,** *132* (3), 153-63.

81. Zhu, Y.; Liao, L., Applications of Nanoparticles for Anticancer Drug Delivery: A Review. *Journal of Nanoscience and Nanotechnology* **2015,** *15*, 4753–4773.

82. Panyam, J.; Labhasetwar, V., Biodegradable nanoparticles for drug and gene delivery to cells and tissue. *Advanced Drug Delivery Reviews* **2003,** *55*, 329–347.

83. Singh, R.; Lillard, J. W., Nanoparticle-based targeted drug delivery. *Experimental and molecular pathology* **2009,** *86* (3), 215-23.

84. Desai, M. P.; Labhasetwar, V.; Amidon, G. L.; Levy, R. J., Gastrointestinal uptake of biodegradable microparticles: effect of particle size *Pharm. Res.* **1996,** *13*, 1838–1845.

85. Ventola, C. L., The Nanomedicine Revolution. Part 1: Emerging Concepts. *Pharmacy &Therapeutics* **2012,** *37*, 512-517.

86. Wang, N. X.; Von Recum, H. A., Affinity-based drug delivery. *Macromolecular bioscience* **2011,** *11* (3), 321-32.

87. Mura, S.; Nicolas, J.; Couvreur, P., Stimuli-responsive nanocarriers for drug delivery. *Nature materials* **2013,** *12* (11), 991-1003.

88. Fleige, E.; Quadir, M. A.; Haag, R., Stimuli-responsive polymeric nanocarriers for the controlled transport of active compounds: concepts and applications. *Adv Drug Deliv Rev* **2012,** *64* (9), 866-84.

89. Taghizadeh, B.; Taranejoo, S.; Monemian, S. A.; Moghaddam, Z. S.; Daliri, K.; Derakhshankhah, H.; Derakhshani, Z., Classification of stimuli-responsive polymers as anticancer drug delivery systems. *Drug delivery* **2015,** *22* (2), 145-55.

90. Masood, F., Polymeric nanoparticles for targeted drug delivery system for cancer therapy. *Materials science & engineering. C, Materials for biological applications* **2016,** *60*, 569-78.

91. Kedar, U.; Phutane, P.; Shidhaye, S.; Kadam, V., Advances in polymeric micelles for drug delivery and tumor targeting. *Nanomedicine : nanotechnology, biology, and medicine* **2010,** *6* (6), 714-29.

92. Esfand, R.; Tomalia, D., Poly(amidoamine) (PAMAM) dendrimers: from biomimicry to drug delivery and biomedical applications. *Drug Discov. Today* **2001,** *6*, 427–436.

93. Fang, R. H.; Hu, C. M.; Luk, B. T.; Gao, W.; Copp, J. A.; Tai, Y.; O'Connor, D. E.; Zhang, L., Cancer cell membrane-coated nanoparticles for anticancer vaccination and drug delivery. *Nano letters* **2014,** *14* (4), 2181-8.

94. Krishnamurthy, S.; Vaiyapuri, R.; Zhang, L.; Chan, J. M., Lipid-coated polymeric nanoparticles for cancer drug delivery. *Biomaterials science* **2015,** *3* (7), 923-36.

95. Misra, C.; Kumar, M.; Sharma, G.; Kumar, R.; Singh, B.; Katare, O. P.; Raza, K., Glycinated fullerenes for tamoxifen intracellular delivery with improved anticancer activity and pharmacokinetics. *Nanomedicine* **2017,** *12*, 1011-1023.

96. Sandhu, P. S.; Kumar, R.; Beg, S.; Jain, S.; Kushwah, V.; Katare, O. P.; Singh, B., Natural lipids enriched self-nano-emulsifying systems for effective co-delivery of tamoxifen and naringenin: Systematic approach for improved breast cancer therapeutics. *Nanomedicine* **2017,** *13* (5), 1703-1713.

97. Thakur, C. K.; Thotakura, N.; Kumar, R.; Kumar, P.; Singh, B.; Chitkara, D.; Raza, K., Chitosan-modified PLGA polymeric nanocarriers with better delivery potential for tamoxifen. *International journal of biological macromolecules* **2016,** *93* (Pt A), 381-389.

98. Majd, H. M.; Asgari, D.; Barar, J.; Valizadeh, H.; Kafil, V.; Abadpour, A.; Moumivand, E.; Mojarrad, J. S.; Rashidi, M. R.; Coukos, G.; Omidi, Y., Tamoxifen loaded folic acid armed PEGylated magnetic nanoparticles for targeted imaging and therapy of cancer. *Colloids and surfaces. B, Biointerfaces* **2013,** *106*, 117-25.

99. Jenkins, R.; Burdette, M. K.; Foulger, S. H., Mini-review: fluorescence imaging in cancer cells using dye-doped nanoparticles. *RSC Adv.* **2016,** *6* (70), 65459-65474.

100. http://www.thermofisher.com/uk/en/home/references/molecular-probes-the-handbook/introduction-to-fluorescence-techniques.

101. Diaspro, A.; Chirico, G.; Usai, C.; Ramoino, P.; Dobrucki, J., Photobleaching. *In Handbook of Biological Confocal Microscopy. J.B. Pawley, editor. Springer -Verlag* **2006**, 690-702.

102. Prasher, D. C.; Eckenrode, V. K.; Ward, W. W.; Prendergast, F. G.; Cormier, M. J., Primary structure of the Aequorea victoria green-fluorescent protein *Gene* **1992,** *111*, 229-233.

103. Chiocchetti, A.; Tolosano, E.; Hirsch, E.; Silengo, L.; Altruda, F., Green fluorescent protein as a reporter of gene expression in transgenic mice. *Biochimica et Biophysica Acta* **1997,** *1352*, 193-202.

104. Sun, J.; Kelemen, G. H.; Abalos, J. M. F.; Bibb, M. J., Green fluorescent protein as a reporter for spatial and temporal gene expression in Streptomyces coelicolor A3(2). *Microbiology* **1999,** *145*, 2221-2227.

105. Elliott, G.; O'Hare, P., Live-Cell Analysis of a Green Fluorescent Protein-Tagged Herpes Simplex Virus Infection. *Journal of virology* **1999,** *73*, 4110-4119.

106. Chalfie, M.; Tu, Y.; Euskirchen, G.; Ward, W. W.; Prashert, D. C., Green fluorescent protein as a marker for gene expression. *Science* **1994,** *63*, 802-805.

107. Murray, C. B.; Noms, D. J.; Bawendi, M. G., Synthesis and Characterization of Nearly Monodisperse CdE (E = S, Se, Te) Semiconductor Nanocrystallites. *J. Am. Chem. Soc.* **1993,** *115*, 8706-8715.

108. Ballou, B.; Lagerholm, B. C.; Ernst, L. A.; Bruchez, M. P.; Waggoner, A. S., Noninvasive Imaging of Quantum Dots in Mice. *Bioconjugate Chem.* **2004,** *15*, 79−86.

109. Chen, F.; Gerion, D., Fluorescent CdSe/ZnS nanocrystal-peptide conjugates for long-term, nontoxic imaging and nuclear targeting in living cells. *Nano Letters* **2004,** *4*, 1827-1832.

110. Derfus, A. M.; Chan, W. C. W.; Bhatia, S. N., Intracellular Delivery of Quantum Dots for Live Cell Labeling and Organelle Tracking. *Advanced Materials* **2004,** *16* (12), 961-966.

111. Voura, E. B.; Jaiswal, J. K.; Mattoussi, H.; Simon, S. M., Tracking metastatic tumor cell extravasation with quantum dot nanocrystals and fluorescence emission-scanning microscopy. *Nature medicine* **2004,** *10* (9), 993-8.

112. Dahan, M.; Levi, S.; Luccardini, C.; Rostaing, P.; Riveau, B.; Triller, A., Diffusion Dynamics of Glycine Receptors Revealed by Single–Quantum Dot Tracking. *Science* **2003,** *302*.

113. Robertson, T. A.; Bunel, F.; Roberts, M. S., Fluorescein derivatives in intravital fluorescence imaging. *Cells* **2013,** *2* (3), 591-606.

114. Galandiuk, S.; Fazio, V. W.; Petras, R. E., Fluorescein Endoscopy - A Technique for Noninvasive Assessment of Intestinal Ischemia. *Dis. Col. & Rec.* **1988,** *31*, 848-853.

115. Bhunchet, E.; Hatakawa, H.; Sakai, Y.; Shibata, T., Fluorescein electronic endoscopy: A novel method for detection of early stage gastric cancer not evident to routine endoscopy. *Gastrointestinal Endoscopy* **2002,** *55* (4), 562-571.

116. Marmor, M. F.; Ravin, J. G., Fluorescein Angiography - Insight and Serendipity a Half Century Ago. *Arch Ophthalmol.* **2011,** *129*, 943-948.

117. Jung, D.; Min, K.; Jung, J.; Jang, W.; Kwon, Y., Chemical biology-based approaches on fluorescent labeling of proteins in live cells. *Molecular bioSystems* **2013,** *9* (5), 862-72.

118. Dong, X.; Wei, C.; Chen, H.; Qin, J.; Liang, J.; Kong, D.; Liu, T.; Lv, F., Real-Time Imaging Tracking of a Dual Fluorescent Drug Delivery System Based on Zinc Phthalocyanine-Incorporated Hydrogel. *ACS Biomaterials Science & Engineering* **2016,** *2* (11), 2001-2010.

119. Saxena, S.; Jayakannan, M., pi-Conjugate Fluorophore-tagged and Enzyme-responsive L-Amino acid Polymer Nano-carrier and their Colour-tunable Intracellular FRET Probe in Cancer Cells. *Biomacromolecules* **2017**.

# Chapter 2

## Synthesis and characterisation of polymerisable coumarin derivatives with dual functionality

# 2. Synthesis and characterisation of polymerisable coumarin derivatives with dual functionality

## 2.1. Introduction

This project targeted the development of novel nanomaterials for two types of applications: as drug delivery system (DDS) of tamoxifen and as sensor unit for the direct detection of the same drug and its metabolites. The common feature of the two systems was the preparation of polymeric matrices with high molecular recognition capability. The polymers were prepared using the molecular imprinting approach based on a template-casting procedure. As described in Chapter 1, prior to polymerisation the functional monomers (FM) assemble around the template (T), forming a pre-polymerisation, monomer-template complex. The polymeric matrix is then formed following the addition of the cross-linker together with the initiator, and 3-D cavities that are complementary in shape and functionalities to the imprinting molecule, are obtained after removal of the template. The interactions between FM and T play a key role in the rebinding properties of imprinted polymers. Usually, the stronger and more stable the complex is, the higher the specificity of the polymer will be. Therefore, considerable effort needs to be invested in the choice of FM and the study of the polymerisation conditions that lead to the formation of the most stable complex. This is true whatever the applications of the polymers, whether it is for sensing purposes, for catalysis or as a drug delivery vehicle. In particular, in the case of detector devices, the functional monomer anchors and interacts with the target and an additional unit provides a detectable signal upon binding of the analyte. A variety of nanosized materials often used for detection of biomolecules are reported in the literature. Such systems are all based on the generation of different signals, such as colorimetric[1]

electrochemical, [2] magnetic, [3] electric[4] signal. Nonetheless, as described in chapter 1 (section 1.4), applications of fluorescence in sensing presents many advantages, compared to other techniques of detection, namely high efficiency, sensitivity and sensibility. It was therefore, decided to focus the attention on this technique and to design a fluorescent tag that would be covalently linked to the polymeric network, as opposed to being simply incorporated.

In the group where this project was developed, a considerable amount of work was previously carried out on the screening and identification of suitable fluorescent monomers.[5] Dansylaminoethylacrylamide, fluorescein O-methacrylate and 7-acrylamidecoumarin-4-trifluoromethyl (TCA), which structures are shown in figure 2.1, were all investigated as potential fluorescent monomers. Several imprinted nanogels were prepared and tested for solubility, particle size and fluorescence intensity, identifying TCA as the fluorescent monomer that ensured the desired characteristics in the final polymer.

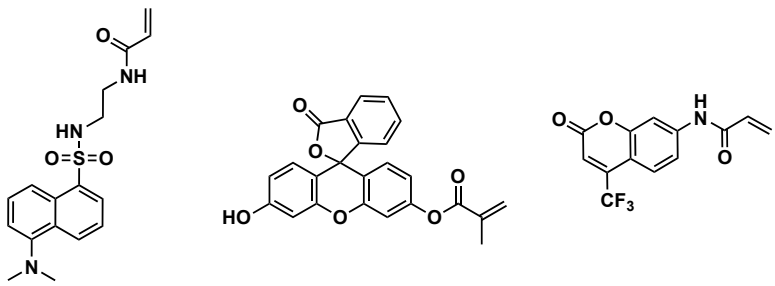


**Figure 2.1.** Structure of fluorescent monomers previously evaluated.

However, one of the main objectives of this work was to design a monomer that could provide fluorescence features to the matrix, as well as enable the interactions with the target. Considering the fundamental role played by the pre-polymerisation complex in the molecular recognition properties of the final imprinted matrix, a careful design of the FM is essential. In fact, the functional monomer should carry appropriate functional

groups to strongly bind the template, thus ensuring the formation of the most stable complex. After studying the optical characteristics of the TCA (identified in the previous study) and evaluating its structure, it was decided to use the same core and to chemically modify it in order to add functional groups to interact with the template. In the following section an account of the coumarins properties and their different possible synthetic approaches will be given.

### 2.1.1. Overview of coumarin properties and synthetic pathways

Coumarin is a natural compound, part of the benzopyrone family, found in many different plants. Its main core can be functionalised, giving rise to several different structures with a variety of biological activities. In fact, coumarins are well known for their analgesic, anti-oxidant, anti-inflammation, anticoagulant, antiviral and anti-bacterial activities.[6] These compounds have also unique photochemical and photophysical properties as well as high photostability and quantum yield.[7] They have large Stokes shift, which is defined as the difference in wavelength between the maximum absorption and emission peaks. Large Stokes shift is desirable for fluorescent molecules as it allows a strong signal while eliminating the overlap between absorption and emission spectra. For this feature, coumarins have been widely used as fluorescent probes for the selective detection of a number of compounds.[8-12] The long excitation and emission maxima that characterise the coumarins make them also largely used in *in vivo* applications, as the background autofluorescence of the cellular components and biological fluids is minimised.

The first appearance of coumarin in literature goes back to 1820 when Vogel isolated this compound from tonka beans, but wrongly classified it as benzoic acid.[13] It was only in 1835 that Guillemette identified the compound isolated by Vogel as coumarin instead

of benzoic acid.[14] Coumarin was employed as precursor in the synthesis of anticoagulant drugs. The most common one is commercialised with the name Coumadin®, which reduces the risk of forming blood clots by inhibiting the vitamin K-dependent synthesis of clotting factors, proteins in the blood that control bleeding.[15]

Perkin was the first scientist to synthesise the simple coumarin in 1868 using the aldol condensation of o-hydroxybenzaldehyde and acid anhydrides (scheme 2.1).

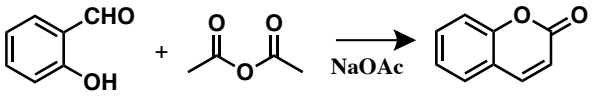


**Scheme 2.1**. Schematic representation of Perkin reaction for synthesis of coumarin.

After that, many other named reactions have been optimised for the synthesis of coumarin and derivatives (scheme 2.2). The most famous ones are the Pechmann reaction, used for the synthesis of 3-, 4- and 7-substituted coumarins; the Kostanecki-Robinson reaction, used for the synthesis of 3- and 4-substituted coumarins; the Reformatsky reaction, involving condensation of aldehydes or ketones with organo-zinc derivatives of α-halo esters; together with the Witting reaction and the Knoevenagel reaction. [16]

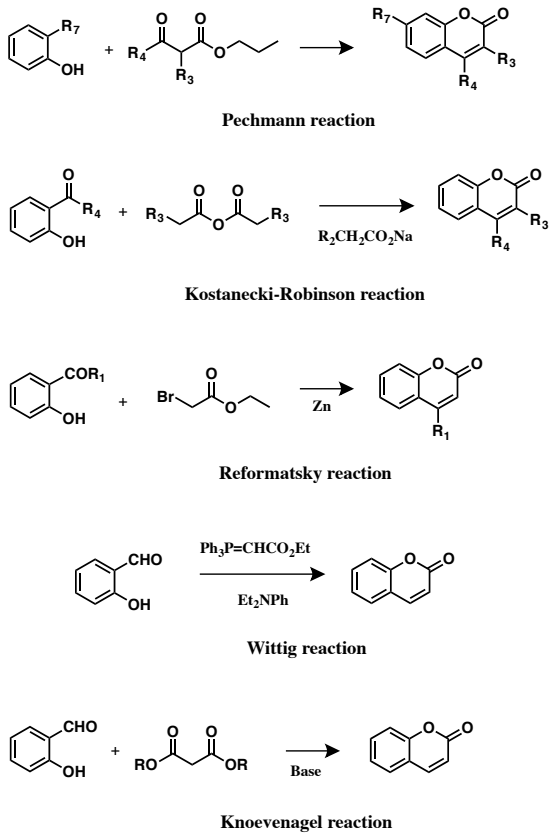


**Scheme 2.2.** Schematic representation of several name reactions for synthesis of coumarins.

## 2.2. Design of functional monomer – coumarin derivatives

As mentioned in section 2.1, TCA (7-acrylamidecoumarin-4-trifluoromethyl), was previously used in the preparation of nanogels with potential DDS applications, together with acrylic acid as functional monomer (figure 2.2). Acrylic acid had the role of capturing and interacting with the target molecule *via* ionic bond, while the coumarin monomer was used as a fluorescent probe to enable nanogel tracking during *in vivo* and *in vitro* experiments.[5]

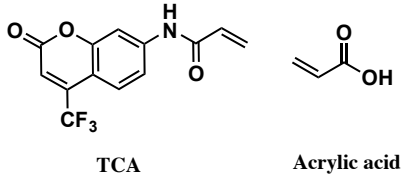


**Figure 2.2.** Molecular structure of the two monomers selected as fluorescent monomer and functional monomer, respectively in the work carried out by Dr. J. V. Ray, in the Resmini's group [5]

Using two separate molecular entities, one for fluorescence properties and one for specific binding interactions with the target, could cause additional issues in the preparation of imprinted polymers. In fact, different reactivity of the involved compounds could result in a different kinetics of their incorporation in the final matrix. This could, therefore, have an impact on the morphology and the physical chemical properties of the polymer. To minimise such potential issues it was decided to design a functional monomer with dual functionality. The fluorescent tag and the anchor unit were combined in one molecular structure. Moreover, such monomer could also cover the role of sensing unit, providing a signal upon binding of the target, when employed in the development of a detector system. Therefore, for the purpose of preparing coumarin-based smart monomers, three main features of the molecules were identified as essential: i) good fluorescence emission and ability to produce a signal when in contact with the analytes; ii) polymerisable unit to covalently link it to the polymer; iii) presence of functional groups to anchor the template.

After careful evaluation of the template structure and also considering the successful results obtained within the research group, it was decided to incorporate a carboxyl group on the coumarin monomer. This would allow ionic interactions between the amine group of the tamoxifen, or its analogues, and the coumarin smart monomer, as showed in figure 2.3.

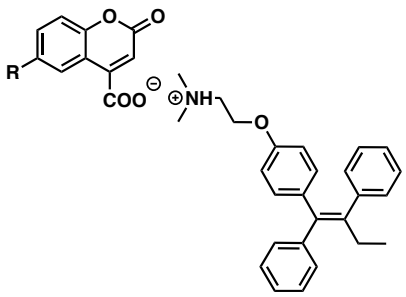


**Figure 2.3.** Proposed interactions between the smart monomer coumarin derivative, in which R represents the polymerisable unit, and the target tamoxifen

After identifying the carboxylic acid as the best choice of anchoring group, different options for the choice of polymerisable unit were evaluated. The polymerisable group plays an important role in the incorporation of the monomers in the final matrix, as the rate of incorporation depends on the kinetic of the different radicals.[17] To ensure that the incorporation ratio of the different component in the polymeric network matches the ratio employed in the pre-polymerisation mixture, polymerisable units with similar chemical structures should be used. Analogous structures should, in fact, lead to similar reaction rates, thus maximising the addition of the monomers in a ratio that is as comparable as possible to the initial mixture.

Following these considerations two smart monomers, represented in figure 2.4, 6-acrylamidecoumarin-4-carboxylic acid (monomer **1a**) and 6-vinylcoumarin-4-carboxylic acid (monomer **1b**), were chosen.

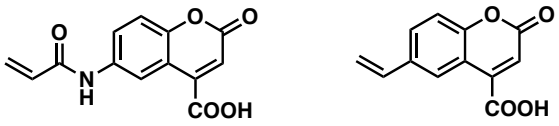


**1 a** **1 b**

**Figure 2.4.** The chosen smart monomers with dual functionality.

Envisaging the incorporation of the monomers into a polymer system with N,N'-methylenebis(acrylamide) used as a cross-linker, the polymerisable acrylamide unit on monomer **1a** was favourite, as the polymerisable groups were the same. However, it was also interesting to study how the vinyl group on monomer **1b** would have affected the overall system. The difference in the chemical structure of the vinyl group compared to the acrylamide group of the cross-linker, involved a different kinetic, which could lead to different incorporation rate. Nevertheless, the reactivity of the monomer **1b** was expected to be higher as he radical formed was stabilised by the resonance in the conjugated system. Moreover, the lack of additional functionalities in monomer **1b**

compared with **1a** could involve the formation of simpler systems with no extra inter- or intra-molecular interactions.

Careful analysis of the chemical structures of the functional group and the target molecule suggested two possible modes for binding interactions. On one hand a π-π stacking between the aromatic rings of the target and the monomer, on the other ionic bond between the carboxyl group on the monomer and the amine group on the target. However, it is important to underline that the strength of the interactions will depend to a certain extent on the type of solvent used. Detailed studies of the interactions are described later in chapter 3.

### 2.2.1. Retrosynthetic analysis

The synthesis of the target monomers could be achieved *via* a number of different approaches. Retrosynthetic analysis (scheme 2.3) showed that both selected monomers **1a** and **1b** could be derived from intermediates **2a** and **2b**, characterised by identical core. The identified precursors were characterised by a carboxylate group in position C4, which could be easily hydroxylated to give the desired carboxylic acid group.

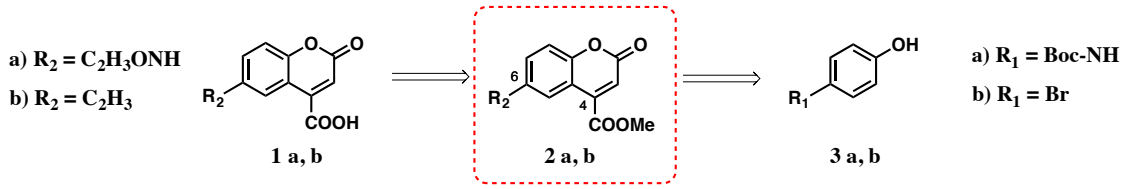


**Scheme 2.3.** Retrosynthetic analysis of the monomers **1a** and **1b**. The compound **2** (**a, b**) was identified as convenient precursors for the synthesis of the monomers.

It was decided to initially focus the efforts on the synthesis and optimisation of the carboxylate precursors **2a** leading to monomer **1a** and **2b** leading to monomer **1b**.

Although the retrosynthetic approach was quite similar, for clarity of explanation the individual synthesis of the two monomers will be described separately.

## 2.3. Synthesis of coumarin monomers

### 2.3.1. Towards the synthesis of 6-acrylamidecoumarin-4-carboxylate (2a)

Different pathways and starting materials were evaluated to obtain the coumarin derivative with an acrylamide group in position C6. The strategy represented in scheme 2.4 was eventually identified as the most convenient in which commercially available N-boc-aminophenol was used as starting material.

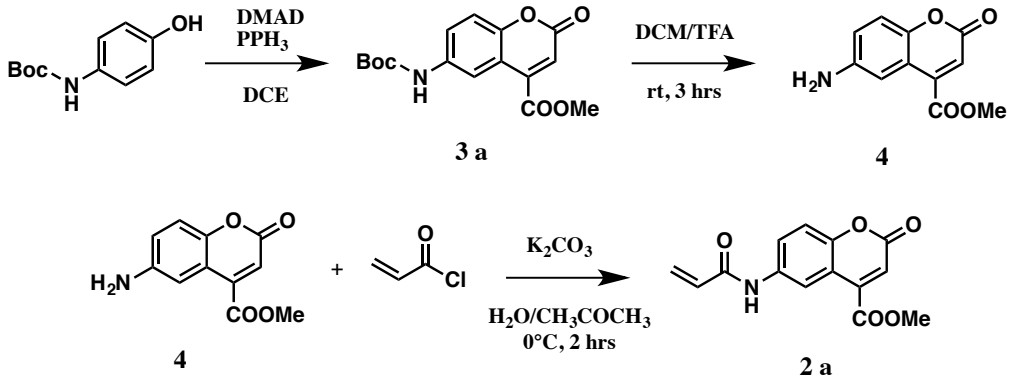


**Scheme 2.4.** Synthetic pathway for the synthesis of precursor **2a**

The first step was based on the formation of a di-substituted coumarin derivative at C4 and C6, followed by Boc cleavage to achieve the 6-aminocoumarin-4-carboxylate (**4**). Compound **4** was further reacted with acryloyl chloride to add polymerisable moiety in position C6 and obtain the desired precursor **2a**.

In the following subsections all the steps of the synthesis are discussed.

#### 2.3.1.1. 1st step – synthesis of 6-N-boc-aminocoumarin-4-carboxylate (3a)

The first attempt focused on the modification of a synthetic strategy already published in 1998.[18] The synthesis proceeded *via* a vinyl triphenylphosphonium salt formed by the initial attack of triphenylphosphine ($PPh_3$) to the dimethyl acetylenedicarboxylate (DMAD), followed by electrophilic aromatic substitution of the salt in *ortho* position to

the hydroxyl group of the starting material, which was the *para*-substitued aminophenol. Further intramolecular lactonization closed the ring, forming the coumarin derivative.

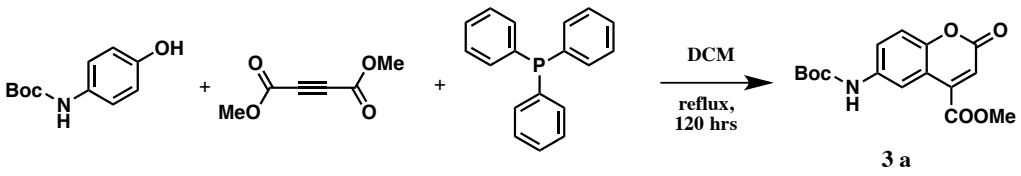


**3 a**

**Scheme 2.5.** Synthetic step for carboxylate derivate **3a**

According to the procedure found in the literature, which was followed carefully in the first instance, the synthesis required reflux for 120 hours (scheme 2.5). However, TLC (thin layer chromatography) of the crude showed four spots, three of them compatible with N-boc-aminophenol, DMAD and $PPh_3$, suggesting that all the starting materials were not completely consumed during the 5 days reaction. Although the extra spot showed the formation of some product, it was decided to leave the reaction for longer, monitoring it with TLC. No changes were observed in the TLC after 7 days, hence the reaction was quenched and the product purified *via* flash chromatographic column. Four fractions were isolated, two of them were the starting materials, the third was a mixture of N-boc-aminophenol and the product, and the fourth fraction was the pure product. The third fraction was further purified to give more pure compound. The product **3a** was successfully obtained with 20% yield and fully characterised. Part of the product was probably lost during the purification step, as an impure fraction of product was isolated after the chromatographic column. Moreover, half of the initial amount of N-boc-aminophenol and DMAD was recovered after purification. This suggested scarce reactivity of the chemicals under the conditions applied, which further explained the low yield obtained.

At this stage, the main purpose was to obtain product **3a** with sufficient yield to allow completion of the three steps synthesis and isolation of sufficient amounts of precursor

**2a**. Given the low yield obtained following the published procedure [18] and the concerns raised by the purification process, an alternative approach was considered. Considering that the product was obtained after refluxing the mixture for over 7 days, it was agreed that the intramolecular lactonization was very energetically demanding. Extensive survey of literature data identified an interesting study by Hekmatshoar *et al*.[19] during which microwave irradiation was used in the synthesis of coumarin derivatives.

Microwaves (MW) are part of the electromagnetic field characterised by wavelengths ranging from 1 millimetre to 1 metre, corresponding to frequencies of 300 GHz to 300 MHz. Microwaves have an effect on the electric charges; polar molecules irradiated by microwaves rotate and align themself with the applied field. The dielectric constant of the material is directly proportional to its ability to convert electromagnetic energy into thermal energy. The bigger the dielectric constant, the more rapidly the material is heated up.[20] MW irradiation applied to organic synthesis has become very popular in the last few years, completely transforming protocols for numerous organic reactions.[21] The use of microwaves, with increased homogenous and rapid heat, accelerates the reactions, allowing the formation of the products in very short time when compared with classical thermal methods. Microwave assisted synthesis has several advantages over conventional reflux, such as uniform and highly efficient heating throughout the material, low operating cost, an increase in process speed and a reduction in unwanted side reactions, obtaining more pure products.[20] Following these considerations, it was decided to adapt the method reported by Hekmatshoar[19] for the synthesis of product **3a**. Although same chemicals were used both in the microwave approach and in the traditional reflux synthesis, significant amount of time was spent in optimising the synthesis and accelerating the process (scheme 2.6).

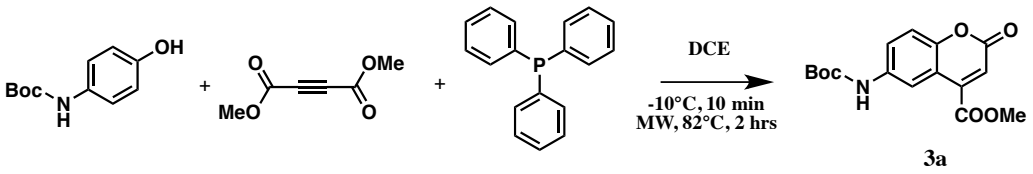


**Scheme 2.6.** Microwave assisted synthesis of monomers **3a**

Generally the optimisation of synthetic procedures tends to focus on two main paramenters: the solvent and temperature. However, in this case the temperature of the reaction was directly dependent on the solvent. The reaction was carried out in a sealed microwave vessels with no possibility for the potential pressure, formed inside the tube, to be released. Hekmatshoar, in his work, used the solvent acetronitrile (ACN). ACN is characterised by a good dielectric constant (ε: 37.5) and high boiling point (82°C), which allows it to reach a high temperature with no concerns about pressure formed inside the microwave tube. ACN was therefore, the first choice in the solvent selection process. However, the reaction mixture was not soluble in this solvent, making it inappropriate for performing the reaction. A suitable alternative choice would have been DCM, which was successfully used in the previous attempt (scheme 2.5) and it was shown to well solubilise the starting materials. However, DCM was discarded upfront due to its low boiling point (bp: 40°C) and low dielectric constant (ε: 8.93). Consequently, dichloroethane was considered as a possible option due to its similarity to DCM in terms of polarity. Although DCE has a dielectric constant smaller than ACN (ε: 10.36), it has a higher boiling point than DCM (bp: 83°C). This allowed to reaching high temperature that seemed to be the key of this step. The reaction was monitored *via* TLC every 30 minutes. After 2 hours no significant changes in the TLCs were noticed; the starting materials were not completely consumed although formation of the product was observed. The reaction was, therefore, quenched and the mixture purified by flash chromatographic column. The product **3a** was isolated in 26.5% yield. The purity of the

target molecule **3a** was confirmed by $^{1}$H-NMR (figure 2.5). The characteristic peaks of the fused rings of the coumarin were assigned using a COSY spectrum, reported in the same figure. The spectrum shows the typical singlet of the boc- protecting group at 1.54 ppm, together with the distinctive peaks of the coumarin moiety in the chemical shift range 8.3 – 7 ppm and the carboxylate singlet at 4 ppm.

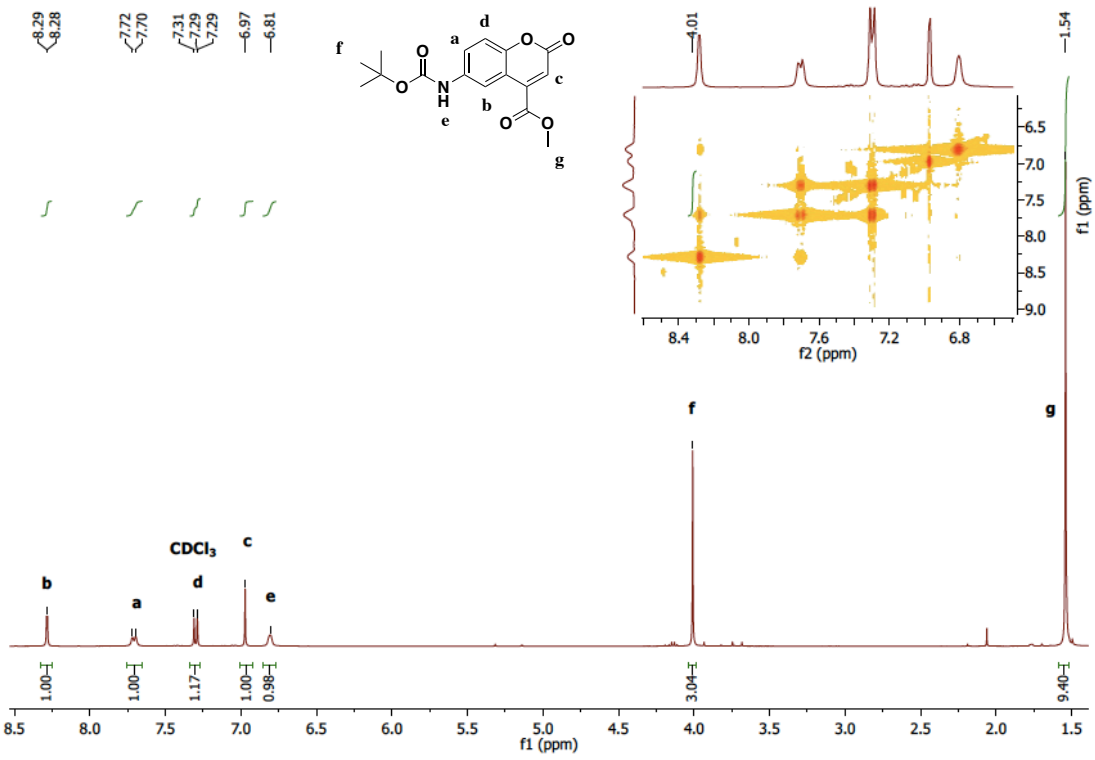


**Figure 2.5.** 400MHz $^{1}$H-NMR and COSY spectrum in $CDCl_3$ of **3a**

Although the yield (26.5%) remained low, more than 5% of product was recovered by using MW assisted synthesis compared to the reflux synthesis previously applied. Moreover, this approach was shown to be incredibly timesaving as the reaction only took 2 hours compared to 7 days of the reflux strategy. It was, therefore, decided to carry on with the rest of the synthetic pathway in order to achieve the synthesis of the monomer **1a**.

### 2.3.1.2: 2nd step – synthesis of 6-aminocoumarin-4-carboxylate (4)

Having obtained compound **3a**, the following step focused on the deprotection of the amine from the Boc group before proceeding to the addition of the acrylic moiety in C6 position.

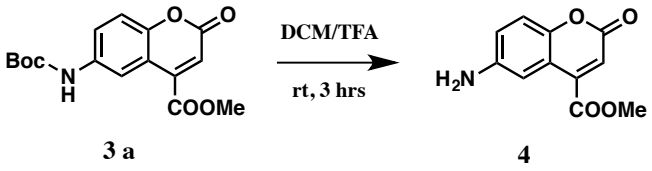


**3 a** **4**

**Scheme 2.7.** Boc cleavage of the compound **3a** to obtain product **4.**

The general approach for Boc cleavage involving TFA in DCM was used to achieve product **4**. The reaction was monitored *via* TLC and quenched only when the starting material was fully consumed. The reaction mixture was then washed with phosphate buffer to remove the TFA salt formed with the amine group, and extracted with DCM. However, after five extractions the TLC of the aqueous phase still showed the presence of the product, suggesting that DCM was not sufficiently polar to allow complete recovery of the product. Ethyl acetate was then used and showed to allow optimal extraction of the product from the aqueous phase, which was obtained with a yield of 86% and fully characterised by $^{1}$H-NMR in $CDCl_3$. The $^{1}$H-NMR spectrum in figure 2.6 shows a shift towards lower ppm of the characteristics peaks of the coumarin moiety. The removed Boc- group exposed the electron-donating amino group, which generated a shielding effect on the aromatic protons, moving the signals. The missing singlet of the Boc group at 1.5 ppm and the new peak at 3.21 ppm, given from the amine, were further confirmation of the successful deprotection.

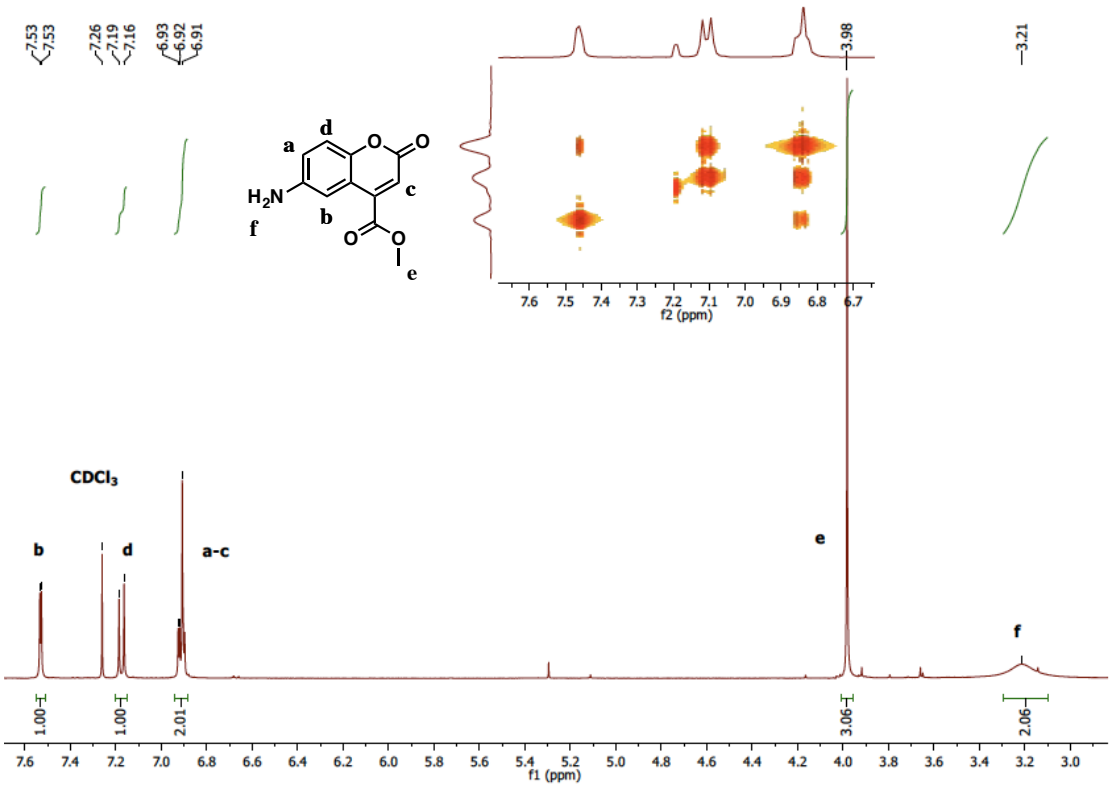


**Figure 2.6.** 400MHz $^1$H-NMR spectrum in $CDCl_3$ of **4**

### 2.3.1.3: 3rd step – synthesis of 6-acrylamidecoumarin-4-carboxylate (2a)

Once product **4** was obtained and characterised, it was possible to add the polymerisable acrylic group.

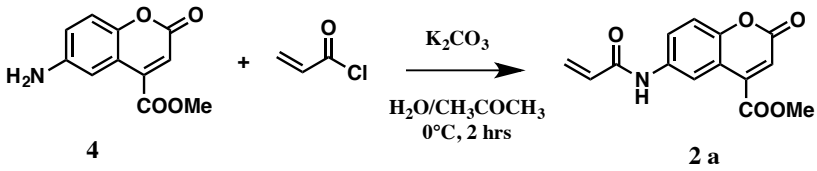


**Scheme 2.8.** Synthesis of precursor **2a**

Product **2a** was successfully obtained in 61% yield by following a method reported in literature by Chanthamath *et al*.[22] The product was insoluble in $CHCl_3$, MeOH and ACN, however it was opportunely solubilised in DMSO and its purity confirmed *via* $^1$H-NMR. COSY spectrum and coupling constant values were used to help assign the correct peaks to the right protons. The spectrum in figure 2.7 shows the characteristic peaks of

the molecule. The singlet at chemical shift 10.45 ppm was originated from the proton of the acrylamide group, which showed the deshielding effect produced by the acrylic group, which caused a shift of the peak to the downfield. The peaks of the acryloyl group in the chemical shift range of 6.47 - 6.27 ppm provided further evidence of the formation of the acrylamide group. Moreover, the typical peaks of the four protons on the fused rings of the coumarin are clearly visible in the chemical shift between 8.47 and 6.91 ppm.

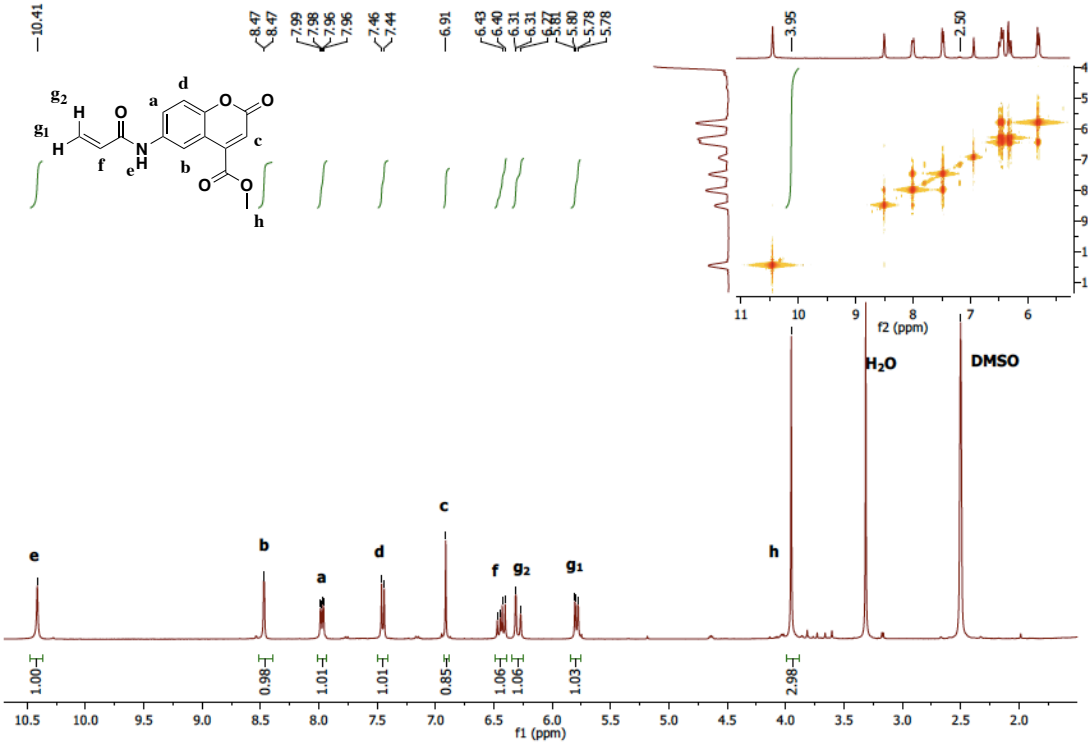


**Figure 2.7.** 400MHz $^{1}$H-NMR spectrum in DMSO of **2a**

### 2.3.2: Towards the synthesis of 6-vinylcoumarin-4-carboxylate (2b)

The strategy represented in scheme 2.9 was identified to achieve the coumarin derivative characterised by the presence of a vinyl group in position C6 (compound 2b).

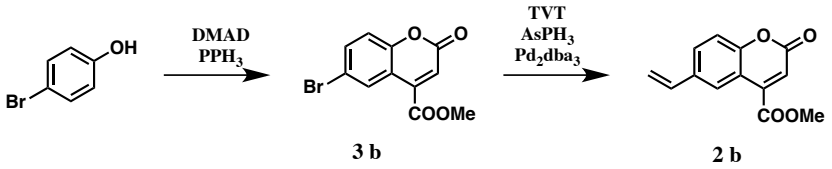


**Scheme 2.9.** Synthetic pathway for the synthesis of precursor **2b**

The two-step synthesis of monomer **2b** was already reported in 2009 by Nguyen *et al*.[23] The first step involved formation of the coumarin skeleton substituted in C6 and characterised by the methyl ester group in C4. The following step involved the addition of the vinyl group in position C6.

### 2.3.2.1. 1st step – synthesis of 6-bromocoumarin-4-carboxylate (3b)

A first attempt to synthesise the product **3b** was carried out by following the procedure published by Nguyen.[23] 4-bromophenol, DMAD and $PPh_3$ were refluxed in DCM for 120 hours, as reported in scheme 2.10. Similar procedure carried out in the synthesis of **3a**, as described in section 2.3.1.1, was applied for the synthesis of **3b**.

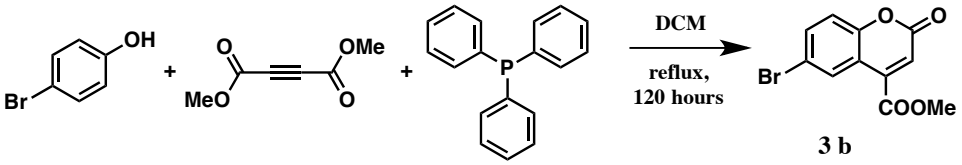


**Scheme 2.10.** Synthetic scheme for **3b**

The literature data reported a purification step based on recrystallization of the crude and further purification of the solid *via* flash chromatography to obtain the product in 52% yield. The same protocol was applied; recrystallization of the crude mixture provided the pure product in 10 % yield. However, TLC showed the presence of residual product in the filtrate. Therefore, the mixture was then evaporated and another recrystallization was carried out, collecting further 6% of pure product. A new TLC showed that the product was not completely recovered, suggesting the inefficacy of the

recrystallization in isolating the product. A flash chromatography column was then performed on the filtrate solution, following the same conditions reported in literature. Unfortunately, no separation of the pure product was achieved in such conditions; the $^{1}$H-NMR spectra showed the presence of both 4-bromophenol and the product in each one of the fractions collected from the column, suggesting a problem in the polarity of the eluent used. The reaction was repeated several times (> 3) and other solvent mixtures commonly used for chromatographic columns, were investigated to obtain a better separation. Although, the maximum yield obtained in one of the attempts was 24% the $^{1}$H-NMR spectrum of the product showed small impurities from the residual starting material 4-bromophenol. Given the similarity in the synthesis of product **3a** and the issues that rose during the product purification and the time-consuming reaction, it was decided to adapt the same approach involving microwave irradiation used and described in section 2.3.1.1. The synthesis was, once again, based on the data published by Hekmatshoar.[19]

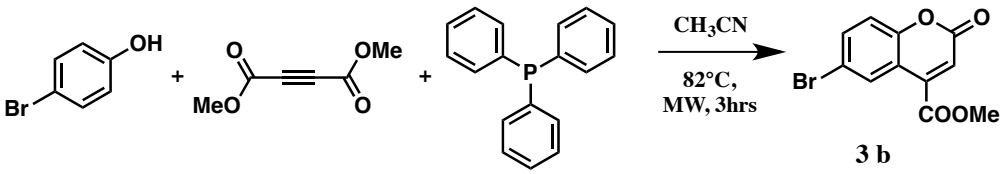


**Scheme 2.11.** Synthesis of **3b** by microwave irradiation.

The synthesis of compound **3b** was carried out in ACN, the same solvent reported in literature [19]. The reaction was monitored *via* TLC and quenched after 3 hours, as no significant differences were observed. The purification step was improved compared to the previous attempt. A gradient elution mode was employed; this allowed to gradually increasing the polarity of the mobile phase to obtain better separation of the compounds. The product **3b** was obtained in 31% yield and the NMR spectrum, reported in figure 2.8, was recorded. The characteristic peaks of the four protons on the coumarin skeleton

were identified in the chemical shift ranging 8.49ppm - 7.01 ppm, whereas the -$CH_3$ of the carboxylate group gave the typical singlet at 4.02 ppm.

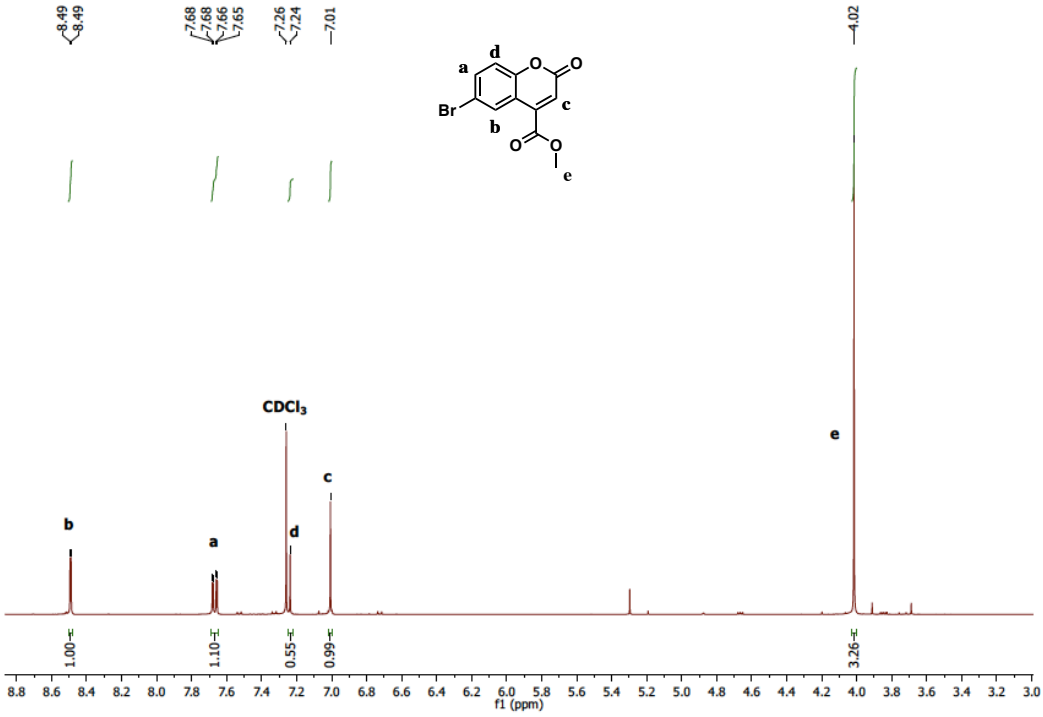


**Figure 2.8.** 400MHz $^1$H-NMR spectrum in $CDCl_3$ of **3b**

### 2.3.2.2: 2nd step – synthesis of 6-vinylcoumarin-4-carboxylate (2b)

The second and final step of the synthesis of the coumarin derivative **2b** was based on the Stille reaction, a C-C coupling between organostannanes and halides catalysed by palladium.[24] The reaction was carried out as reported in literature, by refluxing for 120 hours in THF (tetrahydrofuran).

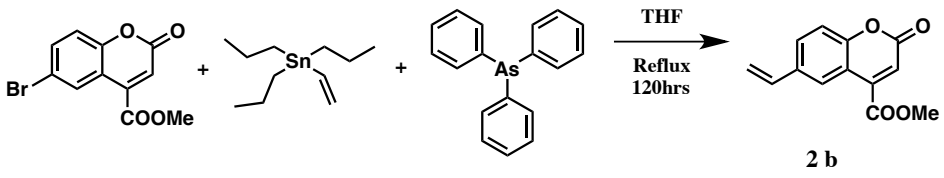


**Scheme 2.12.** Synthesis of compound **2b**

The first attempt to carry out the reaction *via* this approach was a success and product **2b** was obtained with a 30% yield. Nevertheless, this first attempt was done on a small

scale and the final amount obtained (< 10 mg) was insufficient to proceed with the rest of the project. However issues of reproducibility occurred when the reaction was scaled up, in particular in the purification step, which appeared to promote decomposition of the product. Due to time restriction, this approach was not optimised, instead the microwave protocol, which proved to give better results in the synthetic paths already explored, was immediately employed (figure 2.13). The microwave irradiation synthesis was carried out in THF, which was used in the previous attempt involving reflux. Recrystallization from hot ethanol of the crude mixture gave the pure product in 48% yield.

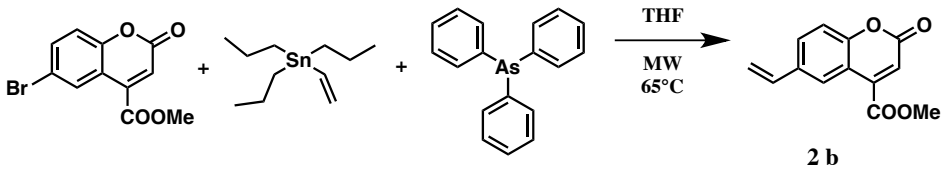


**Scheme 2.13.** Microwave-assisted synthesis of compound **2b**

The spectrum $^{1}$H-NMR, figure 2.9, confirmed the purity of the product showing the doublet of doublet at chemical shift 6.75 ppm derived from the =C<u>H</u>- and the two doublets at 5.78 and 5.33 ppm from the =C<u>H</u>$_2$-, typical of the vinyl group. The usual four peaks of the coumarin and the singlet of the carboxylate are showed in the range 8.27-6.95 ppm and at 4.01 ppm, respectively.

The amount of product **2b** recovered was deemed sufficient to move to the next step.

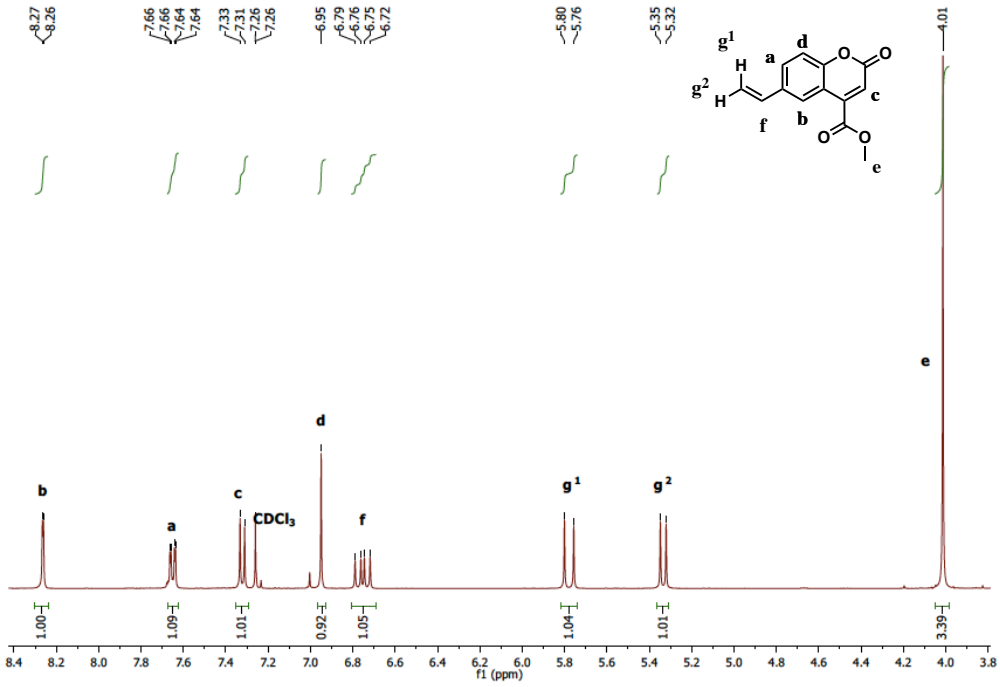


**Figure 2.9.** 400MHz $^{1}$H-NMR spectrum in $CDCl_3$ of **2b**

## 2.4. Fluorescence characterisation of the monomers

The synthesis described in the previous section led to the two precursors, **2a** and **2b**, which purity was assessed by $^{1}$H-NMR. The following step was to evaluate the fluorescence properties of the two precursors. As aforementioned, the high fluorescence yield of the functional monomers is a required feature to provide the final polymer with sufficient fluorescence for future applications. Study the fluorescence properties at this stage of the synthesis was necessary because of the concerns related to the stability of the polymerisable acrylamide group during the hydrolysis step.

### 2.4.1: Fluorescence studies of 6-acrylamidecoumarin-4-carboxylate (2a)

As previously shown during the synthetic procedure, monomer **2a** could only be solubilised in DMSO (see section 2.3.1.3), thus all the fluorescence studies were carried out in this solvent.

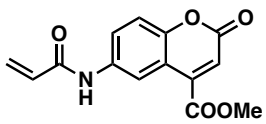


**2 a**

**Figure 2.10.** The molecular structure of precursor **2a**

The UV-Vis spectrum in figure 2.11 shows two peaks at $\lambda_{abs}$= 300nm and $\lambda_{abs}$ = 366 nm. Literature data shows that, although the compound absorbed more at short wavelengths, the emission intensity was higher when the compound was irradiated at longer wavelength.[23] The fluorescence of monomer **2a** was, therefore, evaluated after excitation at $\lambda_{abs}$ = 366 nm.

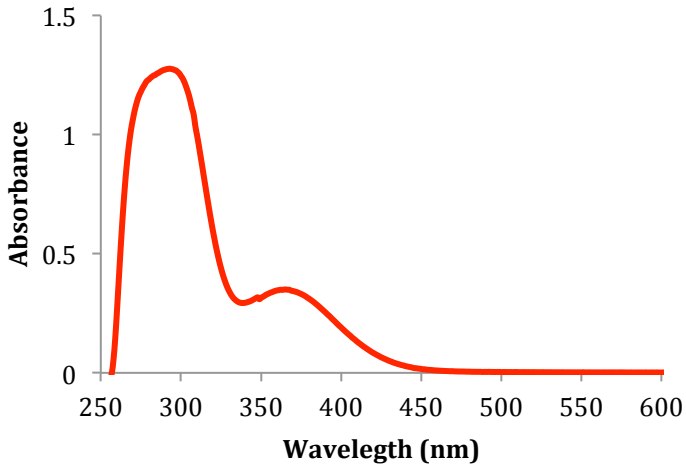


**Figure 2.11.** UV-Vis spectrum of precursor **2a** in DMSO at concentration 0.092mM (0.025mg/mL). Two absorption peaks are shown at $\lambda_{abs}$ = 300 and 366nm

The fluorescence of different solutions of **2a** in DMSO, with varying concentrations, was evaluated in order to identify suitable emission intensity.

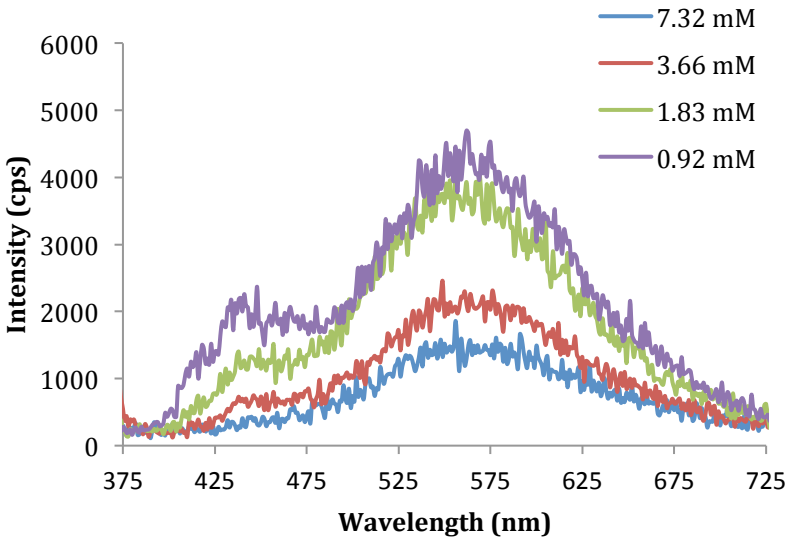


**Figure 2.12.** Fluorescence emission at $\lambda_{em}$ = 557nm following excitation at $\lambda_{abs}$ = 366nm of **2a** in DMSO at different concentration ranging between 0.92 - 7.32mM.

Figure 2.12 shows some evidence of fluorescence emission of **2a**, however the changes in concentrations also provide evidence of quenching. The overall maximum emission was observed at 0.92mM, with no significant change when the concentration was doubled to 1.83mM, suggesting that the emission reached a plateau. Furthermore when the concentration was further increased to 3.66 and 7.32mM respectively, a strong self-quenching effect was observed. This is a regular effect that usually occurs in high concentration and it is caused by the collision of the fluorophore with a neighbouring one. Taking into consideration the requirements in terms of fluorescence intensity for the final polymers, these data clearly indicate that probe **2a** was not a suitable fluorophore for this application.

### 2.4.2. Fluorescence studies of 6-vinylcoumarin-4-carboxylate (2b)

Considering the unexpected results obtained from the fluorescence evaluation of precursor **2a** in DMSO, it was decided to study the fluorescent of monomer **2b** (figure 2.13) in a different solvent.

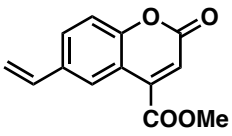


**2 b**

**Figure 2.13.** The molecular structure of precursor **2b**

The UV-Vis spectrum of **2b** was recorded in ACN and showed three main peaks at $\lambda_{abs}$ = 255, 280 and 345nm (figure 2.14).

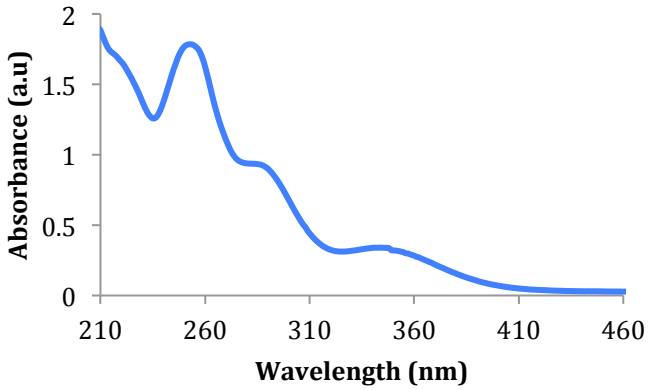


**Figure 2.14.** UV-Vis spectrum of precursor **2b** in ACN at concentration 0.11mM (0.025mg/mL). Three peaks are identified at $\lambda_{abs}$ = 255, 280 and 345nm.

As mentioned in the previous section, in the case of coumarins the long wavelength was selected to have a higher fluorescent emission. Solutions of precursor **2b** were prepared in ACN at different concentration to study the fluorescence emission (figure 2.15).

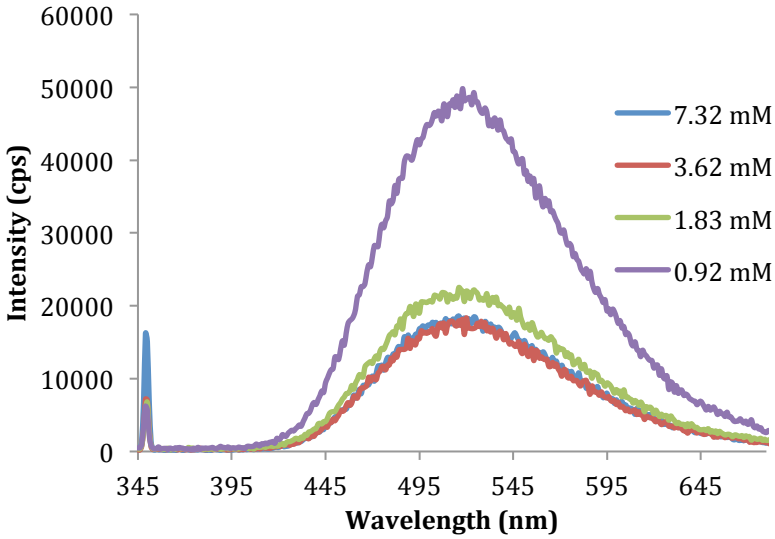


**Figure 2.15.** Fluorescence emission at $\lambda_{em}$ = 510nm, following excitation at $\lambda_{ex}$ = 345nm, of **2b** in ACN in concentrations ranging between 0.92 to 7.32mM.

At a concentration as low as 0.92mM, the precursor **2b** displayed high fluorescence emission, which significantly decreased when the concentration was doubled to 1.83mM, reaching a minimum with 3.62 and 7.32mM. Also in this case a self-quenching effect was observed, as the fluorescence decreases with increasing concentration. However, the overall emission of the precursor **2b** was ten fold higher than what observed for precursor **2a**. This difference could be due to an effect of the solvent. In order to confirm such hypothesis a solution of precursor **2b** at concentration 0.92mM, which reported the highest fluorescence emission in figure 2.15, was prepared in DMSO. The UV-Vis spectrum of **2b** in DMSO (figure 2.16 A) did not show significant differences compared to the spectrum recorded in ACN. Therefore, the **2b** was excited at the lowest wavelength, 345nm (figure 2.16 B).

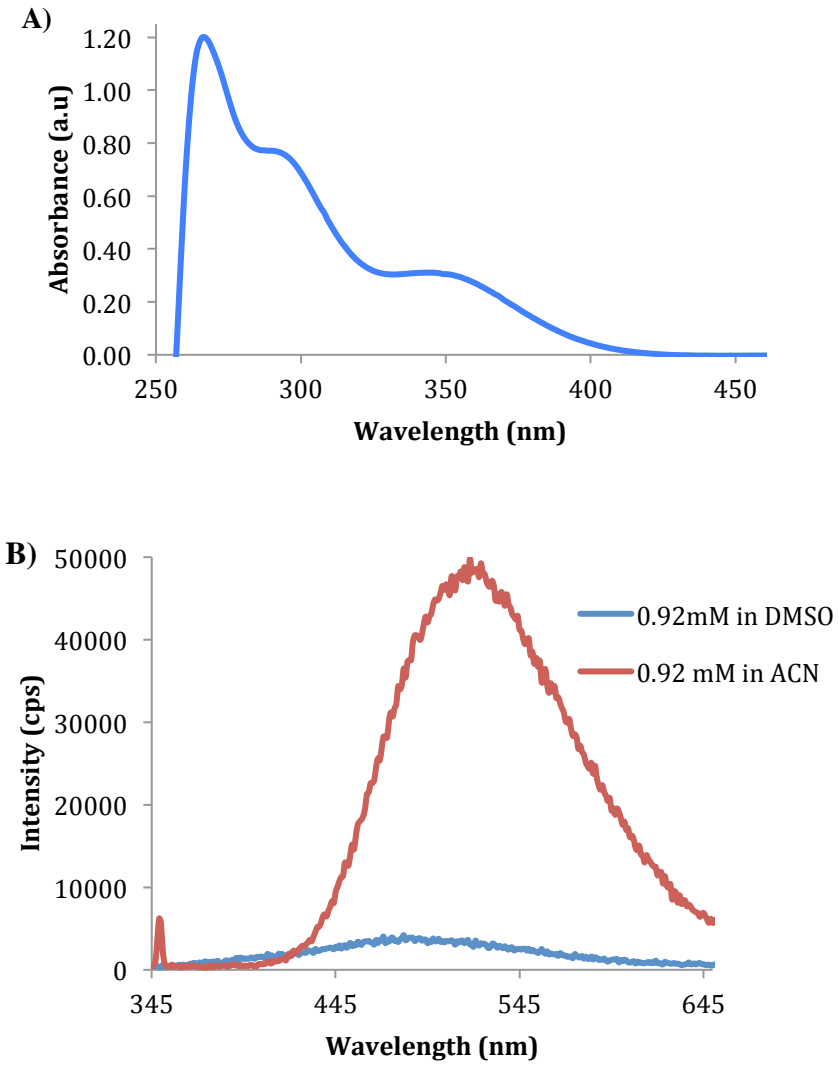


**Figure 2.16.** **A)** UV-Vis spectrum of precursor **2b** in DMSO at 0.11mM (0.025mg/mL). Three peaks are identified at $\lambda_{abs}$ = 270, 280 and 345 nm. **B)** Fluorescent emission at $\lambda_{em}$ = 480 and 510nm, following excitation at $\lambda_{ex}$ = 345nm, of precursor **2b** at the same concentration 0.92mM, but in different solvent.

Figure 2.16 (B) shows the emission of the precursor **2b** in DMSO compared to that in ACN. For equal concentration, the fluorescence in DMSO was significantly lower (<4000cps) than that in ACN (50000cps), clearly proving that the solvent plays a major effect in the fluorescence emission. Although the two molecule **2a** and **2b** had the same core of coumarin, the polymerisable unit demonstrated to have a huge impact on the suitability of using these monomers as fluorescent tags. The change in solubility between the two structures was probably due to a different packing of the molecules in

solution due to intermolecular forces. In fact, the additional groups of the polymerisable acrylamide moiety of the precursor **2a** could generate hydrogen bonding with the carbonyl on the coumarin, contributing in the reduction of fluorescence emission. Only the precursor **2b** showed the required features for further applications. The last step of hydrolysis was carried out on precursor **2b** to obtain the monomer **1b**.

## 2.5. Synthesis of 6-vinylcoumarin-4-carboxylic acid (1b): hydrolysis of 6-vinylcoumarin-4-carboxylate (2b)

The final step of the strategic synthesis required the hydrolysis of the ester group in position C4. The reaction was carried out in basic conditions at 40°C in the dark.

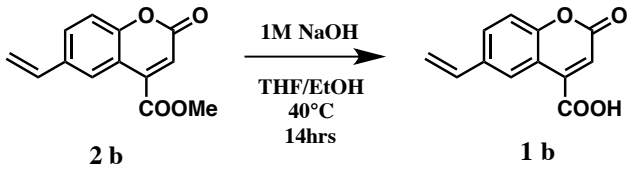


**2 b** **1 b**

**Scheme 2.14.** Basic hydrolysis to achieve monomer **1b**

The reaction was monitored *via* TLC and quenched when the starting materials was completely consumed. The successful of the hydrolysis was assessed by $^{1}$H-NMR. The spectrum, reported in figure 2.17, showed the lack of the singlet of the -COOC$\underline{H}_3$ at δ: 4ppm, confirming the presence of the desired product. The characteristic peaks of the coumarin skeleton and the vinyl group were all identifiable.

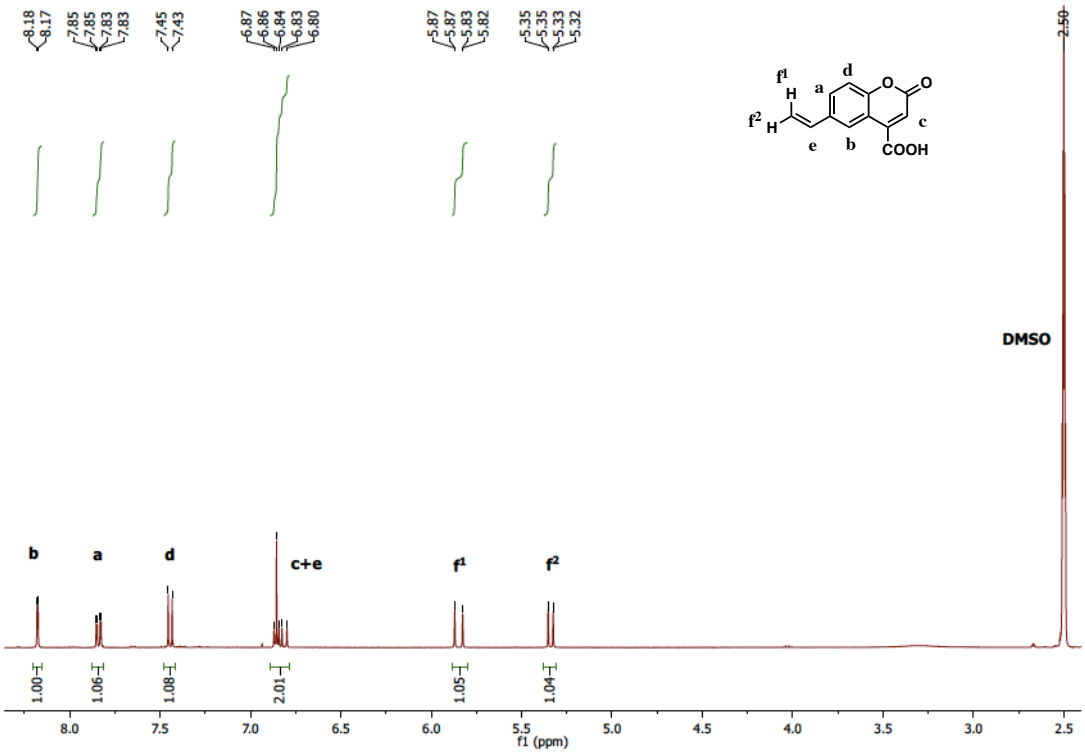


**Figure 2.17.** 400MHz $^{1}$H-NMR spectrum in DMSO of **1b**

## 2.6. Conclusions

The precursors **2a** and **2b** were successfully synthesised and purified with good chemical yields. A new synthetic strategy for the synthesis of coumarin derivatives was identified and optimised. In both cases, data suggested that microwave irradiation significantly improved the synthetic pathway, compared with the more traditional approach based on reflux. By using the novel procedure the reaction time was reduced from 7 days to about 3 hours, with significant reduction of side products, leading to an easier purification protocol, and increased chemical yields.

Fluorescence studies carried out on both monomers identified **2b** as the only suitable compound to be taken forward to the next stage of the work. The fact that **2a** could only be solubilised in DMSO had a clear impact on its fluorescence emission.

The desired monomer **1b** was obtained by hydrolysis of the methyl ester of precursor **2b**. The molecule presented all the necessary characteristics to be used as functional

monomer in the preparation of molecular imprinted polymers for sensing and drug delivery applications.

This will be described in details in the following chapter 3 and 4.

## 2.7. Reference


1. (a) Li, D.; Cheng, W.; Yan, Y.; Zhang, Y.; Yin, Y.; Ju, H.; Ding, S., A colorimetric biosensor for detection of attomolar microRNA with a functional nucleic acid-based amplification machine. *Talanta* **2016,** *146*, 470-6; (b) Zhai, J.; Yong, D.; Li, J.; Dong, S., A novel colorimetric biosensor for monitoring and detecting acute toxicity in water. *The Analyst* **2013,** *138* (2), 702-707.

2. Grieshaber, D.; MacKenzie, R.; Voros, J.; Reimhult, E., Electrochemical Biosensors - Sensor Principles and Architectures. *Sensors* **2008,** *8*, 1400-1458.

3. Josephson, L.; Perez, J. M.; Weissleder, R., Magnetic Nanosensors for the Detection of Oligonucleotide Sequences. *Angew. Chem. Int. Ed.* **2001,** *40*, 3204-3206.

4. Park, S.; Taton, T. A.; Mirkin, C. A., Array-Based Electrical Detection of DNA with Nanoparticle Probes. *Science* **2002,** *295*, 1503-1506.

5. Ray, J. V., Novel molecular imprinted nanogels as drug delivery vehicles for tamoxifen. *A thesis presented in partial fulfillment of the Degree of Doctor of Philosophy at the University of London* **2014**.

6. Wu, L.; Wang, X.; Xu, W.; Farzaneh, F.; Xu, R., The Structure and Pharmacological Functions of Coumarins and Their Derivatives. *Current Medicinal Chemistry* **2009,** *16*, 4236-426.

7. Kangyu, C.; Yuan, G.; Zhenhuan, L.; Bingqin, Y.; Zhen, S., Novel Coumarin-based Fluorescent Probe for Selective Detection of Bisulfite Anion in Water. *Chin. J. Chem* **2010,** *28*, 55-60.

8. Yuan, G.; Jing, A.; Haoyang, T.; Mengjiao, P.; Franck, S., Selective and "turn-off" fluorimetric detection of mercury(II) based on coumarinyldithiolane and coumarinyldithiane in aqueous solution. *Materials Research Bulletin* **2015,** *63*, 155-163.

9. Yin, H.; Zhang, B.; Yu, H.; Zhu, L.; Feng, Y.; Zhu, M.; Guo, Q.; Meng, X., Two-photon fluorescent probes for biological Mg(2+) detection based on 7-substituted coumarin. *The Journal of organic chemistry* **2015,** *80* (9), 4306-12.

10. Wu, J.; Sheng, R.; Liu, W.; Wang, P.; Ma, J.; Zhang, H.; Zhuang, X., Reversible fluorescent probe for highly selective and sensitive detection of mercapto biomolecules. *Inorganic chemistry* **2011,** *50* (14), 6543-51.

11. Liu, Y.; Lv, X.; Liu, J.; Sun, Y. Q.; Guo, W., Construction of a selective fluorescent probe for GSH based on a chloro-functionalized coumarin-enone dye platform. *Chemistry* **2015,** *21* (12), 4747-54.

12. Tran, T. M.; Alan, Y.; Glass, T. E., A highly selective fluorescent sensor for glucosamine. *Chemical communications* **2015,** *51* (37), 7915-7918.

13. Vogel, A., Darstellung von Benzoesäure aus der Tonka-Bohne und aus den Meliloten- oder Steinklee-Blumen" [Preparation of benzoic acid from tonka beans and from the flowers of melilot or sweet clover]. *Blumen. Ann. Phys.* **1820,** *64*, 161-166.

14. Guillemette, A., "Recherches sur la matière cristalline du mélilot" [Research into the crystalline material of melilot]. . *Journal de Pharmacie* **1835,** *21*, 172–178.

15. Freedman, M. D., Oral Anticoagulants: Clinical Indications Pharmacodynamics, and Adverse Effects. *J Clin Pharmacol* **1992,** *32*, 196-209.

16. Borges, F.; Roleira, F.; Milhazes, N.; Santana, L.; Uriarte, E., Simple Coumarins and Analogues in Medicinal Chemistry: Occurrence, Synthesis and Biological Activity. *Current Medicinal Chemistry* **2005,** *12*, 887-916.

17. Alfrey, T.; Price, C. C., Relative reactivities in vinyl copolymerization. *Journal of Polymer Science: Part A: Polymer Chemistry.* **1996,** *34*, 157-162.

18. Yawi, I.; Hekmt-Sboar, R.; Ztmomi, A., A new and efficient route to 6-carboxymethylcoumarins mediated by vinyltriphenylphosphonium Salt. *Tetrahedron Letters* **1998,** *39*, 2391-2392

19. Hekmatshoar, R.; Souri, S.; Rahimifard, M.; Faridbod, F., Novel synthesis of oxygenated coumarins from substituted phenols mediated by vinyl triphenylphosphonium salt under microwave irradiation. *Phosphorus, Sulfur and Silicon* **2002,** *177*, 2827–2833.

20. Ravichandran, S.; Karthikeyan, E., Microwave Synthesis - A Potential Tool for Green Chemistry. *International Journal of ChemTech Research* **2011,** *3*, 466-470.

21. Gawande, M. B.; Shelke, S. N.; Zboril, R.; Varma, R. S., Microwave-assisted chemistry: synthetic applications for rapid assembly of nanomaterials and organics. *Accounts of chemical research* **2014,** *47* (4), 1338-48.

22. Chanthamath, S.; Takaki, S.; Shibatomi, K.; Iwasa, S., Highly stereoselective cyclopropanation of alpha,beta-unsaturated carbonyl compounds with methyl (diazoacetoxy)acetate catalyzed by a chiral ruthenium(II) complex. *Angewandte Chemie* **2013,** *52* (22), 5818-21.

23. Nguyen, T. H.; Ansell, R. J., Fluorescent imprinted polymer sensors for chiral amines. *Organic & biomolecular chemistry* **2009,** *7* (6), 1211-20.

24. Espinet, P.; Echavarren, A. M., The mechanisms of the Stille reaction. *Angewandte Chemie* **2004,** *43* (36), 4704-34.

# Chapter 3

## Development of a detector for tamoxifen and its metabolites based on bulk molecularly imprinted polymers

# 3. Development of a detector for tamoxifen and its metabolites based on bulk molecularly imprinted polymers

## 3.1. Introduction

As already reported in chapter 1, tamoxifen (figure 3.1) is one of the most widely used drugs for anticancer therapy. The drug acts as an antagonist on oestrogen receptors in breast tissues, inhibiting the proliferation of cells and hence the propagation of the tumour.[1] Due to its anti-oestrogen effect, the World Anti-doping Authority (WADA) has listed tamoxifen as one of the prohibited substances. Although the drug is not responsible for enhancing the performance of athletes, it is frequently used in conjunction with doping agents to minimise *gynecomastia* (enlargement of breasts), one of the frequent side effects of doping with steroids.[2] The presence of tamoxifen metabolites in athletes' biological samples is always considered to be a red flag for doping. Unfortunately the evaluation of large numbers of samples is limited by the lack of a fast, cheap and reliable test that would act as a strong deterrent. This was the drive for the development of the work that is described in this chapter and that was published as an article in Analytical Bioanalytical Chemistry.[3]

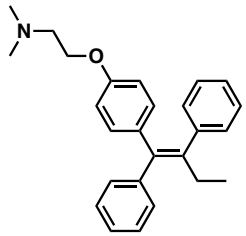


**Figure 3.1.** Molecular structure of tamoxifen

The state of the art regarding the detection of tamoxifen and its metabolites was already discussed in the introduction (session 1.3.2). Although some important advances in terms of accuracy and efficiency were made in the last decade, all reported

methodologies relied heavily on complex instrumentation and trained personnel, which results in associated high cost, limiting the number of samples that can be screened.

Given the high level of interest, one of the objectives of this project was to develop a novel material to be used for the detection of tamoxifen metabolites in athletes' biological samples. The polymer matrix was prepared by molecular imprinting and was characterized based on its optical properties. The results presented in this chapter were organised in two parts, the first one describing the interactions between the functional monomer and the analytes, the second one focusing on the synthesis and characterization of the obtained polymer matrix.

## 3.2. Design of the polymer matrix

The molecular imprinting technique, described in chapter 1 (section 1.2) allows the formation of cavities, which are complimentary in shape and functionalities to the template used. The polymers prepared using this method have the potential to selectively recognise the template molecule. The degree of recognition is highly dependent on the polymer formulation, the monomers structure and ratio, the cross-linking agent, and the experimental conditions. All of the above play an important role and need to be carefully optimised for each application.

### 3.2.1. Functional monomer and template

#### 3.2.1.1. Functional monomer

The functional monomer carries the main functional groups that are relevant for the formation of the interactions with the template *via* covalent, non-covalent or semi-covalent approach (section 1.2). Such interactions play a key role in the formation of imprinted polymers. The stronger and more defined the interactions are, the higher the

selectivity and the imprinting efficiency of the resulting polymer. Molecular imprinting is a promising method for preparing artificial receptors bearing pre-determined binding cavities capable of recognizing target molecules. Molecularly imprinted receptors can also be functionalised in order to produce a specific signal triggered by the binding event. One possible way to obtain this is by functionalising the matrix and incorporating a fluorescent probe close to the binding site. When the analyte is recognised and bound, a change of fluorescence is therefore produced.

Fluorescence spectroscopy is a good technique for sensing analysis, due to its non-invasiveness and high sensitivity (chapter1, section 1.4). Literature data suggested that a common approach for the development of optical sensors involved the use of nanomaterials with intrinsic fluorescent properties, namely quantum dots, carbon dots, carbonanotubes or encapsulation *via* non-covalent interactions of the fluorescent probe in the nanomaterials.[4] However, the latter approach implied a potential decrease in the sensitivity of the nanosensor, due to the possible leakage of the tag. MIPs have largely been employed in the development of optical sensors both for non-fluorescent[5] and fluorescent analytes.[6, 7] An interesting example was reported by Levi *et al.* about the development of optical sensor for the detection of chloramphenicol. The system was based on the competitive displacement of the drug conjugated with the dye methyl red from the cavities of an imprinted polymer.[8] The group prepared different analogous of chloramphenicol in order to determine the ability of the polymer to recognize the target molecule and to better understand the nature of the interactions involved (figure 3.2). This system presented two main drawbacks, HPLC equipment was still required for the analysis and the polymer was not able to sufficiently differentiate the analyte and tiamphenicol, the structural analogue, hence suggesting a lack of specificity.

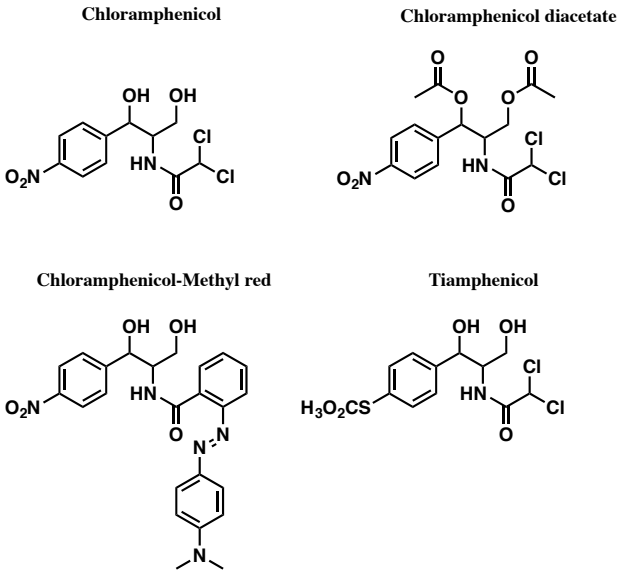


**Figure 3.2.** The target molecule is represented in the top left corner; the chloramphenicol diacetate and the tiamphenicol are the synthesised analogues, while the chloramphenicol-Methyl red is the drug conjugated with the dye

Although the use of expensive and complicated instruments was still largely required when detectors were developed, there was a continuous drive towards innovative applications of MIP in sensing. Two recent interesting examples involved the selective detection of antibiotics, enrofloxacin[9] and vancomycin.[10] Carrasco *et al.* described the preparation of a microarray of optical fibre bundles with MIP microspheres.[9] The advantages of such optical fibres were their reproducibility, resistance to organic solvents and the possibility to be applied in real serum samples with good LOD. While, Korposh and co-workers developed a novel sensor based on a long period grating (LPG) fibre optic. The combination of the LPG with nanomaterials, such as MIPs, produced sensors with high sensitivity and specificity, as demonstrated in their work.[10]

For the purpose of this objective, the efforts focused on the selection of a fluorescent monomer able to give a signal upon binding with the analyte. Chapter 2 described the work done on the design and synthesis of 6-vinylcoumarin-4-carboxylic acid (VCC),

figure 3.3. The fluorescence of VCC, resulting from the conjugation of the benzene and the pyran rings, was evaluated and found to be dependent on the solvent used.

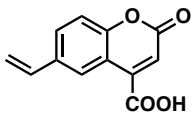


**Figure 3.3.** Structure of 6-vinylcoumarin-4-carboxylic acid, VCC. The monomer designed for this project.

Based on previous knowledge, the monomer and the template were expected to interact *via* π-π stacking and ionic bond, with the strengths of these interactions depending on the solvent system.[11] The aromatic portions of the two molecules, which were the benzene ring fused to a heterocyclic pyran ring and the triphenylethylene moiety, were expected to give rise to π-π stacking, while the amine group of the template could interact with the carboxylic acid of the monomer *via* ionic bonding (figure 3.4).

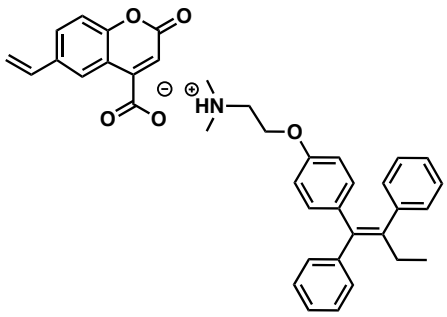


**Figure 3.4.** Schematic representation of the ionic bond between the tertiary amine of tamoxifen and the carboxylic acid of the monomer

### 3.2.1.2. The template

As already mentioned the preparation of MIPs is based on the formation of strong interactions between the imprinting species and the functional monomer. One of the issues that might occur during development of a MIP is that, despite numerous and repetitive washings of the final material, trace amounts of the template (generally <1%) may remain entrapped within the cavities. This could leak during analysis and interfere with accurate determinations.[12] This may not represent a problem for application in

catalysis or separation of mixtures. However, when MIPs are used in sensing and analysis of traces levels, the template bleeding cad cause false positive results. In order to address this issue of potential template contamination of the samples, three main approaches are reported in literature. These are the use of strong solvent in combination with acids, use of specific triggers like temperature, and use of template analogous. Rashid *et al.* were able to quantitatively elute the tamoxifen employed in the preparation of a MISPE (molecularly imprinted solid phase extraction) by using stronger washing conditions.[13] Although a mixture of methanol-acetic acid, in different ratios, was used for washing out the tamoxifen, the drug was not fully recovered and the group experienced some leakage during the application, causing significant interference. A mixture of acetonitrile and acetic acid 4 to 1 was eventually required to completely wash the tamoxifen out. Zander *et al*. demonstrated that by using a combination of heat-treatment and numerous washings of the polymer with strong solvents, 95% of template removal was achieved, compared with removal of 60-90% when weaker solvents were used.[14] Although successful, such protocols were highly dependent on the type of polymer matrix and functional monomers.

A more common approach, identified to avoid false positive during the analysis, is based on the use of a structural analogue of the target molecule as template[15]. This could result in loss of specificity, if the structural similarities are limited, and therefore great care has to be exercised when choosing such analogue. For the synthesis of MIP in this work, clomiphene, a chlorinated analogue of tamoxifen, was chosen as template. Its chemical structure is represented in figure 3.5.[16]

Clomiphene was first synthesised in 1956 at William S. Merrell Company. Although the successive experimentation in rats showed antifertility properties of clomiphene, the evaluation of its biological activity in human females resulted in an unexpected reversed

behaviour.[17] In fact, just like tamoxifen, clomiphene is part of the SEM (selective oestrogen modulators) family, acting both as the agonist or the antagonist in different species, organs, tissues and cell type. Clomiphene was found to induce the ovulation in female patients affected by amenorrhea and anovulation, thus becoming widely and successfully used in the treatments of female infertility. The drug inhibits oestrogen receptors in the hypothalamus, stimulating the release of the two main gonadotropins, the FSH (follicle-stimulating hormone) and LH (luteinizing hormone), leading to follicular growth, ovulation and pregnancy.[18]

The structure of clomiphene is very similar to tamoxifen, with one chlorine atom to replace the ethyl group and a di-ethylamine instead of the di-methylamine (figure 3.5). The use of the analogue was not expected to have a significant impact on the molecular recognition ability of the matrix. The binding sites in the tamoxifen molecule were identified as the amino group, for potential ionic interactions and the three aromatic rings, for π-π stacking. Such moieties were still present in the molecule of clomiphene.

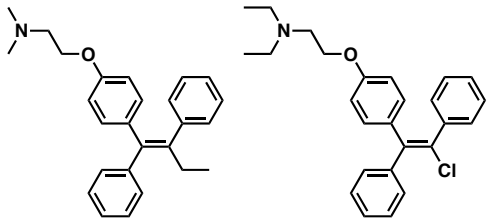


**Figure 3.5.** Molecular structure of tamoxifen and clomiphene. The binding sites, as the tertiary amine and aromatic groups are present in both structures

### 3.2.2. Interaction studies of functional monomers and analytes.

Previous results reported by Nguyen *et al.* demonstrated that VCC could be applied as a fluorescent monomer in the preparation of a molecular imprinted sensor for chiral amines.[19] By using (-)-ephedrine as the template, the group prepared MIPs in which the strong florescence of the coumarin unit was quenched after molecular recognition of the

amines and template. The interactions between the monomer and ephedrine were proved to occur *via* hydrogen bonds between the carboxylic acid on the fluorophore and the amine on the template. Given the similarity of the system described by Nguyen and the system proposed here, a comparable behaviour and a quench of fluorescence upon binding of the analytes were expected. Nevertheless, studies on the interactions between VCC and the analytes were carried out to ensure the formation of a detectable signal triggered by the binding of the target molecules. Three analytes were investigated: clomiphene (CLO), the structural analogue of the drug, tamoxifen (TAM) and 4-hydroxytamoxifen (4-OHT), one of its main metabolites (figure 3.6).

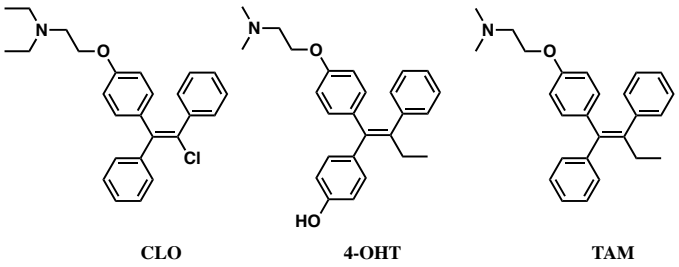


**Figure 3.6.** Structure of the three analytes from left to right: CLO - clomiphene, 4-OHT - 4-hydroxytamoxifen, TAM - tamoxifen

The first step in this work focused on the identification of the optical characteristics of VCC. In order to favour the formation of non-covalent interactions between VCC and TAM a polar, non-protic solvent was necessary. Literature research showed that Ansell's group employed NMR titration and data analysis to study the association of ephedrine and the carboxylic acid of the methacrylic acid. The group successfully demonstrated that strong interactions were obtained using the solvent acetonitrile (ACN).[20] It was, therefore decided to perform the interaction studies in the same solvent. The UV-Vis spectrum of the monomer, recorded in ACN, showed the presence of three main peaks at $\lambda_{abs}$ = 260, 280 and 345nm, respectively (figure 3.7).

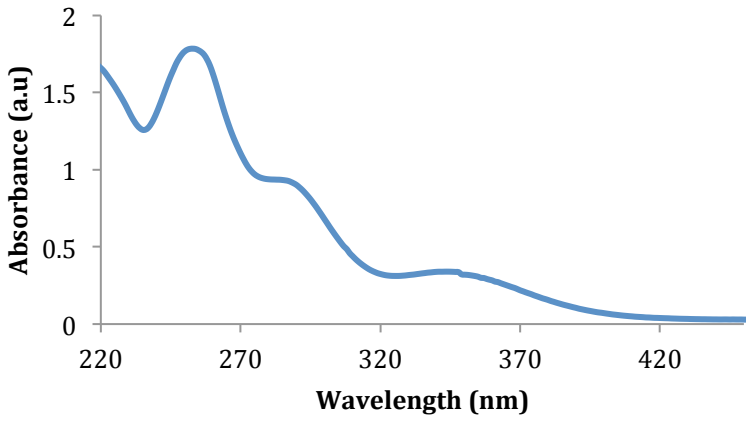


**Figure 3.7.** UV-Vis spectrum of VCC in ACN at 0.11mM. Three main peaks are identified at $\lambda_{abs}$ = 260, 280 and 345nm

Although the UV-Vis spectrum showed $\lambda_{max}$ = 260nm, the fluorescence spectrum was recorded after excitation at $\lambda_{ex}$ = 345nm. In fact, literature data showed that the fluorescence emission of the monomer VCC was more intense after irradiation at $\lambda_{ex}$ = 345nm, rather than $\lambda_{ex}$ = 260 or 280nm.[19] Figure 3.8 shows the strong emission of VCC at $\lambda_{em}$ = 521nm, following excitation at $\lambda_{ex}$ = 345nm.

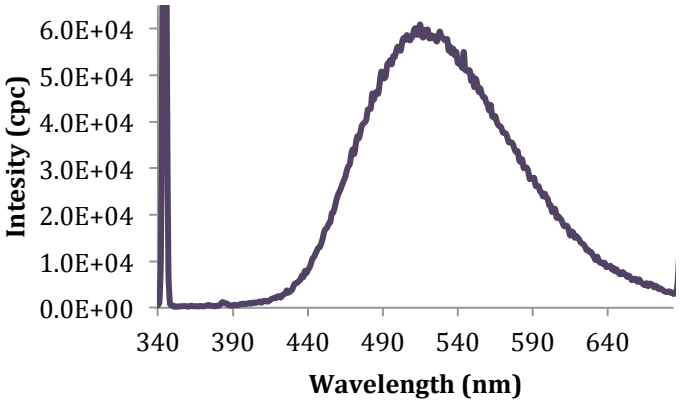


**Figure 3.8.** Emission spectrum of the functional monomer, VCC, at $\lambda_{em}$ = 521nm, after excitation at $\lambda_{ex}$ = 345nm. [VCC] = 2.97x10$^{-4}$ M in ACN, emission slit 1.5

In order to study the effect of the analytes concentration on the fluorescence intensity of VCC, six different solutions containing monomer-analyte ratios ranging between 0 and 5 were prepared (table 3.1).

**Table 3.1.** The appropriate volume of CLO, TAM and 4-OHT from stock was added to 1 mL of VCC stock solution ($5.93x10^{-4}$ M) followed by addition of ACN to give a total volume of 2 mL (the minimum volume required by fluorimeter limitation).

| **Ratio VCC : Analyte** | **Final [VCC] solution** | **Final [Analyte] solution** | **Final volume in ACN** |
|---|---|---|---|
| 1:0 | $2.97x10^{-4}$ M | - | 2 mL |
| 1:0.25 | $2.97x10^{-4}$ M | $7.4x10^{-5}$ M | 2 mL |
| 1:0.5 | $2.97x10^{-4}$ M | $1.49x10^{-4}$ M | 2 mL |
| 1:0.75 | $2.97x10^{-4}$ M | $2.23x10^{-4}$ M | 2 mL |
| 1:1 | $2.97x10^{-4}$ M | $2.97x10^{-4}$ M | 2 mL |
| 1:5 | $2.97x10^{-4}$ M | $1.48x10^{-3}$ M | 2 mL |

Each solution was kept at room temperature for 5 minutes before being analysed. The fluorescence was recorded after irradiation at $\lambda_{ex}$ = 345nm, monitoring the emission between $\lambda_{em}$ = 345-680nm. The data obtained are reported in figure 3.9

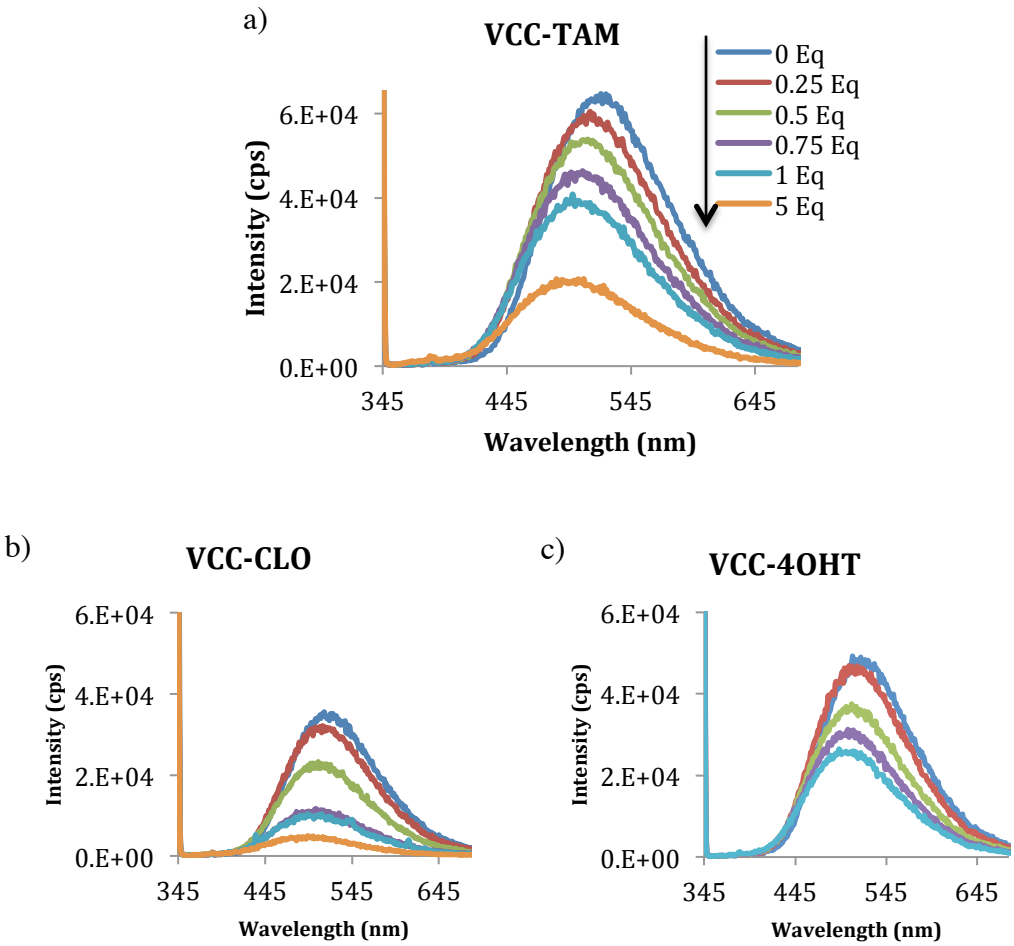


**Figure 3.9.** Fluorescence quenching of the monomer 6-vinylcoumarin-4-carboxylic acid following addition of increasing concentrations of the analytes: tamoxifen **(a)**, clomiphene **(b)** and 4-hydroxytamoxifen **(c)**. Fluorescence spectra recorded after excitation at $\lambda_{ex:}$ 345 nm. [VCC] = $2.97 \times 10^{-4}$ M, $V_{tot}$ = 2 mL.

Figure 3.9-a shows the effect of increasing amount of tamoxifen on the fluorescence emission of VCC, while figure 3.9-b and -c show the effect of clomiphene 4-hydroxytamoxifen, respectively. As expected, based on available literature data, there was a direct relationship between the quenching of VCC fluorescence and the concentration of analytes, together with a mild hypsochromic shift (shift of the emission bands towards shorter wavelength). 4-OHT was expensive to acquire and not easily available, therefore it was decided to evaluate the large monomer-analyte ratio (1:5) only with tamoxifen and clomiphene, which were cheaper and more easily obtained.

Results showed a further quench of fluorescence by TAM and CLO in such conditions. Considering the comparable trend of quenching obtained by the three analytes, it was possible to assume that a further quenching of VCC would be recorded in higher ratios of 4-hydroxytamoxifen.

A potential explanation for the observed fluorescence quench and the hypsochromic shift could be found on the fact that coumarin molecules were not characterized by a big separation in energy between the states π, π* and n, π* and were, therefore, easily perturbed. Moreover, in VCC a π, π* state may lie below the n, π *, this could explain the intense fluorescence of VCC and the blue shift. The π ← π * transitions were more intense than n← π * transitions.

Figures 3.9-a, -b and -c show a variation in the fluorescence intensity of the samples 1:0, containing only the monomer, regardless the quencher. Such variation was probably due to human error while preparing the samples or to errors related to the instruments (balance/fluorometer), however it is possible to assume that the same errors were maintained within each set of sample, prepared and tested at the same time. Therefore, to be able to compare the effects obtained by each analyte, the data were expressed as percentage of VCC residual fluorescence, following addition of the quencher solution (figure 3.10). In order to consistently evaluate the intensity value of fluorescence, it was decided not to take into account the small blue shift effect (hypsochromic shift) and to measure the emission intensity at fixed wavelength $\lambda_{em}$ = 521nm. After averaging the triplicates, the results were then compared with the VCC fluorescence value, which was normalised to 100.

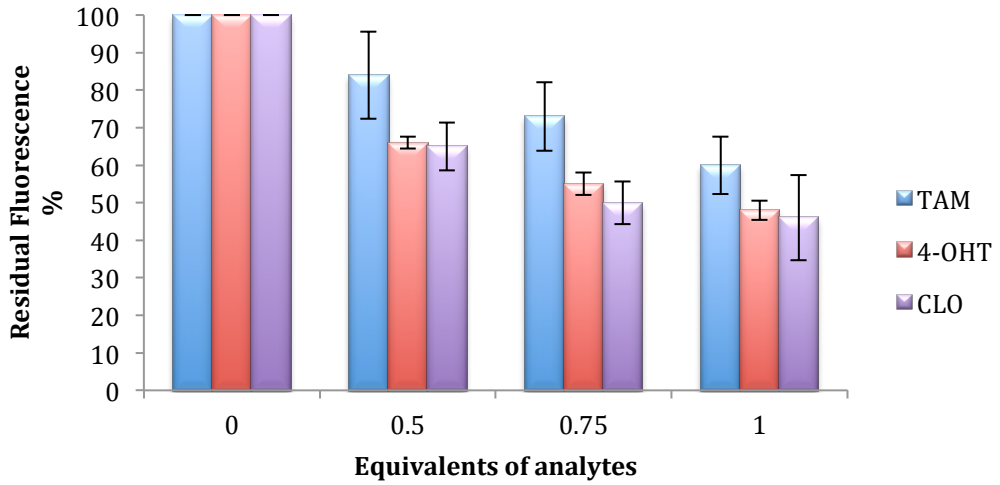


**Figure 3.10.** Percentage of residual 6-vinylcoumarin-4-carboxylic acid monomer (VCC) fluorescence, following addition of the tamoxifen (TAM), 4-hydroxytamoxifen (4-OHT) and clomiphene (CLO) in increasing concentrations in ACN. VCC fluorescence is normalised to 100. Fluorescence spectra recorded after excitation at $\lambda_{ex:}$ 345nm and read at $\lambda_{em:}$ 521nm. [VCC] = $2.97 \times 10^{-4}$ M, $V_{tot}$ = 2 mL

By normalising the values recorded for samples 1:0, containing only VCC, it was possible to minimise the variation in fluorescence previously observed. By using this approach to plot the experimental data, a more significant comparison of the effect of the three different quenchers on VCC fluorescence could be carried out. The three analytes showed progressive and rapid quenching of fluorescence as a function of increasing concentration. The experimental conditions, concentrations, solvent and set-p were all kept constant during the tests. Therefore any variation in the residual fluorescence could be attributed to the variations in chemical structure of the molecule, which, ultimately, influence the interactions with the monomer. CLO and 4-OHT were able to quench 54% and 52%, respectively, of the monomer fluorescence, compared to 40% quenching obtained with TAM. Interestingly, 4-OHT was a stronger quencher than TAM, in any of the ratios. Although the variation in structure was minimal, the presence of the hydroxyl group in the metabolite played a key role in the binding interaction, probably *via* strong hydrogen bonds. However, the smaller quenching of TAM

compared to 4-OHT was not a cause of concern. In fact, tamoxifen is normally metabolised shortly after it is consumed, therefore, in potential applications in real samples, the metabolite 4-OHT would be the main analyte.

Having obtained evidence of interactions between VCC and CLO, TAM, 4-OHT by quenching of the monomer fluorescence, the next step focused on the characterisation of the polymeric matrix.

## 3.3. Preparation of the molecularly imprinted polymer

### 3.3.1. Choice of format polymer

The different polymer formats have been described in chapter 1. Nowadays the imprinted polymers in the bulk format are still very widely used for sensing applications. Bulk polymerisation is considered one of the simplest synthetic processes for MIP. The grinding and sieving procedures of the final monoliths are easy to optimise. The bulk format was therefore chosen for the development of the optical detector. Dr. Judith Ray, a previous member of the Resmni's research group, synthesised the polymers employed in this work during her secondment at Polyintell. This is a French company specialised in bulk MIPs for applications as solid phase extraction (SPE) absorbent material for sample clean-up in food safety or environmental analysis, life science and pharmaceutical R&D.[21,22] The polymers were then shipped to Queen Mary University of London, where they were tested and analysed for their potential applications as detector of tamoxifen and its metabolites.

### 3.3.2. Polymers synthesis (carried out by Dr. Ray)

Although the synthesis of the polymers for sensing application was carried out by Dr. Ray, it is briefly reported in this section for completeness. The synthesis of molecular

imprinted polymers involved a careful evaluation of the possible combination of backbone monomers (BM) and cross-linking agents (XL), which led to the selection of methacrylic acid as BM and EDGMA as cross linker. The chosen porogenic solvent was ACN, as this solvent was shown to favour the formation of strong interactions between FM and T.[20] After different attempts the synthesis of MIP and the corresponding NIP was optimised using the ratio 1:1:3:20, T/FM/BM/XL (clomiphene, 6-vinylcoumarin-4-carboxylic acid, methacrylic acid and EDGMA respectively), with 80% crosslinker and a 1:1 ratio between clomiphene and VCC. 95% template removal was obtained after braking, grounding and sieving the bulk polymers and after several washings with 2.5 % acetic acid in methanol. The template seemed to be hard to remove completely from the MIP; nevertheless the left over template, being it an analogue of the analyte, was not expected have an impact in the analysis. Before being sent to Queen Mary University of London, the size of the particles was confirmed between 45 and 25 μm. Moreover, the different binding capacities of the polymers, both MIP and NIP, towards the analytes were evaluated. The imprinted polymer showed a superior molecular recognition capacity towards clomiphene and tamoxifen compared to the non-imprinted polymer, with an IF =21.7 and 18.7, respectively. Rebinding experiments were also carried out on both MIP and NIP confirming the imprinting effect of MIP. As expected, the imprinted polymer showed higher affinity towards the template than towards tamoxifen, while the non-imprinted polymer showed very little rebinding affinity with similar values for both clomiphene and tamoxifen.

### 3.3.3. Interaction studies of MIP-analytes

The interactions between the polymers and the analytes were investigated as a function of the matrix fluorescence quenching. The amount of VCC incorporated in the polymer ($VCC_{MIP}$) was calculated at Polyintell by fluorescence, using a reference line. It was

found to be $2.36x10^{-4}$ moles of VCC per milligram of imprinted polymer; such value was then used to prepare solutions of known ratios $VCC_{MIP}$-analytes.

#### 3.3.3.1. Optimization of the method

Preliminary studies were carried out by testing the change of MIP fluorescence in relation to tamoxifen, exploring a range of ratio $VCC_{MIP}$-TAM between 0 and 5. Due to lack of polymer the fluorescence measurements were carried out on a plate reader, which allowed using small amounts of material and volumes. The solutions $VCC_{MIP}$-TAM were prepared in ACN into the wells of a standard 96-well plate, in order to minimize as much as possible any loss of material. Control solutions were also prepared with the polymer at the same initial concentrations, to monitor the effect of the dilution on the fluorescence. The results, reported in figure 3.11, showed that the fluorescence of the MIP was gradually quenched as the concentration of tamoxifen increased. The data demonstrated the ability of the polymer to rebind tamoxifen into the cavities and to provide a detectable signal. Moreover, it was proved that VCC maintained its capability to establish interactions with the target molecule, although being incorporated within the polymeric matrix. On the other hand, the control solutions showed a constant value of fluorescence emission, independently from the dilution. This confirmed that the quenching observed in the presence of the drug was a direct result of the interactions between the matrix and tamoxifen, as opposed of an effect due to the dilution of the sample.

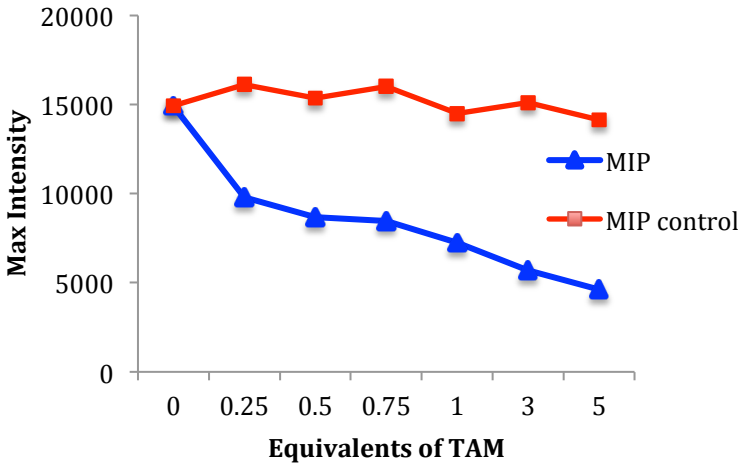


**Figure 3.11.** Fluorescence intensity of MIP (5 mg/mL in ACN, $1.18 \times 10^{-3}$ M in VCC), following the addition of increasing amount of tamoxifen, compared to successive dilution of MIP solution. Fluorescence recorded with FLUOstar OPTIMA plate reader; the excitation filter used was 340-10 and the emission filter was 510-20

Once established that the methodology used provided encouraging results, it was then applied to evaluate the interactions between the polymer and the other analytes.

### 3.3.3.2. Fluorescence studies of MIP-analytes.

The same procedure described in the previous section was employed to investigate the interactions of MIP with TAM, 4-OHT and CLO. Five solutions containing $VCC_{MIP}$-analytes, with ratio ranging between 0 and 1, were prepared as showed in table 3.2.

**Table 3.2.** Solutions of MIP/NIP containing an increasing amount of analytes compared to the functional monomer incorporated for fluorescence quenching studies.

| Ratio $VCC_{MIP}$-Analyte | n° of moles of VCC in MIP | n° of moles of Analyte |
|---|---|---|
| 1:0 | $2.36x10^{-7}$ mol | - |
| 1:0.25 | $2.36x10^{-7}$ mol | $5.9x10^{-8}$ mol |
| 1:0.5 | $2.36x10^{-7}$ mol | $1.18x10^{-7}$ mol |
| 1:0.75 | $2.36x10^{-7}$ mol | $1.77x10^{-7}$ mol |
| 1:1 | $2.36x10^{-7}$ mol | $2.36x10^{-7}$ mol |

The data presented here were expressed as a percentage of MIP residual fluorescence following addition of the quencher to the solution. After averaging the duplicates, the results were then compared with the value obtained by the MIP fluorescence, which was normalised to 100.

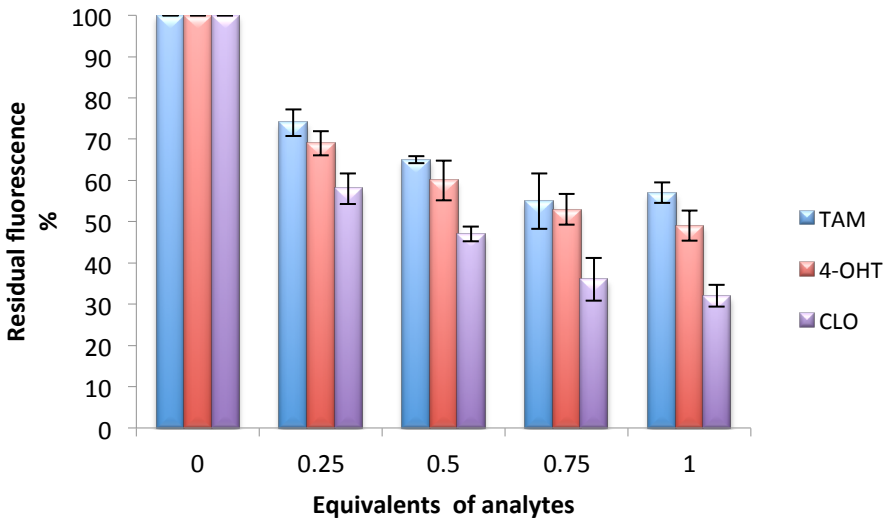


**Figure 3.12.** Residual fluorescence of MIP (5 mg/mL in ACN, $1.18x10^{-3}$ M in VCC), following the addition of varying equivalents of analytes (tamoxifen, 4-hydroxytamoxifen and clomiphene). Fluorescence recorded with FLUOstar OPTIMA plate reader; the excitation filter used was 340-10 and the emission filter was 510-20. Data are presented as percentage of residual fluorescence compared to the MIP fluorescence

The results, showed in figure 3.12, confirmed the formation of interactions between MIP and all the analytes, which generated a quench of the matrix fluorescence.

Interestingly, the progressive quenching of the MIP followed the same trend already showed in figure 3.10 in which the fluorescence of the non-polymerised VCC, quenched by the analytes, was reported. This suggested that the incorporation of the functional monomer within the polymeric network did not affect its binding sites, maintaining the ability of VCC to interact with the target molecules. Clomiphene showed to be the strongest quencher, followed by 4-hydroxytamoxifen and tamoxifen. This result confirmed the higher affinity of the polymeric matrix towards the template, already measured with the re-binding experiments carried out at Polyintell. Table 3.3 shows a summary of the percentage of MIP/VCC fluorescence quenching following addition of the analytes. Higher quenching by each of the analytes was obtained in case of MIP, providing clear evidence of the formation of selective 3D cavities that involve tighter interactions with the target molecules. This was noticed in particular when using a ratio $VCC_{MIP}$/VCC-CLO 1:0.5 in which the quenching of MIP was 1.5 times bigger than what observed in case of VCC functional monomer. However, the difference in quenching, between the MIP and VCC, decreased as the ratio increased, probably as the saturation point of the MIP was being approached.

**Table 3.3.** Summary of percentage of MIP/VCC fluorescence quenching following addition of analytes.

| Ratio | VCC:TAM | MIP:TAM | VCC:4OHT | MIP:4OHT | VCC:CLO | MIP:CLO |
|---|---|---|---|---|---|---|
| 0.5 | 16% | 35% | 34% | 40% | 35% | 53% |
| 0.75 | 27% | 45% | 45% | 47% | 50% | 64% |
| 1 | 40% | 43% | 52% | 64% | 54% | 68% |

### 3.3.4. Visual detection of clomiphene

One of the main objectives of this work was to develop a polymeric matrix with potential application as detector for fast and easy screening, without using complex

equipment. Having confirmed the generation of a signal, detectable with a fluorimeter/plate reader, the feasibility of using the MIP as material for the development of a visual detector was evaluated. A new set of preliminary experiments was, therefore, designed and optimised in order to assess with the naked eye the quenching of MIP fluorescence in relation with the strong quencher clomiphene. Four glass vials were prepared containing MIP and NIP in ACN. To each vial, an increasing amount of clomiphene was added to obtain a ratio $VCC_{MIP}$:CLO ranging between 1:0 to 1:1. The samples were placed in a dark room under a standard 365nm UV light and observed with the naked eye. Figure 3.13 (A and B) shows the images taken in such conditions. When the four vials containing NIP and CLO were irradiated with the UV lamp, no significant changes in the fluorescence brightness were visible, regardless the concentration of CLO (figure 3.13-A). While, when the vials containing MIP and CLO were placed in the same conditions, a clear difference in emission between the vials was detected (figure 3.13-B). In particular, the fluorescence brightness of the solutions decreased as the amount of CLO increased from 0 to 1 equivalent.

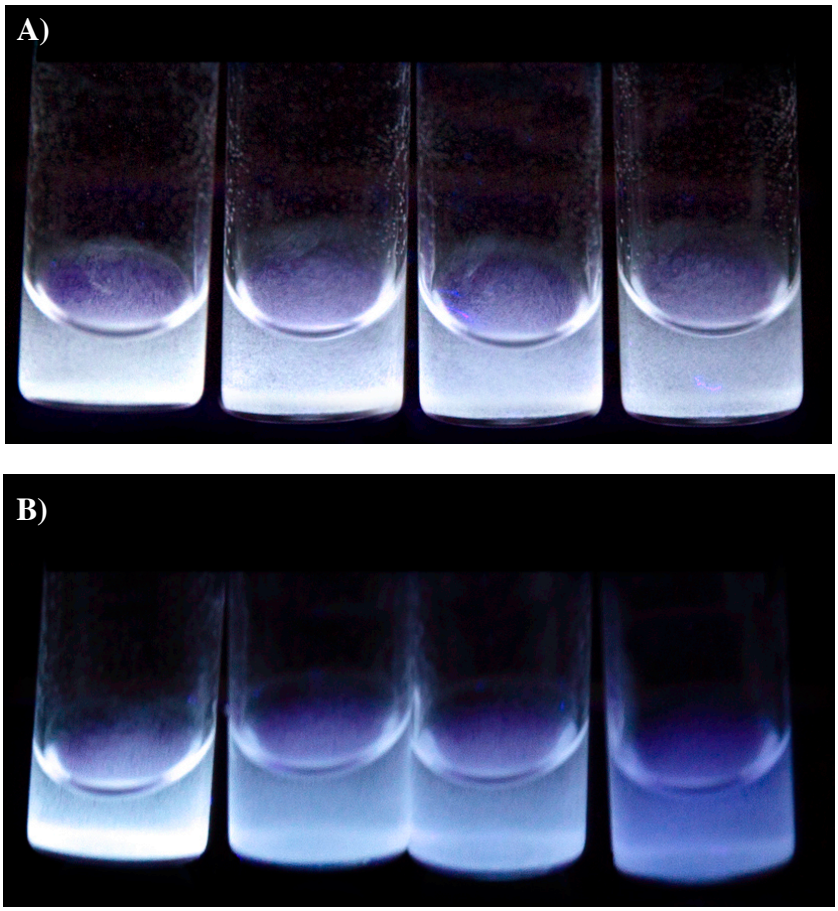


**Figure 3.13.** Visual detection of clomiphene with NIP and MIP by using a standard 365 nm UV light. **A) NIP** solutions from left to right, ratio of fluorophore - clomiphene 1:0, 1:0.5, 1:0.75, 1:1. No significant variation in fluorescence by increasing the amount of clomiphene can be detected. **B) MIP** solutions from left to right, ratio of fluorophore - clomiphene 1:0, 1:0.5, 1:0.75, 1:1. A clear quenching of fluorescence by increasing the amount of clomiphene from 0 to 1 equivalents is shown

These preliminary results were very encouraging, as it represented a first step towards the use of this material in the development of a visual sensor for easy detection of the drug. Moreover, the difference between the two matrices reinforced the HPLC data previously obtained, which showed the higher binding affinity of the imprinted polymer towards the template, when compared to the non-imprinted counterpart. The very little change of fluorescence in the NIP, in comparison to the significant fluorescence quenching observed in the MIP, suggested a lack of cavities in the non-imprinted network that would allow tighter interactions with CLO, and thus higher quenching.

## 3.4. Conclusion and future work

VCC was identified as a suitable fluorescent functional monomer for the preparation of MIP with potential application as detector of tamoxifen and its metabolites. Data demonstrated that interactions between the functional monomer and clomiphene, tamoxifen and 4-hydroxytamoxifen provided a measurable effect on the fluorescence of the monomer. In fact, the residual fluorescence of VCC progressively reduced as the amount of CLO, 4-OHT and TAM increased from 0 to 1 equivalents.

Having confirmed the interactions between the monomer and the targets, an imprinted polymer was obtained in bulk format using clomiphene as template. The use of structural analogues of analyte is a very common technique in the synthesis of MIP intended for detection and trace analysis. This way any potential bleeding of analyte during the analysis, which could lead to false positive results, is minimised. The imprinted polymer was characterized by good molecular recognition properties in ACN towards clomiphene and tamoxifen, with imprinting efficiencies of 21.7 and 18.7, respectively. The larger affinity of the MIP towards clomiphene was also confirmed by fluorescence study. Although significant fluorescence quenching was obtained when the MIP was in contact with each of the analytes, CLO provided a bigger quenching. This was proved to be consistent with the data obtained with the non-polymerised VCC and the analytes. Finally, the MIP was tested for visual detection in comparison with the NIP. The results showed that the quenching of the MIP can be seen with the naked eye, while the NIP fluorescence remains almost unaltered. The results reported in this chapter put the bases for the production of a detector of drug metabolites based on a switchable polymer, which can be used by a layperson.

The polymer obtained in this work is expected to perform in combination with SPE (solid phase extraction) cartridge. Tamoxifen and its metabolites are insoluble in water

and are excreted in urine as conjugates of glucuronic acid. Therefore, a pre-treatment involving hydrolysis, in order to obtain the free drug/metabolite, followed by a SPE step, to concentrate the sample, is essential before the analysis. At this point, the polymer here developed can be used to carry out the detection of the analytes in organic solvent, as ACN, where the interactions between the FM and the target are favoured.

Future work should involve the determination of the lower detection limit of the bulk polymer and the evaluation of the characteristics of this detector system in real samples. Moreover, the sensitivity of the system could be increased by reducing the size of the polymer and preparing it in the format of nanoparticles. By increasing the surface-to-volume ratio, more active sites could be available to rebind the drug, thus providing a lower detection limit

## 3.6. Reference

1. Bentrem, D. J.; Gaiha, P.; Jordan, V. C., Oestrogens, Oestrogen Receptors and Breast Cancer. *European Journal of Cancer Supplements* **2003,** *1* (1), 1-12.

2. Baker, J. S.; Graham, M. R.; Davies, B., Steroid and prescription medicine abuse in the health and fitness community: A regional study. *European journal of internal medicine* **2006,** *17* (7), 479-84.

3. Mirata, F.; Ray, J. V.; Perollier, C.; Arotcarena, M.; Bayoudh, S.; Resmini, M., Smart coumarin-tagged imprinted polymers for the rapid detection of tamoxifen. *Analytical and bioanalytical chemistry* **2016,** *408* (7), 1855-61.

4. Li, Q.; Liu, L.; Liu, J.-W.; Jiang, J.-H.; Yu, R.-Q.; Chu, X., Nanomaterial-based fluorescent probes for live-cell imaging. *TrAC Trends in Analytical Chemistry* **2014,** *58*, 130-144.

5. Leung, M. K. P.; Chow, C.-F.; Lam, M. H. W., A sol–gel derived molecular imprinted luminescent PET sensing material for 2,4-dichlorophenoxyacetic acid. *Journal of Materials Chemistry* **2001,** *11* (12), 2985-2991.

6. Suárez-Rodrıguez, J.; Dıaz-Garcıa, M., Flavonol fluorescent flow-through sensing based on a molecular imprinted polymer. *Analytica Chimica Acta* **2000,** *405*, 67-76.

7. Piletsky, S. A.; Piletskaya, E. V.; Yano, K.; Kugimiya, A.; Elgersma, A. V.; Levi, R.; Kahlow, U.; Takeuchi, T.; Karube, I.; Panasyuk, T. I.; El'skaya, A. V., A Biomimetic Receptor System for Sialic Acid Based on Molecular Imprinting. *Analytical Letters* **1996,** *29* (2), 157-170.

8. Levi, R.; McNiven, S.; Piletsky, S. A.; Cheong, S.; Yano, K.; Karube, I., Optical Detection of Chloramphenicol Using Molecularly Imprinted Polymers. *Analitical Chemistry* **1997,** *69*, 2017-2021.

9. Carrasco, S.; Benito-Pena, E.; Walt, D. R.; Moreno-Bondi, M. C., Fiber-optic array using molecularly imprinted microspheres for antibiotic analysis. *Chem. Sci.* **2015,** *6*, 3139-3147.

10. Korposh, S.; Chianella, I.; Guerreiro, A.; Caygill, S.; Piletsky, S.; James, S. W.; Tatam, R. P., Selective vancomycin detection using optical fibre long period gratings functionalised with molecularly imprinted polymer nanoparticles. *The Analyst* **2014,** *139* (9), 2229-36.

11. Ray, J. V., Novel Molecular Imprinted Nanogels As Drug Delivery Vehicles For Tamoxifen. *Thesis submitted to Queen Mary University, School of Biological and Chemical Sciences*.

12. Lanza, F.; Sellegren, B., TheApplication of Molecular Imprinting Technologyto Solid Phase Extraction. *Chromatographia* **2001,** *53*, 599-611.

13. Rashid, B. A.; Briggs, R. J.; Hay, J. N.; Stevenson, D., Preliminary Evaluation of a Molecular Imprinted Polymer for Solid-phase Extraction of Tamoxifen. *Analytical Communications* **1997,** *34* (10), 303-306.

14. Zander, A.; Findlay, P.; Renner, T.; Sellergren, B., Analysis of Nicotine and Its Oxidation Products in Nicotine Chewing Gum by a Molecularly Imprinted Solid-Phase Extraction. *Anal. Chem.* **1998,** *70*, 3304-3314.

15. (a) Andersson, L. I.; Paprica, A.; Arvidsson, T., A Highly Selective Solid Phase Extraction Sorbent for Pre- Concentration of Sameridine Made by Molecular Imprinting. *Chromatographia* **1997,** *46*; (b) Andersson, L. I.; Hardenborg, E.; Sandberg-Ställ, M.; Möller, K.; Henriksson, J.; Bramsby-Sjöström, I.; Olsson, L.-I.; Abdel-Rehim, M., Development of a molecularly imprinted polymer based solid-phase extraction of local anaesthetics from human plasma. *Analytica Chimica Acta* **2004,** *526* (2), 147-154.

16. Claude, B.; Morin, P.; Bayoudh, S.; de Ceaurriz, J., Interest of molecularly imprinted polymers in the fight against doping. Extraction of tamoxifen and its main metabolite from urine followed by high-performance liquid chromatography with UV detection. *Journal of chromatography. A* **2008,** *1196-1197*, 81-8.

17. Greenblatt, R. B.; Barfield, W. E.; Jungck, E. C.; Ray, A. W., Induction of ovulation with MRL/41. Preliminary report. *JAMA* **1961,** *178* (101), 249-251.

18. Clark J.H; B.M, M., The agonistic-antagonistic properties of clomiphene: a review *Pharmacology & Therapeutics* **1982,** *15*, 467-519.

19. Nguyen, T. H.; Ansell, R. J., Fluorescent imprinted polymer sensors for chiral amines. *Organic & biomolecular chemistry* **2009,** *7* (6), 1211-20.

20. Ansell, R. J.; Wang, D.; Kuah, J. K., Imprinted polymers for chiral resolution of +/--ephedrine. Part 2: Probing pre-polymerisation equilibria in different solvents by NMR. *The Analyst* **2008,** *133* (12), 1673-83.

21. Ali, W. H.; Derrien, D.; Alix, F.; Perollier, C.; Lepine, O.; Bayoudh, S.; Chapuis-Hugon, F.; Pichon, V., Solid-phase extraction using molecularly imprinted polymers for selective extraction of a mycotoxin in cereals. *Journal of chromatography. A* **2010,** *1217* (43), 6668-73.

22. Lucci, P.; Nunez, O.; Galceran, M. T., Solid-phase extraction using molecularly imprinted polymer for selective extraction of natural and synthetic estrogens from aqueous samples. *Journal of chromatography. A* **2011,** *1218* (30), 4828-33.

# Chapter 4

## pH-responsive molecularly imprinted nanogels for delivery of tamoxifen

# 4. pH-responsive molecularly imprinted nanogels for delivery of tamoxifen

## 4.1. Introduction

The results described in the thesis have so far centred on the synthesis of the fluorescent functional monomer 6-vinylcoumarin-4-carboxylic acid (VCC), reported in chapter 2, and its use for the preparation of bulk imprinted polymers for sensing applications, described in chapter 3.

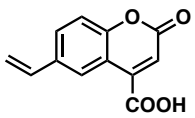


**Figure 4.1.** 6-vinylcoumarin-4-carboxylic acid, VCC.

The fluorescence studies reported in chapter 3 highlighted the strength of the interactions occurring between VCC and tamoxifen, suggesting the possibility of using the same monomer for the preparation of a new MIP with potential application as drug delivery vehicle. The sections in this chapter will describe the work done and discuss the results obtained.

### 4.1.1. Molecularly imprinted nanogels as drug delivery vehicles

As mentioned in chapter 1 (section 1.3.2), one of the main requirements of new drug delivery systems (DDS) is the capacity to provide sustained and tailored drug release. The use of the molecular imprinting approach for loading drugs has shown interesting results. Researchers have largely explored the potential of MIPs as DDS and many reviews have been published during the past few years.[1-3] The use of functional monomers to create specific interactions with the drug can allow a certain degree of

control of the release profile, by altering the strengths of the interactions.[1] For examples, MIPs have been studied as transdermal carriers for enantioselective-controlled delivery.[4] The particularly high specificity and selectivity of MIPs make these materials ideal vehicles in cases of chiral drugs delivery in which one of the enantiomers is more active than the other. By delivering only the active enantiomer, instead of a mixture, the efficiency of the drug increase and the potential toxicity and side effects, caused by the inactive enantiomer, decrease considerably. The use of MIPs represents a good alternative to the methodologies employed for the production of pure single enantiomers, which are expensive and time-consuming. Moreover, the risk associated with the racemization of a single enantiomer of the chiral drug, both in raw material and pharmaceutical products, requires constant control of the substance.

In the group where this project was developed, there is a strong expertise in polymeric nanoparticles, developed for a variety of applications, as well as considerable knowledge in the area of molecular imprinting. In particular the group was the first to report the development of imprinted nanogels as enzyme mimics, to catalyse carbonate hydrolysis.[5] The design of nanogels (already discussed in chapter 1) has evolved during the years, together with different synthetic approaches that can be used to prepare them.[6] The literature abounds with reviews that explain in detail the different methods employed, such as suspension polymerisation, photolithographic technique, (inverse) mini- or micro- or emulsion, precipitation, high dilute free radical or living radical polymerisation (figure 4.2).[7]

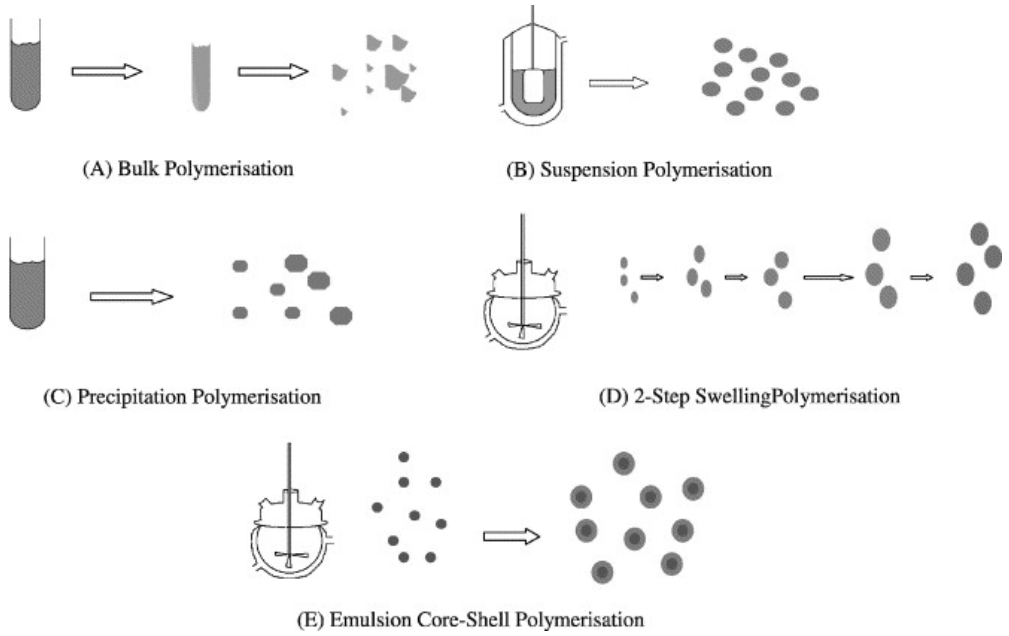


**Figure 4.2.** Schematic representation of the synthetic steps in some of the existent polymerisation procedures. Image reproduced with permission from Moral and Mayes[8]

Each polymerisation method produces final materials characterised by different rebinding ability, morphology and particle size, as reported in 2004 by Moral and Mayes.[8] The choice of the most appropriate synthetic approach is therefore important in order to tailor the size and the morphology of the particles, to suit the different applications. The emulsion polymerizations, micro- or mini-, are heterogeneous processes and depend on the nature of the monomers. If the monomers are hydrophilic the polymerisation is carried out in aqueous droplets in organic solvents, vice versa if the monomers are hydrophobic. Such approaches resort to the use of surfactants in order to disperse the monomers in the continuous phase, stabilise the system and inhibit the aggregation of particles.[9] Whereas, high dilution radical polymerisation is based on the use of low concentration of the monomers to increase the distance between the growing polymer chains, therefore favouring the intramolecular rather than intermolecular crosslinking and preventing macrogelation. Conversely from the emulsion

polymerisation, the high dilution is a homogeneous process in which the components are completely soluble in the polymerisation solvent.[9]

In the Resmini's group high dilution radical polymerisation has been optimised as the prevalent synthetic approach for the preparation of nanogels.[5, 10, 11] The high dilution does not require the presence of the surfactants for stabilising the particles; this is one of the main reasons for selecting this particular approach. Surfactants are useful in stabilising the systems, but they can also be toxic and difficult to remove during purification. Furthermore, surfactants can alter the recognitions properties of the matrix and compete with the formation of hydrogen bonds thus weakening the binding affinity of the network towards the substrate.

## 4.2. Imprinted nanogels formulation

The first part of the work towards the development of imprinted nanogels to be used potentially for the delivery of tamoxifen, involved some fundamental studies to identify the key parameters, essential to obtain the best polymer formulation. This involved the selection of the most suitable monomers, the crosslinker, and the initiator. Other important factors to consider during the design of imprinted polymers were the porogenic solvent and the concentration of monomers ($C_M$) as these have been shown to influence the particle size. In the following sections the choice of each component of the polymer mixture is discussed.

### 4.2.1. Choice of the functional and backbone monomers

- THE FUNCTIONAL MONOMER

As already discussed in chapter 1, the formation of a stable template-functional monomer complex is a key requirement to the formation of polymers with high recognition characteristics. The VCC monomer (6-vinylcoumarin-4-carboxylic acid),

whose synthesis is described in chapter 2, was selected as functional monomer as a result of the strong interactions that occur with the target drug tamoxifen, in addition to its fluorescent properties. The latter in particular is very important, because it allows monitoring carefully the fate of the nanoparticles both *in vivo* and *in vitro*, in addition to allowing the investigation of the internalisation mechanism.

Careful evaluation of the structures of VCC and tamoxifen suggested the formation of two possible main interactions, strongly dependant on the chosen solvent system. Hydrophobic interactions can take place as a result of π-π stacking of the aromatic units, as well as ionic bond between the carboxylic group on VCC and the amino group on TAM (figure 4.3). However, given that the primary target for this work was to develop a system in which the drug release could be controlled by pH, it was required to ensure good ionic interactions. For this purpose a polar, aprotic organic solvent, with dielectric constant sufficiently high to allow solubilisation of all the components, will be necessary for the polymerisation. Section 4.2.4 will cover more in details the choice of the polymerisation solvent.

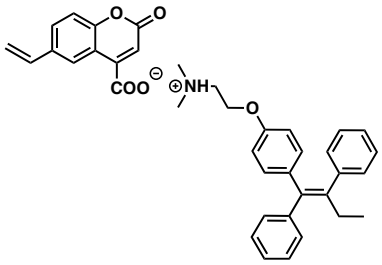


**Figure 4.3.** Representation of the ionic interaction that take place between the amine group of the tamoxifen and the carboxylic acid in VCC.

The pH-sensitive drug vehicles, as the one proposed, are based on the lower pH values existing in inflamed, infected and malignant tissues. These tissues are slightly more acidic than the physiological pH of 7.4, due to high glycolytic activity that produces acids equivalents in the cell.[12, 13] Tamoxifen, as anti-cancer drug, is expected to be

internalised in cancer cells in which the intracellular pH was shown to vary between 4 and 6.[14] However, pH 5.5 is conventionally reported in the literature when studying the release of novel materials as proof of concepts.[15, 16] The carboxylic acid of the VCC has a pKa of 2.50 in water (SciFinder prediction tool) thus existing predominantly in its deprotonated form. Whereas the amine group of tamoxifen, with a pKa 8.9 in water, is mainly protonated, favouring the formation of an ionic bond. This project was developed on the hypothesis that the low pKa of VCC would significantly hinder the release of tamoxifen in healthy cells at physiological pH, while a slow release of the drug could be favoured inside cancer cells. In fact, the more acidic intracellular environment would disrupt the interactions between the monomer and the drug allowing the free tamoxifen to link on the oestrogen receptors and exert its biological actions.

- COLLOIDAL STABILITY AND THE BACKBONE MONOMER

Nanogels have polymeric networks able to absorb water and form a stable, dispersed colloidal solution, which is directly linked to the chemical structure and the solvent system used. In this chapter the term solubility, when referred to nanogels, will be used to identify the degree of stability of the colloidal dispersion. In this context the applications of nanogels also need to be considered, and for this project applications in water are targeted.

Considering the hydrophobicity of the functional monomer, VCC, it was necessary to choose a backbone monomer that could maximise the solubility of the nanogels in water. During previous studies carried out in the research group of Prof. Resmini, the hidrophilic acrylamide was often used as backbone monomer in the preparation of nanogels for a variety of applications (figure 4.4).[17,5,10] Although the monomer acrylamide is well known to be neurotoxic, genotoxic and carcinogenic, once the monomers react to form long polymer chains the toxicity is no longer present.

Furthermore, the FDA approved the use of polyacrylamide as a film former in the imprinting of soft-shell gelatin capsules when the polymer does not contain more than 0.2% acrylamide monomer.[18]

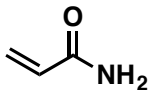


**Figure 4.4.** Representation of the structure of acrylamide monomer

However, there was a concern that acrylamide-based nanogels would display low solubility in aqueous systems and would therefore not be suitable for drug delivery studies.[17] In order to overcome this issue, work was carried out to develop nanogels using N-isopropylacrylamide (NIPAM, figure 4.5) as backbone monomer, as this monomer was previously used and showed to have much more suitable characteristics in terms of solubility.[19, 11] This is an interesting monomer, characterised by the isopropyl group as a substituent on the N atom of the amide, and when polymerised gives rise to matrices that can show thermoresponsive properties.

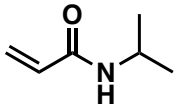


**Figure 4.5.** Representation of the structure of N-isopropylacrylamide (NIPAM)

Thermoresponsive N-isopropylacrylamide (NIPAM) based polymers, formed by long linear chains of the units, display a phase transition above or below a particular temperature defined as lower critical solution temperature (LCST).[20] The polymer can loose about 90% of its own volume when heated above the LCST in water, passing from a swollen hydrate state to a shrunken dehydrated state. Below the critical temperature water molecules form a hydrated shell around the hydrophobic moieties of the polymer, assuming the most thermodynamically stable state, whereas above the

LCST a de-solvation of the hydrophobic moieties of the polymer chains occurs (figure 4.6). The entropy of the water molecules increases, resulting in the collapse of the polymer as the hydrophobic interactions polymer-polymer increase.[21, 22]

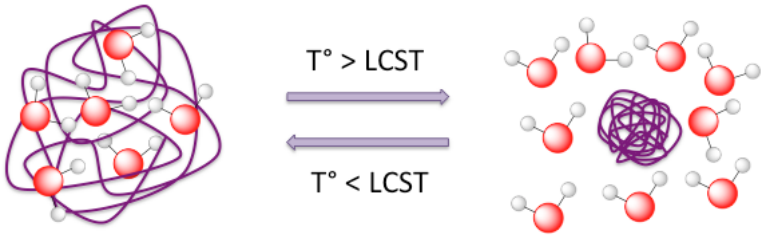


**Figure 4.6.** Graphic illustration of the thermo-responsiveness characteristics of p-NIPAM. On the left, when the temperature is below the LCST, the polymer (purple line) is hydrated and swollen. On the right, when temperature rises above the LCST, the polymer is dehydrated and shrunk

Linear poly-N-isopropylacrylamide (p-NIPAM) show a LCST at 32°C. However, in cross-linked gels, changes in the chemical compositions can lead to values closer to the human body temperatures (36.5 – 37.5°C). The degree of flexibility of the polymer matrix has been shown to have an impact on the temperature at which the phase transition occurs (Salinas *et al*. unpublished data). This particular characteristic contributed to make p-NIPAM promising stimuli-responsive drug delivery carriers, in which the release of the drug is triggered by a difference in temperature.[23] Therefore, by using NIPAM as backbone monomer in the nanogels here presented, a new, extra feature could be added to the final system. If the right combination of monomers and crosslinkers were used, it would be possible to obtain a carrier able to respond to double stimuli for drug release: a change in pH and also change in temperature. As mentioned, there is plenty of research showing that cancer cells have more acidic pH compared to the healthy cells. In the same way tumours are subject to mild hyperthermia, generally 1 or 2°C warmer than healthy cells, due to the higher replication rate of cancer cells, which release energy. Thermo-responsive drug delivery system, with phase transition temperature at 38-39°C, have been developed in order to deliver the drug only in the

vicinity of cancer cells. In the hyperthermia conditions of the tumour environment the polymers collapse and become hydrophobic, favouring the release of the drugs. Whereas in normal tissue the polymers are in their hydrophilic, thermodynamic stable state, and the drugs remain encapsulated within the matrix.[24]

### 4.2.2. Choice of initiator

The initiator is the component responsible for the activation of the free radical polymerisation. Two main general types of free radical initiators are commercially available, the organic peroxides and the azocompounds, both of which decompose thermally to produce two radicals. In the peroxides groups (R-O-O-R'), the cleavage of the oxygen-oxygen bond produces two free radicals, while in the azocompounds (R-N=N-R') the decomposition causes the scission of the two carbon-nitrogen bonds producing nitrogen and two alkyl radicals. Some peroxides show a considerable solvent and concentration effect, i.e. the decomposition rate increases/decreases depending on the solvent and concentration used. On the other hand the decomposition rate of azocompounds is not affected by concentration, solvent or environment, making them more stable and generally safer than the peroxide initiators.[25] Among azocompounds, azobisisobutyronitrile (AIBN) is a very common initiator, widely used in radical polymerisations. AIBN was selected as initiator for the preparation of the imprinted and non-imprinted nanogels. This initiator undergoes a thermal decomposition at 60°C, following the mechanism illustrated in figure 4.7.

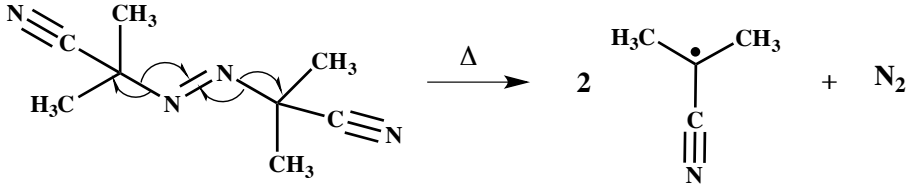


**Figure 4.7.** Mechanism of the thermal decomposition of the initiator AIBN when heated over 60°C

In case of high dilution radical polymerisation, AIBN is generally used in 1% mol of double bonds in the mixture. However, this amount requires each time optimisation, especially when chemical compounds that can act as radical quenchers are present in the polymerisation mixture.

### 4.2.3. Choice of the cross-linker

The cross-linking agent is one of the essential components involved in the preparation of imprinted nanogels. The cross-linker (XL) allows the formation of a three-dimensional network by linking different polymer chains; it stabilizes the imprinted binding sites and influences the morphology and physico-chemical characteristics of the system. [26] The chemical structure of the XL impacts mainly on the physico-chemical properties; whereas the content of XL impacts on the rigidity of the matrix and binding sites. Moreover the XL has to be chosen accordingly to the environment in which the polymer will be applied, weather it is aqueous or organic. Depending on the applications that has been targeted, which is either catalysis, sensor or drug delivery, the content of cross-linker in a polymer system can vary ranging from 80-90%, for very cross-linked and rigid system, to as low as 10-5%. [27-29]

The chemical structure of the polymerisable unit of the different components has an effect on the rate of the polymerization, which potentially lead to a different degree of incorporation. [30] The pre-polymerisation mixture is prepared using a well-defined ratio of functional monomer (FM) to backbone monomer (BM) to crosslinker (XL) to template (T). The main target is to maintain this ratio also in the final polymer. However, such aim can be seriously affected if the polymerisable groups on the different components have dissimilar chemical structures. The difference in chemical structures can lead to a different kinetics of reaction, resulting in a variation of the ratio

FM:BM:XL:T in the final product. Given the random nature of the radical polymerization it is quite difficult to establish subsequently the percentage of incorporation. This becomes significantly important if the chemical yield is below 80-85%. In such cases the incorporation of the monomers in the final polymer could not reflect the ratio used in the pre-polymerisation mixture. Given the choice of the functional and backbone monomer, which contains a vinyl and an acrylamide group, respectively, it is necessary to find a cross-linker with similar functional group. Taking into account these considerations, cross-linker agents widely used that have all the requirements listed above are the N,N' - methylenebis(acrylamide) (MBA) or N,N' - ethylenebis(acrylamide) (EBA) represented in figure 4.8.

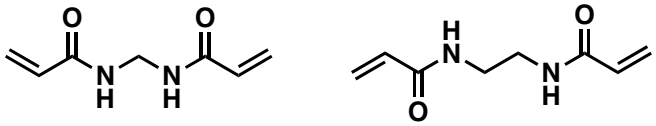

**Figure 4.8.** From left to right, structure of cross-linking agents N,N' - methylenebis(acrylamide) (MBA) and N,N' - ethylenebis(acrylamide) (EBA)

Both MBA and EBA cross-linkers are water soluble, they carry the same polymerisable unit as the backbone monomer, and they do not have any other major functional groups that could give rise to any additional interactions, with the exception of the carbonyl and the -NH- group. However, the presence of an extra methylene group in the EBA, compared to MBA, could contribute to make the matrix too flexible, in addition to increasing the hydrophobicity. In fact, although a certain degree of flexibility is desirable, it is important to achieve tight cavities to prevent the risk of non-specific binding. Both the structure and the amount of cross-linker influence the rigidity of the final network, which is important for retaining the structure of the cavities. High cross-linker content, usually between 70% and 80%, involves a lack of flexibility and high rigidity, limiting the swelling of the particles, hence the solubility of the nanogels in the

appropriate solvent. In the case of DDS it is important to have cavities that enclose the drug, but in order to allow the release of the template, the network should not be partly flexible. Papadimitriou *et al*. demonstrated that polymers prepared with 20% XL showed good uploading and good release profile of the therapeutic cargo. [19] Therefore, the content of MBA was fixed at 20% for the preparation of nanogels, which would exhibit its function in aqueous environment and would be able to release the drug from the cavities.

### 4.2.4. Choice of the polymerisation solvent

The nature of the solvent plays an important role in the polymerisation process. It is necessary for the polymerisation solvent to completely solubilise the components involved in the process so that a homogeneous solution can be obtained. As reported by Beltran *et al*. the imprinted polymers would work better if the solvent used during the polymerisation was the same as the final solvent required by the applications. [31] The nanogels will potentially be used in aqueous environment, however, using water as polymerisation solvent could be problematic. Tamoxifen, as a large percentage of commercially available small molecule drugs, is hydrophobic and therefore a homogeneous solution could not be achieved in water, preventing interactions between the drug and the functional monomer. Water was, therefore, discarded as polymerisation solvent, as well as other protic solvents. In fact, protic solvents would interfere with the formation of potential hydrogen bonds between tamoxifen and the monomers, thus limiting the specificity of the cavities. However, considering the choice of using VCC, NIPAM and MBA as functional monomer, backbone monomer and cross-linker, respectively, a polar solvent is required in order to solubilise the components. Inspired by previous published works, it was decide to use the polar aprotic dimethylsulfoxide

(DMSO) as polymerisation solvent. [5, 11,17,19]

### 4.2.5. Concentration of monomers ($C_M$)

To generate nanosized intramolecular crosslinked particles, the prevention of intermolecular particle-particle interactions in the polymerisation mixture is a key requirement. As demonstrated by Graham *et al*., this is achievable by considering combination of good polymerisation solvent and overall monomer concentration ($C_M$).[32] In fact, nanogels can be formed only when the $C_M$ is below a well defined value referred to as critical gelation concentration, which depends on the polymerisation solvent and its solubility parameter (figure 4.9).[33,34] In such conditions the swollen particles are dilute enough not to create intermolecular connections, acting as steric stabilisers against aggregations.

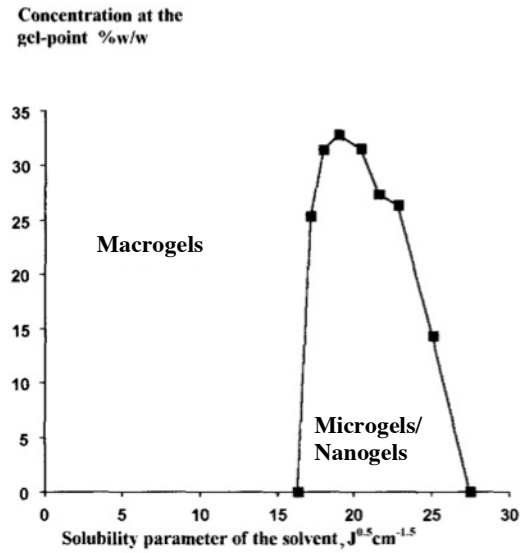


**Figure 4.9.** Plot of monomer concentration at gel point *versus* solubility parameter of the used polymerisation solvent. The two regions in which the formation of macrogels or micro/nanogels occurs are clearly labelled. Figure reproduced with permission from Graham *et al*.[33]

The considerable amount of work carried out by the Resmini's group and others has shown a direct correlation between the values of $C_M$, the particle size and the polydispersity obtained. An easy way to predict the formation of small particles is to

observe the aspect of the mixture after polymerisation. A low viscosity, clear solution suggests the formation of small particles, while high viscous mixture or gelatinous lumps suggests macrogelation.

It was previously shown that value of $C_M$ equal to 0.5% produced nanogels with small particle size and low polydispersity index, while maintaining good chemical yields.[35-37] It was therefore decided to use this as initial value for the preparation of nanogels and to optimise it if necessary.

## 4.3. Synthesis and characterisation of nanogels

The polymerisation was based on an established procedure, involving two days polymerisation at 70°C, after degassing the mixture.[10,17] The final nanogel solution was dialysed against water for two days, by changing dialysis water 3 times a day. Dialysis is an important step for the purification. Previous work indicated that the use of membranes with pore size of 3.5 KDa were suitable for ensuring isolation of polymers with the desired size.[38] Therefore, only the remaining un-reacted components, as well as smaller polymer chains, were removed from the mixture through the pores. The resulting aqueous solution, containing the nanogels, was freeze-dried and fluffy solids were recovered. All polymers were prepared in DMSO with 20% MBA and NIPAM as backbone monomer. A recent work published by Zielinska *et al*.[11] has shown that the content of cross-linker influences the volume phase transition temperature (VPTT), feature provided by the presence of the thermo-responsive backbone polymer. The work demonstrated that polymers containing 20% MBA showed a phase transition at around 39°C and were considered suitable for drug delivery applications. However at this stage of the development the thermoresponsive properties were not considered essential and

therefore the polymer preparations were instead evaluated based on yields, solubility, particle size and fluorescence properties.

### 4.3.1. Characteristics of the nanogels

Here below a brief explanation of the different parameters, used to judge the polymers and guide the optimisation process, is given.

#### 4.3.1.2. Chemical yield

The chemical yield is the first parameter taken in consideration during evaluation of the nanogels. Preparations with chemical yields lower than 30% were discarded, as the loss of material during purification was too high and the exact composition of the resulting polymer could not be confirmed. The yield was determined after the polymerisation process and the dialysis purification step. The solid polymer, obtained after the freeze-dryer, was weighted out and compared with the amount of material that was initially inserted in the pre-polymerisation mixture (equation 4.1).

$$\%\, Chemical\ Yield = \frac{Actual\ Yield}{Theoretical\ Yield} \times 100 \qquad \textbf{Equation 4.1}$$

#### 4.3.1.3. Solubility in water

As already mentioned, the solubility of the nanogels is an important characteristic for drug delivery applications. The solubility was evaluated as the amount of polymer that would give rise to a stable and clear colloidal dispersion in water, which would not show any particles visible to the naked eye. The evaluation started with a concentration of 2mg/mL. The polymer was weighted out and the correct volume of water was added to give the desired concentration. The sample was then sonicated for 10 minutes and its aspect was observed. The sample was then diluted down with the addition of further

portions of water in case insoluble material was present. At that point the sonication step and the visual evaluation were repeated.

#### 4.3.1.4 Particle size (Zetasizer)

The size of the nanogels was measured by Dynamic Light Scattering (DLS) technique. This technique consists of a laser beam that illuminates the particles contained in the sample solution and a detector placed at 90°C to the source of laser, which measures the light scattered by such particles. The zetasizer system interprets the size of the particles present in the sample by correlating the Brownian motion of such particles and the scattered light.[39, 40] The Brownian motion is defined as "the erratic random movement of particles in a liquid due to the bombardment by the molecules that surround them". The smaller the particles are, the quicker they move around, vice versa the larger ones move slower. This continuous diffusion of the particles suspended in the liquid samples, involve a fluctuation of the intensity of the scattered light, accordingly to the size of the particles. In particular, if the particles are large and move slowly then the intensity fluctuates slowly as well, while a quick fluctuation is expected in case of small particles. By using a correlation function, the zetasizer system measures the rate of the intensity fluctuation and the degree of similarity between two signals over time. This information is then used to calculate the size distribution. The standard size distribution obtained from the zetasizer is by light intensity, which can be converted into volume and number distribution using the Mie theory (figure 4.10). As the names suggest, the number distribution reflects the number of particles with different sizes. In other words, if there were equal number of particles with different size, the graph would show two peaks with the same intensity. The volume distribution gives a measurement of the volume size of the particles. Bigger particles have a larger volume and give bigger contribution,

therefore, considering the same example as above, the graph would show two peaks, one of which $10^3$ fold larger than the other, accordingly to the volume of a sphere (4/3 πr3). Whereas the intensity distribution is a measurement of the amount of light scattered by the particles. Big particles scatter more light and generate higher contribution than small ones. The graph would show two peaks, one of which $10^6$ fold bigger than the other, accordingly to Rayleigh's approximation.

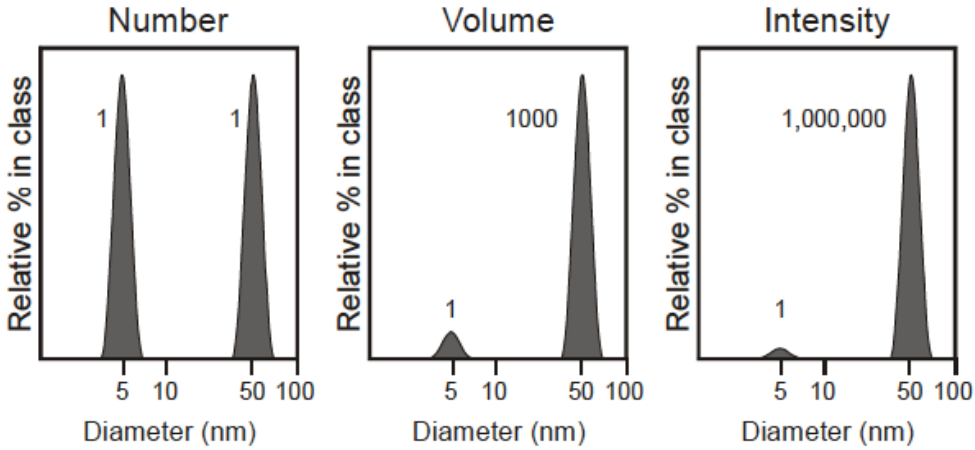


**Figure 4.10.** Number, Volume and intensity distributions of a sample containing two populations of particles, one with 5 nm and one with 50 nm diameters[39]

It is important to note that the actual properties of the material are taken into account only when the size is expressed by volume or number distributions. The intensity has a multimodal particle size distribution and it is proportional to the square of the molecular weight, therefore this distribution could be misleading in real samples. The intensity distribution can be dominated by other particles in case large impurities like dust or small number of aggregates are present in solution. Figure 4.11 represents a schematic illustration of the intensity distribution graph in the case in which a large number of particles with size 10 nm are present in a sample together with only one particle of 100 nm. The graph shows two peaks with same intensity for the two different particles size.

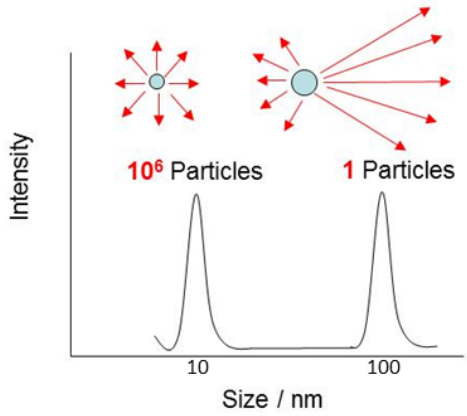


**Figure 4.11.** Schematic representation of the contribution to size distribution by intensity of particles of different size

Therefore, in the cases of small particles, number and volume distribution give the most accurate representation of the actual size.

Only the size distribution by number of the nanogels prepared will be shown in this section, however it is possible to find the intensity and volume distribution graphs in the appendix at the end of this thesis.

After polymerisation, every preparation has been dialysed against water before being freeze-dried and stored as a solid at room temperature in the dark. The particle size of all the nanogels were measured at 0.5 mg/mL in water at pH = 5.5. In order to break down any possible aggregates formed in the solution, the samples were prepared by filtering the mixture on a 0.45μm GHP filter after sonication for 10 minutes.

#### 4.3.1.5. Fluorescence properties

When developing a novel drug delivery system it is of high importance to be able to monitor *in vitro* the pathway taken by the vehicle. By studying the cellular uptake and the distribution of the DDS, it is possible to predict the accumulation, the safety, and efficiency of such materials within the body. As described in chapter 1 (section 1.4),

fluorescence is widely used as imaging technique due to its high sensitivity, low radiation, and non-invasiveness.

Considering that the final application of nanogels will be in aqueous environment, the fluorescence spectra were recorded in water. The UV-Vis of the fluorescent monomer was initially recorded in the same solvent, as shown in figure 4.12.

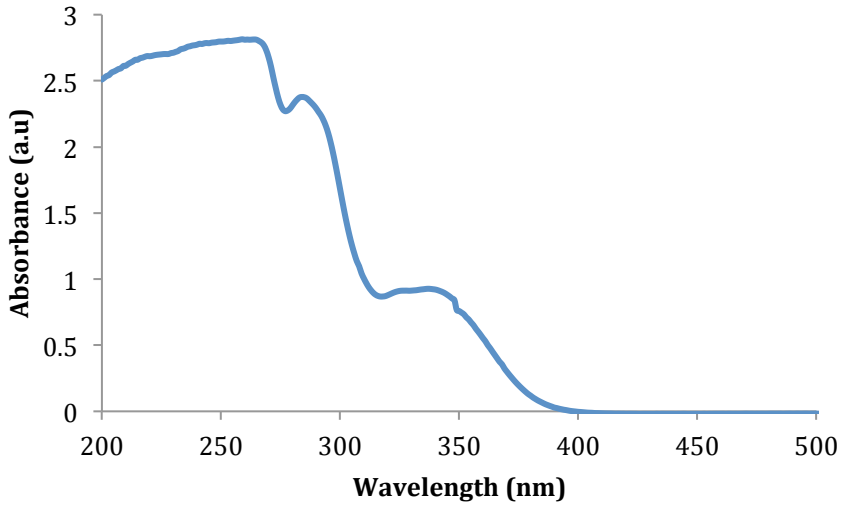


**Figure 4.12.** UV-Vis spectrum of VCC functional monomer in water. [VCC]= 0.28mM. Two main peaks are visible, $\lambda_{abs}$ = 350 and 285nm

VCC in water showed two main peaks, one with $\lambda_{abs}$ = 350nm and another one, with higher absorbance, at $\lambda_{abs}$ = 285nm. However, the fluorescence emission of the polymers was carried out after excitation at $\lambda_{exc}$ = 360nm. This value was chosen to ensure that none of the other functional groups in the polymeric matrix were excited. The lower the wavelength of excitation is, the higher the risk to irradiate other components that can influence the emission. The fluorescence of the nanogels was therefore measured by emission at wavelength $\lambda_{em}$ = 470nm following excitation at wavelength $\lambda_{exc}$ = 360nm.

### 4.3.2. Nanogels preparation

The first polymer preparation that was attempted was **FM-P1**. The content of functional monomer is a fundamental parameter to take in consideration in the synthesis of nanogels. It directly influences the amount of drug incorporated within the matrix and deeply affects the morphology of the final polymers. When hydrophobic monomers, such as VCC, are introduced in the nanogels the risk of obtaining insoluble polymers is very high. Previous work in the group identified the content of such functional monomers between 10% and 20% as the ideal percentage. Given the hydrophobicity of the VCC, it was decided to prepare the first nanogel, **FM-P1**, with 10% of functional monomer.

**Table 4.1.** Preparation of the first NIP. Polymerisation was carried out at 70 °C for 2 days in DMSO. Dialysis was performed against water for two days followed by freeze-drier.

| | MIP/NIP | MBA | VCC | AIBN | $C_M$ | Yield | Solubility in Water |
|---|---|---|---|---|---|---|---|
| **FM-P1** | NIP | 20% | 10 % | 2 % | 0.5 % | 5% | 2 mg/mL |

This polymer was prepared using 10% of VCC and 2% of AIBN. Considering the anti-oxidant effect of coumarin derivatives, described in chapter 2, and the high likelihood that the formed free radicals would be quenched by the functional monomer, it was decided to use a higher content of initiator to overcome such effect of the VCC (section 4.2.2). Although the solubility in water and the particle size were satisfying, (figure 4.13), this formulation was discarded. The chemical yield was 5%, which was considered too low to be accepted for any purposes. Such little yield was probably due to the radical quenching effect of the VCC and to the insufficient content of initiator. The media, in which nanogels are formed when high dilution radical polymerisation is

employed, is so diluted that the few radicals formed do not hit each other very frequently. Therefore the obtained polymer chains are too small to be retained within the dialysis membrane during the purification process, hence obtaining a low yield.

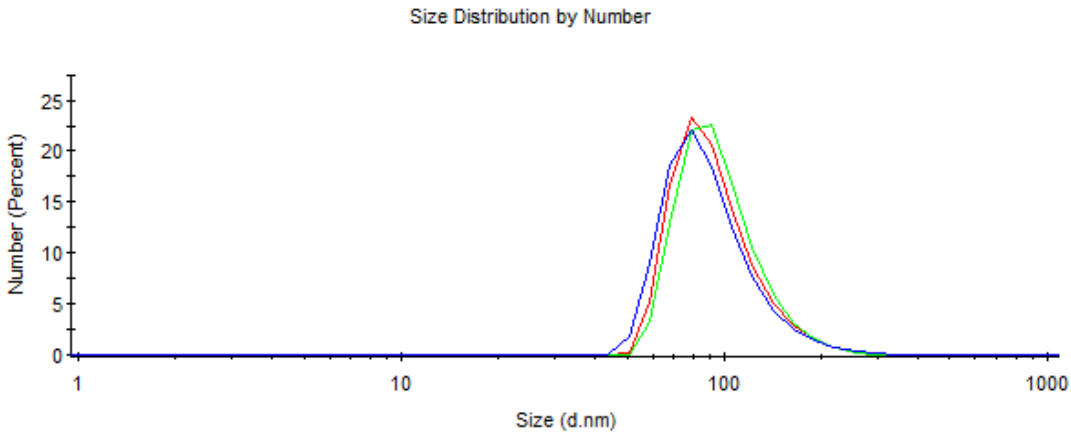


**Figure 4.13.** Particle size of **FM-P1** at 1 mg/ml in water, distribution by number. The measurements were recorded as triplicates. The particle size by number of **FM-P1** was 96 ± 32 nm with PDI = 0.110. Each line represents the average particle size over 15-17 scans of the nanogel.

In the subsequent preparation the content of VCC was lowered to 5% while maintaining all the other parameters constants.

**Table 4.2.** Preparation of the NIP. Polymerisation was carried out at 70 °C for 2 days in DMSO. Dialysis was performed against water for two days followed by freeze-drier.

| | MIP/NIP | MBA | VCC | AIBN | $C_M$ | Yield | Solubility in Water |
|---|---|---|---|---|---|---|---|
| **FM-P2** | NIP | 20% | 5 % | 2 % | 0.5 % | 8.5% | 2 mg/mL |

The chemical yield of **FM-P2** slightly increased compared to **FM-P1**, although very marginally, therefore suggesting that probably the content of VCC was still having an important effect in the polymerisation process.

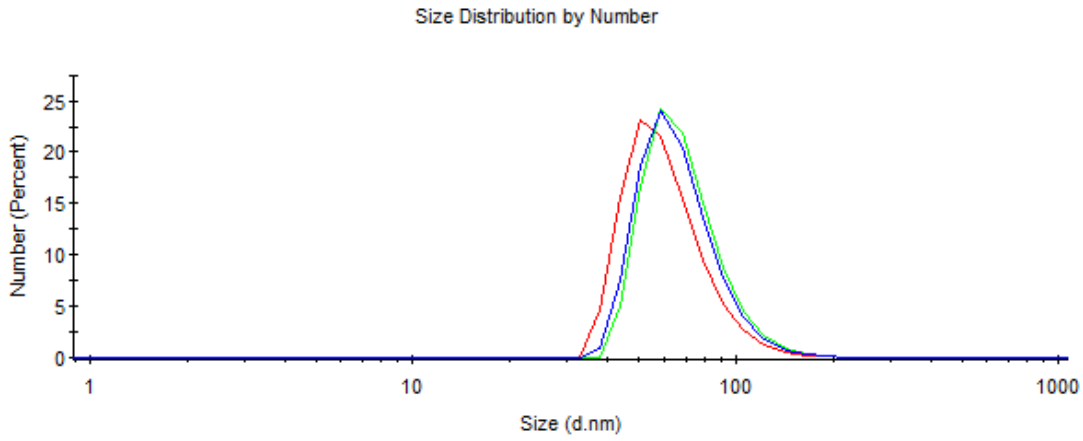


**Figure 4.14.** Particle size of **FM-P2** at 1 mg/ml in water, distribution by number. The measurements were recorded as triplicates. Each line represents the average particle size over 15-17 scans of the nanogel. The particle size by number of **FM-P2** was 61 ± 19 nm with PDI = 0.130

The new preparation showed good solubility and small particle size, however the chemical yield was not sufficiently high to consider this formulation any further. The low yield implies poor incorporation of the monomers within the polymeric matrix. Also, due to the random aspect of the free radical polymerisation process, the cross-linker may polymerise first. The cross-linker agent has faster kinetic because of the presence of two units of polymerisable moiety in the same molecule, thus involving slower incorporation of the monomers. Interestingly, the VCC content in both preparations was higher than AIBN, so it was decided to investigate what would happen if the proportion was inverted.

Two new polymers were synthesised: a non-imprinted nanogel, NIP **FM-P3** and the corresponding imprinted nanogel (MIP **FM-P4)**, using 5% of AIBN and 2.5% of VCC, while CM was reduced to 0.2% as an attempt to keep small particles size.

**Table 4.3.** Preparation of the NIP/MIP. Polymerisation was carried out at 70 °C for 2 days in DMSO. Dialysis was performed against water for two days followed by freeze-drier.

| | MIP/NIP | MBA | VCC | AIBN | $C_M$ | Yield | Solubility in Water |
|---|---|---|---|---|---|---|---|
| **FM-P3** | NIP | 20% | 2.5 % | 5 % | 0.2 % | 18.3% | 2 mg/mL |
| **FM-P4** | MIP | 20% | 2.5 % | 5 % | 0.2 % | 22% | 1 mg/mL |

By using AIBN in double concentration of VCC an improvement in the yield was observed. From < 10% obtained with **FM-P2** the chemical yield raised to around 20% for **FM-P3** and **P4**. This result confirmed the essential part played by the ratio AIBN-VCC. The particle size by number distribution was in the right range for the potential application of the nanogels, as shown in figure 4.15, with the size for both NIP and MIP found to be around < 30nm. However, the chemical yield was still particularly low, which meant there was a risk that the final polymer would be characterised by a very different ratio of the components used in the pre-polymerisation mixture.

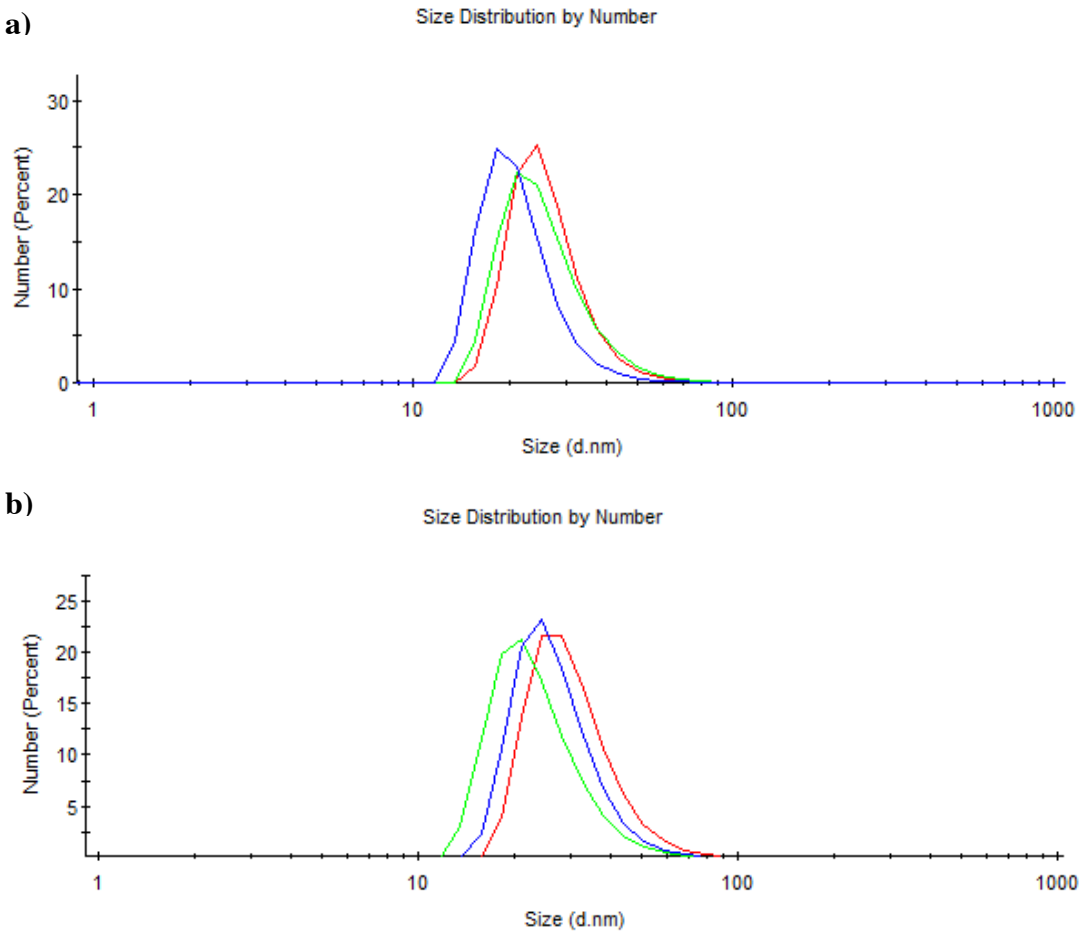


**Figure 4.15. a)** Particle size of NIP **FM-P3** was 27 ± 8 nm with PDI = 0.418. **b)** Particle size of MIP **FM-P4** (bottom graph) was 27 ± 8 nm with PDI = 0.303. The measurements were recorded as triplicates. Each line represents the average particle size over 15-17 scans of the nanogel

The fluorescence emission of the two nanogels was recorded after excitation at $\lambda_{exc}$ = 360 nm (figure 4.16).

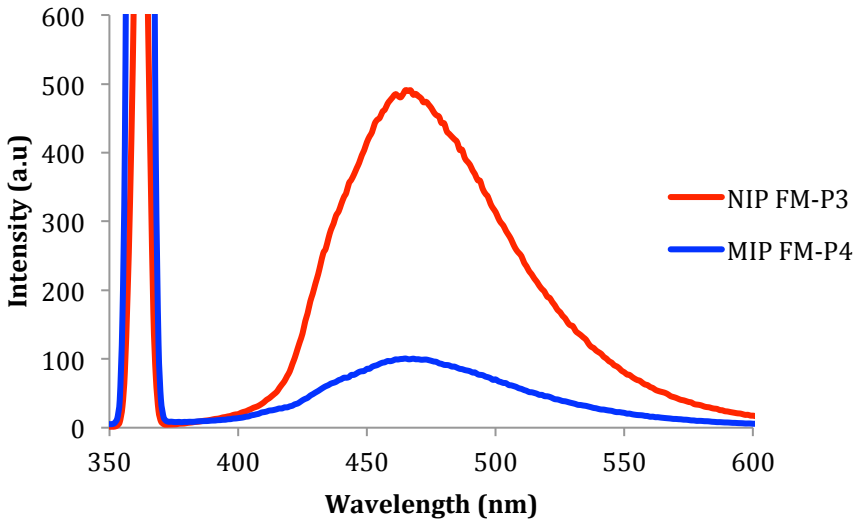


**Figure 4.16.** Fluorescence emission at $\lambda_{em}$ = 460nm of **FM-P3** (NIP) and **FM-P4** (MIP) at 1 mg/mL in water after excitation at $\lambda_{exc}$ = 360nm

The data show a very clear difference between the emission of **FM-P3** and MIP **FM-P4**. There are two possible explanation for this observation: on one side this could be the result of the fluorescent monomer being incorporated in different percentages in the two matrices, while another explanation could be based on the assumption that the drop in fluorescence for the MIP is the result of the quenching due to the presence of tamoxifen. As demonstrated in chapter 3 the fluorescence of the polymers is quenched by interactions between the functional monomer and the drug. Although further studies, aiming to quantify the functional monomer and tamoxifen, would help clarify such behaviour, these two nanogels were discarded due to low chemical yield. As previously mentioned, such little yield was probably due to the formation of a large portion of low molecular weight polymeric chains, which are not retained within the dialysis bag during the isolation step.

Following the first sets of preparation and careful analysis of the data the need for more work was very clear. At this stage there was a serious concern that the combination of low $C_M$ used in the preparation together with the balance between functional monomer

and initiator was having a negative impact on the polymerisation reaction and also on the yields. Therefore it was decided to try to further reduce VCC to 1% while increasing $C_M$ to 0.5%. This experiment was done only to evaluate the impact of these changes, as it was understood that polymers with 1% tag would not have sufficient cavities and fluorescence. The polymers NIP **FM-P5** and MIP **FM-P6** were prepared and characterised with the results shown in the table below.

**Table 4.4.** Preparation of the NIP/MIP. Polymerisation was carried out at 70 °C for 2 days in DMSO. Dialysis was performed against water for two days followed by freeze-drier.

| | MIP/NIP | MBA | VCC | AIBN | $C_M$ | Yield | Solubility in Water |
|---|---|---|---|---|---|---|---|
| **FM-P5** | NIP | 20% | 1 % | 5 % | 0.5 % | 86.3 % | 1 mg/mL |
| **FM-P6** | MIP | 20% | 1 % | 5 % | 0.5 % | 87.2 % | 0.75 mg/mL |

It was very interesting to observe that the chemical yield increased dramatically to over 85%. The results suggested that the combination of decreasing VCC while increasing $C_M$ led to this result. It was evident at this stage that the challenge was to find a balance between two key factors, the presence of sufficient initiator to counter balance the quenching effect of VCC while maintain a concentration of monomers in solutions sufficiently high to allow for the formation of particles that would not be lost during the purification step. Figure 4.17 shows that the particle size have increased in size, although remaining in the range (<100nm) required for the desired applications.

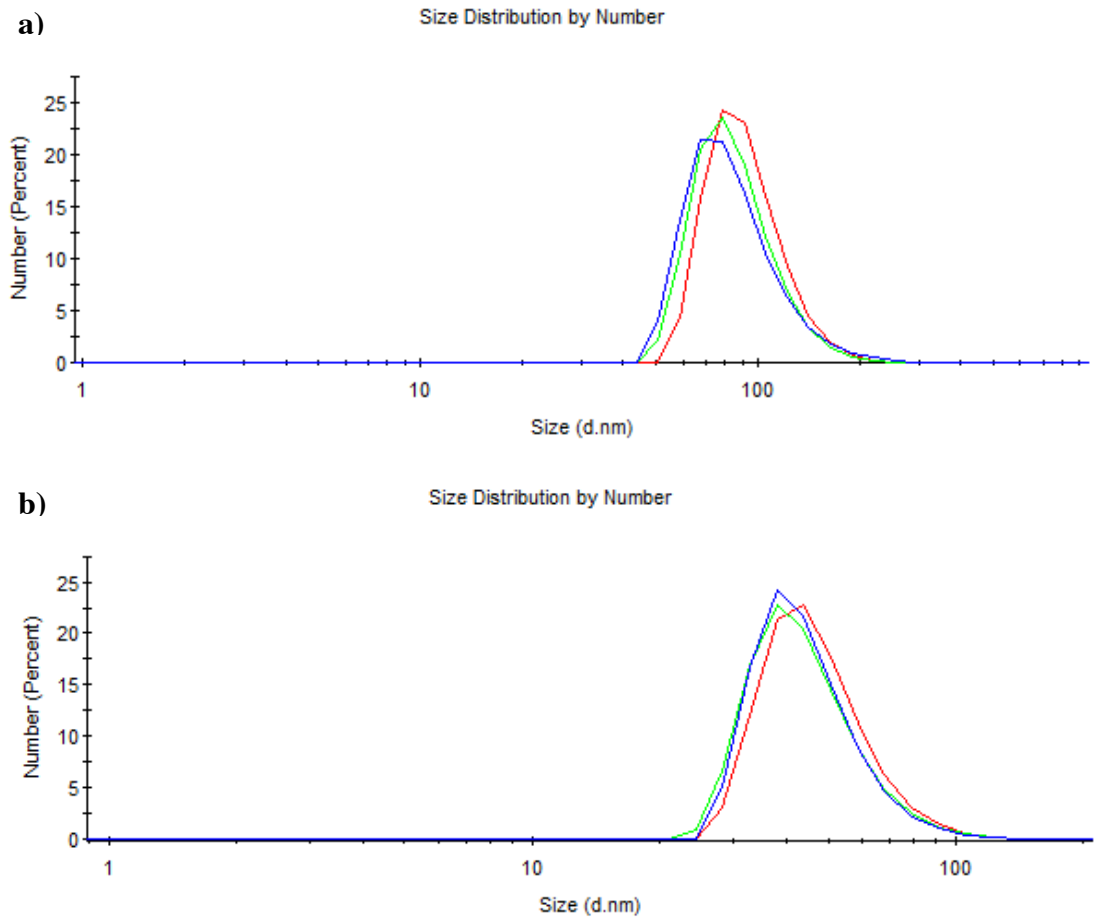


**Figure 4.17. a)** Particle size of NIP **FM-P5** (top graph) was 93 ± 25 nm with PDI = 0.284. **b)** Particle size of MIP **FM-P6** (bottom graph) was 48 ± 15 nm with PDI = 0.207. The measurements were recorded as triplicates. Each line represents the average particle size over 15-17 scans of the nanogel

Although the issue of the radical quenching was overcome by using a low concentration of the VCC functional monomer, such low content also affected the fluorescence of the nanogels. Intensity < 50 a.u. was showed by **FM-P5** and **FM-P6** (figure 4.18).

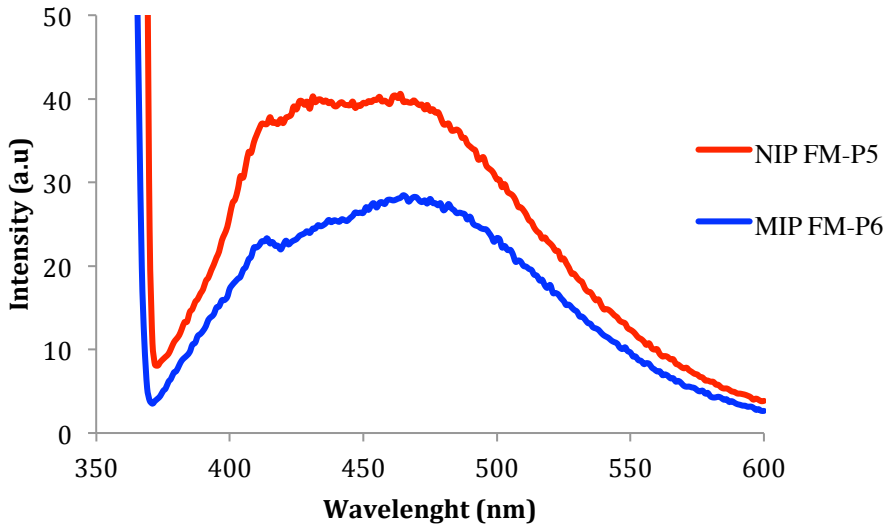


**Figure 4.18.** Fluorescence emission at $\lambda_{em}$ = 460nm of **FM-P5** (NIP) and **FM-P6** (MIP) at 1 mg/mL in water after excitation at $\lambda_{exc}$ = 360nm

The two preparations were obtained with very good chemical yields while maintaining the particle size in the desired range, however the fluorescent level displayed by the particles at the concentration of 1 mg/mL, required for further experiments, were not deemed sufficient.

The next step focused on the synthesis of two new polymers, **FM-P7** and **FM-P8**. Considering the low fluorescence intensity obtained with **FM-P5** and **P6**, the content of VCC in the new preparations was increased to 2.5%. Moreover, after evaluating the previous results, it was clear that the amount of initiator had a big impact on the formation of the nanogels and on their chemical yields. It was, therefore, decided to double the content of AIBN to 10% in order to increase the amount of radicals in solution and to push the formation of polymer with higher molecular weight that could be retained during the purification step.

**Table 4.5.** Preparation of the NIP/MIP. Polymerisation was carried out at 70 °C for 2 days in DMSO. Dialysis was performed against water for two days followed by freeze-drier.

| | MIP/NIP | MBA | VCC | AIBN | $C_M$ | Yield | Solubility in Water |
|---|---|---|---|---|---|---|---|
| **FM-P7** | NIP | 20% | 2.5 % | 10 % | 0.5 % | 53 % | 1 mg/mL |
| **FM-P8** | MIP | 20% | 2.5 % | 10% | 0.5 % | 40 % | 1 mg/mL |

Table 4.5 shows the content of each component for the new polymers **FM-P7** and **P8**. Unfortunately the chemical yields obtained were not as high as the previous ones (**FM-P5/P6**). However, recently, Mr. Pengfei Liu, a member of the Resmini's group, carried out NMR studies on the preparation of nanogels based on 20%MBA and 80%NIPAM, a very similar formulation to what was used in the synthesis of **FM-P7** and **FM-P8**. Results showed that increased amount of AIBN involved a faster polymerisation. After 48hrs the totality of MBA was consumed when 5% of initiator to the double bonds in the mixture was used. However, some NIPAM was left unreacted, thus confirming the first hypothesis that cross-linking agent was more reactive than the other monomers. Therefore, considering the higher amount (10%) of AIBN used in the preparation of **FM-P7/P8**, it was possible to assume a successful polymerisation of each monomer. This being said, the low chemical yield was likely due to the formation of polymeric chains with low molecular weight, lost during the isolation process, rather than a scarce incorporation of the monomers. Mr. Liu kindly provided the NMR spectra, which are reported in the annex at the end of this thesis.

The particle size of the imprinted polymer, 82nm, was bigger than the non-imprinted counterpart, 30nm (figure 4.19). One hypothesis is that the larger particle size was due to the presence of tamoxifen molecules trapped in the matrix. On the other side it is

known that the absence of template can change significantly the structure of the polymer.

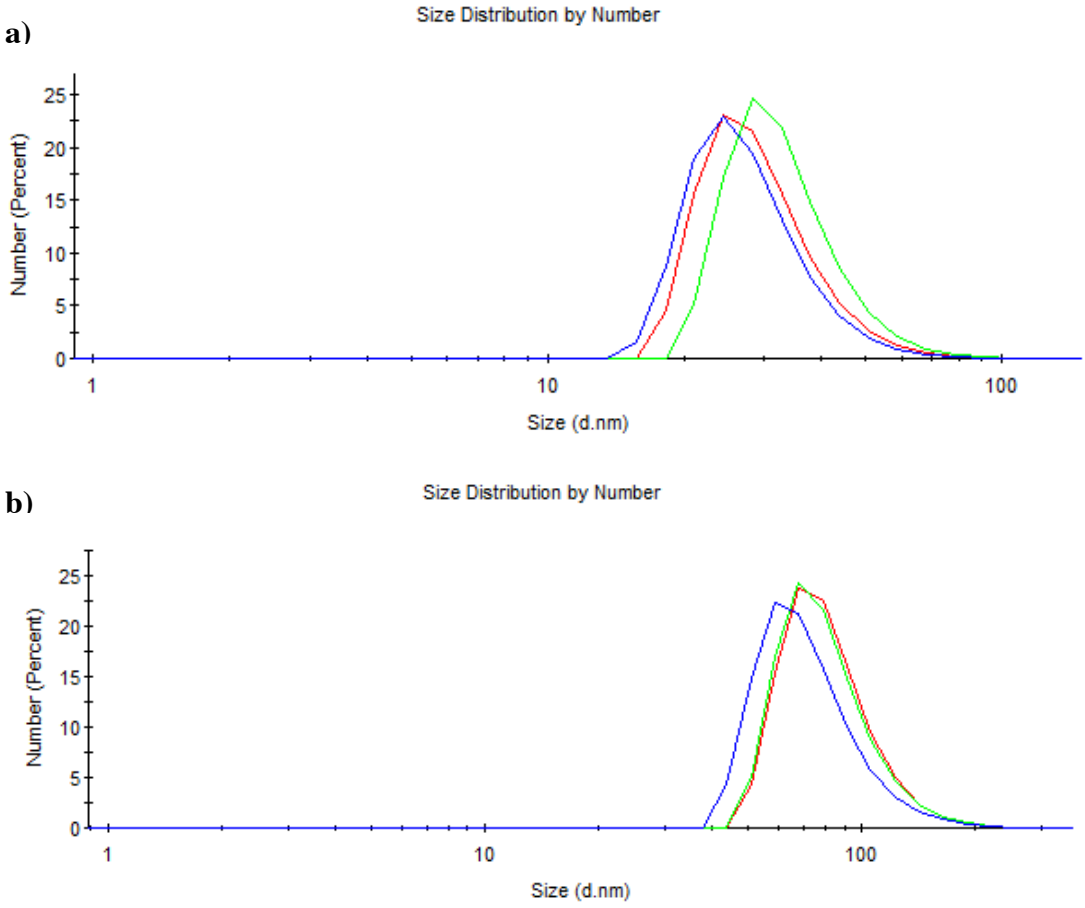


**Figure 4.19. a)** Particle size of **FM-P7** (top graph) was 30 ± 9 nm with PDI = 0.284. **b)** Particle size of **FM-P8** (bottom graph) was 82 ± 24 nm with PDI = 0.207. The measurements were recorded as triplicates. Each line represents the average particle size over 15-17 scans of the nanogel

In terms of fluorescence, NIP **FM-P7** showed a suitable intensity, as a result of the higher chemical yield obtained, which reflects the incorporation of the fluorescent monomer. The fluorescence spectrum of the MIP **FM-P8** was quite different compared to the NIP, showing significantly lower intensity (figure 4.20). Interestingly, the same trend previously observed in the other sets was maintained. Also in this case two possible scenarios were hypothesised. On one hand, the presence of the tamoxifen in the

imprinted nanogels, which quenches the VCC, on the other a different percentage of VCC incorporated in the two matrices.

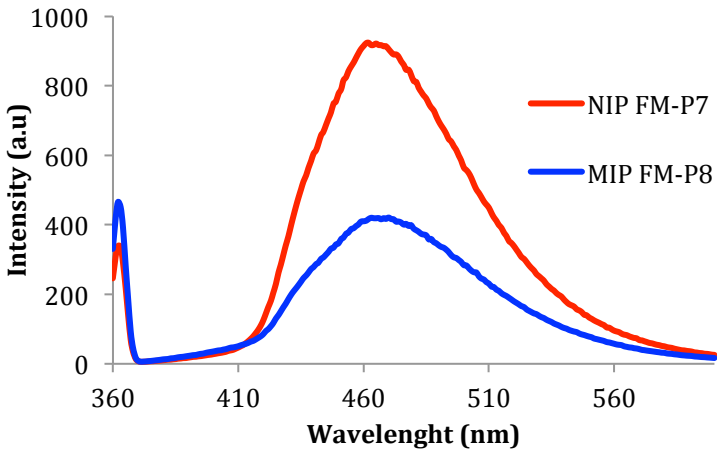


**Figure 4.20.** Fluorescence emission at $\lambda_{em}$ = 460nm of **FM-P7** (NIP) and **FM-P8** (MIP) at 1 mg/mL in water after excitation at $\lambda_{exc}$ = 360nm

Although, increasing the $C_M$ to 1% or incrementing the ratio between VCC and AIBN, would have probably provided better characteristics to the polymer, lack of time prevented the optimisation to be carried any further. Nevertheless, the two nanogels were shown to have a combination of good solubility, small particle size and high fluorescence that allowed these polymers to be taken to the next stage.

The thermo-responsiveness of the polymers **FM-P7** and **P8** was also investigated. NIPAM-based polymers are characterised by a phase transition or lower critical solution temperature. The cross-linked nanogels obtained by using this monomer show the same ability of swelling below the critical temperature and shrinking above it, as described in section 4.2.1. In the case of hydrogels/nanogels such temperature is known as volume phase transition temperature (VPTT), while the LCST is a term used for linear thermoresponsive polymers.[41] The VPTT/LCST is often determined by turbidimetry, which is the process of measuring the loss of intensity of transmitted light of a known

wavelength due to the scattering effect of particles suspended in the sample. VPTT is the temperature at which the transmittance (T) reaches 50% or, in other words, the temperature at the inflection point of the transmittance curve.

The VPTT of the nanogels was determined from the absorbance at λ = 500nm measured against temperature. The wavelength λ = 500nm was selected as this value was in the range of wavelength in which collapsed/shrunk nanogels where shown to absorb.[11] VPTT measurements were carried out on UV-Vis spectrophotometer coupled with a temperature controller in which the heating rate was set at 1°C every minute. The absorbance was transformed into transmittance in a second step. The analyses were performed on a solution of polymer dispersed in water at pH = 5.5, in order to relate the thermo-responsiveness to the potential environment of action of the nanogels, which is cancer cells characterised by acidic pH. The samples were prepared at a concentration of 1 mg/mL and were filtered on a 0.45µm GHP filter after 10 minutes sonication.

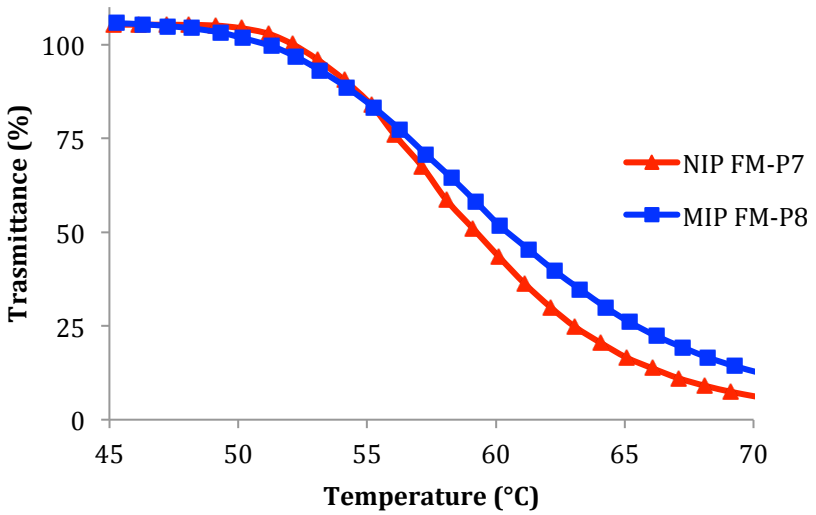


**Figure 4.21.** VPTT of NIP FM-P7 and MIP FM-P8. Absorption at $\lambda_{abs}$ = 500 nm, heating rate 1°C per minute. Samples concentration: 1 mg/mL in water at pH = 5.5

The NIP **FM-P7** showed 50% of transmittance at T = 58°C, while the MIP **FM-P8** at T = 60°C. The VPTT of the two preparations was particularly high and outside the range

of temperature reached by cancer cells in hyperthermia conditions (Section 4.2.1: colloidal stability and the backbone monomer). Comparison of these results with literature data provides evidence that the addition of a functional monomer, such as VCC, leads to very significant changes in the characteristics and morphologies of the polymers, probably also due to changes in the hydrophobicity of the matrix. By varying the amount of the cross-linker, the VPTT could be lowered to values closer to the required ones for biological applications; however, this would have required to further reducing the content of cross-linker. This would have had a significant impact on the possibility of creating well-defined three-dimensional pockets.

In order to demonstrate the formation of a covalent bond between the fluorescent functional monomer and the polymeric network, the two nanogels were further studied using fluorescence spectroscopy. Solutions of NIP and MIP **FM-P7** and **P8** were prepared in a mixture of 50:50 $H_2O$/MeOH at 0.5mg/mL. After stirring for 2 hours, the two solutions were dialysed against 10% MeOH in $H_2O$, changing the dialysis mixture three times in 24 hours, with the last change being 100% $H_2O$. The nanogels solutions were freeze-dried and reconstituted in $H_2O$ at the same original concentration, sonicated and filtrated before recording their fluorescence spectra.

This procedure aimed to cleave any possible non-covalent interactions between the VCC and the polymeric network, using a polar, protic organic solvent. MeOH was chosen, as it was previously demonstrated that this solvent was not sufficiently strong to disrupt the ionic interactions between tamoxifen and the acidic moiety of the functional monomer. To achieve it a mixture of MeOH and acidic acid was necessary to achieve drug release. [42, 43] Figure 4.22 shows the fluorescence spectrum of the two nanogels after treatment.

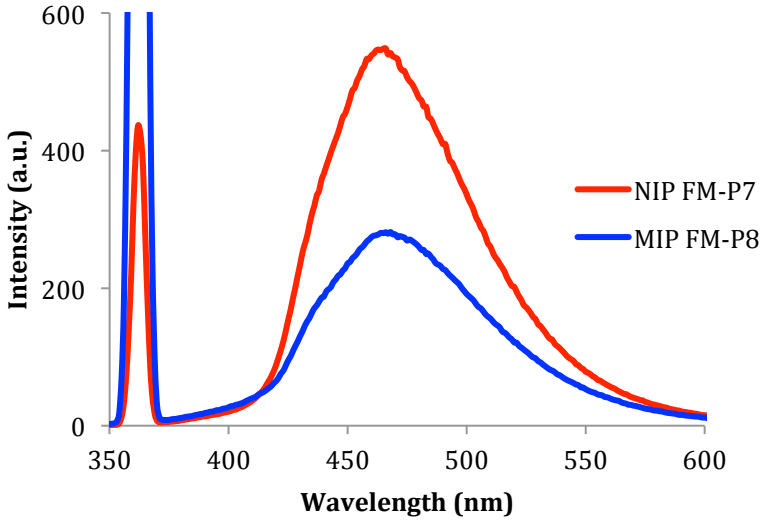


**Figure 4.22.** Fluorescence emission at $\lambda_{em}$ = 460nm after excitation at $\lambda_{exc}$ = 360nm of NIP **FM-P7** and MIP **FM-P8** at 0.5 mg/mL in $H_2O$ after MeOH treatment and dialysis

Due to lack of **FM-P7** and **P8**, it was decided to work with concentration of 0.5 mg/mL and to compare the results obtained in figure 4.22 with the fluorescence spectrum recorded during the characterisation of the polymers reported in figure 4.23.

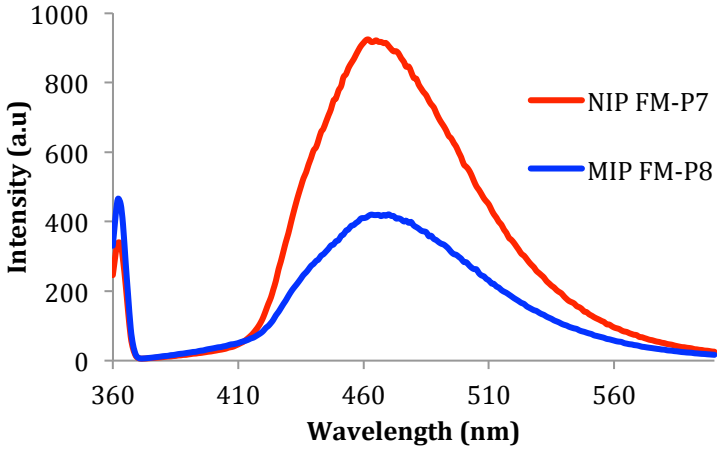


**Figure 4.23.** Fluorescence emission at $\lambda_{em}$ = 460nm of **FM-P7** (NIP) and **FM-P8** (MIP) at 1 mg/mL in water after excitation at $\lambda_{exc}$ = 360nm

Although different concentrations were compared, it was possible to confirm that the VCC was covalently linked within the polymer. In fact, the fluorescence emission of the

two nanogels treated with MeOH, showed in figure 4.22, ensured that no loss of fluorescent monomer occurred during the treatment. This result also suggested that the difference in emission between the imprinted and non-imprinted polymers was mainly due to the presence of the drug, which quenched the fluorescence, rather than a different percentage in the incorporation of fluorophor.

## 4.4. Quantification of the drug loaded in the polymeric matrix

As described in chapter 1 a number of different methods are available for the detection of tamoxifen (TAM). One of the most common modern methods of detection involves the use of high performance liquid chromatography (HPLC). HPLC is an efficient and accurate technique, which provides more precise and reproducible results compared to other approaches already mentioned (section 1.3.1). Moreover, it is characterised by low detection limits, which are important, given the small amount of tamoxifen that is expected in the nanogels. It was, therefore, decided to employ the HPLC to attempt a quantitative evaluation of the amount of TAM loaded in MIP **FM-P8**.

A new methodology was developed and optimised. It was found that good conditions for analysing tamoxifen in the column Hichrom C18 25mm were 85:15 methanol to water acidified with 0.5% acetic acid at a flow rate of 0.5 mL/min. This gave a peak at 6.8 minutes. Initially a reference line of tamoxifen in ACN was established (figure 4.24).

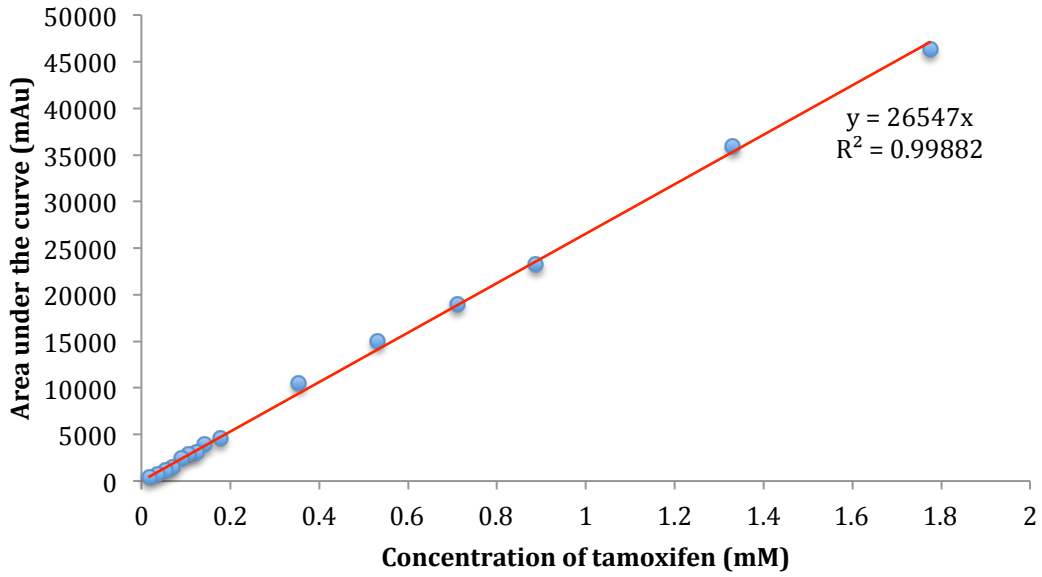


**Figure 4.24.** Reference line of the area under the curve obtained *via* HPLC against the concentration of tamoxifen injected. 20µL were injected in acetonitrile measuring the absorbance at 270nm. Flow rate was 0.5 mL/min using 85% MeOH, 15% water acidified with 0.5% acetic acid

Once the reference line was obtained and it was demonstrated to be reproducible by repeating the measurements, nanogel **FM-P8** was analysed using the same methodology developed. After polymerisation the nanogel was purified *via* dialysis against water in order to remove the polymeric chains with small molecular weight as well as the unreacted components. After dialysis the nanogel was freeze-dried, weighted and stored in the dark at room temperature. The nanogel was reconstituted in acidic MEOH/ACN 5:5 and stirred overnight in order to disrupt the interactions between the drug and functional monomer. The mixture was then filtered with a 20 nm filter to remove the polymer from the solution, leaving only the free tamoxifen in the filtrate. 20µL of the filtrate was then injected in HPLC. After such treatment of the sample, a clear HPLC profile with only one peak of the tamoxifen released from the nanogel was expected. Figure 4.25 shows the HPLC graph of the filtrate of **FM-P8** in acidic MEOH/ACN.

Although a peak compatible with tamoxifen was visible at retention time 7.4 minutes, other peaks were also present.

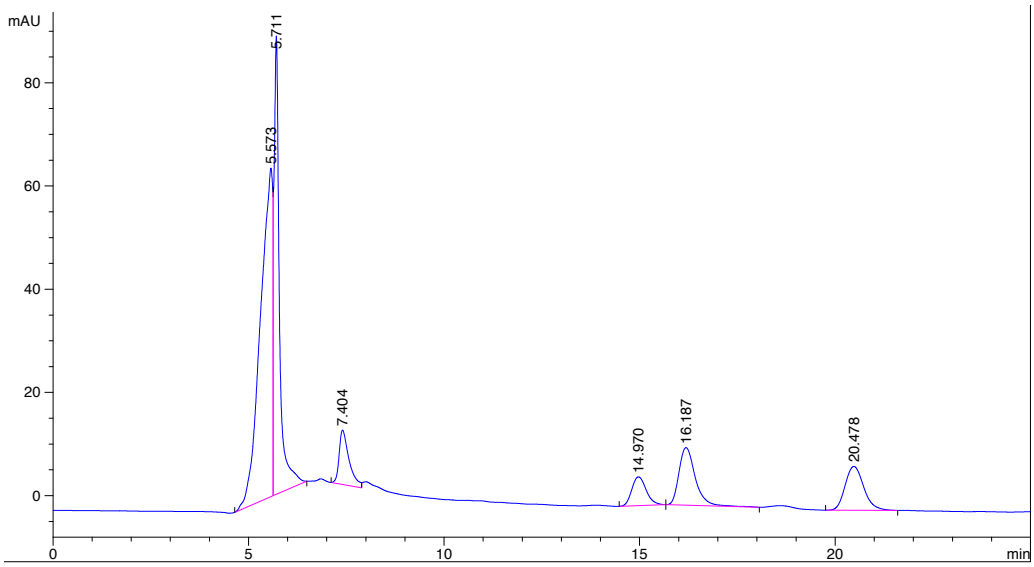


**Figure 4.25.** HPLC profile of the **FM-P8** at 1 mg/mL in acidic MEOH/ACN 50:50 after filtration with 20 nm filter. The peak at 7.4 min is compatible with tamoxifen

The peaks at shorter retention time, 5.57 and 5.71 minutes, could be caused by equilibrium between different isomers of tamoxifen or other issues arisen because of the presence of the polymeric matrix. In fact, the peaks at retention time 14.97, 16.18 and 20.47 minutes could probably be polymer peaks. Although the mixture was first filtered with a 20 nm filter, the nanogels are not all consistent in terms of size; therefore some small particles might have passed through the filter and be separated in HPLC giving the peaks. To ensure that the peak at retention time 7.404 min was tamoxifen, the same filtrate solution was spiked with a known concentration of tamoxifen free drug in the same solvent (figure 4.26).

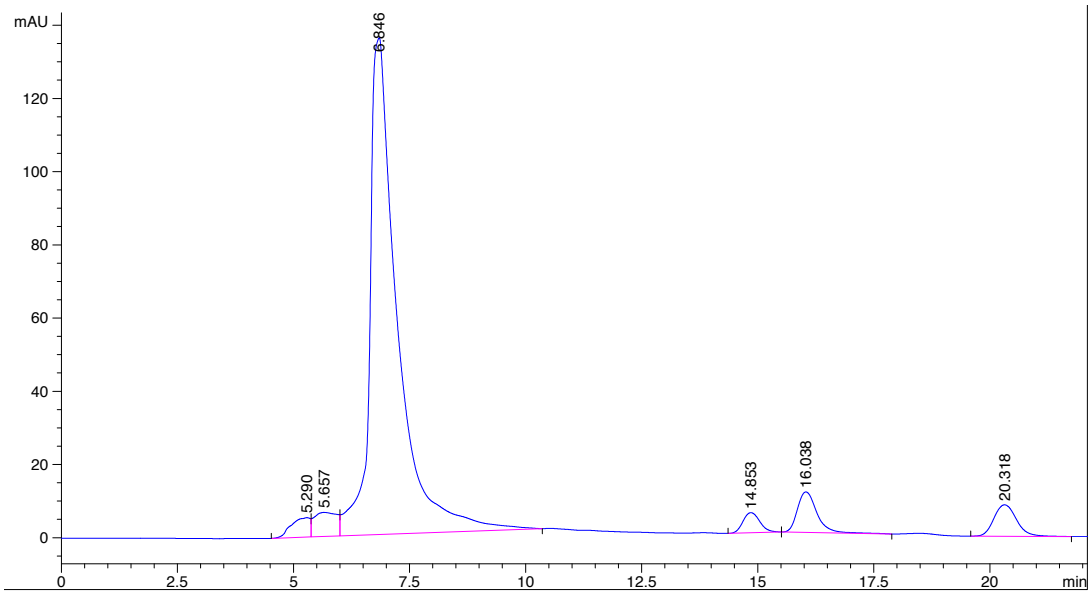


**Figure 4.26.** Solution of MIP **FM-P8** in acidic MEOH/ACN 50:50 filtrated with 20 nm filter and spiked with 70 µg/mL of tamoxifen in ACN

As shown in the figure above, a big peak appeared at retention time in between the other peaks (6.84 minutes). This suggested that the peak obtained at 7.4 min, in figure 4.25, was given by tamoxifen present in the polymeric network. However, the peak of tamoxifen was broad and not separated from the other peaks at the baseline, making an exact reading of the area under the curve for quantification of the drug very difficult. A number of other treatments of the samples were carried out to eliminate the components that interfered with tamoxifen's peak. However, a clearer and more defined HPLC profile was not achieved.

A possible explanation of the difficulties encountered in the evaluation of the amount of loaded drug could lie in the instability of tamoxifen, which is well known and documented in literature. [44, 45] Tamoxifen absorbs light in the solar irradiations UVB and UVA region and undergo to photochemical reactions. Products of such reactions include geometrical isomerisation, oxidation product of the C=C double bod or ring cyclisation to form phenantrene derivatives. As described in chapter 1, the photocyclisation of tamoxifen and the formation of fluorescent phenantrene derivatives

were used in the past for detecting the drug using HPLC coupled with fluorimeter. Given the inconclusive results obtained by using the available HPLC system and the pressure on time to provide evidence that tamoxifen was loaded in the matrix, as opposed to its precise quantification, it was decided to develop a new approach.

### 4.4.1. Photocyclisation of tamoxifen

This new method for the evaluation of tamoxifen was based on the formation of the drug's phenantrene derivative after UV irradiation and its visualisation using UV-Vis spectroscopy. The irradiation of a solution of tamoxifen in MeOH led to the presence of three new peaks in the UV spectrum of drug at $\lambda_{max}$ = 360, 344 and 300nm (figure 4.27). The intensity of the new peaks increased over time, reaching a maximum after 4 hours.

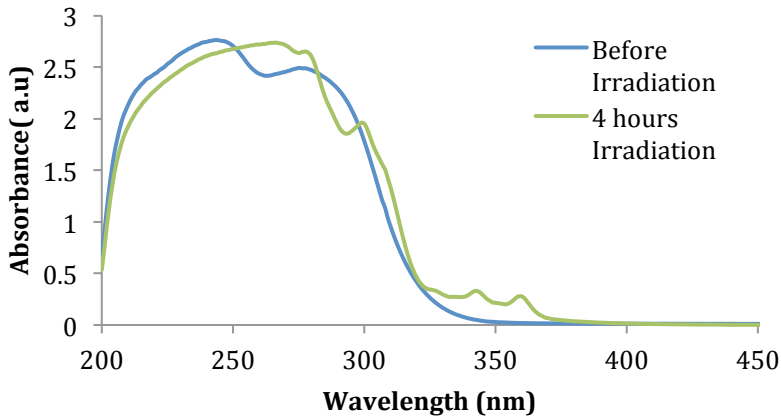


**Figure 4.27.** UV-Vis spectrum of tamoxifen in MeOH at 0.202μM before irradiation and after 4 hours irradiation. Three new peaks at $\lambda_{max}$ = 360, 344 and 300nm are formed after irradiation

Initially a reference line after 4 hours UV irradiation of tamoxifen in MeOH was recorded. After careful evaluation of the three peaks of the irradiated tamoxifen, it was chosen to monitor the peak at $\lambda_{abs}$ = 360nm, as it was more stable over time compared to the other peaks.

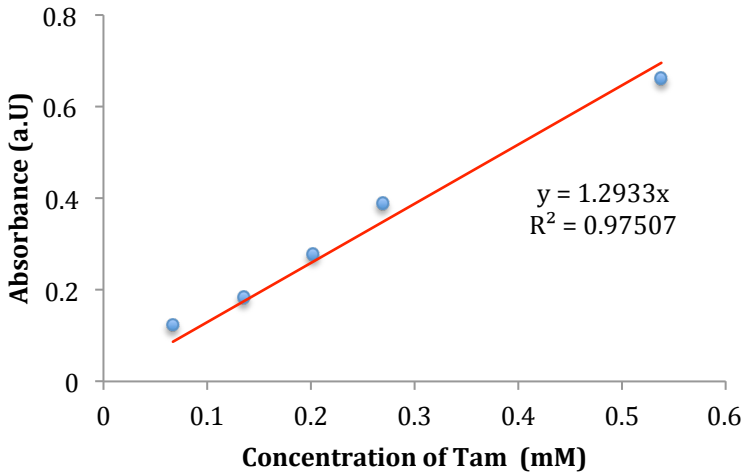


**Figure 4.28.** Reference line of tamoxifen in MeOH after 4 hours irradiation using a standard UV lamp at 365nm. The intensity of the peak at $\lambda_{max}$ = 360nm is reported against the concentration of tamoxifen

Once the calibration curve was obtained, solutions of NIP **FM-P7** and MIP **FM-P8** in MeOH were irradiated under UV lamp and the formation of new species at $\lambda_{abs}$ = 360nm was monitored *via* UV-Vis spectroscopy, as shown in figure 4.29. Figure 4.29 (a) shows the UV spectrum of NIP **FM-P7**. As expected, considering the lack of tamoxifen in the matrix, no peak was formed at $\lambda_{abs}$ = 360nm and no difference were visible after irradiation. Figure 4.29(b), shows the UV spectrum of **FM-P8** and, in figure 4.29(c), an enlargement between $\lambda_{abs}$ = 350-370nm shows more in details the presence of a peak at $\lambda_{abs}$ = 360nm.

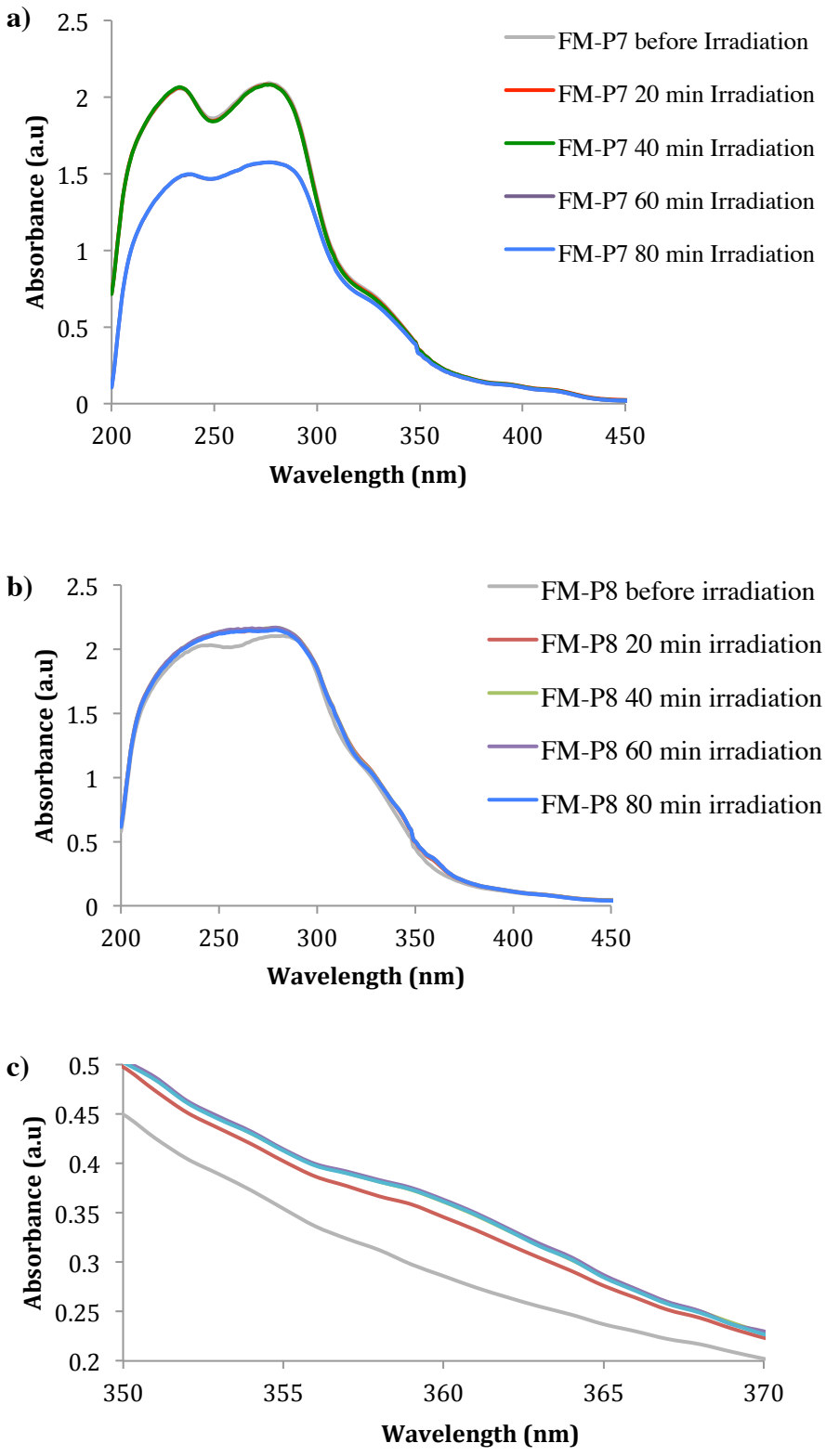


**Figure 4.29.** UV-Vis spectra of 1mg/mL in MeOH of **a)** NIP **FM-P7**; **b)** MIP **FM-P8**; **c)** Enlargement between $\lambda_{abs}$ = 350 and 370nm of the UV-Vis spectrum of MIP **FM- P8**.

The formation of this new peak, which was not observed before irradiation, suggested the presence of tamoxifen within the MIP matrix. MeOH, used to dissolve the polymer, disrupted the ionic interactions between the drug and the functional monomer, allowing the tamoxifen to be released in solution. Once the tamoxifen was free from the matrix, it photoreacted forming a new derivative, which absorbed at $\lambda_{abs}$ = 360nm. After 40 minutes irradiation the intensity of the peak in the MIP solutions reached a maximum, suggesting that the total amount of tamoxifen was transformed. Using the spectrum recorded before the irradiation as baseline, the maximum absorbance at $\lambda_{abs}$ = 360nm was determined. According to the reference line previously recorded, the evaluation of the loaded drug gave a value of 0.058mM of tamoxifen per mg of polymer. Once that the loaded tamoxifen was determined the percentage of drug incorporated in the matrix could be assessed. The percentage of tamoxifen incorporated was calculated as a ratio of the actual drug loaded in the matrix and the amount of drug used in the pre-polymerisation mixture, taking into account the chemical yield of the polymer (equation 4.2), which was found to be 31.2%.

$$\%\ of\ TAM = \frac{Actual\ Drug\ incorporated}{Theoreticanl\ Drug\ incorporated} \times 100 \qquad \textbf{Equation 4.2}$$

The 31.2% of the total amount of tamoxifen added in the mixture during the preparation of nanogels was successfully incorporated within the polymeric matrix. The rest could have been lost together with the rest of smaller polymeric chains during the purification. These results provided interesting preliminary data and an estimate of the drug loading in the polymers. Although this method may seem as a convoluted way of quantification and it was based on a chemical transformation, which could lead to by-products, it presented evidence of the presence of tamoxifen in the nanogel **FM-P8**. Therefore, it was agreed to use the preparations **FM-P7** and **P8** to carry out *in vivo* experiments, described in chapter 5.

## 4.5. Conclusions and future work

The molecular imprinting approach and high dilution polymerisation technique were employed in the preparation of water soluble nanogels with potential application as stimuli-responsive drug delivery carrier. The optimisation of the synthesis of nanogels containing 6-Vinylcoumarin-4-carboxylic acid (VCC) and N-isopropylacrylamide (NIPAM) led to the formulation of **FM-P7** and **FM-P8**. Evidence showed that VCC was successfully polymerised and the polymers presented good water solubility of 1 mg/mL, high fluorescence emission and small particles size in the range of 30-82nm. Initial issues, encountered during quantification of the loaded drug using HPLC, were overcome resorting to photochemical transformation of tamoxifen. UV-irradiation of MIP solutions gave a new absorbance peak, which was used to evaluate the amount of loaded drug. According to the reference line, previously obtained by irradiating solution of tamoxifen at different concentrations, the amount of drug incorporated in **FM-P8** was 0.058mM per mg of polymer.

Future works should involve further optimisation of the HPLC-based method for quantification of the loaded drug. In fact, by using the HPLC quantification of the drug would become a lot faster and more sensible compared to the method applied in this project. Modification of the methodology, for example by changing the retention time of tamoxifen and the eluent solvent, could give better separation between the peak of TAM and contaminants. This would allow a clearer reading of the area under the curve, allowing more accurate quantification. Another way to optimise the quantification of the drug would be to adapt the HPLC approach to the detection of photocyclisation products. This could be possible by irradiate the sample with UV light, separate it in the chromatographic column and use a fluorescence detector to increase the sensitivity. Once an easier and more precise evaluation of the amount of TAM would be possible,

the next step for the **FM-P8** nanogel would be to carry out drug release studies at pH: 5.5, the conventionally chosen pH for anticancer drug delivery system test. The determination of the drug release profile would give information on the ability of the system to provide a sustained drug release.

## 4.6. References

1. Zaidi, S. A., Molecular imprinted polymers as drug delivery vehicles. *Drug delivery* **2016,** *23* (7), 2262-2271.

2. Wang, N. X.; Von Recum, H. A., Affinity-based drug delivery. *Macromolecular bioscience* **2011,** *11* (3), 321-32.

3. Lulinski, P., Molecularly imprinted polymers as the future drug delivery devices. *Acta Poloniae Pharmaceutica* **2013,** *70*, 601-609

4. Suedee, R.; Srichana, T.; Rattananont, T., Enantioselective Release of Controlled Delivery Granules Based on Molecularly Imprinted Polymers. *Drug delivery* **2002,** *9*, 19-30.

5. Maddock, S. C.; Pasetto, P.; Resmini, M., Novel imprinted soluble microgels with hydrolytic catalytic activity. *Chem Commun* **2004,** (5), 536-7.

6. Sultana, F.; Manirujjaman.; Imran-Ul-Haque; Arafat, M.; Sharmin, S., An Overview of Nanogel Drug Delivery System. *Journal of Applied Pharmaceutical Science* **2013,** *3*, S95-S105.

7. Oh, J. K.; Drumright, R.; Siegwart, D. J.; Matyjaszewski, K., The development of microgels/nanogels for drug delivery applications. *Prog. Polym. Sci.* **2008,** *33*, 448–477.

8. Pérez-Moral, N.; Mayes, A. G., Comparative study of imprinted polymer particles prepared by different polymerisation methods. *Analytica Chimica Acta* **2004,** *504*, 15–21.

9. Sanson, N.; Rieger, J., Synthesis of nanogels/microgels by conventional and controlled radical crosslinking copolymerization. *Polymer Chemistry* **2010,** *1* (7), 965.

10. Carboni, D.; Flavin, K.; Servant, A.; Gouverneur, V.; Resmini, M., The first example of molecularly imprinted nanogels with aldolase type I activity. *Chemistry* **2008,** *14* (23), 7059-65.

11. Zielinska, K.; Sun, H.; Campbell, R. A.; Zarbakhsh, A.; Resmini, M., Smart nanogels at the air/water interface: structural studies by neutron reflectivity. *Nanoscale* **2016,** *8* (9), 4951-60.

12. Gao, W.; Chan, J. M.; Farokhzad, O. C., pH-Responsive nanoparticles for drug delivery. *Molecular pharmaceutics* **2010,** *7* (6), 1913-20.

13. Vaupel, P.; Kallinowski, F.; Okunieff, P., Blood Flow, Oxygen and Nutrient Supply, and Metabolic Microenvironment of Human Tumors: A Review *CANCER RESEARCH* **1989,** *49*, 6449-6465.

14. Fleige, E.; Quadir, M. A.; Haag, R., Stimuli-responsive polymeric nanocarriers for the controlled transport of active compounds: concepts and applications. *Adv Drug Deliv Rev* **2012,** *64* (9), 866-84.

15. (a) Yang, B.; Li, Y.; Sun, X.; Meng, X.; P., C.; Liu, N., A pH-responsive drug release system based on doxorubicin conjugated amphiphilic polymer coated quantum dots for tumor cell targeting and tracking. *Journal of Chemical Technology and Biotechnology* **2013,** *88*, 2169--2175; (b) Dai, X.; Hong, C.; Pan, C., pH-Responsive

Double-Hydrophilic Block Copolymers: Synthesis and Drug Delivery Application. *Macromolecular Chemistry and Physics,* **2012,** *213*, 2192--2200.

16. Fang, C.; Kievit, F. M.; Veiseh, O.; Stephen, Z. R.; Wang, T.; Lee, D.; Ellenbogen, R. G.; Zhang, M., Fabrication of magnetic nanoparticles with controllable drug loading and release through a simple assembly approach. *Journal of controlled release : official journal of the Controlled Release Society* **2012,** *162* (1), 233-41.

17. Pasetto, P.; Maddock, S. C.; Resmini, M., Synthesis and characterisation of molecularly imprinted catalytic microgels for carbonate hydrolysis. *Analytica Chimica Acta* **2005,** *542* (1), 66-75.

18. Amended final report on the safety assessment of polyacrylamide and acrylamide residues in cosmetics. *International journal of toxicology* **2005,** *24 Suppl 2*, 21-50.

19. Papadimitriou, S. A.; Robin, M. P.; Ceric, D.; O'Reilly, R. K.; Marino, S.; Resmini, M., Fluorescent polymeric nanovehicles for neural stem cell modulation. *Nanoscale* **2016,** *8* (39), 17340-17349.

20. Yoshida, R.; Sakai, K.; Okano, T.; Sakurai, Y., Modulating the phase transition temperature and thermosensitivity in N-isopropylacrylamide copolymer gels. *Journal of Biomaterials Science, Polymer Edition* **1994,** *6*, 585-598.

21. Dimitrova, I.; Trzebicka, B.; Muller, A.; Dworak, A.; Tsvetanov, C., Thermosensitive water-soluble copolymers with doubly responsive reversibly interacting entities. *Prog. Polym. Sci.* **2007,** *32*, 1275–1343.

22. Grinberg, N.; Dubovik, A.; Grinberg, V.; Kuznetsov, D.; Makhaeva, E.; Grosberg, A.; Tanaka, T., Studies of the Thermal Volume Transition of Poly(N-isopropylacrylamide) Hydrogels by High-Sensitivity Differential Scanning Microcalorimetry. 1. Dynamic Effects. *Macromolecules* **1999,** *32*, 1471-1475.

23. Bikram, M.; West, J., Thermo-responsive systems for controlled drug delivery *Expert Opin. Drug Deliv.* **2008,** *5*, 1077-1091.

24. Abulateefeh, S. R.; Spain, S. G.; Aylott, J. W.; Chan, W. C.; Garnett, M. C.; Alexander, C., Thermoresponsive polymer colloids for drug delivery and cancer therapy. *Macromolecular bioscience* **2011,** *11* (12), 1722-34.

25. Sheppard, C. S.; Kamath, V. R., The Selection and Use of Free Radical Initiators. *Polymer Engineering and Science* **1979,** *19*, 597-606.

26. Golker, K.; Karlsson, B. C. G.; Olsson, G. D.; Rosengren, A. M.; Nicholls, I. A., Influence of Composition and Morphology on Template Recognition in Molecularly Imprinted Polymers. *Macromolecules* **2013,** *46* (4), 1408-1414.

27. Muhammad, T.; Nur, Z.; Piletska, E. V.; Yimit, O.; Piletsky, S. A., Rational design of molecularly imprinted polymer: the choice of cross-linker. *The Analyst* **2012,** *137* (11), 2623-8.

28. Henschel, H.; Kirsch, N.; Hedin-Dahlström, J.; Whitcombe, M. J.; Wikman, S.; Nicholls, I. A., Effect of the cross-linker on the general performance and temperature dependent behaviour of a molecularly imprinted polymer catalyst of a Diels–Alder reaction. *Journal of Molecular Catalysis B: Enzymatic* **2011,** *72* (3-4), 199-205.

29. (a) Erturk, G.; Mattiasson, B., Molecular Imprinting Techniques Used for the Preparation of Biosensors. *Sensors* **2017,** *17* (2); (b) Kueseng, P.; Noir, M. L.;

Mattiasson, B.; Thavarungkul, P.; Kanatharana, P., Molecularly imprinted polymer for analysis of trace atrazine herbicide in water. *Journal of environmental science and health. Part. B, Pesticides, food contaminants, and agricultural wastes* **2009,** *44* (8), 772-80.

30. Alfrey, T.; Price, C. C., Relative Reactivities in Vinyl Copolymerization. *Jounul of Polymer Science: Part A: Polymer Cbmiatry* **1996,** *34*, 157-162

31. Beltran, A.; Borrull, F.; Cormack, P. A. G.; Marce, R. M., Molecularly-imprinted polymers: useful sorbents for selective extractions. *Trends in Analytical Chemistry* **2010,** *29*, 1363-1375.

32. Graham, N. B.; Cameron, A., Nanogels and microgels: The new polymeric materials playground. *Pure &Appl. Chem.* **1998,** *70*, 1271-1275.

33. Graham, N. B.; Hayes, C. M. G., MICROGELS 1 : Solution Polymerization Using Vinyl Monomers. *Macromol. Symp.* **1995,** *93*, 293-300.

34. Biffis, A.; Graham, N. B.; Siedlaczek, G.; Stalberg, S.; Wulff, G., The Synthesis, Characterization and MolecularRecognition Properties of Imprinted Microgels. *Macromol. Chem. Phys.* **2001,** *202*, 163-171.

35. Ray, J. V., Novel Molecular Imprinted Nanogels As Drug Delivery Vehicles For Tamoxifen. *A thesis presented in partial fulfillment of the Degree of Doctor of Philosophy at the University of London* **2014**.

36. Servant, A., Synthesis And Characterisation Of Molecularly Imprinted Nanoparticles With Enzyme-Like Catalytic Activity For The Kemp Elimina Tion. *A thesis presented in partial fulfillment of the Degree of Doctor of Philosophy at the University of London* **2010**.

37. Sun, H., Structural and interactions studies of thermoresponsive NIPAM nanogels at interfaces. *School of Biological and Chemical Sciences, Queen Mary University of London* **2015**.

38. Tashakori-Sabzevar, F.; Mohajeri, S. A., Development of ocular drug delivery systems using molecularly imprinted soft contact lenses. *Drug development and industrial pharmacy* **2015,** *41* (5), 703-13.

39. Malvern, Zetasizer Nano User Manual. *Malvern Instrument Ltd.* **2004**.

40. Arzenšek, D., Dynamic light scattering and application to proteins in solutions. *Seminar for University of Ljubljana* **2010**, 1-18.

41. Constantin, M.; Cristea, M.; Ascenzi, P.; Fundueanu, G., Lower critical solution temperature versus volume phase transition temperature in thermoresponsive drug delivery systems. *Express Polymer Letters* **2011,** *5* (10), 839-848.

42. Rashida, B. A.; Briggs, R. J.; Hay, J. N.; Stevenson, D., Preliminary Evaluation of a Molecular Imprinted Polymer for Solid-phase Extraction of Tamoxifen. *Analytical Communications1* **1997,** *34*, 303-305.

43. Claude, B.; Morin, P.; Bayoudh, S.; de Ceaurriz, J., Interest of molecularly imprinted polymers in the fight against doping. Extraction of tamoxifen and its main metabolite from urine followed by high-performance liquid chromatography with UV detection. *Journal of chromatography. A* **2008,** *1196-1197*, 81-8.

44. Furr, B. J. A.; Jordan, V. C., The Pharmacology And Clinical Uses Of Tamoxifen. *Pharmac. Ther.* **1984,** *25* 127-205.

45. Wang, L.; Wang, S.; Yin, J. J.; Fu, P. P.; Yu, H., Light-Induced Toxic Effects of Tamoxifen: A Chemotherapeutic and Chemopreventive Agent. *Journal of photochemistry and photobiology. A, Chemistry* **2009,** *201* (1), 50-56.

# Chapter 5

## *In vivo* system for toxicity and drug visualisation studies

# 5. *In vivo* system for toxicity and drug visualisation studies

## 5.1. Introduction

Given the recent growth in the design of nanomaterials for therapeutic uses, a thorough understanding of the associated systemic and local toxicity as well as the biodistribution of the nanomaterials is of high importance.[1] These materials have different characteristics compared to their bulk counterpart, mainly due to their nano-size. The small particle size, the increased surface-to-volume ratio, the shape and the surface chemistry altogether influence the potential toxicity of the nanoparticles. [2] As already described in the previous chapter, small particles are expected to be easily internalised into the cells and to penetrate and translocate across epithelial and endothelial cells. For these reasons, nanoparticles tend to accumulate in tissues with high phagocytic activity like spleen, kidneys, liver and lungs, where they may interfere with the biological functions of the tissues. [3] As nanotechnology is a relatively recent field, the medium and long-term effects of such nanoparticles are still not completely known. Moreover, the use of nanoparticles with unknown toxicological properties represents hazards not only for human health but also for the environment and wildlife.

International guidelines for assessing the effects of chemicals on human health and environment were first drawn up in 1980 and are constantly updated by the Organisation for Economic Cooperation and Development (OECD). Animals with similar genetics and physiology to humans are often used for testing potential human treatments. *In vivo* testing can provide important information regarding the absorption, distribution, metabolism and toxicity of nanomaterials. As expected, there are laws that regulate the use of animals in science, with particular attention to their care and welfare.[4] The Animal (scientific procedures) Act, compiled in the UK in 1986, requires

scientists to obtain a personal licence, in order to perform procedures on animals, and also a licence for the project in which the animals are used; another licence is necessary for the institute where the animals are housed. Research proposals are fully assessed in terms of potential harm to the animals and the procedures or experiments are examined in details, before the licences are issued. Animal research is also governed by the principles of the 3Rs: Refinement, Replacement and Reduction, that were first defined by Russel and Burch. [5] "Refinement" means reducing the amount of stress and pain an animal is exposed to. In order to do so, it is important to employ the least invasive techniques and control the pain of the animal throughout the procedure. "Replacement" denotes the substitution of the living models with *in vitro* testing, computer modelling and statistical assessment, whenever it is possible. "Reduction" intends keeping the number of animals used in the experiments to a minimum. As a result of the above, all the experiments described in this chapter were done in compliance with these principles and carried out under the project licence, number P6D11FBCD, and the personal licence, number ICC74C01A1, issued by the Home Office.

## 5.2. Review of *in vivo* models – Toxicity screening

It is essential to screen the new therapeutics for pharmacological activity and potential toxicity, before starting human clinical trials. Pre-clinical toxicity screening on animal models shows toxic effects of the tested compound in relation to the organs, the dose and species. [6] The same amount of comprehensive information could not be obtained by using only animal-free alternatives, such as *in vitro* testing or computer modelling. Although these strategies are useful for initial indication of toxicity, the results obtained are significantly different from the information provided by *in vivo* experimentation.

A number of different animal species are used depending on the specific toxicity test carried out. For example, rabbits[7] and guinea pigs[8] are employed in acute toxicity testing for topical preparation, with particular attention on eyes and skin irritation; hamsters and gerbils are used for testing chronic toxicity and carcinogenesis bioassays; [9] non-humans primates[10] and dogs[11] are often employed for toxicokinetic studies. However, mice represent the most widely used *in vivo* system. [12, 13] This is primarily due to the model's physiological similarity to humans as well as the incredibly high amount of available mutant loci, either spontaneous or chemically induced, that gives rise to a number of potential models of different human diseases. Therefore, several treatment strategies are pre-clinically tested on mice, contributing to increasing the importance of mouse models. Examples of nanoparticle toxicity investigations carried out in mice are abundant in the literature. In 2007, for example, Cha and Myung tested the acute toxic effect of metal-based nanoparticles using a mouse model. [14] Non-specific toxicity manifested as a haemorrhage in the heart, lymphocytic infiltration in the liver, stomach and intestine, and medullary congestion in the spleen. The group was able to demonstrate that the acute toxicity was not dependent on the size of the nanoparticles but was instead due to the presence of the inorganic particles. Also magnetic iron oxide nanoparticles, with potential imaging and therapeutic functions, were widely tested in mice. [15] Quan *et al*. developed human serum albumin coated iron oxide nanoparticles, encapsulated with doxorubicin, to be subcutaneously injected into anesthetised mice. [16] Such formulation was not toxic to the mice. In addition *in vivo* imaging as well as *ex vivo* biodistribution confirmed the tumour targeting characteristics of the nanoparticles and the tumour suppression effect of the encapsulated doxorubicin. Nanomaterials, other than metal nanoparticles, such as micelles, [17] nanotubes, [18] solid lipid nanoparticles[19] and many others[20, 21] have also been tested in mice over the years. As

already mentioned, animal testing is a necessary first step towards the development of new materials with therapeutic potential. Such compounds can move forward to human clinical trials only when their toxic levels and efficacy in the therapy have been evaluated in animals first.

## 5.3. Zebrafish as novel *in vivo* system

Although mammals are widely used as human pathology models and for toxicity screening, they present some disadvantages. Life cycles and developmental stages are time-consuming and involve high housing costs. Moreover, foetal experiments are difficult, due to internal fertilisation, which would require embryonic manipulations inside the mother.

Recently, *Denio rerio*, more commonly known as zebrafish, has seen an exponential growth as a novel alternative to mammalian models for development, disease, and toxicological studies. Zebrafish is a species of tropical freshwater fish commonly found in slow-moving or stagnant water. [22] Females can spawn every 2-3 days producing between 100 and 200 eggs per clutch. [23] When fertilised, the eggs are only 0.7 mm in diameter and are optically transparent, thus allowing easy monitoring through all developmental stages. The development of the embryos is very rapid. In only 36 hours post fertilisation (hpf) it is possible to observe precursors of the major organs and at 3 days post fertilisation (dpf) the embryos hatch, entering into their larval period. By 5 dpf, the organs and tissues are fully developed; larvae grow their swim bladder, they start swimming actively, they show active avoidance behaviour (escape responses), respiratory movements and they start seeking for and swallowing food (figure 5.1). [24]

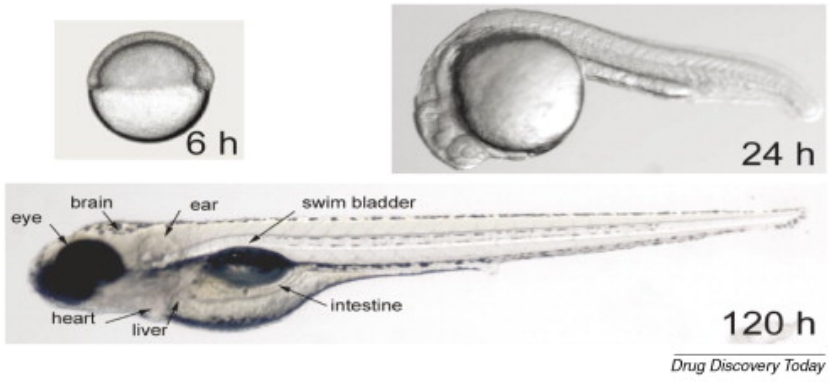


**Figure 5.1.** A representative image of zebrafish developmental stages at 6, 24 and 120 hpf. By 120 hpf, the larvae are fully developed and start swimming and searching for food. Image reproduced with permission from McGrath *et al*.[24]

Zebrafish are characterised by a series of features that make them complementary to the mammalian models. Their genome, brain patterning and structure/function of many neural, physiological and anatomical systems are similar to rodents and humans. [25] They also show an innate immune system, monocyte/macrophages, and adaptive immune systems. [26] Regarding the similarity with humans, the fully mapped genome of zebrafish shows that 70% of human genes have at least one obvious zebrafish orthologue, suggesting that there could be a match of the genes involved in human diseases to the zebrafish genome.[27] Furthermore, targeted genetic modifications have been introduced in zebrafish embryos in order to generate mutant alleles that copy human disease loci, making this animal system a good human pathology model. [22]

The characteristics of zebrafish, including their small size, ease of handling, rapid development, transparency, high number of eggs per clutch and low housing costs, make them ideal for fast and reliable pre-clinical screenings of materials with therapeutic applications. [28, 29] The drug and toxicology screening procedure simply requires the dispersion of the chemical compounds under examination in water. Larvae at the same developmental stage are immersed in the solution and checked for physical

or behavioural changes caused by the molecules at different concentrations. In case of hydrophobic compounds or large molecules, it is safe to use DMSO up to 1% v/v as the carrier or to inject such compounds into the yolk sac, the sinus venosus or the circulatory system. Fish larvae can live for seven days in a single well of a standard 96-well plate with no food, only supported by nutrients stored in the yolk sac. This is a significant advantage over mammalian models, which require higher maintenance efforts. Zebrafish larvae younger than 5 dpf can absorb any analyte, dispersed in the surrounding media, through their skin and gills; after 5 dpf they actively begin to swallow the materials. Another advantage of using zebrafish compared to other animals lies in the opportunity to use significantly larger numbers of zebrafish for each assay, with lower associated costs compared to mammals. Moreover, the larvae maintain their transparency for several days, therefore allowing an easier monitoring of the effect of the tested compounds. [24]

Literature review indicates that nanotoxicity screening using zebrafish has increased considerably in the last 10 years (figure 5.2).

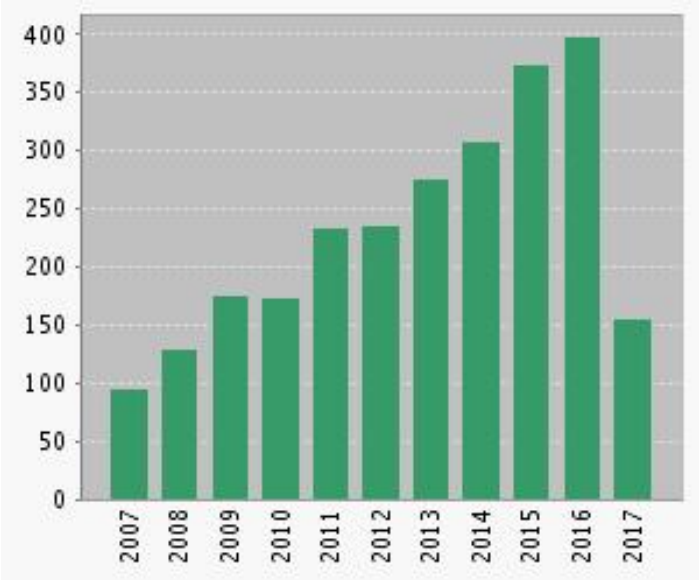


**Figure 5.2.** Increasing trend in the number of publications in zebrafish research (2006–2016). Keyword "zebrafish" searched performed on web of knowledge database and refined by "toxicology" and "nanoscience/nanotechnology". Search conducted on 19th May 2017.

Recent examples found in the literature involve toxicity studies for graphen oxide, [30] a number of different nanoparticles[31, 32] and carbon nanotubes functionalised with polyethylene glycol. [33] Zebrafish were examined in terms of survival rate and altered morphology, as well as hatching rate and spontaneous movement.

### 5.3.1. LoxP - Cre$^{ERt}$ system for tamoxifen release studies

Among the transgenic lines of zebrafish available at the moment, the Cre/loxP system is the most interesting for the purpose of this thesis. The Cre/lox is a site-specific recombination system, which was first employed in mice and gradually adapted for a variety of animal models, including zebrafish. [34] The Cre/loxP site-specific recombination is a technique commonly used to artificially control, either spatially or temporally, gene expression by recombination of DNA *in vivo*. This technique utilises the enzyme Cre recombinase, which recognises a specific 34 base pair DNA sequence, named loxP site (locus X-over in P1 bacteriophage). The Cre recombinase catalyses recombination of the particular genetic sequence contained between two loxP sites, called loxP-floxed genes. According to the orientation of the loxP sites, the Cre recombinase can catalyse deletion, translocation or inversion of the loxP-floxed genes (figure 5.3). [35]

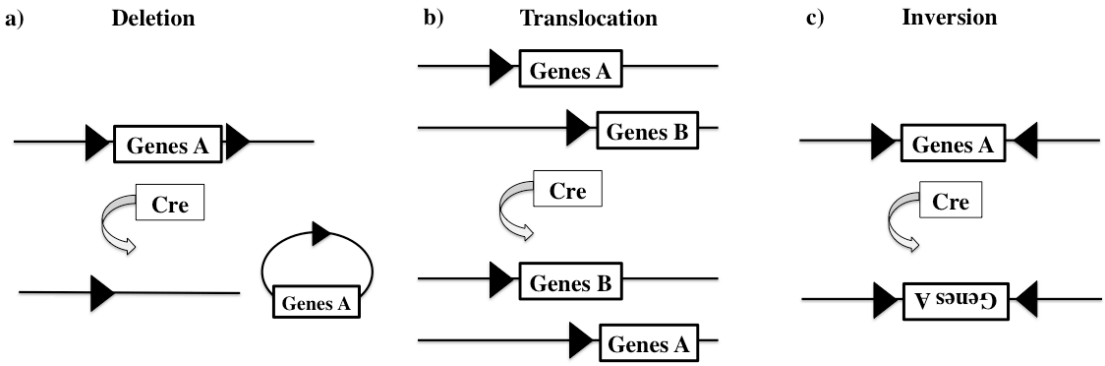


**Figure 5.3.** Schematic representation of the Cre/loxP system. Gene A/B represents the loxP-floxed genetic sequence of interested, flanked by loxP sites represented by black triangles. **a)** The Cre recombinase catalyses the deletion of the flanked genes when the loxP sites are oriented in parallel (head-to-tail). **b)** The translocation of genes A and B is promoted by the Cre recombinase when the loxP sites are on separate DNA strands. **c)** Cre recombinase catalyses the inversion of genes A when the loxP sites have an anti-parallel orientation (head-to-head)

A very useful application of this approach lies in the generation of transgenic zebrafish lines designed to switch fluorescence from green to red (G2R) by knocking out or expressing two different fluorescent proteins: GFP (green fluorescent protein) and RFP (red fluorescent protein). [36] This is achieved by flanking the genetic sequence that expresses the GFP with two loxP sites. When the Cre recombinase becomes expressed in the tissue, it excises the loxP-floxed GFP, leading to its knockout. Only at this point, under the control of a ubiquitous promoter, the RFP, which is called cargo genes, becomes expressed and the fluorescence changes from green to red (figure 5.4). The ubiquitous promoter is a region of DNA, located next to the loxP sites, where the transcription takes place, which initiates the transcription of particular genes. The promoter helps to enhance the expression of the RFP ubiquitously.

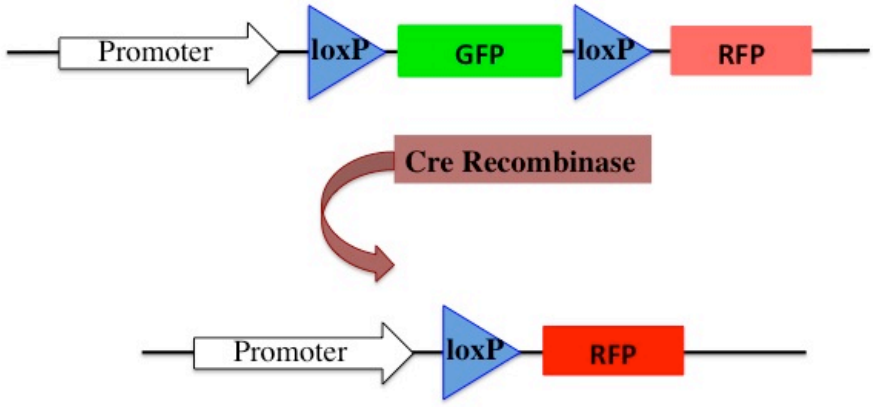


**Figure 5.4.** Schematic representation of the Cre/loxP site-specific recombination. A second gene of interest, the cargo gene, follows the loxP-floxed GFP. The cargo gene expresses the second fluorescent protein, the RFP. When the Cre recombinase is expressed in the system, the loxP-floxed GFP is knocked out and the cargo gene is brought closer to the promoter, hence switching expression of proteins

It is possible to control the gene knockout and the RFP expression by inducing a temporal activity of Cre recombinase. A construct $Cre^{ERt2}$ is obtained by fusing a mutant ligand-binding domain of the human oestrogen receptor (ER) together with the Cre recombinase. In this case, the activation of the recombination event depends only on the presence of anti-oestrogen. Mutant versions of the ER ligand-binding domain were employed in order to circumvent the potential binding and activation of the $Cre^{ERt2}$ by endogenous oestrogens. The $Cre^{ERt2}$ is, in fact, insensitive to the natural oestrogens and it is activated when the anti-oestrogen tamoxifen (TAM) or 4-hydroxytamoxifen (4-OHT, tamoxifen metabolite) are introduced in to the system. [37] Tamoxifen binds the ER fused with the Cre recombinase, which penetrates into the nucleus producing the targeted mutation. This system was successfully employed by Hans *et al*. in 2009[38] and by Mosimann *et al*. in 2011. [39] The two groups explored the efficiency of the different available ubiquitous promoters, finding that they become progressively inactive during the course of development. Hans and co-workers discovered that the loxP-floxed genes knockout occurs within 2-4 hours of the administration of TAM or 4-OHT, however the

promoter they used (EF1α) only expresses in the early developing stages (from 5 to 24 hpf).[38] The reliability of loxP excision is required throughout all the stages of development, Mosimann's group, therefore, employed a *ubiquitin* (*ubi*) locus in zebrafish to generate an ubiquitously expressed transgene driver, that would not be dependent on the developmental stage. [39] A new transgenic line, named *ubi*:switch, which contains GFP was therefore prepared by Mosimann.

The loxP sites, as well as the Cre recombinase, are not native to the animal genome; it is necessary to artificially insert the sequences using transgenic technology. In order to obtain *in vivo* models containing the Cre/loxP site-specific recombination, two different transgenic lines were required: (a) one line containing the loxP-floxed GFP cassette, which express GFP and emits green fluorescence ubiquitously from 24 hpf; (b) one containing the $Cre^{ERt2}$, which emits green fluorescence only in the heart from 48 hpf. Only the offspring of the crossbreed $Cre^{ERt2}$ × LoxP that inherited both genes will give rise to the *ubi*:switch line. Figure 5.5 shows the possible allele combinations of the offspring in the progeny of heterozygous or homozygous adults.

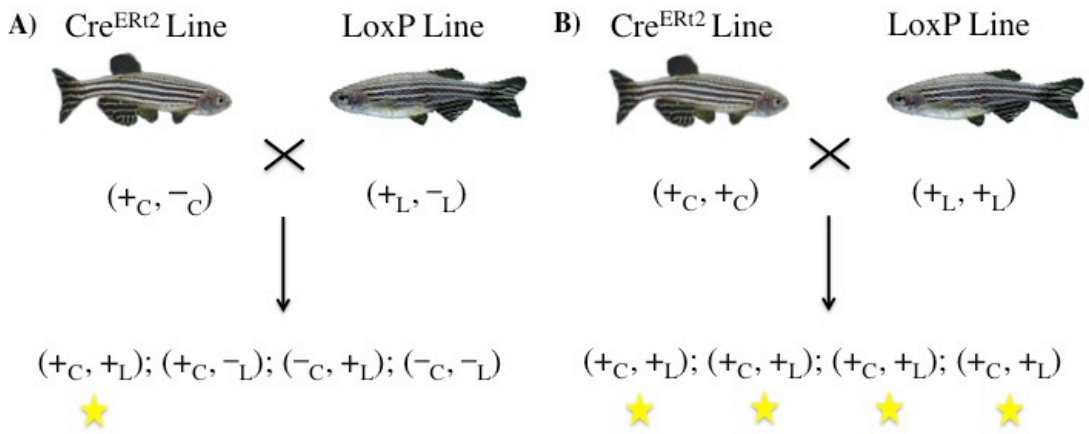


**Figure 5.5.** Schematic of zebrafish allele inheritance to form a *ubi*:switch transgenic zebrafish. **A)** crossbreeding of two heterozygous $cre^{ERt2}$ and loxP lines, in this case only 25% of the offspring inherit the two alleles and form *ubi*:switch tg line. **B)** crossbreeding of two homozygous $cre^{ERt2}$ and loxP species, in this case 100% of the offspring inherit the two alleles, forming *ubi*:switch tg line

Only 25% of the offspring generated from heterozygous fish and 100% of the offspring generated from homozygous fish inherit the two alleles and respond to the presence of tamoxifen by generating red fluorescence.

This tamoxifen reporter line ubi:loxP-EGFP-loxP-mCherry (ubi:switch) was selected to test the presence of tamoxifen in the MIP **FM-P8** matrix, discussed in chapter 4.

#### 5.3.1.1. Genotyping by breeding

The two transgenic zebrafish lines were acquired from University College London's fish facility, where they were maintained as heterozygous lines. The lines were subsequently maintained for a number of years according to the breeding program employed at Queen Mary University of London's biological service unit. This resulted in both the lines being maintained in tanks containing a mendelian distribution of homozygous, heterozygous and wild type genotypes. As previously mentioned, using homozygous fish from both transgenic lines increases the percentage of the offspring that inherit both alleles and that are responsive to tamoxifen to 100%. It was therefore decided to identify the homozygous fish and only use them for future tests. A genotyping by breeding strategy was required in order to identify the homozygous fishes of the tg:loxP and tg:$Cre^{ERt2}$.

$Cre^{ERt2}$ males and loxP females were individually housed in separated and labelled tanks, which were then crossbred with female and male wild type (WT), respectively. The eggs generated from the tg:$Cre^{ERt2}$ exhibit a green fluorescence heart at 48 hpf, while the ones obtained from tg:loxP show a green fluorescence in the whole body at 24 hpf. In cases of heterozygous $Cre^{ERt2}$ or loxP adults, 50% of the offspring would express GFP at 48hpf or 24hpf, respectively, whereas in case of homozygous adults, the totality of the

offspring would display GFP. Figure 5.6 shows a schematic representation of this strategy.

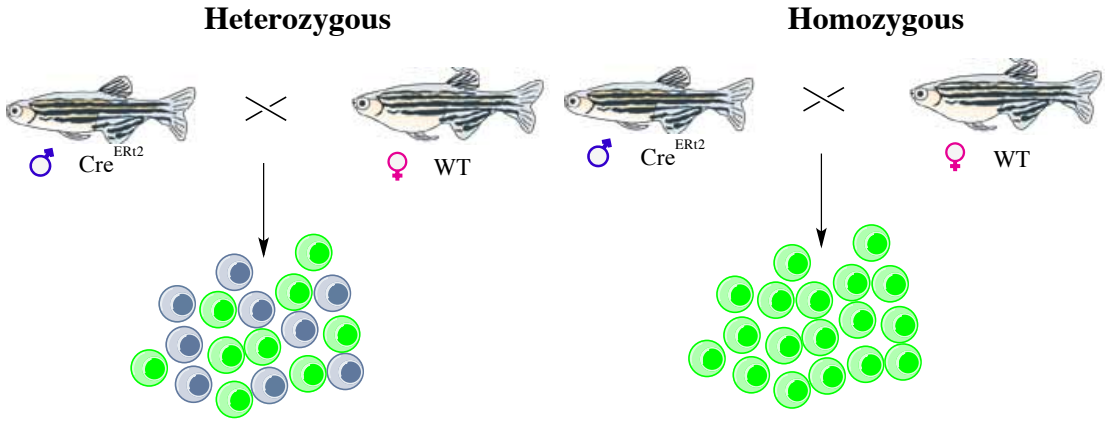


**Figure 5.6.** Schematic representation of the genotyping by breeding strategy, using the CreERt2 as example. The same process was applied for the genotyping of loxP adults. Only the heterozygous give the totality of the embryos that express GFP

The fish identified as homozygous were kept in separate, labelled tanks and used for the crossbreeding $Cre^{ERt2}$ × loxP in order to obtain *ubi*:switch.

## 5.4. Tamoxifen - induced switch

It was necessary to evaluate the reliability of the Cre/loxP system for the visual detection of tamoxifen prior to the evaluation of drug loading in the polymeric matrix MIP - **FM-P8**. The homozygous $Cre^{ERt2}$ males were crossbred with homozygous loxP females. One $Cre^{ERt2}$ fish and one loxP fish were paired together in a tank equipped with a removable insert with a perforated mesh at the bottom. The mesh allows the eggs to pass through and sink to the bottom of the outer box, preventing the adults from eating them. The following morning, the clutch from each couple was collected in different petri dishes using a strainer. Using a microscope, the embryos were sorted into petri dishes contained 50 healthy and fertilised eggs. The dishes were kept in an incubator at 28°C and checked regularly. A high percentage of embryos can spontaneously die

during the first 24 hours and, if not removed from the dish, can cause the death of the entire group. The embryos were also sorted for ubiquitously expression of GFP at 24 hpf. All of the embryos showed green emission under the fluorescence microscope, confirming that the adult fishes were homozygous and that the embryos contained the full loxP-Cre$^{ERt2}$ system, which express red fluorescence (mcherry) on exposure to tamoxifen. Figure 5.7 shows an embryo of *ubi*:switch at 24 hpf in which the GFP expression is visible in the entire body.

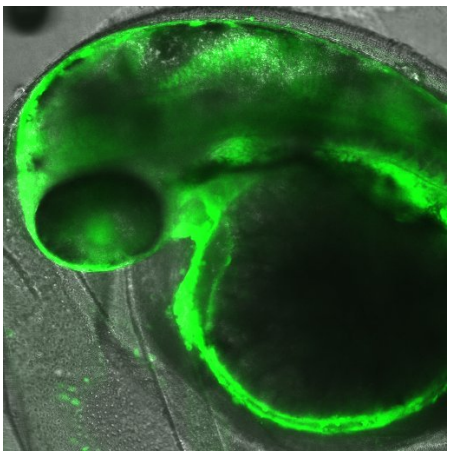

**Figure 5.7.** Confocal image of an embryo ubi:loxP-EGFP-loxP-mCherry at 24 hpf. GFP is expressed everywhere in the body

Together with the evaluation of the efficacy of the system, the potential dose-dependent toxicity of tamoxifen at larval stages was assessed. Larvae at 4 dpf were chosen for this experiment, as at this stage the fish have already hatched and start seeking food. The drug dispersed in water can therefore be internalised by the larvae following two main routes, absorption through the skin and the gills or ingestion and absorption in the GI (gastro intestinal) tract.

A literature review suggested that the concentration of tamoxifen and metabolites generally used to induce the recombination in zebrafish is in the range 5-10μM. [38-40] It was therefore decided to investigate the effect of tamoxifen at the limits of this range. Two concentrations of the free drug tamoxifen citrate, 5 and 10μM, were fed to two

different groups of zebrafish at 4dpf. The test was carried out in a 6-well plate, using 2 wells for each concentration of TAM plus 2 wells for internal plate and negative controls. Figure 5.8 shows the set-up of the experiment; thirty larvae at 4dpf were immersed in each well. The plate was kept in an incubator at 28°C.

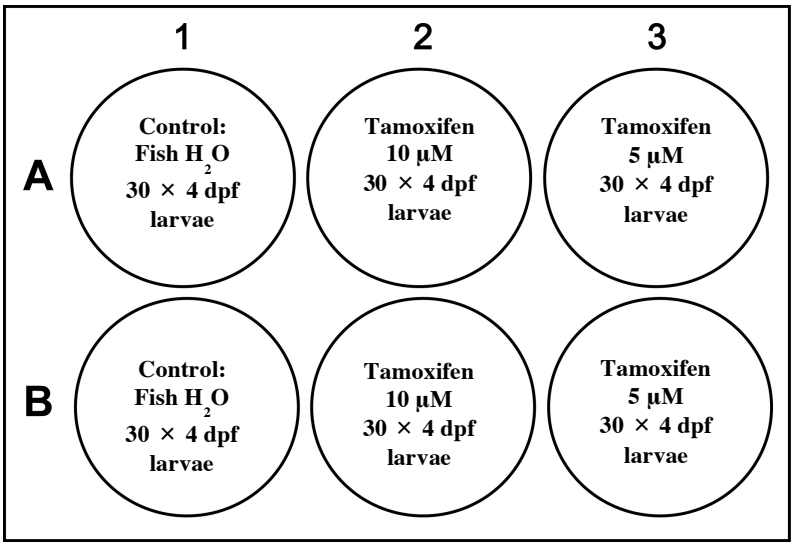


**Figure 5.8.** Schematic representation of the experimental set-up

This experiment lasted 5 days. Throughout the whole time zebrafish were monitored daily in terms of survival rate and any alterations in motility or morphological deformation. After only 4 hours the fish treated with both concentrations of TAM showed a lack of motility and response to touch, compared to the control groups. Although no deaths were recorded during the experiment, the fish displayed signs of stress and dorsal curvature of the body was observed in every fish treated with TAM. According to Mosimann *et al*. the mcherry expression was expected after 3 days of treatment.[39] Given the *ubiquitin* promoter used in the Cre/loxP system, the intensity of red fluorescence was not expected to decrease over time. Two days later, five random fish per concentration were chosen as a representative sample and were prepared for imaging. The fish were first anesthetised and immersed for 2 hours in paraformaldehyde

(PFA) to fix the tissues, before mounting them on microscope slides using a solution of 1% w/v agarose in PBS for imaging.

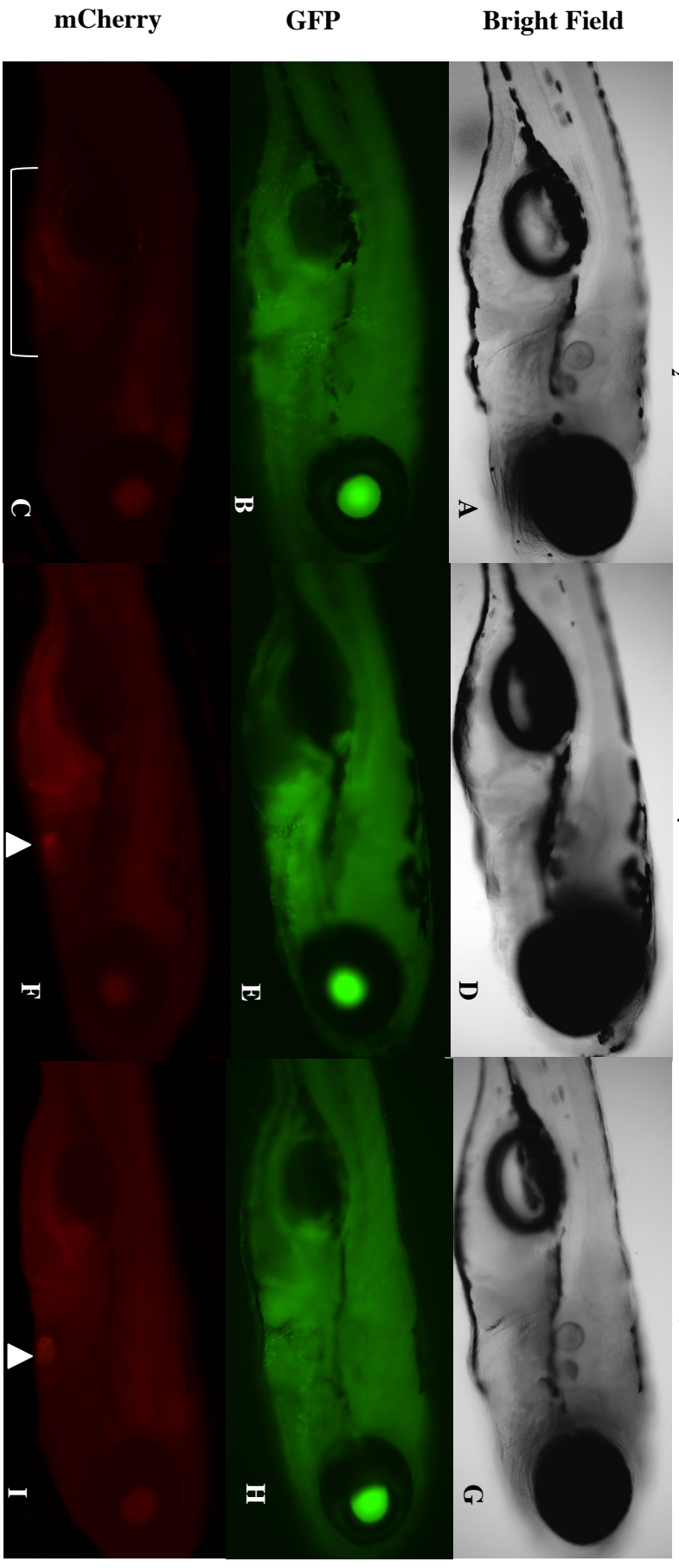
Bright Field
GFP
mCherry
Control Fish H2O
TAM 5 µM
TAM 10 µM
A
B
C
D
E
F
G
H
I

**Figure 5.9.** Cre-mediated recombination fluorescence microscope images. **A-I)** Head and trunk lateral views of 9dpf larvae, anterior to the right. **A-C)** Control fish immersed in fish water. This larva retains the green signal and does not show any mcherry expression, a part from the autofluorescent red signal in the yolk (bracket). **D-F)** Fish treated with tamoxifen 5μM. The mcherry is expressed everywhere in the fish tissues and in particular in the heart (arrow). **G-I)** Fish treated with tamoxifen 10μM. The mcherry is expressed everywhere in the fish tissues and in particular in the heart (arrow)

Fluorescence microscope images of represented larvae are shown in figure 5.9. No mcherry expression was visible in the untreated fish (figure 5.9 C) apart from autofluorescence in the yolk. The fish treated with a solution of tamoxifen at different concentrations showed mcherry expression ubiquitously in the tissues, particularly in the heart. Every larva prepared for imaging displayed mcherry fluorescence in the tissues, however, for simplicity of representation, only one larva per concentration is shown in figure 5.9.

The results obtained confirm the $Cre^{ERt2}$/loxP system to be useful for the visual detection of tamoxifen with the presence of the drug inducing mcherry fluorescence.

## 5.5. Toxicity and visualisation studies *in vivo* using ubi:switch zebrafish system

Once it was demonstrated that the presence of tamoxifen could induce the switch of fluorescence in the $Cre^{ERt2}$/loxP system available in the BSU at Queen Mary University of London, it was decided to use zebrafish to obtain preliminary data using the tamoxifen loaded nanogels **FM-P8,** obtained using the molecular imprinting approach for the drug incorporation. For comparison, the counterpart polymer non-imprinted **FM-P7** was also used in parallel. The experiments were designed to assess two important objectives: i) to assess the toxicity of the tamoxifen-loaded nanogels and to compare the data with the ones obtained for the nanogels alone; ii) to demonstrate the potential for nanogels to be used as drug delivery vehicles by showing the effective incorporation of

tamoxifen in the polymeric matrix. Given the limited time available to complete the work, it was decided to focus the work on only two concentrations of polymers and to follow the fish embryo acute toxicity test guidelines given by the OECD (Organisation for Economic Cooperation and Development).[41] Embryonic stage *ubi:*switch zebrafish were exposed to two different concentrations of NIP **FM-P7** and MIP **FM-P8** at 24 hpf for a period of 96 hours. The embryos were monitored every 24 hours with particular attention to indicators of lethality, as stated in the test guidelines but using the later stage responses for embryos and larvae. The indicators were: immobility, absence of respiratory movement, lack of heartbeat, insufficient reaction to stimulus and abnormalities of body forms. Four standard 24-well plates were used, one plate for each concentration and nanogel. Twenty embryos per concentration, one embryo per well, were exposed to the nanogels. The remaining four wells in the plate were the control groups. Controls consisted of one embryo per well immersed in fresh fish water and used both as negative control and as internal plate control. The layout of the plates is reported in figure 5.10.

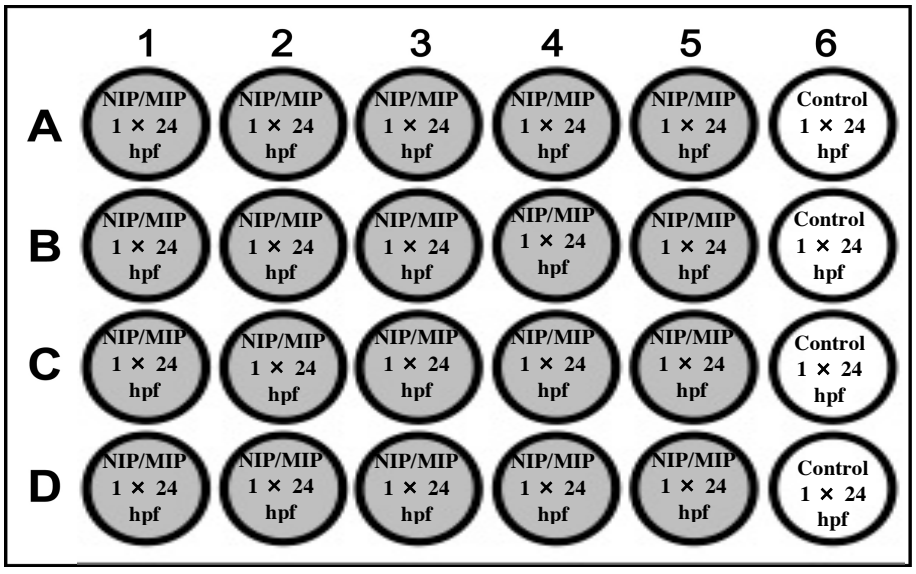


**Figure 5.10.** Layout of the 24-well plates used in the evaluation of toxicity of two solutions of NIP **FM-P7** and MIP **FM-P8**. In the same time the presence of tamoxifen in the matrix of the MIP was investigated by monitoring the expression of mcherry fluorescence

Having demonstrated the successful activation of the Cre recombinase in the zebrafish following the incubation with tamoxifen at 5µM and 10µM, the subsequent step investigated the effect of polymeric matrix when a similar amount of drug is uploaded. Two solutions of MIP **FM-P8** were prepared in fish water at a concentration of 84.7µg/mL and 169.4µg/mL, with content of tamoxifen estimated to be approximately 5µM and 10µM. Two solutions of the corresponding NIP **FM-P7** counterpart at the same polymer concentrations of 84.7µg/mL and 169.4µg/mL were also prepared. The mixtures were sonicated for 10 minutes and filtered over a 0.45µm GHP filter immediately before transferring one embryo at 24 hpf to each well. The plates were then randomly positioned in the incubator at 28°C.

At the end of the exposure period, no acute toxicity was observed for any of the solutions tested; no negative outcome in any of the indicators of lethality was recorded (figure 5.11).

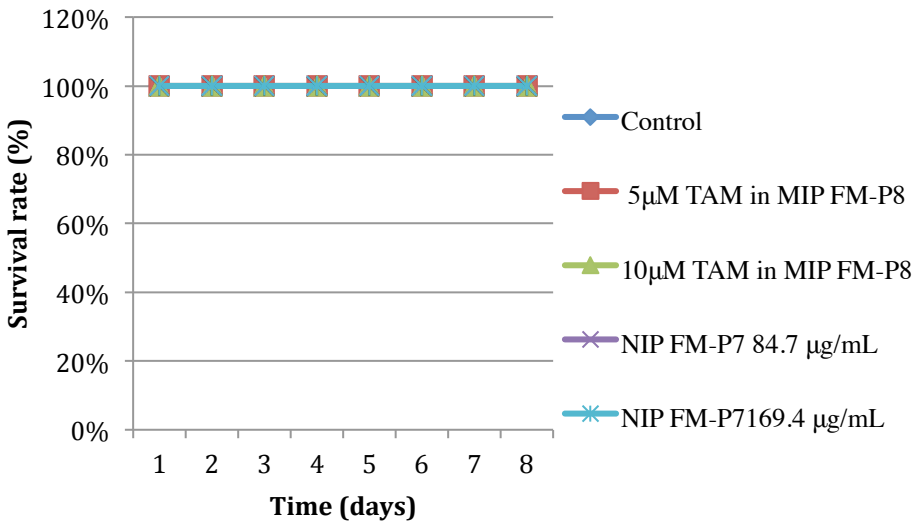


**Figure 5.11.** Effect of nanogels on 24hpf zebrafish embryos. Two concentrations of nanogels **FM-P7** (84.7µg/mL and 169.4µg/mL) and **FM-P8**, containing an estimation of 5µM and 10µM of tamoxifen, were fed to 24hpf zebrafish embryos for 8 days. Each solution was tested on 20 embryos and they all were well and alive

The data obtained were very encouraging. As shown in figure 5.11, the tested concentration of nanogels, chosen accordingly to the concentration of free tamoxifen investigated in section 5.4, showed no toxicity in zebrafish. Comparison of toxicity data for these nanoparticles with previously obtained data[42] demonstrates that these NIPAM-based nanogels can be safely use at these concentrations as there is no evidence of significant toxicity. This result is very important and will play an important role for future applications.

Evaluation of the presence of tamoxifen in the MIP was carried out by fluorescence microscopy. After 8 days of treatment, five random fish per concentration were chosen as a representative sample and prepared for imaging. However, for simplicity of representation only one larva per concentration is shown in figure 5.12. The fish were then anesthetised and immersed for 2 hours in paraformaldehyde (PFA) to fix the tissues, before mounting them on microscope slides using a solution of 1% w/v agarose in PBS for imaging.

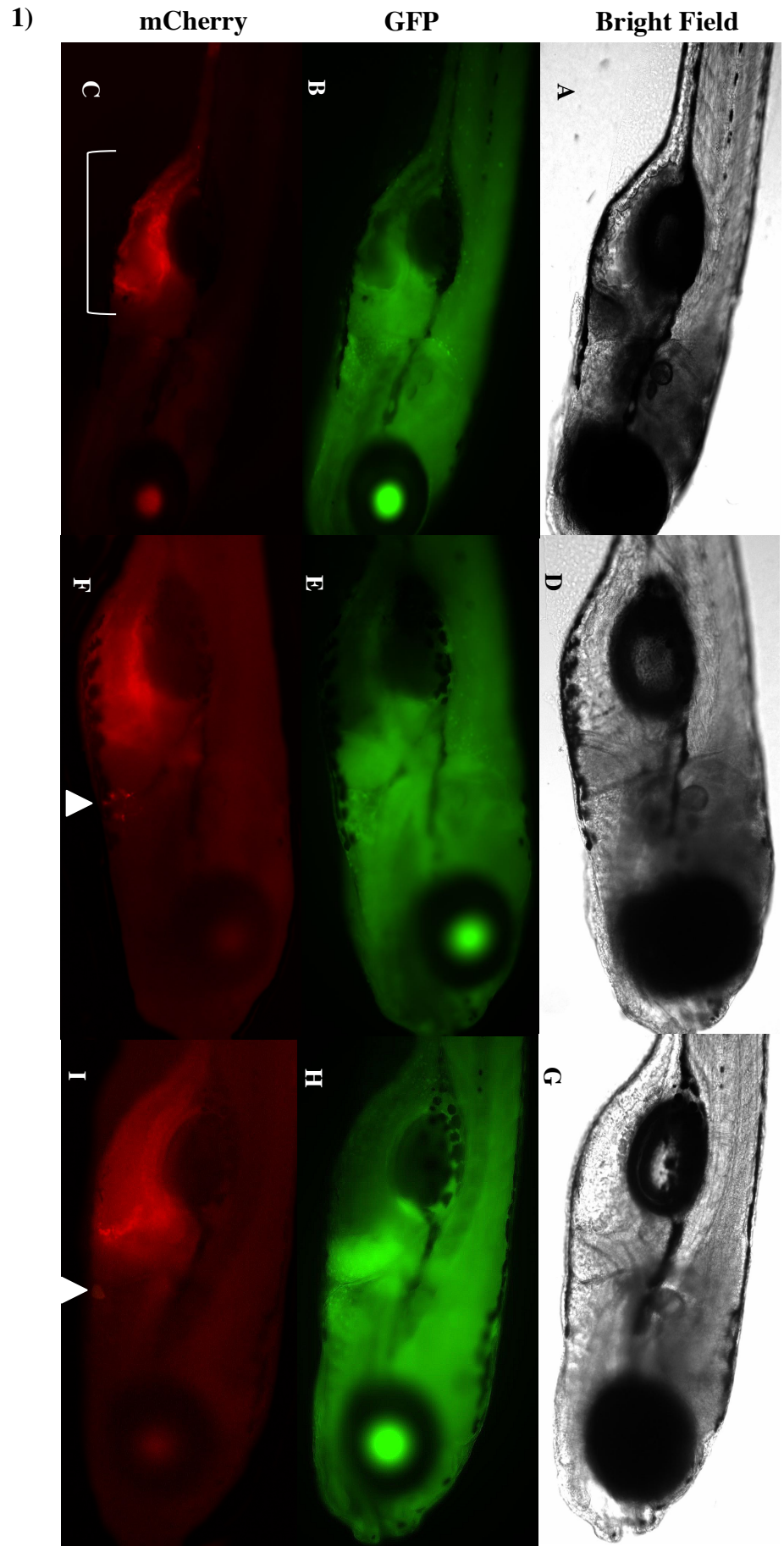
1)
mCherry
GFP
Bright Field
A
B
C
D
E
F
G
H
I
NIP FM-P7
TAM 10 µM
in MIP FM-P8
TAM 5 µM
in MIP FM-P8

**NIP FM-P7**

**2)**


**TAM 10 µM**
**in MIP FM-P8**

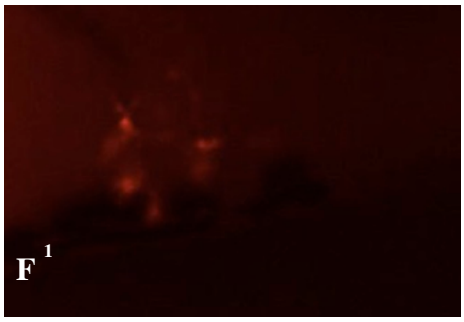


**TAM 5µM**
**in MIP FM-P8**


**Figure 5.12. 1) A-I)** Head and trunk lateral views of represented 8dpf larvae, anterior to the right. *Ubi*:switch 8dpf fish treated with NIP **FM-P7** (**A-C**), MIP **FM-P8** containing 5µM tamoxifen (**D-F**) and MIP **FM-P8** containing 10µM tamoxifen (**G-I**). **A-C)** Control fish treated only with NIP show no mcherry expression; only the autofluorescent red signal is visible in the yolk (bracket). **D-F)** Fish treated with MIP containing 10µM tamoxifen. The mcherry is expressed everywhere in the fish tissues, particularly in the heart (arrow). **G-I)** Fish treated with MIP containing 5µM tamoxifen. The mcherry is expressed everywhere in the fish tissues.

**2)** Enlargement of the region around the heart of **C[1])** NIP treated fish, **F[1])** MIP containing 10µM tamoxifen and **I[1])** MIP containing 5µM tamoxifen

The data represented in figure 5.12, which report the fluorescence microscope images taken of one set of fish treated with NIP 169.4μg/mL, MIP 84.7μg/mL and MIP 169.4μg/mL respectively, show evidence for the presence of tamoxifen in the polymeric matrix. In fact the generation of mcherry fluorescence in the fish tissues and heart treated with MIP (figure 5.12 (1) **D-F** and **G-I**), compared to the lack of red signals on fish treated with NIP (figure 5.12 (1) **A-C**) confirmed that the drug was loaded in the polymeric network during the polymerisation process. The results also suggested a dose-dependent response of the Cre/loXP system to tamoxifen. The mcherry expression in the heart of the fish treated with the strongest concentration of MIP (figure 5.12 (2) panel $F^{1}$) displayed a more intense fluorescence compared to the lowest concentration (figure 5.12 (2) panel $I^{1}$).

## 5.6. Conclusion and future work

In conclusion the $Cre^{ERt2}$/loxP proved to be a useful system for the visual detection of tamoxifen contained in the polymeric matrix. The presence of tamoxifen in the organism induces the activation of the recombination event producing red fluorescence in the fish tissues and in the heart.

The nanogels were tested on zebrafish both for tamoxifen evaluation and for toxicity studies. Using the same array for both investigations saves time, money and reduces the number of animals needed. This preliminary study showed promising results as mcherry expression was only observed in the fish treated with two solutions of MIP at different concentrations, which means tamoxifen was loaded in MIP **FM-P8**. These results suggest that the imprinting process during the polymerisation step was successful.

The zebrafish showed good tolerance to the coumarin-based imprinted polymers at the tested concentrations. However, a further toxicity screening, which could test a higher

number of concentrations, is needed to evaluate the $LC_{50}$ of these polymers (lethal concentration at which half of the sample population is killed).

Future work should involve the study of the drug release mechanism in the fish, which probably takes place in the acidic pH of the stomach after ingestion. Moreover, once the $LC_{50}$ has been assessed in zebrafish, it would be essential to carry out *in vivo* testing on small mammals, such as mice. This is an important step to test the efficacy of the system as a drug delivery vehicle. Mice, unlike zebrafish, have breast tissue on which analogous human breast cancer could be grown. This could allow investigation of the potential advantage of using the nanogels over the free drug in reducing the tumour and preventing further growth.

## 5.7. References


1. Khan, H. A.; Shanker, R., Toxicity of Nanomaterials. *BioMed research international* **2015,** *2015*, 521014.

2. Sharifi, S.; Behzadi, S.; Laurent, S.; Forrest, M. L.; Stroeve, P.; Mahmoudi, M., Toxicity of nanomaterials. *Chemical Society reviews* **2012,** *41* (6), 2323-43.

3. Clichici, S.; Filip, A., In vivo Assessment of Nanomaterials Toxicity. **2015**.

4. Festing, S.; Wilkinson, R., The ethics of animal research. Talking Point on the use of animals in scientific research. *EMBO Rep.* **2007,** *8* (6), 526–530.

5. Russell, W. M. S.; Burch, R. L., The Principles of Humane Experimental Technique. *Methuen, London* **1959**.

6. Parasuraman, S., Toxicological screening. *Journal of pharmacology & pharmacotherapeutics* **2011,** *2* (2), 74-9.

7. York, M.; Steiling, W., A Critical Review of the Assessment of Eye Irritation Potential using the Draize Rabbit Eye Test. *J. Appl. Toxicol.* **1998,** *18*, 233–240.

8. Van Loveren, H.; Cockshott, A.; Gebel, T.; Gundert-Remy, U.; de Jong, W. H.; Matheson, J.; McGarry, H.; Musset, L.; Selgrade, M. K.; Vickers, C., Skin sensitization in chemical risk assessment: report of a WHO/IPCS international workshop focusing on dose-response assessment. *Regulatory toxicology and pharmacology : RTP* **2008,** *50* (2), 155-99.

9. Homburger, F.; Van Dongen, C. G.; Adams, R. A.; Soto, E., Hamsters and Gerbils: Advantages and Disadvantages as Models in Toxicity Testing. *Journal of the american college of toxicology* **1985,** *4*, 1-15.

10. Weinberg, A. D.; Thalhofer, C.; Morris, N.; Walker, J. M.; Seiss, D.; Wong, S.; Axthelm, M. K.; Picker, L. J.; Urba, W. J., Anti-OX40 (CD134) Administration to Nonhuman Primates: Immunostimulatory Effects and Toxicokinetic Study. *J. Immunother. 29*, 575-585.

11. Suzuki, T.; Ichihara, M.; Hyodo, K.; Yamamoto, E.; Ishida, T.; Kiwada, H.; Ishihara, H.; Kikuchi, H., Accelerated blood clearance of PEGylated liposomes containing doxorubicin upon repeated administration to dogs. *International journal of pharmaceutics* **2012,** *436* (1-2), 636-43.

12. Bedell, M. A.; Jenkins, N. A.; Copeland, N. G., Mouse models of human disease. Part I: Techniques and resources for genetic analysis in mice. *Genes & Development* **1997,** *11*, 1-10.

13. Bedell, M. A.; Largaespada, D. A.; Jenkins, N. A.; Copeland, N. G., Mouse models of human disease. Part II: Recent progress and future directions. *Genes & Development* **1997,** *11*.

14. Cha, K. E.; Myung, H., Cytotoxic Effects of Nanoparticles Assessed In Vitro and In Vivo. *J. Microbiol. Biotechnol.* **2007,** *17*, 1573–1578.

15. Liu, G.; Gao, J.; Ai, H.; Chen, X., Applications and potential toxicity of magnetic iron oxide nanoparticles. *Small* **2013,** *9* (9-10), 1533-45.

16. Quan, Q.; Xie, J.; Gao, H.; Yang, M.; Zhang, F.; Liu, G.; Lin, X.; Wang, A.; Eden, H. S.; Lee, S.; Zhang, G.; Chen, X., HSA coated iron oxide nanoparticles as drug delivery vehicles for cancer therapy. *Molecular pharmaceutics* **2011,** *8* (5), 1669-76.

17. Yamamoto, Y.; Hyodo, I.; Takigahira, M.; Koga, Y.; Yasunaga, M.; Harada, M.; Hayashi, T.; Kato, Y.; Matsumura, Y., Effect of combined treatment with the epirubicin-incorporating micelles (NC-6300) and 1,2-diaminocyclohexane platinum (II)-incorporating micelles (NC-4016) on a human gastric cancer model. *International journal of cancer* **2014,** *135* (1), 214-23.

18. Ciofani, G.; Raffa, V.; Vittorio, O.; Cuschieri, A.; Pizzorusso, T.; Costa, M.; Bardi, G., In vitro and in vivo biocompatibility testing of functionalized carbon nanotubes. *Methods in molecular biology* **2010,** *625*, 67-83.

19. Athawale, R. B.; Jain, D. S.; Singh, K. K.; Gude, R. P., Etoposide loaded solid lipid nanoparticles for curtailing B16F10 melanoma colonization in lung. *Biomedicine & pharmacotherapy = Biomedecine & pharmacotherapie* **2014,** *68* (2), 231-40.

20. El-Gogary, R. I.; Rubio, N.; Wang, J. T., Polyethylene Glycol Conjugated Polymeric Nanocapsules for Targeted Delivery of Quercetin to Folate-Expressing Cancer Cells in Vitro and in Vivo. *Acs Nano* **2014,** *8* 1384–1401.

21. Liu, Y.; Feng, L.; Liu, T.; Zhang, L.; Yao, Y.; Yu, D.; Wang, L.; Zhang, N., Multifunctional pH-sensitive polymeric nanoparticles for theranostics evaluated experimentally in cancer. *Nanoscale* **2014,** *6* (6), 3231-42.

22. Tavares, B.; Santos Lopes, S., The Importance of Zebrafish in Biomedical Research. *Acta Med. Port.* **2013,** *26*, 583-592.

23. Spence, R., Zebrafish Ecology and Behaviour. *Zebrafish Models in Neurobehavioral Research* **2010,** *52*, 1-46.

24. McGrath, P.; Li, C. Q., Zebrafish: a predictive model for assessing drug-induced toxicity. *Drug discovery today* **2008,** *13* (9-10), 394-401.

25. Ali, S.; Champagne, D. L.; Spaink, H. P.; Richardson, M. K., Zebrafish embryos and larvae: a new generation of disease models and drug screens. *Birth defects research. Part C, Embryo today : reviews* **2011,** *93* (2), 115-33.

26. Goldsmith, J. R.; Jobin, C., Think small: zebrafish as a model system of human pathology. *Journal of biomedicine & biotechnology* **2012,** *2012*, 817341.

27. Howe, K.; Clark, M. D.; Torroja, C. F., The zebrafish reference genome sequence and its relationship to the human genome. *Nature* **2013,** *496* (7446), 498-503.

28. Lessman, C. A., The developing zebrafish (Danio rerio): a vertebrate model for high-throughput screening of chemical libraries. *Birth defects research. Part C, Embryo today : reviews* **2011,** *93* (3), 268-80.

29. Lee, H. Y.; Inselman, A. L.; Kanungo, J.; Hansen, D. K., Alternative models in developmental toxicology. *Systems biology in reproductive medicine* **2012,** *58* (1), 10-22.

30. Chen, Y.; Hu, X.; Sun, J.; Zhou, Q., Specific nanotoxicity of graphene oxide during zebrafish embryogenesis. *Nanotoxicology* **2016,** *10* (1), 42-52.

31. Kovriznych, J. A.; Sotnikova, R.; Zeljenkova, D.; Rollerova, E.; Szabova, E.; Wimmerova, S., Acute toxicity of 31 different nanoparticles to zebrafish (Danio rerio)

tested in adulthood and in early life stages - comparative study. *Interdisciplinary toxicology* **2013,** *6* (2), 67-73.

32. Chakraborty, C.; Sharma, A. R.; Sharma, G.; Lee, S. S., Zebrafish: A complete animal model to enumerate the nanoparticle toxicity. *Journal of nanobiotechnology* **2016,** *14* (1), 65.

33. Girardi, F. A.; Bruch, G. E.; Peixoto, C. S.; Dal Bosco, L.; Sahoo, S. K.; Goncalves, C. O.; Santos, A. P.; Furtado, C. A.; Fantini, C.; Barros, D. M., Toxicity of single-wall carbon nanotubes functionalized with polyethylene glycol in zebrafish (Danio rerio) embryos. *Journal of applied toxicology : JAT* **2017,** *37* (2), 214-221.

34. Lakso, M.; Sauer, B.; Mosinger, B.; Lee, E. J.; Manningt, R. W.; Yu, S.-H.; Mulder, K. L., Targeted oncogene activation by site-specific recombination in transgenicmice. *Genetics* **1992,** *89*, 6232-6236.

35. Carter, M.; Shieh, J. C., Making and Using Transgenic Organisms. *Guide to Research Techniques in Neuroscience* **2010,** *13*, 243-262.

36. Yoshikawa, S.; Kawakami, K.; Zhao, X. C., G2R Cre reporter transgenic zebrafish. *Developmental dynamics : an official publication of the American Association of Anatomists* **2008,** *237* (9), 2460-5.

37. Feil, R.; Brocard, J.; Mascrez, B.; Lemeur, M.; Metzger, D.; Chambon, P., Ligand-activated site-specific recombination in mice. *Genetics* **1996,** *93*, 10887-10890,.

38. Hans, S.; Kaslin, J.; Freudenreich, D.; Brand, M., Temporally-Controlled Site-Specific Recombination in Zebrafish. *PLoS ONE* **2009,** *4*, 1-7.

39. Mosimann, C.; Kaufman, C. K.; Li, P.; Pugach, E. K.; Tamplin, O. J.; Zon, L. I., Ubiquitous transgene expression and Cre-based recombination driven by the ubiquitin promoter in zebrafish. *Development* **2011,** *138* (1), 169-77.

40. Felker, A.; Nieuwenhuize, S.; Dolbois, A.; Blazkova, K.; Hess, C.; Low, L. W.; Burger, S.; Samson, N.; Carney, T. J.; Bartunek, P.; Nevado, C.; Mosimann, C., In Vivo Performance and Properties of Tamoxifen Metabolites for CreERT2 Control. *PLoS One* **2016,** *11* (4), e0152989.

41. OECD Guidelines For The Testing Of Chemicals. **2013**.

42. Ray, J. V., Novel Molecular Imprinted Nanogels As Drug Delivery Vehicles For Tamoxifen. *Thesis submitted within Queen Mary University of London*

# Chapter 6

## Materials and Methods

# 6. Materials and methods

## 6.1. Chemicals and Materials

### 6.1.1. Chemicals and materials for the synthesis of functional monomers

N-Boc-4aminophenol, dimethyl acetylenedicarboxylate, triethylamine, trifluoroacetic acid, palladium catalyst, tributyl(vinyl)tin and sodium fluoride were all purchased from Aldrich. Magnesium sulphate, sodium hydroxide and sodium chloride were purchased from Fisher. 4-bromophenol was purchased from Acros Organics, triphenylarsine from Alfa Aesar, triphenylphosphine from Fluka and potassium carbonate from BDH. Dry solvents dichloromethane ($CH_2Cl_2$) and tetrahydrofuran (THF) were supplied from MBRAUN MB SPS-800 solvent purification system. Dry dichloroethane was purchased from Acros Organics. Hexane, ethyl acetate, petroleum ether, acetone and acetonitrile were all purchased from VWR. Flash column chromatography was performed on reaction mixtures using VWR silica gel. Analytical thin layer chromatography (TLC) was carried out using pre-coated aluminium plates TLC Silica gel 60 $F_{254}$, purchased from Merck. The plates were visualized under an ultraviolet lamp at $\lambda$ = 254/365 nm.

### 6.1.2. Fluorescence studies on bulk polymers for detection of clomiphene, tamoxifen and 4-hydroxytamoxifen

Acetonitrile was purchased from VWR. Hamilton syringes were used for making the solutions for UV-Vis and fluorescent spectroscopy experiments. 96-well plates were purchased from FALCON and used on the plate reader. High precision quartz cell with light path of 10mm and total volume 1 mL, where purchased from Hellma Analytics and used for UV-Vis. High precision quartz cell with light path of 10mm and total

volume 2 mL, where purchased from Hellma Analytics and used for fluorescence experiments.

### 6.1.3. Chemicals and materials for synthesis of nanogels for DDS

N-isopropyacrylamide (NIPAM), N-N'-methylenebis(acrylamide) (MBA) and dry DMSO were purchased from Aldrich. Azobisisobutyronitrile (AIBN) was purchased from Acros Fisher Scientific UK and recrystallized from methanol before use. Tamoxifen citrate (98%) was purchased from Cambridge Bioscience. Dialysis membrane for nanogel isolation was purchased from MediCell International Ltd, 22 mm diameter and molecular cut off 3.5 KDa. Dialysis bag Float-A-Lyzer® G2 (5mL volume) with MWCO = 3.5-5.0 KDa were purchased from Spectrum Europe BV. GHP Acrodisc ® 13mm syringe filter with 0.45μm GHP membrane were purchased from PALL. Inorganic membrane filter Anotop ™ 10mm, 0.02μm, were purchased from Whatman. Solvent resistant disposable cuvettes in polystyrene 10x10x45 (DTS0012, Malvern) were used to record the size at the DLS.

### 6.1.4. Chemicals and materials for the *in vivo* studies

Phosphate buffered saline (PBS) was purchased from Sigma. Agarose low gelling point was purchased from BDH and used in a solution of 1% w/v in PBS at pH: 7.4. Paraformaldehyde (PFA) was purchased from Prolabo and used in a solution of 4% w/v in PBS pH: 7.4. Microscope slide and cover glass were purchased from BDH. Polystyrene 24- and 6-well cell culture plates were purchased from Corning Incorporated.

## 6.2. Instruments

### 6.2.1. NMR Spectroscopy

$^{1}$H-NMR, 2D-NMR and $^{13}$C-NMR spectra were recorded on a Bruker AV400 MHz (Avance and Avance III) or Bruker AV600 MHz (AV 600) spectrometers. Deuterated solvents, $CDCl_3$ and DMSO-$d_6$, were used depending on the solubility of the compounds. Chemical shifts in NMR spectra are reported as $\delta$ (in parts per million, ppm) relative to residual solvent signals: $CDCl_3$ $\delta$H = 7.26 ppm; $\delta$C = 77.23 ppm or DMSO-$d_6$ $\delta$H = 2.50; $\delta$C = 39.51.

$^{1}$H-NMR peak multiplicity were reported as follow: s = singlet, d = doublet, t = triplet, q = quartet, m = multiplet. Coupling constants (*J*) were measured in hertz. MestReNova software was used to analyse the NMR data.

### 6.2.2. UV-VIS Spectroscopy

UV-Vis spectra were recorded using Cary 100 UV-Vis Spectrophotometer (Agilent technologies), equipped with an internal thermostat.

### 6.2.3. Fluorescent Spectroscopy

All fluorescence data for the characterisation of the detector developed in chapter 3 was accomplished on a Flouromax-3 with emission slit set at 1.5. The other fluorescence studies were carried out on a Cary Eclipse Fluorescence Spectrophotometer (Agilent technologies).

### 6.2.4. Plate Reader

The interaction studies between MIP and the analytes were carried out on a BMG LABTECH FLUOstar OPTIMA Microplate Reader. Fluorescence was recorded using

the 340-10 excitation filter and the 510-20 emission filter.

### 6.2.5. Zetasizer (Dynamic light scattering)

DLS measurements were performed on a Malvern Zetersizer NaNo ZS. The instrument was equipped with a 4mV He-Ne laser operating at λ = 633nm, an avalanche photodiode detector with high quantum efficiency and an ALV/LSE-5003 multiple tau digital correlator electronics system.

### 6.2.6. Freeze-dryer

The polymers were freeze-dried using a Labcoco FreeZone 6 Freeze Dry System.

### 6.2.7. High performance liquid chromatography (HPLC)

All data was recorded on a manual injector Aglient Technologies 1220 Infinity LC fitted with a HiChrom 5 μm - C18 column 250 mm x 4.6mm id. The data were analysed using Agilent ChemStation software.

### 6.2.8. Confocal Microscope

Leica SP5 confocal laser scanning microscope.

### 6.2.9. Fluorescent Microscope

Leica DMRA2 fluorescence microscope, coupled with Hamamatsu ORCA-ER digital camera.

### 6.2.10. UV lamp for irradiation

UVP, UV GL 58 handheld UV lamp, 254/365nm.

## 6.3. Methods

### 6.3.1. Synthesis of functional monomers

#### 6.3.1.1. Synthesis of 6-N-boc-aminocoumarin-4-carboxylate (3a)

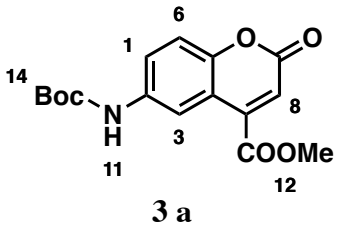


**3 a**

**Reflux synthesis:**

Under a $N_2$ atmosphere, N-Boc-4-aminophenol (0.5 g, 2.39 mmol) and $PPh_3$ (0.6267 g, 2.39 mmol) were dissolved in dry DCM (5 mL). The mixture was cooled to -10°C in dry ice and acetone bath and dimethyl acetylenedicarboxylate (0.2934 mL, 2.39 mmol) was added drop-wise. The reaction was stirred at -10°C for 1 hour and then refluxed for 168 hours at 40°C. The solvent was reduced *in vacuo* and the crude was purified with flash chromatography. Two columns were necessary to isolate the product. In the first column a gradient elution mode was used starting from hex/EtOAc 80:20 and the second column started from DCM to arrive to DCM/EtOAc 90:10. The combination of the fractions containing pure compound gave the product **3a** in a 20% yield.

**Microwave irradiation:**

$PPh_3$ (1.31 g, 5 mmol), and N-Boc-4-aminophenol (1.046 g, 5 mmol) were added in a microwave tube. Once it was sealed, vacuum/nitrogen cycles were performed in order to remove any traces of oxygen. Dry DCE (7.5 mmol) was then added. The mixture was cooled at -10°C (dry ice/acetone bath) and a solution of dimethyl acetylenedicarboxylate (614.5 µl, 5 mmol) in DCE (4 mL) was added dropwise over 10 min. After 10 min stirring at room temperature, the mixture was irradiated in a

microwave oven for 2 hours at 83°C. The solvent was reduced *in vacuo* and the crude was purified with flash chromatography. Two columns were necessary to isolate the product. In the first column a gradient elution mode was used starting from hex/EtOAc 80:20 and the second column started from DCM to arrive to DCM/EtOAc 90:10. The combination of the fractions containing pure compound gave the product **3a** in a 26.5% yield.

**$^{1}$H-NMR** (400 MHz, $CDCl_3$) δ 8.26 (d, J = 2.5 Hz, 1H, **H3**), 7.68 (d, J = 8.0 Hz, 1H, **H1**), 7.27 (d, J = 8.0 Hz, 1H, **H6**), 6.94 (s, 1H, **H8**), 6.78 (s, 1H, **H11**), 3.98 (s, 3H, **H12**), 1.51 (s, 9H, **H14**).

**$^{13}$C NMR** (101 MHz, $CDCl_3$) δ 164.14, 160.05, 152.73, 149.98, 141.77, 135.45, 123.47, 120.03, 117.53, 115.87, 81.05, 60.40, 53.21, 28.30.

### 6.3.1.2. Synthesis of 6-aminocoumarin-4-carboxylate (4)

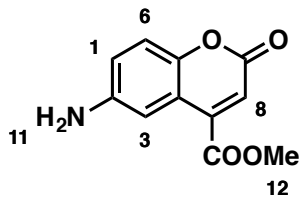


**4**

The compound **3a** (0.1147 g, 0.359 mmol) was dissolved in DCM (2 mL) at 0°C (ice bath). Trifluoroacetic acid (2 mL) was added to the solution drop wise. After keeping the reaction mixture in ice bath for 10 minutes, it was left stirring at room temperature until completion. TLC monitoring (DCM/EtOAc: 9/1 plus few drops of triethylamine) showed the reaction to be complete after 3 hours. The solvent was reduced *in vacuo* and the solid re-dissolved in EtOAc (5mL) and washed with phosphate buffer pH: 8 (4 x 15mL). The organic phase was dried over $MgSO_4$, filtered and evaporated to give 0.068g of product **4** in an 86% yield.

**$^{1}$H-NMR** (400 MHz, $CDCl_3$) δ 7.53 (d, J = 2.7 Hz, 1H, **H3**), 7.17 (d, J = 8.8 Hz, 1H, **H6**), 6.92 (d, J = 2.7 Hz, 1H, **H1**), 6.91 (s, 1H, **H8**), 3.98 (s, 3H, **H12**), 3.21 (s, 2H, **H11**).

**$^{13}$C-NMR** (151 MHz, $CDCl_3$) δ 164.47, 160.37, 147.72, 143.21, 141.81, 120.25, 119.75, 117.85, 116.35, 110.70, 53.06.

#### 6.3.1.3. Synthesis of 6-acrylamidecoumarin-4-carboxylate (2a)

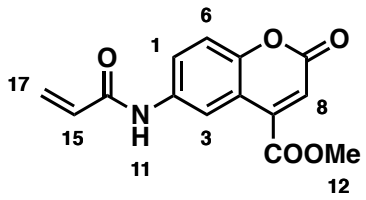


**2 a**

$K_2CO_3$ (63.05mg, 0.456 mmol) was suspended in 5 mL of a mixture of $H_2O$/Acetone (1:4 mL) and cooled down at 0°C (ice bath). The compound **4** (50 mg, 0.228 mmol) was solubilised in 1 mL of the same mixture and added to the cold $K_2CO_3$ solution drop wise. The reaction mixture was left to stir at 0°C. TLC monitoring (DCM/EtOAc: 9/1) showed the reaction to be complete after 2 hours. The mixture was filtered and the organic solvent evaporated at reduced pressure. The resulting water phase was extracted with DCM (3x15mL). The organic phase was dried over $MgSO_4$, filtered and evaporated to give 38.1 mg of product **2a** in a 61% yield.

**$^{1}$H-NMR** (400 MHz, DMSO) δ 10.41 (s, 1H, **H11**), 8.47 (d, J = 2.1 Hz, 1H, **H3**), 7.97 (dd, J = 9.0, 2.2 Hz, 1H, **H1**), 7.45 (d, J = 9.0 Hz, 1H, **H6**), 6.91 (s, 1H, **H8**), 6.44 (dd, J = 17.0, 10.0 Hz, 1H, **H15**), 6.29 (dd, J = 16.9, 1.6 Hz, 1H, **H17a**), 5.79 (dd, J = 10.0, 1.6 Hz, 1H, **H17b**), 3.31 (s, 3H, **H12**).

**$^{13}$C-NMR** (101 MHz, DMSO) δ 165.95, 165.52, 162.12, 153.43, 142.45, 134.32, 129.59, 124.04, 123.25, 122.83, 120.09, 119.16, 119.10.

### 6.3.1.4. Synthesis of 6-bromocoumarin-4-carboxylate (3b)

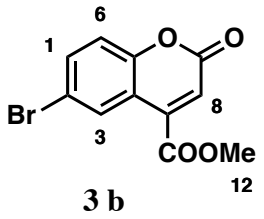


**3 b**

**Reflux synthesis:**

Under a $N_2$ atmosphere, 4-bromophenol (1 g, 5.78 mmol) and $PPh_3$ (1.51 g, 5.78 mmol) were dissolved in dry DCM (15 mL). The mixture was cooled to -10°C in dry ice and acetone bath and dimethyl acetylenedicarboxylate (0.525 mL, 5.78 mmol) was added drop-wise. The reaction was stirred at -10°C for 1 hour and then refluxed for 120 hours at 40°C. The DCM was evaporated at reduced pressure and the product was purified by flash chromatography (DCM/Pet Ether: 75/25), which gave 389mg of product **3b** with a yield of 24%.

**Microwave irradiation:**

$PPh_3$ (700 mg, 4.046 mmol) and 4-bromophenol (1.06 g, 4.046 mmol) were added in a microwave tube. Once it was sealed, vacuum/nitrogen cycles were performed in order to remove any traces of oxygen. Dry ACN (6.069 mmol) was then added. The mixture was cooled at -10°C (dry ice/acetone bath) and a solution of DMAD (498 µl, 4.046 mmol) in ACN (4 mL) was added dropwise over 10 min. After 10 min stirring at room temperature, the mixture was irradiated in a microwave oven for 2 hours at 83°C. The solvent was reduced *in vacuo* and the crude was purified with a gradient elution mode flash chromatography (hex/DCM 50:50) to give product **3a** in a 31% yield.

**$^1$H-NMR** (400 MHz, $CDCl_3$) δ 8.49 (d, J = 2.3 Hz, 1H, **H3**), 7.67 (dd, J = 8.8, 2.3 Hz, 1H, **H1**), 7.24 (s, 1H, **H6**), 7.01 (s, 1H, **H8**), 4.02 (s, 3H, **H12**).

**$^{13}$C-NMR** (101 MHz, $CDCl_3$) δ 165.52, 162.12, 152.78, 142.45, 137.05, 131.76, 121.56, 121.12, 120.09, 119.16.

#### 6.3.1.5. Synthesis of 6-vinylcoumarin-4-carboxylate (2b)

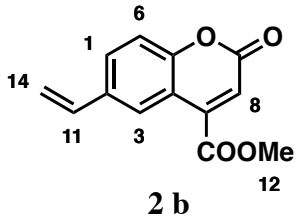


**2 b**

**Reflux synthesis:**

Under a $N_2$ atmosphere, 6-bromocoumarin-4-carboxylate **3b** (30.54 mg, 0.106 mmol) and $AsPh_3$ (6.59 mg, 0.02118 mmol) were dissolved in dry THF (5 mL) and the palladium catalyst (2.46 mg) was added to the mixture. The mixture was stirred for 10 min, before adding tributyl(vinyl)tin (38.69 µl, 0.132 mmol) and refluxing for 192 h at 70 °C. The reaction solution was left to cool to room temperature before adding 4 ml saturated sodium fluoride solution and 3 mL distilled water and stirring for 1 h. Following filtration, the solution was extracted with DCM (3x10 mL) and washed with saturated salt solution (2x10 mL). The extracts were dried over magnesium sulphate, filtered and evaporated *in vacuo*. The crude was purified by flash chromatography (DCM/Pet Ether 80/20) to give 7.4 mg of product **3b** in a 30% yield.

**Microwave irradiation:**

6-bromocoumarin-4-carboxylate **3b** (694.8 mg, 2.45 mmol), $AsPh_3$ (150.3 mg, 0.49 mmol) and the palladium catalyst (83.28 mg) were added in a microwave tube. Once it was sealed, vacuum/nitrogen cycles were performed in order to remove any traces of oxygen. Dry THF (2 ml) was then added followed by tributyl(vinyl)tin (896.68 µl, 3.068 mmol). The mixture was irradiated in a microwave oven for 3 hours at 65°C. The reaction solution was left to cool to room temperature before adding 2 mL saturated

sodium fluoride solution and 1 mL distilled water and stirring for 1 h. Following filtration, the solution was extracted with DCM (3x5 mL) and washed with saturated salt solution (2x5 mL). The extracts were dried over magnesium sulphate, filtered and evaporated *in vacuum*. The crude was purified by recrystallization from hot EtOH to give 272 mg of product **3b** in a 48% yield.

**$^{1}$H-NMR** (400 MHz, $CDCl_3$) δ 8.26 (d, J = 2.0 Hz, 1H, **H3**), 7.65 (dd, J = 8.6, 2.0 Hz, 1H, **H1**), 7.32 (d, J = 8.6 Hz, 1H, **H6**), 6.95 (s, 1H, **H8**), 6.75 (dd, J = 17.6, 10.9 Hz, 1H, **H11**), 5.78 (d, J = 17.6 Hz, 1H, **H14a**), 5.33 (d, J = 10.9 Hz, 1H, **H14b**), 4.01 (s, 3H, **H12**).

**$^{13}$C-NMR** (101 MHz, $CDCl_3$) δ 164.19, 159.86, 153.75, 142.13, 135.29, 134.43, 129.79, 128.65, 124.69, 119.73, 117.38, 115.16, 53.17.

### 6.3.1.6. Synthesis of 6-vinylcoumarin-4-carboxylic acid (1b)

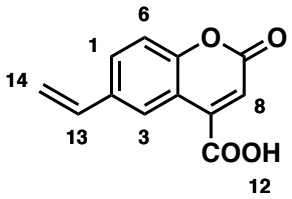


**1 b**

6-vinylcoumarin-4-carboxylate **2b** (184 mg, 0.796 mmol) was dissolved in a solution of 4 mL THF and 10 mL ethanol. Sodium hydroxide (2 mL, 2 M) was added to the reaction and the solution was left to stir at 40°C under nitrogen and in the dark for 14 h. Solvents were removed under *vacuum* and 20 ml of water were added to the residue, which was washed with DCM (2 × 25 mL) and ethyl acetate (2 × 25 mL), before being acidified with concentrated hydrochloric acid. The aqueous phase was then extracted with ethyl acetate (3 × 25 mL) and the combined organic phase washed with a saturated NaCl solution (2 × 25 mL). The organic phase was dried over magnesium sulphate and evaporated to dryness to give 144.7 mg of product **1b** in an 84% yield.

**$^{1}$H-NMR** (400 MHz, DMSO) δ 8.17 (d, J = 2.1 Hz, 1H, **H3**), 7.84 (dd, J = 8.7, 2.1 Hz, 1H, **H1**), 7.44 (dd, J = 8.7, 2.3 Hz, 1H, **H6**), 6.88 – 6.78 (m, 2H, **H8** and **H13**), 5.84 (dd, J = 17.6, 0.7 Hz, 1H, **H14a**), 5.34 (dd, J = 11.0, 0.6 Hz, 1H, **H14b**).

**$^{13}$C-NMR** (101 MHz, DMSO) δ 165.22, 159.42, 153.34, 143.85, 135.33, 133.67, 129.57, 124.47, 118.15, 117.22, 115.82, 115.22.

### 6.3.2. Fluorescence studies chapter 3

#### 6.3.2.1. Interaction studies between VCC and analytes

Solutions of VCC ($5.9 \times 10^{-3}$ M) were mixed with varying volumes of analytes stocks in acetonitrile, to give a final monomer to analytes ratio ranging from 1:0 to 1:5. All the samples were allowed to mix for 5 min at room temperature before being analysed. Triplicate experiments were carried out per each concentration. The fluorescence spectra were recorded at $\lambda_{exc}$ = 521 nm following excitation at $\lambda_{em}$ = 345 nm.

#### 6.3.2.2. Interaction studies between MIP and analytes

Solutions of the imprinted polymer (5 mg/mL in ACN) were placed in 96-well plate and various amounts of analytes were added to give a VCC-analyte ratio ranging from 0 to 0.25,0.5, 0.75 and 1. The solutions were left for 5 min after which the residual fluorescence was measured using a plate reader. Duplicate experiments were carried out per each concentration. The fluorescence spectra were recorded at $\lambda_{exc}$ = 521 nm following excitation at $\lambda_{em}$ = 345 nm

#### 6.3.2.3. Visual detection of clomiphene

A suspension of 2 mg of either MIP or NIP in 400 μl of ACN (5 mg/mL of polymer, $1.18 \times 10^{-3}$ M in VCC) was prepared in glass vials. To each vial, a combination of ACN and clomiphene stock solution ($1.42 \times 10^{-2}$ M) was added to give a total volume of 500

μl and a ratio of VCC to clomiphene ranging from 1:0 to 1:1. The mixtures were allowed to stand for 5 min at room temperature and were then placed under the UV lamp.

### 6.3.3. Synthesis and characterisation of nanogels for drug delivery

#### 6.3.3.1. Tamoxifen extraction from its citrate form

Tamoxifen citrate was dispersed in a sodium carbonate solution (10 mM) and extracted with dichlorometane. The extracts were dried over $MgSO_4$ and evaporated to dryness.

#### 6.3.3.2. General synthesis of nanogels

Tamoxifen imprinted polymers (MIPs) and their non-imprinted counterpart (NIPs) were prepared by using the standard protocol of high dilution radical polymerization. Both nanogels were systhesised using the same conditions, with the only difference in the presence of tamoxifen when MIPs were prepared. The percentage of cross-linking agent MBA was fixed at 20%, while the other components were varied as described in chapter 4, section 4.3.1. The chemicals involved were weighted out and added in a Wheaton glass bottle. After sealing the bottle, dry DMSO was added and cycles *vacuum*/nitrogen were performed. The solution was then polymerised for two days at 70°C in oven.

#### 6.3.3.3. General purification method and reconstitution of nanogels

After polymerisation the nanogel solution was dialysed against non-distilled water for two days, with 2 water exchanges per day. The dialysis membrane used had pore size of 3500 Daltons. On completion of dialysis the solutions were frozen in liquid nitrogen and freeze-dried. White, lightweight powders were obtained and stored in the dark at room temperature.

#### 6.3.3.4. Particle size characterisation-zetasizer

Solutions of nanogels were prepared in distilled water at 1 mg/mL and sonicated at room temperature for 10 minutes. The samples were then filtered with GHP 0.45μm filter (Acrodisc Pall) before being measured with the DLS.

#### 6.3.3.5. Fluorescence characterisation

Solution at concentration 1mg/mL were prepared in a total volume of 2mL and sonicated at room temperature for 10 minutes. The samples were then filtered with GHP 0.45μm filter (Acrodisc Pall) before being transferred into high precision quartz cell with light path of 10mm and total volume 2mL. Experiments were carried out on Cary Eclipse Fluorescence Spectrophotometer, slit:1.5. $\lambda_{exc}$ = 360 nm, $\lambda_{em}$ = 460 nm.

#### 6.3.3.6. Lower Critical Solution Temperature characterisation

Solutions of nanogels were prepared in distilled water at 1 mg/mL and sonicated at room temperature for 10 minutes. The samples were then filtered with GHP 0.45μm filter (Acrodisc Pall) before being transferred into high precision quartz cell with light path of 10mm and total volume 1 mL. Cary 100 UV-Vis Spectrophotometer (Agilent technologies), equipped with an internal thermostat was employed. The wavelength was fixed at 500nm, SBW (spectral bandwidth) was 1nm and the average time 1 seconds. The initial and final temperatures were set to 45°C and 70°C, respectively. Data interval was 1°C and the rate was 1°C/min.

#### 6.3.3.7. Establishing the polymerisation of functional monomer

Solutions of NIP and MIP were prepared at 0.5 mg/mL in a mixture $H_2O$/MeOH and stirred for two hours. The two solutions were dialysed against 10% MeOH in $H_2O$, changing the dialysis mixture three times in 24 hours, with the last change being 100%

$H_2O$. The nanogels solutions were freeze-dried and reconstitute in $H_2O$ at 0.5mg/mL, sonicated and filtrated with GHP 0.45μm filter (Acrodisc Pall) before being transferred before being transferred into high precision quartz cell with light path of 10mm and total volume 2 mL for fluorescence readings.

#### 6.3.3.8. Tamoxifen calibration curve via HPLC

Two stock solutions of tamoxifen citrate at different concentrations were prepared independently by weight in acetonitrile. The solutions were cross-diluted to generate 16 solutions with different concentrations ranging from 0.035 to 1.77 mM. 20 μl of each solution was injected into the HPLC using an eluent of 85:15 methanol to water acidified at 0.5% (v/v) with acetic acid at a flow rate of 0.5 mL/min. Tamoxifen eluted at approximately 7 minutes and the area under the curve was plotted against concentration to form a reference curve. Thus obtaining a value for b in the equation:

$$y = bx + c \qquad \textbf{Equation 1}$$

Where y= area under the curve, x = concentration, b = slope of the curve and due to the curve passing through the origin c=0.

#### 6.3.3.9. Analysis of nanogels via HPLC

The MIP was reconstituted in a mixture of acidic MEOH/ACN 5:5 (pH=3) at a concentration 1 mg/mL and stirred overnight to release the drug. The mixture was then filtered with a 20 nm PTFE filter to remove the polymer. 20 μl of the solution was injected into the HPLC using the same eluent and flow rate as used to obtained the calibration curve.

#### 6.3.3.10. Tamoxifen calibration curve *via* photoreaction and UV-Vis spectroscopy

Concentrations of tamoxifen uploaded onto the nanogels were evaluated by means of calibration curve established using UV-Vis spectrophotometer after UV irradiation. Two stock solutions of tamoxifen at different concentrations were prepared independently by weight in MeOH. The solutions were cross-diluted to generate 5 solutions with different concentrations ranging from 0.067 to 0.538 mM. The solutions were transferred into 1mL high precision quartz cells and irradiated for 4 hours with ultraviolet lamp (max output 254nm) placed 10cm from the quartz cells. The UV-Vis spectrum for each solution was then recorded and the max absorbance of the peak at $\lambda_{abs}$ = 360nm was plotted against concentration to form a reference curve.

$$y = bx + c \qquad \textbf{Equation 1}$$

Where y= area under the curve, x = concentration, b = slope of the curve and due to the curve passing through the origin c=0.

#### 6.3.3.11. Evaluation of tamoxifen loaded in MIP

A solution of MIP in MeOH at 1mg/mL was transferred in high precision 1mL high precision quartz cell and irradiated for a maximum of 80 minutes with ultraviolet lamp (max output 254nm) placed 10cm from the quartz cell. The UV-Vis spectrum of the solution was recorded every 20 minutes. The max absorbance of the peak at $\lambda_{abs}$ = 360nm gave a value for Y in the equation in equation 1and b could be substituted from the slope of the calibration curve hence giving the concentration of tamoxifen present in the sample.

## 6.4. *In vivo* experiments, chapter 5

All fish were maintained at 28.5 °C in 'fish water' which is a salt water solution comprised of sodium bicarbonate, marine salts and calcium sulphate in a ratio of 7.5:1.8:0.84 g in 100 L of reverse osmosis (R/O) purified water. All test solutions were formed using fish water. Adult fish were maintained on a 14 hrs /10 hrs light dark cycle following standard husbandry protocols. Embryos/larvae used for *in vivo* nanogel analysis were maintained at 28.5 °C in the dark. For breeding, fish were housed in pairs overnight in 1 L tank equipped with a removal-mating sieve with a mesh net at the bottom. Embryos were collected the following morning within 2 hpf and placed in separate petri-dishes (n*50/dish). After identification, homozygous $Cre^{ERt2}$ (-Tg(3.5ubb:creERT2,my17:EGFP) males and homozygous loxP (-Tg(3.5ubb:loxP-EGFP-loxP-mcherry) females adults were separated housed in 5 L tank, one couple per tank separated by a clear divisor for easier identification. All procedures were carried out under the Animals (Scientific Procedures) Act, 1986, and under local ethical guidelines (Queen Mary, University of London).

### 6.4.1. Genotyping by breeding

Female loxP adult zebrafish were crossed with a wild type zebrafish in a 1 L mating tank. Embryos were collected, sorted and maintained at 28°C. Each loxP adult was identified as homozygous if at 24 hpf the embryos of the produced clutch showed all over GFP fluorescence. The loxP who produced embryos who did not show GFP fluorescence was discarded. Male $Cre^{ERt2}$ adult zebrafish were crossed with a wild type zebrafish in a 1 L mating tank. Embryos were collected, sorted and maintained at 28°C. $Cre^{ERt2}$ adult was identified as homozygous if at 48 hpf the embryos of the produced

clutch showed GFP fluorescence in their hearts. The $Cre^{ERt2}$ who produced embryos who did not show GFP fluorescence in the heart was discarded.

### 6.4.2. Tamoxifen - induced switch

Homozygous loxP female were crossed with and homozygous $Cre^{ERt2}$ male to produce homozygous *ubi:*switch. Embryos were collected, sorted and maintained at 28°C.

Two solutions of 5 and 10µM of tamoxifen citrate were prepared in fish water and sonicated. Two wells of a 6-well pate were filled with 10 mL of 5µM tamoxifen, two wells were filled with 10 mL of 10µM tamoxifen and the remaining two wells were filled with fish water and used as internal plate control. Thirty larvae at 4dpf *ubi:*switch were added in each well containing either tamoxifen solution or fish water. The plates were labelled and maintained at 28°C.

### 6.4.3. Toxicity and visualisation studies *in vivo* using *ubi*:switch system

Homozygous loxP female were crossed with and homozygous $Cre^{ERt2}$ male to produce homozygous *ubi:*switch. Embryos were collected, sorted and maintained at 28°C.

Four 50 mL solutions of 84.7µg/mL and 169.4µg/mL of NIP **FM-P7** and MIP **FM-P8** were prepared in fish water. The solutions were sonicated and filtrated over 0.45µm GHP filter before transferring 2 mL of each solution in 20 wells of 24-well plates. The other 4 wells of the plate were filled with fresh fish water and served as internal plate control. One *ubi:*switch embryo at 24 hpf was added in each well containing either the nanogels solution or fish water. The plates were labelled and maintained at 28°C.

### 6.4.4. Preparation of the fish for imaging

An average of five fish per each tested solution were transferred into a solution of 4% w/v paraformaldehyde in phosphate buffered solution for 2 hours to fix the tissues. The fish were then mounted on microscope slides using agarose solution 1% w/v in PBS.

# Appendix

# Appendix

## Chapter 4

### 1) Zetasizer

### FM-P1

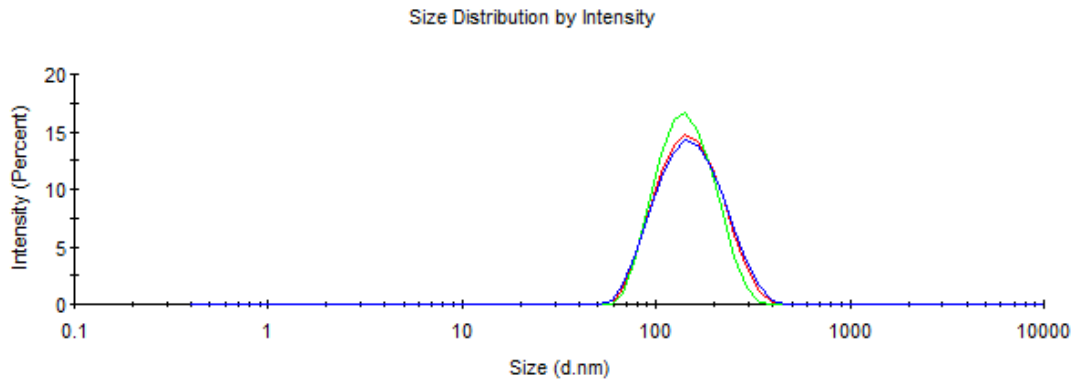


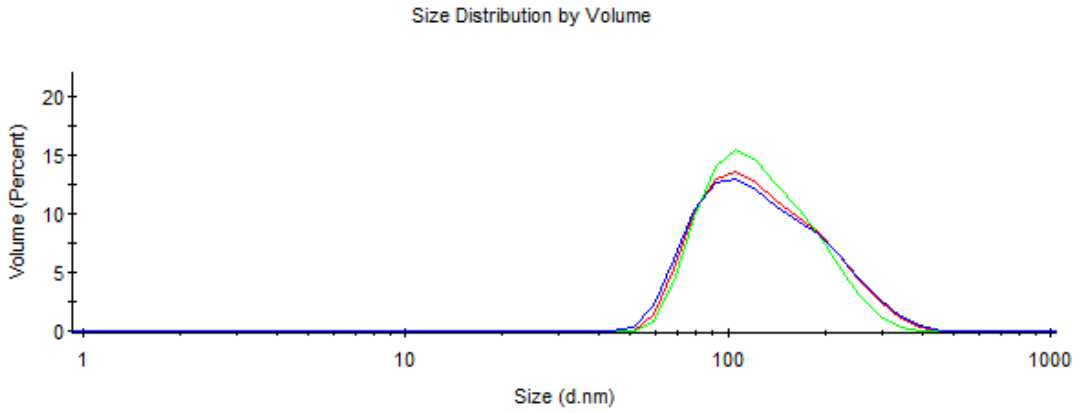

**FM-P2**

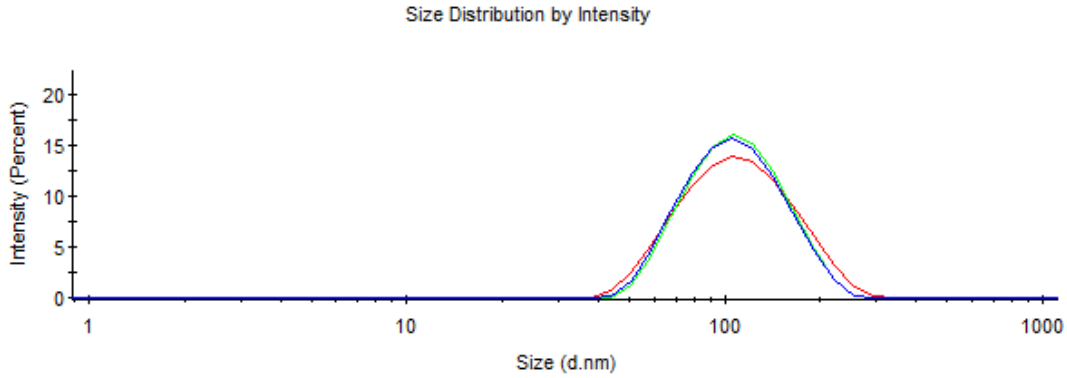
Size Distribution by Intensity
Intensity (Percent)
20
15
10
5
0
1
10
100
1000
Size (d.nm)

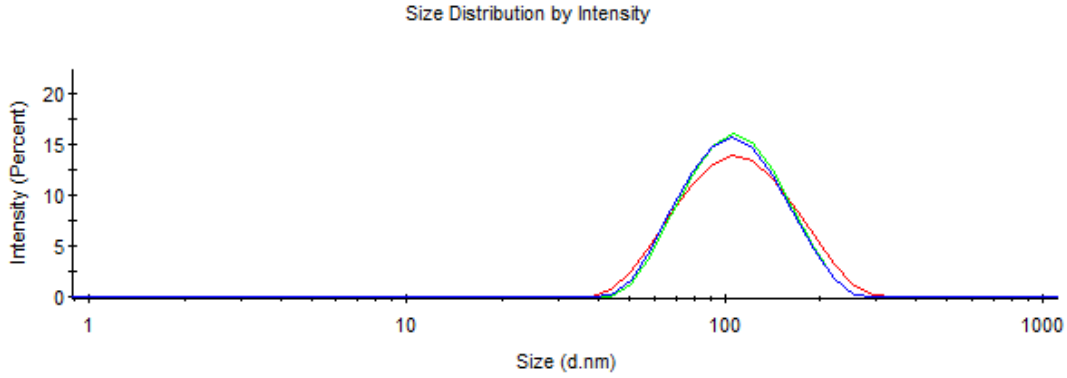
Size Distribution by Intensity
Intensity (Percent)
20
15
10
5
0
1
10
100
1000
Size (d.nm)

**FM-P3**

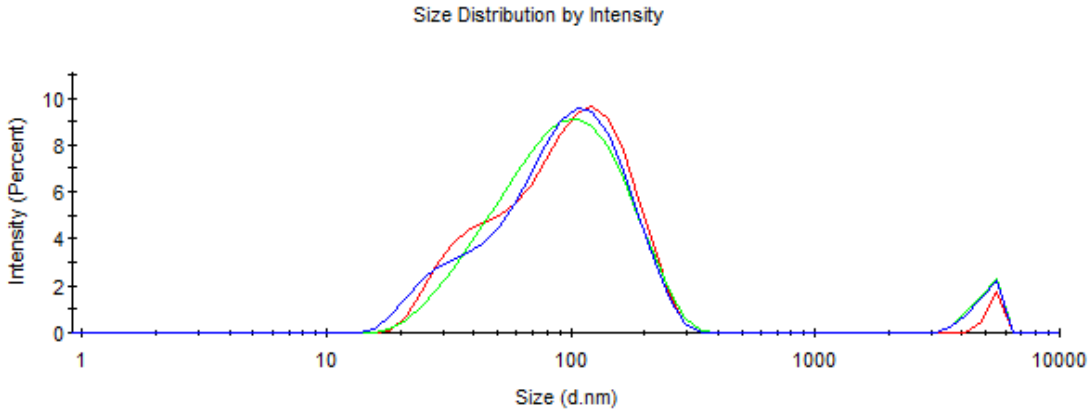
Size Distribution by Intensity
Intensity (Percent)
0
2
4
6
8
10
1
10
100
1000
10000
Size (d.nm)

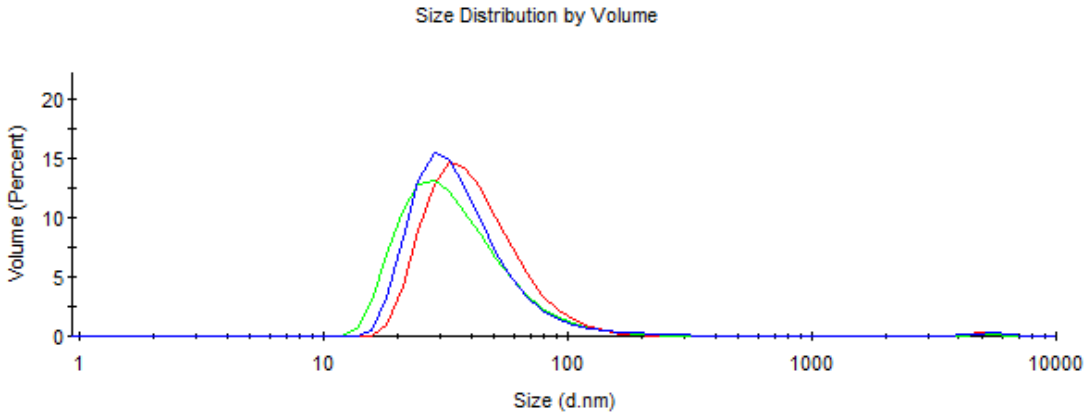
Size Distribution by Volume
Volume (Percent)
0
5
10
15
20
1
10
100
1000
10000
Size (d.nm)

**FM-P4**

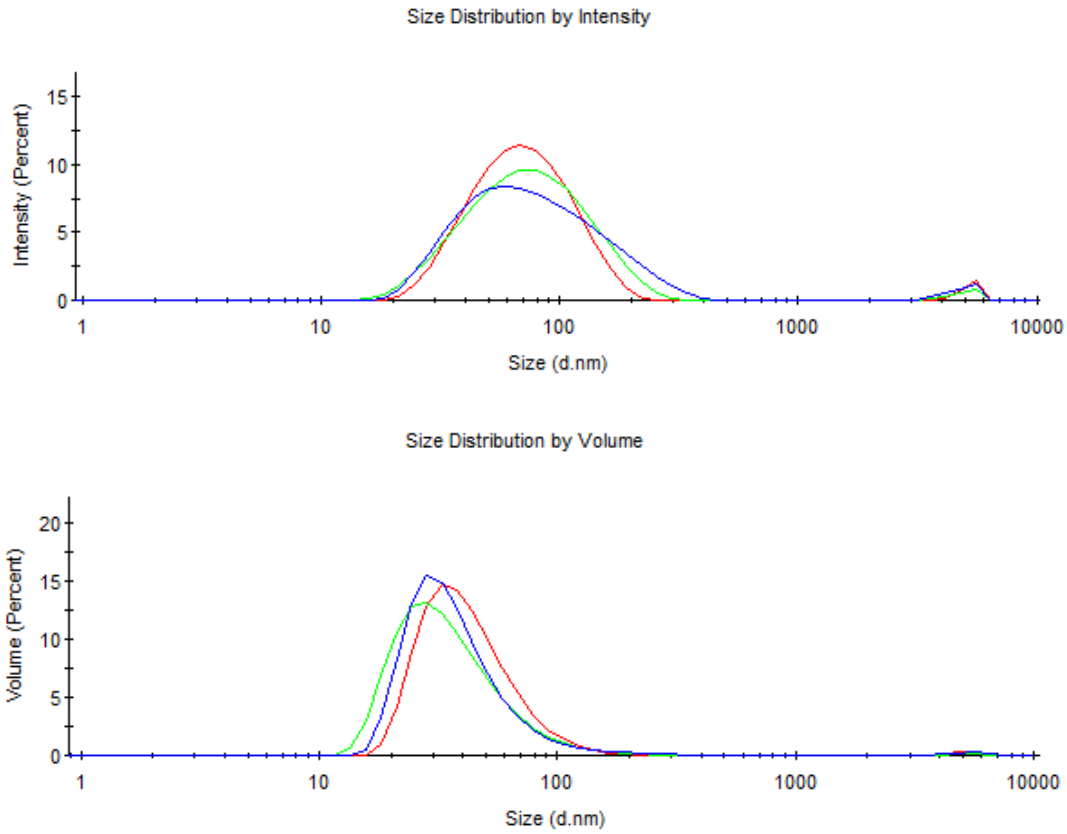
Size Distribution by Intensity
Intensity (Percent)
15
10
5
0
1
10
100
1000
10000
Size (d.nm)
Size Distribution by Volume
Volume (Percent)
20
15
10
5
0
1
10
100
1000
10000
Size (d.nm)

**FM-P5**

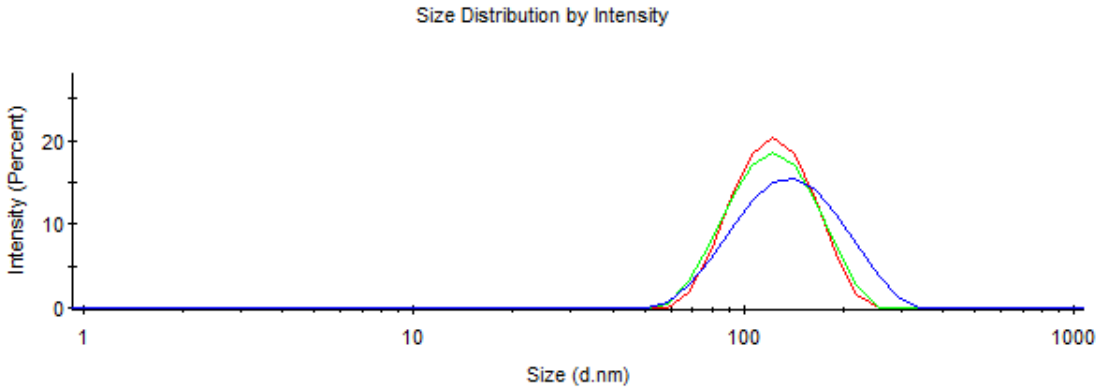
Size Distribution by Intensity
Intensity (Percent)
20
10
0
1
10
100
1000
Size (d.nm)

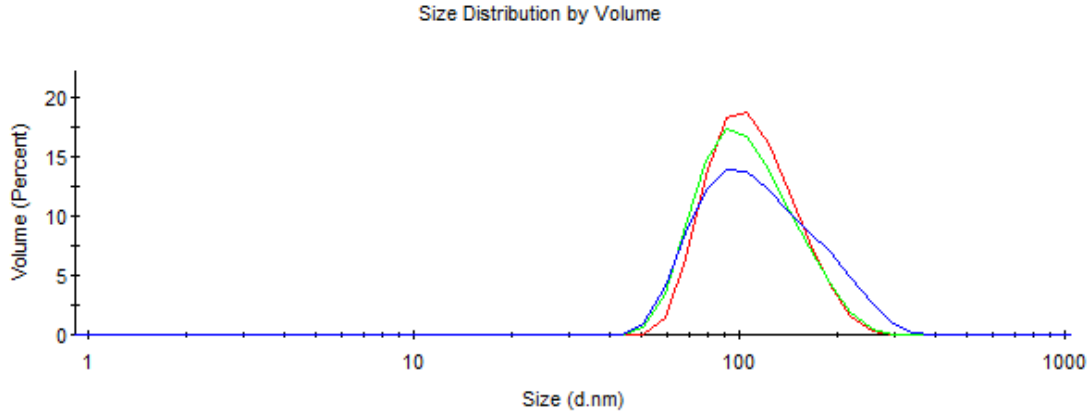
Size Distribution by Volume
Volume (Percent)
20
15
10
5
0
1
10
100
1000
Size (d.nm)

**FM-P6**

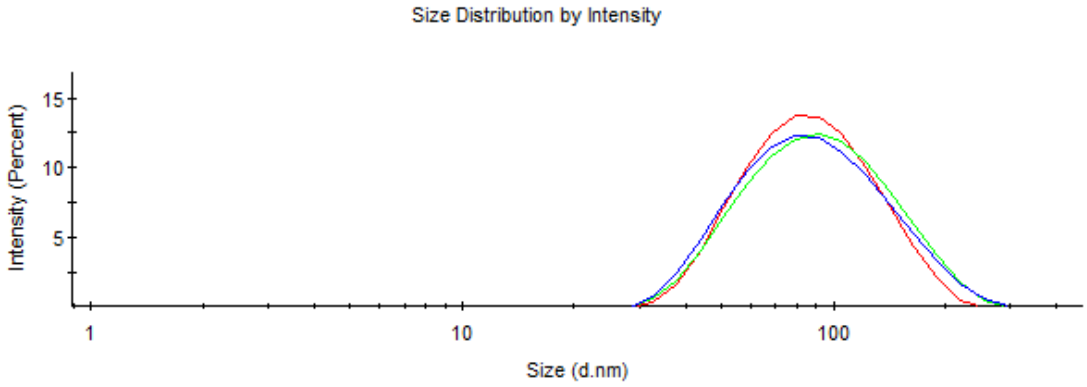
Size Distribution by Intensity
Intensity (Percent)
15
10
5
1
10
100
Size (d.nm)

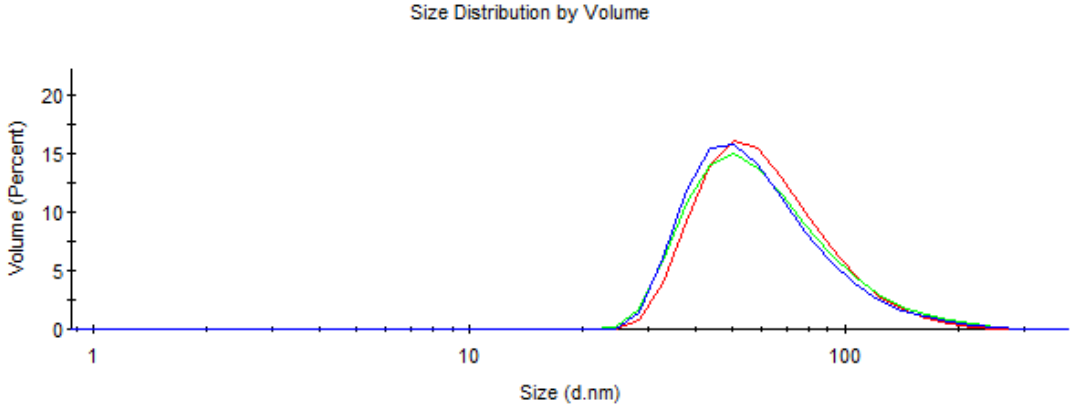
Size Distribution by Volume
Volume (Percent)
20
15
10
5
0
1
10
100
Size (d.nm)

**FM-P7**

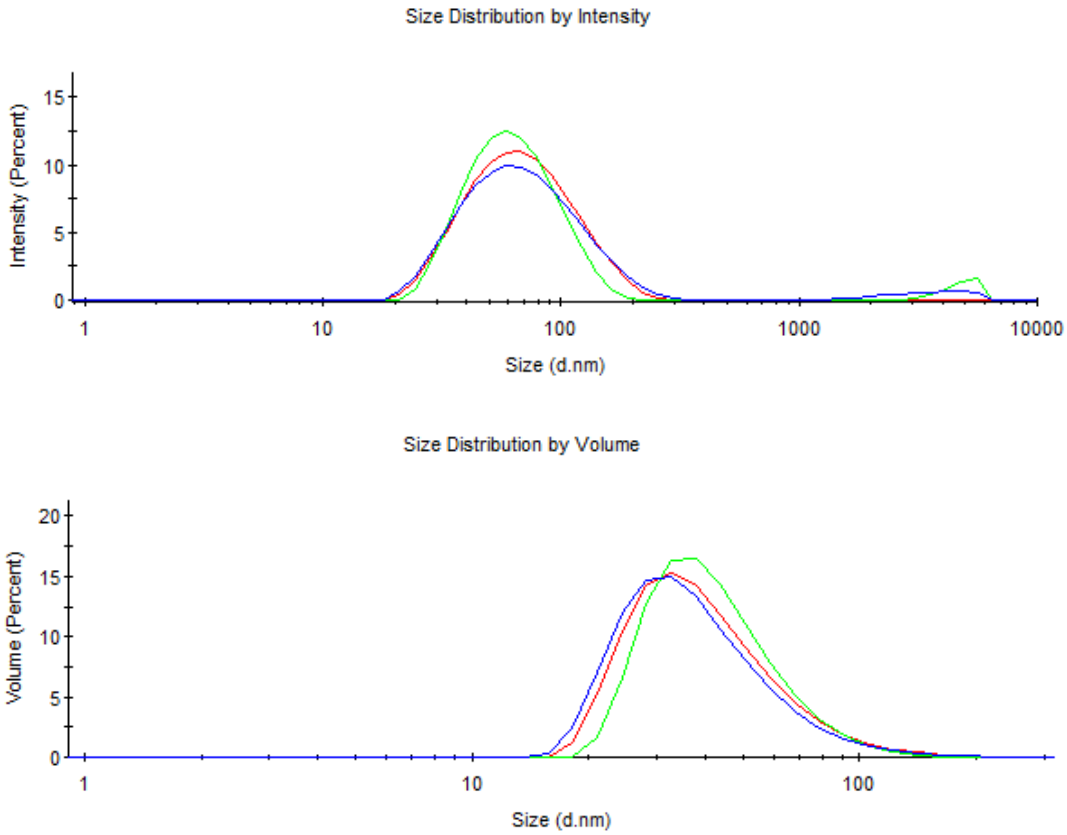
Size Distribution by Intensity
Intensity (Percent)
15
10
5
0
1
10
100
1000
10000
Size (d.nm)
Size Distribution by Volume
Volume (Percent)
20
15
10
5
0
1
10
100
Size (d.nm)

**FM-P8**

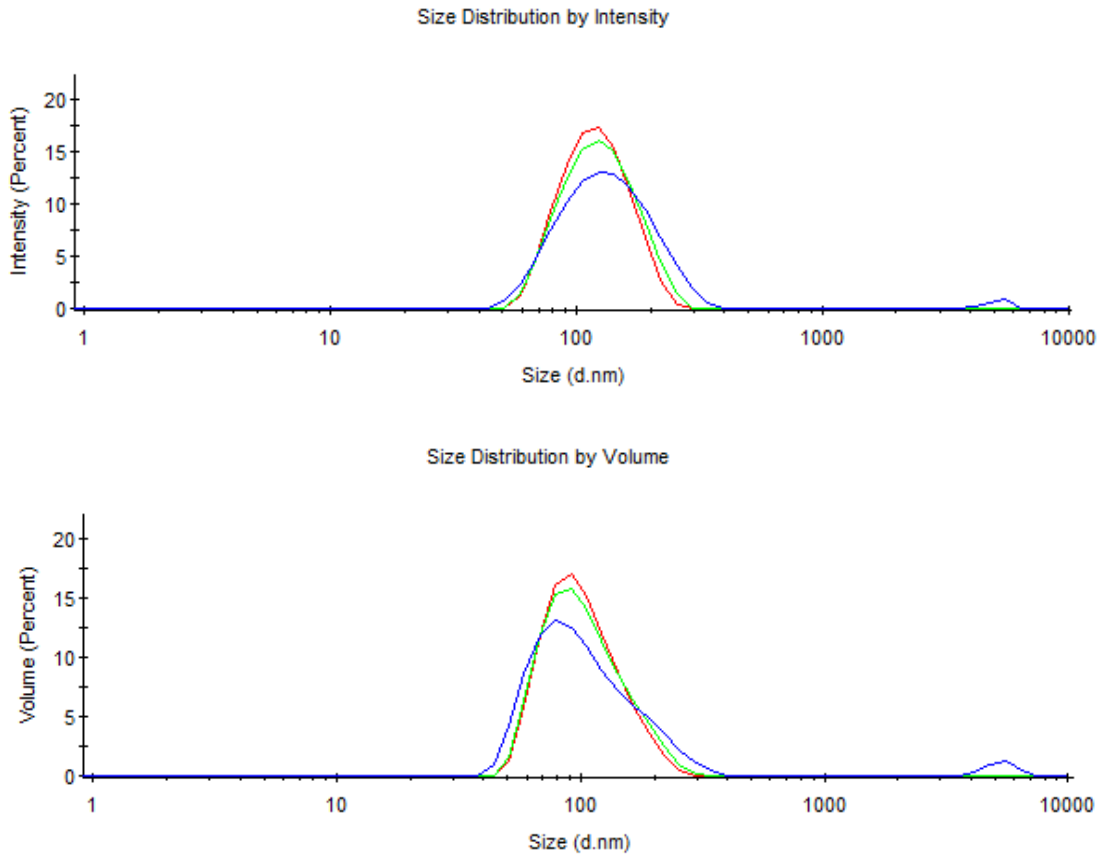
Size Distribution by Intensity
Intensity (Percent)
20
15
10
5
0
1
10
100
1000
10000
Size (d.nm)
Size Distribution by Volume
Volume (Percent)
20
15
10
5
0
1
10
100
1000
10000
Size (d.nm)

**Table 1.** Summary of nanogels size by distribution, intensity, volume and number. Nanogels samples prepared at 0.5 mg/ml in water at pH = 5.5 and filtrated on 0.45 μm filter.

| | **Size Intensity** $(nm)_{AVG}$ | **Size Volume** $(nm)_{AVG}$ | **Size Number** $(nm)_{AVG}$ | **PDI** |
|---|---|---|---|---|
| **FM-P2** | 116.0 ± 44.9 | 87.28 ± 39.80 | 61.70 ± 16.59 | 0.130 |
| **FM-P3** | 79.91 ± 23.39 | 55.23 ± 18.89 | 44.26 ± 12.04 | 0.296 |
| **FM-P4** | 68.01 ± 35.48 | 35.35 ± 18.50 | 23.91 ± 7.933 | 0.233 |
| **FM-P5** | 144.1 ± 49.86 | 123.3 ± 51.85 | 86.03 ± 28.78 | 0.362 |
| **FM-P6** | 92.01 ± 36.13 | 64.98 ± 27.86 | 47.68 ± 14.62 | 0.207 |
| **FM-P7** | 75.15 ± 38.38 | 42.23 ± 21.32 | 29.63 ± 9.339 | 0.269 |
| **FM-P8** | 123.4 ± 37.94 | 105.5 ± 37.90 | 81.77 ± 23.63 | 0.340 |

## 2) UV-vis Spectra of nanogels

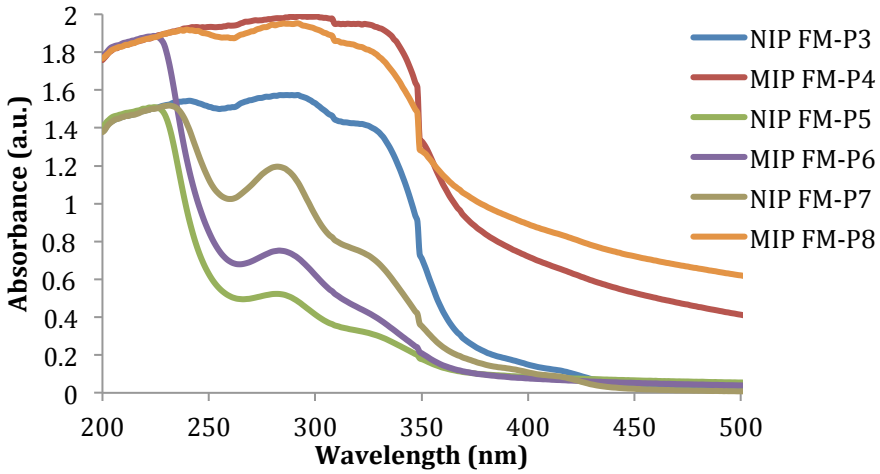


**Figure 1.** Summary of UV-Vis spectrum of every preparation at 1mg/mL in $H_2O$

**3) Non-imprinted nanogel without fluorescence functional monomer.**

| | MIP/NIP | MBA | VCC | NIPAM | AIBN | $C_M$ | Yield | Solubility in Water |
|---|---|---|---|---|---|---|---|---|
| **FM-P9** | NIP | 20% | - | 80% | 10 % | 0.5 % | 68 % | >1 mg/ml |

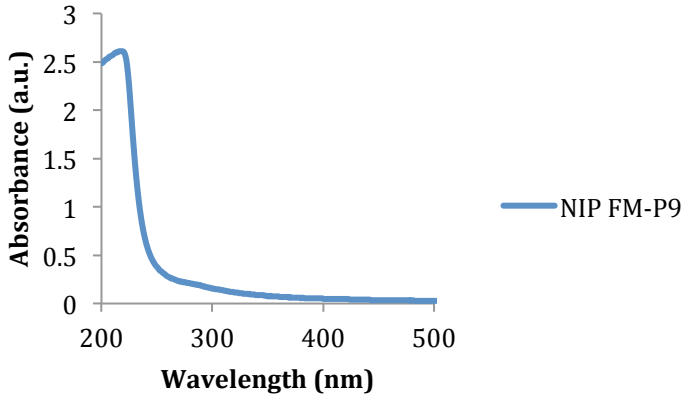


**Figure 2.** UV-Vis spectrum of a non-imprinted polymer prepared following the same procedure as the set of polymers already presented, but without the fluorescent monomer VCC, 1mg/mL in $H_2O$

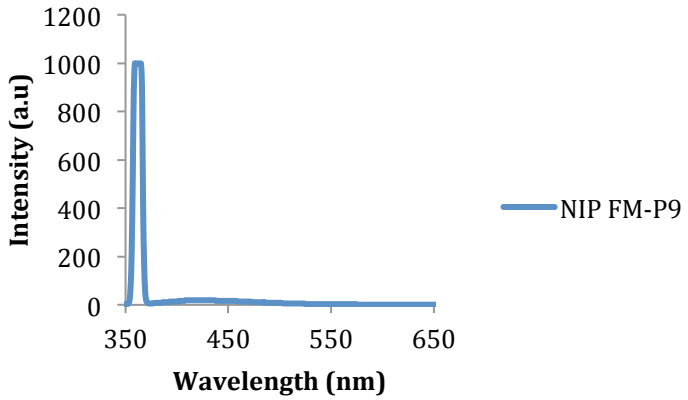


**Figure 3.** Fluorescence emission followed irradiation at λ = 360nm of a non-imprinted polymer prepared following the same procedure as the set of polymers already presented, but without the fluorescent monomer VCC, 1mg/mL in $H_2O$.

## 4) NMR data provided by Mr. Pengfei Liu

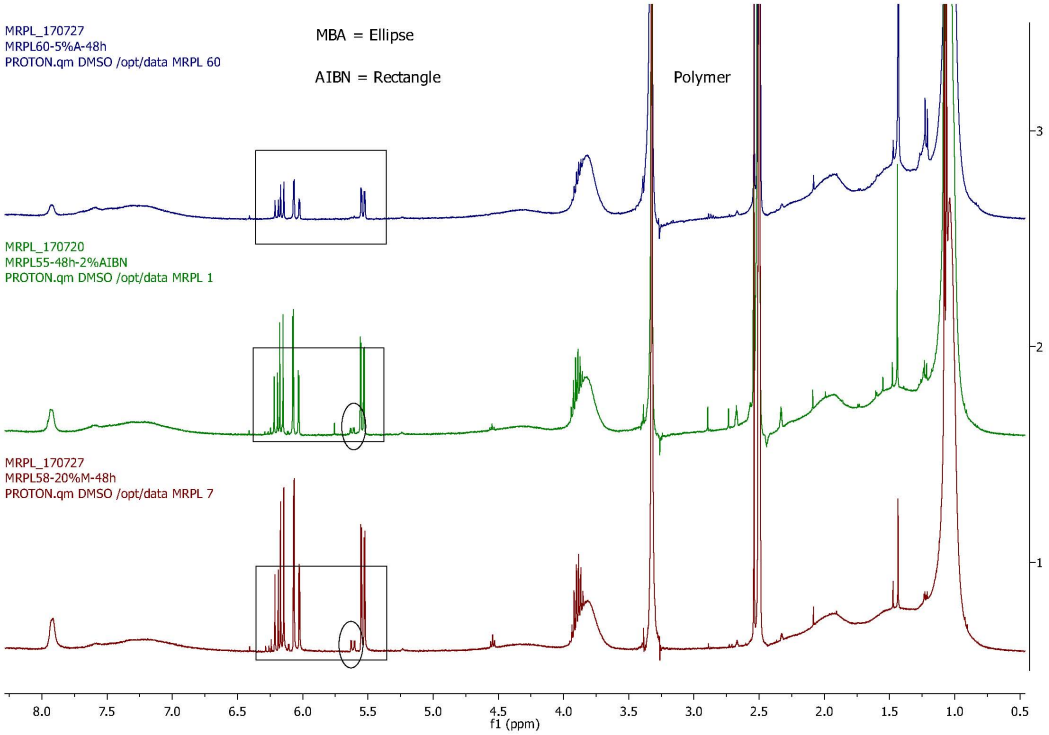


**Figure 4.** Nanogels based on 20% MBA and 80% NIPAM at $C_M$1% after 48hrs polymerisation. From the bottom to the top: 1%, 2% and 5% of AIBN, respectively.

The characteristic peaks of the acrylic group in the NIPAM are highlighted by a rectangle, while the residue peak of the MBA is indicated with an ellipse. It is clearly shown that after 48hrs, when 5% AIBN was employed, no MBA peaks were visible. This suggested the complete polymerisation of the cross-linker, confirming its faster kinetic.